Magnetic Resonance Spectroscopy and Imaging: NMR, MRI and ESR

Contents

Articles

References

Article Licenses

Nuclear Magnetic Resonance

Version 3.0

Relaxation

Relaxation stands quite generally for a release of tension, a return to equilibrium.

In the sciences, the term is used in the following ways:

- Relaxation (physics), and more in particular:
  - Relaxation (NMR), processes by which nuclear magnetization returns to the equilibrium distribution
  - Dielectric relaxation, the delay in the dielectric constant of a material
  - Structural relaxation, responsible for the glass transition
- In mathematics:
  - Relaxation technique (mathematics), a technique for transforming hard constraints into easier ones
  - Relaxation method, for numerically solving elliptic partial differential equations
- In computer science:
  - Relaxation, the act of substituting alternative program code during linking

In Physiology, Hypnotism, Meditation, Recreation:

- Relaxation technique, an activity that helps a person to relax
- Relaxed in Flow (psychology), a state of arousal, flow, over-learned self-control and relaxation
- Relaxation (psychology), the emotional state of low tension

See also:

- Tension (music)

Chemical Shift

In nuclear magnetic resonance (NMR), the **chemical shift** describes the dependence of nuclear magnetic energy levels on the electronic environment in a molecule.[1] [2] [3] Chemical shifts are relevant in NMR spectroscopy techniques such as proton NMR and carbon-13 NMR.

An atomic nucleus can have a magnetic moment (nuclear spin), which gives rise to different energy levels and resonance frequencies in a magnetic field. The total magnetic field experienced by a nucleus includes local magnetic fields induced by currents of electrons in the molecular orbitals (note that electrons have a magnetic moment themselves). The electron distribution of the same type of nucleus (e.g. ^{1}H, ^{13}C, ^{15}N) usually varies according to the local geometry (binding partners, bond lengths, angles between bonds, ...), and with it the local magnetic field at each nucleus. This is reflected in the spin energy levels (and resonance frequencies). The variations of nuclear magnetic resonance frequencies of the same kind of nucleus, due to variations in the electron distribution, is called the chemical shift. The size of the chemical shift is given with respect to a reference frequency or reference sample (see also *chemical shift referencing*), usually a molecule with a barely distorted electron distribution.

The chemical shift is of great importance for NMR spectroscopy, a technique to explore molecular properties by looking at nuclear magnetic resonance phenomena.

Operating frequency

The operating (or Larmor) frequency ω_0 of a magnet is calculated from the Larmor equation

$$\omega_0 = \gamma * B_0$$

where B_0 is the actual strength of the magnet in units like teslas or gauss, and γ is the gyromagnetic ratio of the nucleus being tested which is in turn calculated from its magnetic moment μ and spin number I with the nuclear magneton μ_N and the Planck constant h:

$$\gamma = \frac{\mu\,\mu_N}{hI}$$

Thus, the proton operating frequency for a 1 T magnet is calculated as:

$$\omega_0 = \gamma B_0 = \frac{2.79 \times 5.05 \times 10^{-27}\,\text{J/T}}{6.62 \times 10^{-34}\,\text{Js} \times (1/2)} \times 1\,\text{T} = 42.5\,\text{MHz}$$

Chemical shift referencing

Chemical shift δ is usually expressed in parts per million (ppm) by frequency, because it is calculated from:

$$\delta = \frac{\text{difference in precession frequency between two nuclei}}{\text{operating frequency of the magnet}}$$

Since the numerator is usually in hertz, and the denominator in megahertz, delta is expressed in ppm.

The detected frequencies (in Hz) for ^{1}H, ^{13}C, and ^{29}Si nuclei are usually referenced against TMS (tetramethylsilane) or DSS, which is assigned the chemical shift of zero. Other standard materials are used for setting the chemical shift for other nuclei.

Thus, an NMR signal at 300 Hz from TMS at an applied frequency of 300MHz has a chemical shift of:

$$\frac{300\,\text{Hz}}{300 \times 10^6\,\text{Hz}} = 1 \times 10^{-6} = 1\,\text{ppm}$$

Although the frequency depends on the applied field the chemical shift is independent of it. On the other hand the resolution of NMR will increase with applied magnetic field resulting in ever increasing chemical shift changes.

The induced magnetic field

The electrons around a nucleus will circulate in a magnetic field and create a secondary induced magnetic field. This field opposes the applied field as stipulated by Lenz's law and atoms with higher induced fields (i.e., higher electron density) are therefore called *shielded*, relative to those with lower electron density. The chemical milieu of an atom can influence its electron density through the polar effect. Electron-donating alkyl groups, for example, lead to increased shielding while electron-withdrawing substituents such as nitro groups lead to *deshielding* of the nucleus. Not only substituents cause local induced fields. Bonding electrons can also lead to shielding and deshielding effects. A striking example of this are the pi bonds in benzene. Circular current through the hyperconjugated system causes a shielding effect at the molecule's center and a deshielding effect at its edges. Trends in chemical shift are explained based on the degree of shielding or deshielding.

Nuclei are found to resonate in a wide range to the left (or more rare to the right) of the internal standard. When a signal is found with a higher chemical shift:

- the applied effective magnetic field is lower, if the resonance frequency is fixed, (as in old traditional CW spectrometers)
- the frequency is higher, when the applied magnetic field is static, (normal case in FT spectrometers)
- the nucleus is more deshielded
- the signal or shift is **downfield** or at **low field** or paramagnetic

Conversely a lower chemical shift is called a **diamagnetic shift**, and is **upfield** and more shielded.

Diamagnetic shielding

In real molecules protons are surrounded by a cloud of charge due to adjacent bonds and atoms. In an applied magnetic field ($\mathbf{B}_0$) electrons circulate and produce an induced field ($\mathbf{B}_i$) which opposes the applied field. The effective field at the nucleus will be $\mathbf{B} = \mathbf{B}_0 - \mathbf{B}_i$. The nucleus is said to be experiencing a diamagnetic shielding
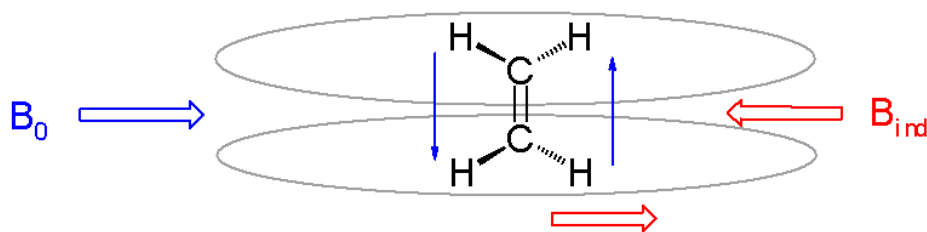
Factors causing chemical shifts

Important factors influencing chemical shift are electron density, electronegativity of neighboring groups and anisotropic induced magnetic field effects.

Electron density shields a nucleus from the external field. For example in proton NMR the electron-poor tropylium ion has its protons downfield at 9.17 ppm, those of the electron-rich cyclooctatetraenyl anion move upfield to 6.75 ppm and its dianion even more upfield to 5.56 ppm.
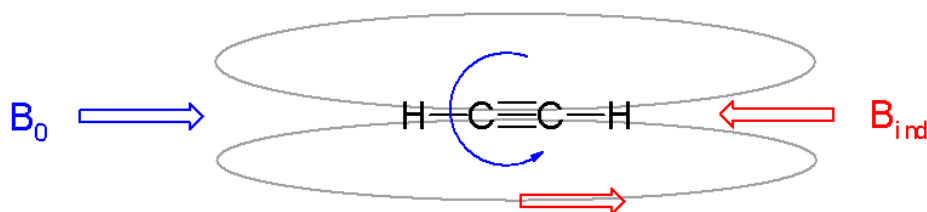
A nucleus in the vicinity of an electronegative atom experiences reduced electron density and the nucleus is therefore deshielded. In proton NMR of methyl halides (CH_3X) the chemical shift of the methyl protons increase in the order I < Br < Cl < F from 2.16 ppm to 4.26 ppm reflecting this trend. In carbon NMR the chemical shift of the carbon nuclei increase in the same order from around −10 ppm to 70 ppm. Also when the electronegative atom is removed further away the effect diminishes until it can be observed no longer.

Anisotropic induced magnetic field effects are the result of a local induced magnetic field experienced by a nucleus resulting from circulating electrons that can either be paramagnetic when it is parallel to the applied field or diamagnetic when it is opposed to it. It is observed in alkenes where the double bond is oriented perpendicular to the external field with pi electrons likewise circulating at right angles. The induced magnetic field lines are parallel to the external field at the location of the alkene protons which therefore shift downfield to a 4.5 ppm to 7.5 ppm range. The three-dimensional space where a nucleus experiences diamagnetic shift is called the shielding zone with a cone-like shape aligned with the external field.

The protons in aromatic compounds are shifted downfield even further with a signal for benzene at 7.73 ppm as a consequence of a diamagnetic ring current.

Alkyne protons by contrast resonate at high field in a 2−3 ppm range. For alkynes the most effective orientation is the external field in parallel with electrons circulation around the triple bond. In this way the acetylenic protons are located in the cone-shaped shielding zone hence the upfield shift.

Magnetic properties of most common nuclei

^{1}H and ^{13}C aren't the only nuclei susceptible to NMR experiments. A number of different nuclei can also be detected, although the use of such techniques is generally rare due to small relative sensitivities in NMR experiments (compared to ^{1}H) of the nuclei in question, the other factor for rare use being their slender representation in nature/organic compounds.

Isotope	Occurrence in nature (%)	spin number l	Magnetic moment μ[4]	Electric quadrupole moment ($e \times 10^{-24}$ cm^2)	Operating frequency at 7 T (MHz)	Relative sensitivity
^{1}H	99.984	1/2	2.79628		300.13	1
^{2}H	0.016	1	0.85739	2.8 x 10^{-3}	46.07	0.0964
^{10}B	18.8	3	1.8005	7.4 x 10^{-2}	32.25	0.0199
^{11}B	81.2	3/2	2.6880	2.6 x 10^{-2}	96.29	0.165
^{12}C	98.9	0				
^{13}C	1.1	1/2	0.70220		75.47	0.0159
^{14}N	99.64	1	0.40358	7.1 x 10^{-2}	21.68	0.00101
^{15}N	0.37	1/2	−0.28304		30.41	0.00104
^{16}O	99.76	0				
^{17}O	0.0317	5/2	−1.8930	−4.0 x 10^{-3}	40.69	0.0291
^{19}F	100	1/2	2.6273		282.40	0.834
^{28}Si	92.28	0				
^{29}Si	4.70	1/2	−0.55548		59.63	0.0785

^{31}P	100	1/2	1.1205		121.49	0.0664
^{35}Cl	75.4	3/2	0.92091	-7.9×10^{-2}	29.41	0.0047
^{37}Cl	24.6	3/2	0.68330	-6.2×10^{-2}	24.48	0.0027
Magnetic properties of common nuclei[5]						

^1H, ^{13}C, ^{15}N, ^{19}F and ^{31}P are the five nuclei that have the greatest importance in NMR experiments:

- ^1H because of high sensitivity and vast occurrence in organic compounds
- ^{13}C because of being the key component of all organic compounds despite occurring at a low abundance (1.1%) compared to the major isotope of carbon ^{12}C, which has a spin of 0 and therefore is NMR inactive.
- ^{15}N because of being a key component of important biomolecules such as proteins and DNA
- ^{19}F because of high relative sensitivity
- ^{31}P because of frequent occurrence in organic compounds and moderate relative sensitivity

Other chemical shifts

The related Knight shift (first reported in 1949) is observed with pure metals. The NMR chemical shift in its present day meaning first appeared in journals in 1950. Chemical shifts with a different meaning appear in X-ray photoelectron spectroscopy as the shift in atomic core-level energy due to a specific chemical environment. The term is also used in Mössbauer spectroscopy, where similarly to NMR it refers to a shift in peak position due to the local chemical bonding environment. As is the case for NMR the chemical shift reflects the electron density at the atomic nucleus. [6]

See also

- Carbon-13 NMR
- MRI
- NMR spectroscopy
- 2D-FT NMRI and Spectroscopy
- Nuclear magnetic resonance
- Protein NMR
- Proton NMR
- Solid-state NMR
- Zeeman effect

External links

- www.chem.wisc.edu [7]
- BioMagResBank [8]
- wwwchem.csustan.edu [9]
- Proton chemical shifts [7]
- Carbon chemical shifts [10]
- Online tutorials (these generally involve combined use of IR, ^1H NMR, ^{13}C NMR and mass spectrometry)
  - Problem set 1, advanced [11] (see also this link [12] for more background information on spin-spin coupling)
  - Problem set 2, moderate [13]
  - Problem set 4, moderate, German language (don't let that scare you away!) [14]
  - Problem set 5, the best! [15]

- Combined solutions to problem set 5 (Problems 1–32) [16] and (Problems 33–64) [17]

References

[1] *Spectrometric Identification of organic Compounds* Silverstein, Bassler, Morrill 4th Ed. ISBN 047109700

[2] *Organic Spectroscopy* William Kemp 3rd Ed. ISBN 0333417674

[3] *Basic ^1H - ^{13}C-NMR spectroscopy* Metin Balei ISBN 0444518118

[4] In units of the nuclear magneton

[5] CRC Handbook of Chemistry and Physics 65Th Ed

[6] *A Short History of Three Chemical Shifts* Shin-ichi Nagaoka Vol. 84 No. 5 May **2007** Journal of Chemical Education 801

[7] http://www.chem.wisc.edu/areas/reich/handouts/nmr-h/hdata.htm

[8] http://www.bmrb.wisc.edu

[9] http://wwwchem.csustan.edu/Tutorials/NMRTABLE.HTM

[10] http://www.chem.wisc.edu/areas/reich/handouts/nmr-c13/cdata.htm

[11] http://www.chem.ucla.edu/~webspectra/

[12] http://drx.ch.huji.ac.il/nmr/whatisnmr/whatisnmr.html

[13] http://orgchem.colorado.edu/hndbksupport/spectprob/problems.html

[14] http://www.chem.uni-potsdam.de/tools/kombi1.htm

[15] http://www.nd.edu/~smithgrp/structure/workbook.html

[16] http://www.nd.edu/~smithgrp/structure/answers1-32.GIF

[17] http://www.nd.edu/~smithgrp/structure/answers33-64.GIF

Knight shift

The **Knight shift** is a shift in the nuclear magnetic resonance frequency of a paramagnetic substance first published in 1949 by the American physicist Walter David Knight.

The Knight shift is due to the conduction electrons in metals. They introduce an "extra" effective field at the nuclear site, due to the spin orientations of the conduction electrons in the presence of an external field. This is responsible for the shift observed in the nuclear magnetic resonance. The shift comes from two sources, one is the Pauli paramagnetic spin susceptibility, the other is the s-component wavefunctions at the nucleus.

Depending on the electronic structure, Knight shift may be temperature dependent. However, in metals which normally have a broad featureless electronic density of states, Knight shifts are temperature independent.

Robinson oscillator

The **Robinson oscillator** (or **Robinson marginal oscillator**) is an electronic circuit used in the field of Nuclear Magnetic Resonance (NMR). The oscillator forms the underlying basis of Magnetic Resonance Imaging (MRI) systems used in many hospitals. It was invented by the British physicist Neville Robinson.

References

- Deschamps, P., Vaissiére, J. and Sullivan, N. S., Integrated circuit Robinson oscillator for NMR detection [1], *Review of Scientific Instruments*, 48(6):664–668, June 1977. DOI 10.1063/1.1135103
- Wilson, K. J. and Vallabhan, C. P. G., An improved MOSFET-based Robinson oscillator for NMR detection [2], *Meas. Sci. Technol.*, 1(5):458-460, May 1990. DOI 10.1088/0957-0233/1/5/015

References

[1]   http://content.aip.org/RSINAK/v48/i6/664_1.html

[2]   http://www.iop.org/EJ/abstract/0957-0233/1/5/015

Fourier transform

In mathematics, the **Fourier transform** (often abbreviated **FT**) is an operation that transforms one complex-valued function of a real variable into another. In such applications as signal processing, the domain of the original function is typically time and is accordingly called the *time domain*. The domain of the new function is typically called the frequency domain, and the new function itself is called the *frequency domain representation* of the original function. It describes which frequencies are present in the original function. This is analogous to describing a musical chord in terms of the notes being played. In effect, the Fourier transform decomposes a function into oscillatory functions. The term Fourier transform refers both to the frequency domain representation of a function, and to the process or formula that "transforms" one function into the other.

The Fourier transform and its generalizations are the subject of Fourier analysis. In this specific case, both the time and frequency domains are unbounded linear continua. It is possible to define the Fourier transform of a function of several variables, which is important for instance in the physical study of wave motion and optics. It is also possible to generalize the Fourier transform on discrete structures such as finite groups, efficient computation of which through a fast Fourier transform is essential for high-speed computing.

Fourier transforms
Continuous Fourier transform
Fourier series
Discrete Fourier transform
Discrete-time Fourier transform
Related transforms

Definition

There are several common conventions for defining the Fourier transform of an integrable function $f : \mathbf{R} \to \mathbf{C}$ (Kaiser 1994). This article will use the definition:

$$\hat{f}(\xi) = \int_{-\infty}^{\infty} f(x)\ e^{-2\pi i x \xi}\ dx, \quad \text{for every real number } \xi.$$

When the independent variable x represents *time* (with SI unit of seconds), the transform variable ξ represents frequency (in hertz). Under suitable conditions, f can be reconstructed from $\hat{f}$ by the **inverse transform**:

$$f(x) = \int_{-\infty}^{\infty} \hat{f}(\xi)\ e^{2\pi i x \xi}\ d\xi, \quad \text{for every real number } x.$$

For other common conventions and notations, including using the angular frequency ω instead of the frequency ξ, see Other conventions and Other notations below. The Fourier transform on Euclidean space is treated separately, in which the variable x often represents position and ξ momentum.

Introduction

The motivation for the Fourier transform comes from the study of Fourier series. In the study of Fourier series, complicated periodic functions are written as the sum of simple waves mathematically represented by sines and cosines. Due to the properties of sine and cosine it is possible to recover the amount of each wave in the sum by an integral. In many cases it is desirable to use Euler's formula, which states that $e^{2\pi i \theta} = \cos 2\pi\theta + i \sin 2\pi\theta$, to write Fourier series in terms of the basic waves $e^{2\pi i \theta}$. This has the advantage of simplifying many of the formulas involved and providing a formulation for Fourier series that more closely resembles the definition followed in this article. This passage from sines and cosines to complex exponentials makes it necessary for the Fourier coefficients to be complex valued. The usual interpretation of this complex number is that it gives you both the amplitude (or size) of the wave present in the function and the phase (or the initial angle) of the wave. This passage also introduces the need for negative "frequencies". If θ were measured in seconds then the waves $e^{2\pi i \theta}$ and $e^{-2\pi i \theta}$ would both complete one cycle per second, but they represent different frequencies in the Fourier transform. Hence, frequency no longer measures the number of cycles per unit time, but is closely related.

We may use Fourier series to motivate the Fourier transform as follows. Suppose that f is a function which is zero outside of some interval $[-L/2, L/2]$. Then for any $T \geq L$ we may expand f in a Fourier series on the interval $[-T/2, T/2]$, where the "amount" (denoted by c_n) of the wave $e^{2\pi i n x/T}$ in the Fourier series of f is given by

$$\hat{f}(n/T) = c_n = \int_{-T/2}^{T/2} e^{-2\pi i n x/T} f(x)\ dx$$

and f should be given by the formula

$$f(x) = \frac{1}{T} \sum_{n=-\infty}^{\infty} \hat{f}(n/T) e^{2\pi i n x/T}.$$
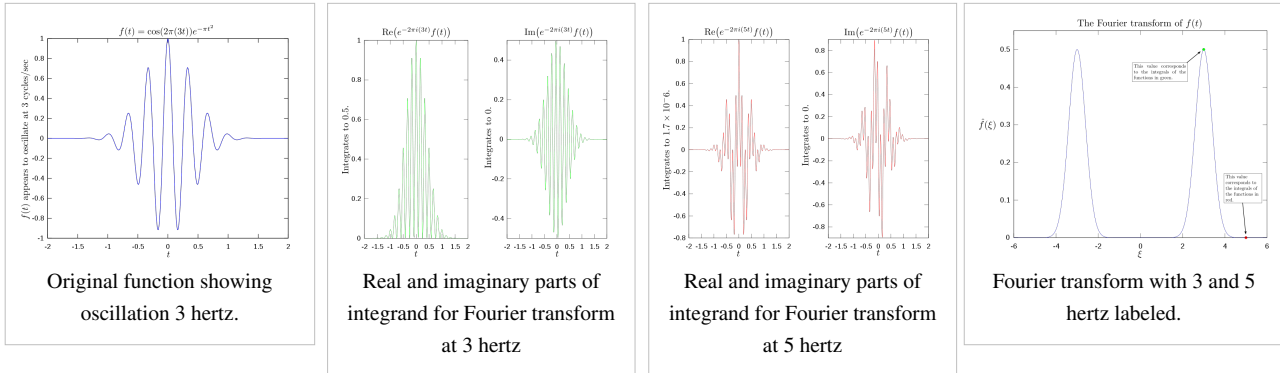
If we let $\xi_n = n/T$, and we let $\Delta\xi = (n + 1)/T - n/T = 1/T$, then this last sum becomes the Riemann sum

$$f(x) = \sum_{n=-\infty}^{\infty} \hat{f}(\xi_n) e^{2\pi i x \xi_n} \Delta\xi.$$

By letting $T \to \infty$ this Riemann sum converges to the integral for the inverse Fourier transform given in the Definition section. Under suitable conditions this argument may be made precise (Stein & Shakarchi 2003). Hence, as in the case of Fourier series, the Fourier transform can be thought of as a function that measures how much of each individual frequency is present in our function, and we can recombine these waves by using an integral (or "continuous sum") to reproduce the original function.

The following images provide a visual illustration of how the Fourier transform measures whether a frequency is present in a particular function. The function depicted $f(t) = \cos(6\pi t) e^{-\pi t^2}$ oscillates at 3 hertz (if t measures

seconds) and tends quickly to 0. This function was specially chosen to have a real Fourier transform which can easily be plotted. The first image contains its graph. In order to calculate $\hat{f}(3)$ we must integrate $e^{-2\pi i(3t)}f(t)$. The second image shows the plot of the real and imaginary parts of this function. The real part of the integrand is almost always positive, this is because when $f(t)$ is negative, then the real part of $e^{-2\pi i(3t)}$ is negative as well. Because they oscillate at the same rate, when $f(t)$ is positive, so is the real part of $e^{-2\pi i(3t)}$. The result is that when you integrate the real part of the integrand you get a relatively large number (in this case 0.5). On the other hand, when you try to measure a frequency that is not present, as in the case when we look at $\hat{f}(5)$, the integrand oscillates enough so that the integral is very small. The general situation may be a bit more complicated than this, but this in spirit is how the Fourier transform measures how much of an individual frequency is present in a function $f(t)$.

| Original function showing oscillation 3 hertz. | Real and imaginary parts of integrand for Fourier transform at 3 hertz | Real and imaginary parts of integrand for Fourier transform at 5 hertz | Fourier transform with 3 and 5 hertz labeled. |

Properties of the Fourier transform

An *integrable function* is a function f on the real line that is Lebesgue-measurable and satisfies

$$\int_{-\infty}^{\infty} |f(x)|\, dx < \infty.$$

Basic properties

Given integrable functions $f(x)$, $g(x)$, and $h(x)$ denote their Fourier transforms by $\hat{f}(\xi)$, $\hat{g}(\xi)$, and $\hat{h}(\xi)$ respectively. The Fourier transform has the following basic properties (Pinsky 2002).

Linearity

 For any complex numbers a and b, if $h(x) = af(x) + bg(x)$, then $\hat{h}(\xi) = a \cdot \hat{f}(\xi) + b \cdot \hat{g}(\xi)$.

Translation

 For any real number x_0, if $h(x) = f(x - x_0)$, then $\hat{h}(\xi) = e^{-2\pi i x_0 \xi}\hat{f}(\xi)$.

Modulation

 For any real number ξ_0, if $h(x) = e^{2\pi i x\xi_0}f(x)$, then $\hat{h}(\xi) = \hat{f}(\xi - \xi_0)$.

Scaling

 For a non-zero real number a, if $h(x) = f(ax)$, then $\hat{h}(\xi) = \dfrac{1}{|a|}\hat{f}\left(\dfrac{\xi}{a}\right)$. The case $a = -1$ leads to the

time-reversal property, which states: if $h(x) = f(-x)$, then $\hat{h}(\xi) = \hat{f}(-\xi)$.

Conjugation

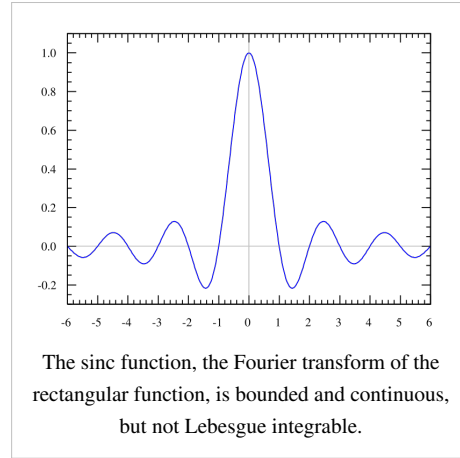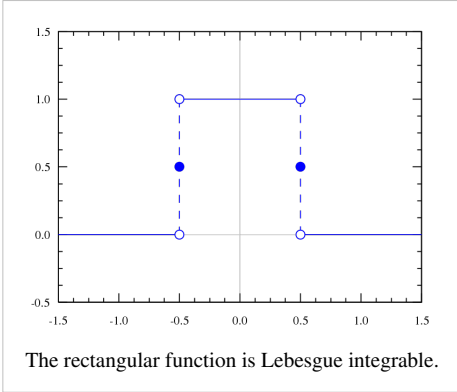 If $h(x) = \overline{f(x)}$, then $\hat{h}(\xi) = \overline{\hat{f}(-\xi)}$.

 In particular, if f is real, then one has the *reality condition* $\hat{f}(-\xi) = \overline{\hat{f}(\xi)}$.

 And if f is purely imaginary, then $\hat{f}(-\xi) = -\overline{\hat{f}(\xi)}$.

Convolution

If $h(x) = (f * g)(x)$, then $\hat{h}(\xi) = \hat{f}(\xi) \cdot \hat{g}(\xi)$.

Uniform continuity and the Riemann–Lebesgue lemma

The rectangular function is Lebesgue integrable.

The sinc function, the Fourier transform of the rectangular function, is bounded and continuous, but not Lebesgue integrable.

$$\hat{f}(\xi) \to 0 \text{ as } |\xi| \to \infty.$$

The Fourier transform $\hat{f}$ of an integrable function f is bounded and continuous, but need not be integrable − for example, the Fourier transform of the rectangular function, which is a step function (and hence integrable) is the sinc function, which is not Lebesgue integrable, though it does have an improper integral: one has an analog to the alternating harmonic series, which is a convergent sum but not absolutely convergent.

It is not possible in general to write the *inverse transform* as a Lebesgue integral. However, when both f and $\hat{f}$ are integrable, the following inverse equality holds true for almost every x:

$$f(x) = \int_{-\infty}^{\infty} \hat{f}(\xi) e^{2i\pi x\xi} \, d\xi.$$

Almost everywhere, f is equal to the continuous function given by the right-hand side. If f is given as continuous function on the line, then equality holds for every x.

A consequence of the preceding result is that the Fourier transform is injective on $L^1(\mathbf{R})$.

The Plancherel theorem and Parseval's theorem

Let $f(x)$ and $g(x)$ be integrable, and let $\hat{f}(\xi)$ and $\hat{g}(\xi)$ be their Fourier transforms. If $f(x)$ and $g(x)$ are also square-integrable, then we have Parseval's theorem (Rudin 1987, p. 187)**:**

$$\int_{-\infty}^{\infty} f(x)\overline{g(x)} \, dx = \int_{-\infty}^{\infty} \hat{f}(\xi)\overline{\hat{g}(\xi)} \, d\xi,$$

where the bar denotes complex conjugation.

The Plancherel theorem, which is equivalent to Parseval's theorem, states (Rudin 1987, p. 186)**:**

$$\int_{-\infty}^{\infty} |f(x)|^2 \, dx = \int_{-\infty}^{\infty} \left| \hat{f}(\xi) \right|^2 \, d\xi.$$

The Plancherel theorem makes it possible to define the Fourier transform for functions in $L^2(\mathbf{R})$, as described in Generalizations below. The Plancherel theorem has the interpretation in the sciences that the Fourier transform preserves the energy of the original quantity. It should be noted that depending on the author either of these theorems might be referred to as the Plancherel theorem or as Parseval's theorem.

See Pontryagin duality for a general formulation of this concept in the context of locally compact abelian groups.

Poisson summation formula

The Poisson summation formula provides a link between the study of Fourier transforms and Fourier Series. Given an integrable function f we can consider the periodization of f given by:

$$\bar{f}(x) = \sum_{k \in \mathbb{Z}} f(x + k),$$

where the summation is taken over the set of all integers k. The Poisson summation formula relates the Fourier series of $\bar{f}$ to the Fourier transform of f. Specifically it states that the Fourier series of $\bar{f}$ is given by:

$$\bar{f}(x) \sim \sum_{k \in \mathbb{Z}} \hat{f}(k) e^{2\pi i k x}.$$

Convolution theorem

The Fourier transform translates between convolution and multiplication of functions. If $f(x)$ and $g(x)$ are integrable functions with Fourier transforms $\hat{f}(\xi)$ and $\hat{g}(\xi)$ respectively, then the Fourier transform of the convolution is given by the product of the Fourier transforms $\hat{f}(\xi)$ and $\hat{g}(\xi)$ (under other conventions for the definition of the Fourier transform a constant factor may appear).
This means that if**:**

$$h(x) = (f * g)(x) = \int_{-\infty}^{\infty} f(y) g(x - y)\, dy,$$

where $*$ denotes the convolution operation, then**:**

$$\hat{h}(\xi) = \hat{f}(\xi) \cdot \hat{g}(\xi).$$

In linear time invariant (LTI) system theory, it is common to interpret $g(x)$ as the impulse response of an LTI system with input $f(x)$ and output $h(x)$, since substituting the unit impulse for $f(x)$ yields $h(x) = g(x)$. In this case, $\hat{g}(\xi)$ represents the frequency response of the system.

Conversely, if $f(x)$ can be decomposed as the product of two square integrable functions $p(x)$ and $q(x)$, then the Fourier transform of $f(x)$ is given by the convolution of the respective Fourier transforms $\hat{p}(\xi)$ and $\hat{q}(\xi)$.

Cross-correlation theorem

In an analogous manner, it can be shown that if $h(x)$ is the cross-correlation of $f(x)$ and $g(x)$:

$$h(x) = (f \star g)(x) = \int_{-\infty}^{\infty} \overline{f(y)}\, g(x + y)\, dy$$

then the Fourier transform of $h(x)$ is:

$$\hat{h}(\xi) = \overline{\hat{f}(\xi)}\, \hat{g}(\xi).$$

As a special case, the autocorrelation of function $f(x)$ is:

$$h(x) = (f \star f)(x) = \int_{-\infty}^{\infty} \overline{f(y)} f(x + y)\, dy$$

for which

$$\hat{h}(\xi) = \overline{\hat{f}(\xi)}\, \hat{f}(\xi) = |\hat{f}(\xi)|^2.$$

Eigenfunctions

One important choice of an orthonormal basis for $L^2(\mathbf{R})$ is given by the Hermite functions

$$\psi_n(x) = \frac{2^{1/4}}{\sqrt{n!}}\, e^{-\pi x^2} H_n(2x\sqrt{\pi}),$$

where $H_n(x)$ are the "probabilist's" Hermite polynomials, defined by $H_n(x) = (-1)^n \exp(x^2/2)\, \mathrm{D}^n \exp(-x^2/2)$. Under this convention for the Fourier transform, we have that

$$\hat{\psi}_n(\xi) = (-i)^n \psi_n(\xi).$$

In other words, the Hermite functions form a complete orthonormal system of eigenfunctions for the Fourier transform on $L^2(\mathbf{R})$ (Pinsky 2002). However, this choice of eigenfunctions is not unique. There are only four different eigenvalues of the Fourier transform (± 1 and $\pm i$) and any linear combination of eigenfunctions with the same eigenvalue gives another eigenfunction. As a consequence of this, it is possible to decompose $L^2(\mathbf{R})$ as a direct sum of four spaces H_0, H_1, H_2, and H_3 where the Fourier transform acts on H_k simply by multiplication by i^k. This approach to define the Fourier transform is due to N. Wiener (Duoandikoetxea 2001). The choice of Hermite functions is convenient because they are exponentially localized in both frequency and time domains, and thus give rise to the fractional Fourier transform used in time-frequency analysis (Boashash 2003).

Fourier transform on Euclidean space

The Fourier transform can be in any arbitrary number of dimensions n. As with the one-dimensional case there are many conventions, for an integrable function $f(x)$ this article takes the definition:

$$\hat{f}(\xi) = \mathcal{F}(f)(\xi) = \int_{\mathbb{R}^n} f(x) e^{-2\pi i x \cdot \xi}\, dx$$

where x and ξ are n-dimensional vectors, and $x \cdot \xi$ is the dot product of the vectors. The dot product is sometimes written as $\langle x, \xi \rangle$.

All of the basic properties listed above hold for the n-dimensional Fourier transform, as do Plancherel's and Parseval's theorem. When the function is integrable, the Fourier transform is still uniformly continuous and the Riemann–Lebesgue lemma holds. (Stein & Weiss 1971)

Uncertainty principle

Generally speaking, the more concentrated $f(x)$ is, the more spread out its Fourier transform $\hat{f}(\xi)$ must be. In particular, the scaling property of the Fourier transform may be seen as saying: if we "squeeze" a function in x, its Fourier transform "stretches out" in ξ. It is not possible to arbitrarily concentrate both a function and its Fourier transform.

The trade-off between the compaction of a function and its Fourier transform can be formalized in the form of an **Uncertainty Principle**, and is formalized by viewing a function and its Fourier transform as conjugate variables with respect to the symplectic form on the time–frequency domain: from the point of view of the linear canonical transformation, the Fourier transform is rotation by 90° in the time–frequency domain, and preserves the symplectic form.

Suppose $f(x)$ is an integrable and square-integrable function. Without loss of generality, assume that $f(x)$ is normalized:

$$\int_{-\infty}^{\infty} |f(x)|^2\, dx = 1.$$

It follows from the Plancherel theorem that $\hat{f}(\xi)$ is also normalized.

The spread around $x = 0$ may be measured by the *dispersion about zero* (Pinsky 2002) defined by

$$D_0(f) = \int_{-\infty}^{\infty} x^2 |f(x)|^2 \, dx.$$

In probability terms, this is the second moment of $|f(x)|^2$ about zero.

The Uncertainty principle states that, if $f(x)$ is absolutely continuous and the functions $x \cdot f(x)$ and $f'(x)$ are square integrable, then

$$D_0(f) D_0(\hat{f}) \geq \frac{1}{16\pi^2} \quad \text{(Pinsky 2002).}$$

The equality is attained only in the case $f(x) = C_1 \, e^{-\pi x^2/\sigma^2}$ (hence $\hat{f}(\xi) = \sigma C_1 \, e^{-\pi \sigma^2 \xi^2}$) where $\sigma > 0$ is arbitrary and C_1 is such that f is L^2–normalized (Pinsky 2002). In other words, where f is a (normalized) Gaussian function, centered at zero.

In fact, this inequality implies that:

$$\left(\int_{-\infty}^{\infty} (x - x_0)^2 |f(x)|^2 \, dx \right) \left(\int_{-\infty}^{\infty} (\xi - \xi_0)^2 |\hat{f}(\xi)|^2 \, d\xi \right) \geq \frac{1}{16\pi^2}$$

for any x_0, ξ_0 in **R** (Stein & Shakarchi 2003).

In quantum mechanics, the momentum and position wave functions are Fourier transform pairs, to within a factor of Planck's constant. With this constant properly taken into account, the inequality above becomes the statement of the Heisenberg uncertainty principle (Stein & Shakarchi 2003).

Spherical harmonics

Let the set of homogeneous harmonic polynomials of degree k on $\mathbf{R}^n$ be denoted by $\mathbf{A}_k$. The set $\mathbf{A}_k$ consists of the solid spherical harmonics of degree k. The solid spherical harmonics play a similar role in higher dimensions to the Hermite polynomials in dimension one. Specifically, if $f(x) = e^{-\pi |x|} 2P(x)$ for some $P(x)$ in $\mathbf{A}_k$, then $\hat{f}(\xi) = i^{-k} f(\xi)$. Let the set $\mathbf{H}_k$ be the closure in $L^2(\mathbf{R}^n)$ of linear combinations of functions of the form $f(|x|)P(x)$ where $P(x)$ is in $\mathbf{A}_k$. The space $L^2(\mathbf{R}^n)$ is then a direct sum of the spaces $\mathbf{H}_k$ and the Fourier transform maps each space $\mathbf{H}_k$ to itself and is possible to characterize the action of the Fourier transform on each space $\mathbf{H}_k$ (Stein & Weiss 1971). Let $f(x) = f_0(|x|)P(x)$ (with $P(x)$ in $\mathbf{A}_k$), then $\hat{f}(\xi) = F_0(|\xi|)P(\xi)$ where

$$F_0(r) = 2\pi i^{-k} r^{-(n+2k-2)/2} \int_0^{\infty} f_0(s) J_{(n+2k-2)/2}(2\pi r s) s^{(n+2k)/2} \, ds.$$

Here $J_{(n+2k-2)/2}$ denotes the Bessel function of the first kind with order $(n + 2k - 2)/2$. When $k = 0$ this gives a useful formula for the Fourier transform of a radial function (Grafakos 2004).

Restriction problems

In higher dimensions it becomes interesting to study *restriction problems* for the Fourier transform. The Fourier transform of an integrable function is continuous and the restriction of this function to any set is defined. But for a square-integrable function the Fourier transform could be a general *class* of square integrable functions. As such, the restriction of the Fourier transform of an $L^2(\mathbf{R}^n)$ function cannot be defined on sets of measure 0. It is still an active area of study to understand restriction problems in L^p for $1 < p < 2$. Surprisingly, it is possible in some cases to define the restriction of a Fourier transform to a set S, provided S has non-zero curvature. The case when S is the unit sphere in $\mathbf{R}^n$ is of particular interest. In this case the Tomas-Stein restriction theorem states that the restriction of the Fourier transform to the unit sphere in $\mathbf{R}^n$ is a bounded operator on L^p provided $1 \leq p \leq (2n + 2) / (n + 3)$.

One notable difference between the Fourier transform in 1 dimension versus higher dimensions concerns the partial sum operator. Consider an increasing collection of measurable sets E_R indexed by $R \in (0,\infty)$: such as balls of radius R centered at the origin, or cubes of side $2R$. For a given integrable function f, consider the function f_R defined by:

$$f_R(x) = \int_{E_R} \hat{f}(\xi) e^{2\pi i x \cdot \xi} \, d\xi, \quad x \in \mathbb{R}^n.$$

Suppose in addition that f is in $L^p(\mathbf{R}^n)$. For $n = 1$ and $1 < p < \infty$, if one takes $E_R = (-R, R)$, then f_R converges to f in L^p as R tends to infinity, by the boundedness of the Hilbert transform. Naively one may hope the same holds true for $n > 1$. In the case that E_R is taken to be a cube with side length R, then convergence still holds. Another natural candidate is the Euclidean ball $E_R = \{\xi : |\xi| < R\}$. In order for this partial sum operator to converge, it is necessary that the multiplier for the unit ball be bounded in $L^p(\mathbf{R}^n)$. For $n \geq 2$ it is a celebrated theorem of Charles Fefferman that the multiplier for the unit ball is never bounded unless $p = 2$ (Duoandikoetxea 2001). In fact, when $p \neq 2$, this shows that not only may f_R fail to converge to f in L^p, but for some functions $f \in L^p(\mathbf{R}^n)$, f_R is not even an element of L^p.

Generalizations

Fourier transform on other function spaces

It is possible to extend the definition of the Fourier transform to other spaces of functions. Since compactly supported smooth functions are integrable and dense in $L^2(\mathbf{R})$, the Plancherel theorem allows us to extend the definition of the Fourier transform to general functions in $L^2(\mathbf{R})$ by continuity arguments. Further $\mathcal{F} : L^2(\mathbf{R}) \to L^2(\mathbf{R})$ is a unitary operator (Stein & Weiss 1971, Thm. 2.3). Many of the properties remain the same for the Fourier transform. The Hausdorff–Young inequality can be used to extend the definition of the Fourier transform to include functions in $L^p(\mathbf{R})$ for $1 \leq p \leq 2$. Unfortunately, further extensions become more technical. The Fourier transform of functions in L^p for the range $2 < p < \infty$ requires the study of distributions (Katznelson 1976). In fact, it can be shown that there are functions in L^p with $p>2$ so that the Fourier transform is not defined as a function (Stein & Weiss 1971).

Fourier–Stieltjes transform

The Fourier transform of a finite Borel measure μ on $\mathbf{R}^n$ is given by (Pinsky 2002):

$$\hat{\mu}(\xi) = \int_{\mathbb{R}^n} \mathrm{e}^{-2\pi i x \cdot \xi} \, d\mu.$$

This transform continues to enjoy many of the properties of the Fourier transform of integrable functions. One notable difference is that the Riemann–Lebesgue lemma fails for measures (Katznelson 1976). In the case that $d\mu = f(x) \, dx$, then the formula above reduces to the usual definition for the Fourier transform of f. In the case that μ is the probability distribution associated to a random variable X, the Fourier-Stieltjes transform is closely related to the characteristic function, but the typical conventions in probability theory take $e^{ix \cdot \xi}$ instead of $e^{-2\pi i x \cdot \xi}$ (Pinsky 2002). In the case when the distribution has a probability density function this definition reduces to the Fourier transform applied to the probability density function, again with a different choice of constants.

The Fourier transform may be used to give a characterization of continuous measures. Bochner's theorem characterizes which functions may arise as the Fourier–Stieltjes transform of a measure (Katznelson 1976).

Furthermore, the Dirac delta function is not a function but it is a finite Borel measure. Its Fourier transform is a constant function (whose specific value depends upon the form of the Fourier transform used).

Tempered distributions

The Fourier transform maps the space of Schwartz functions to itself, and gives a homeomorphism of the space to itself (Stein & Weiss 1971). Because of this it is possible to define the Fourier transform of tempered distributions. These include all the integrable functions mentioned above and have the added advantage that the Fourier transform of any tempered distribution is again a tempered distribution.

The following two facts provide some motivation for the definition of the Fourier transform of a distribution. First let f and g be integrable functions, and let $\hat{f}$ and $\hat{g}$ be their Fourier transforms respectively. Then the Fourier transform obeys the following multiplication formula (Stein & Weiss 1971),

$$\int_{\mathbb{R}^n} \hat{f}(x)g(x)\,dx = \int_{\mathbb{R}^n} f(x)\hat{g}(x)\,dx.$$

Secondly, every integrable function f defines a distribution T_f by the relation

$$T_f(\varphi) = \int_{\mathbb{R}^n} f(x)\varphi(x)\,dx \quad \text{for all Schwartz functions } \varphi.$$

In fact, given a distribution T, we define the Fourier transform by the relation

$$\hat{T}(\varphi) = T(\hat{\varphi}) \quad \text{for all Schwartz functions } \varphi.$$

It follows that

$$\hat{T}_f = T_{\hat{f}}.$$

Distributions can be differentiated and the above mentioned compatibility of the Fourier transform with differentiation and convolution remains true for tempered distributions.

Locally compact abelian groups

The Fourier transform may be generalized to any locally compact abelian group. A locally compact abelian group is an abelian group which is at the same time a locally compact Hausdorff topological space so that the group operations are continuous. If G is a locally compact abelian group, it has a translation invariant measure μ, called Haar measure. For a locally compact abelian group G it is possible to place a topology on the set of characters $\hat{G}$ so that $\hat{G}$ is also a locally compact abelian group. For a function f in $L^1(G)$ it is possible to define the Fourier transform by (Katznelson 1976):

$$\hat{f}(\xi) = \int_G \xi(x)f(x)\,d\mu \qquad \text{for any } \xi \in \hat{G}.$$

Locally compact Hausdorff space

The Fourier transform may be generalized to any locally compact Hausdorff space, which recovers the topology but loses the group structure.

Given a locally compact Hausdorff topological space X, the space $A=C_0(X)$ of continuous complex-valued functions on X which vanish at infinity is in a natural way a commutative C*-algebra, via pointwise addition, multiplication, complex conjugation, and with norm as the uniform norm. Conversely, the characters of this algebra A, denoted Φ_A, are naturally a topological space, and can be identified with evaluation at a point of x, and one has an isometric isomorphism $C_0(X) \to C_0(\Phi_A)$. In the case where $X=\mathbf{R}$ is the real line, this is exactly the Fourier transform.

Non-abelian groups

The Fourier transform can also be defined for functions on a non-abelian group, provided that the group is compact. Unlike the Fourier transform on an abelian group, which is scalar-valued, the Fourier transform on a non-abelian group is operator-valued (Hewitt & Ross 1971, Chapter 8). The Fourier transform on compact groups is a major tool in representation theory (Knapp 2001) and non-commutative harmonic analysis.

Let G be a compact Hausdorff topological group. Let Σ denote the collection of all isomorphism classes of finite-dimensional irreducible unitary representations, along with a definite choice of representation $U^{(\sigma)}$ on the Hilbert space H_σ of finite dimension d_σ for each $\sigma \in \Sigma$. If μ is a finite Borel measure on G, then the Fourier–Stieltjes transform of μ is the operator on H_σ defined by

$$\langle \hat{\mu}\xi, \eta \rangle_{H_\sigma} = \int_G \langle \overline{U}_g^{(\sigma)}\xi, \eta \rangle \, d\mu(g)$$

where $\overline{U}^{(\sigma)}$ is the complex-conjugate representation of $U^{(\sigma)}$ acting on H_σ. As in the abelian case, if μ is absolutely continuous with respect to the left-invariant probability measure λ on G, then it is represented as

$$d\mu = f \, d\lambda$$

for some $f \in L^1(\lambda)$. In this case, one identifies the Fourier transform of f with the Fourier–Stieltjes transform of μ.

The mapping $\mu \mapsto \hat{\mu}$ defines an isomorphism between the Banach space $M(G)$ of finite Borel measures (see rca space) and a closed subspace of the Banach space $\mathbf{C}_\infty(\Sigma)$ consisting of all sequences $E = (E_\sigma)$ indexed by Σ of (bounded) linear operators $E_\sigma : H_\sigma \to H_\sigma$ for which the norm

$$\|E\| = \sup_{\sigma \in \Sigma} \|E_\sigma\|$$

is finite. The "convolution theorem" asserts that, furthermore, this isomorphism of Banach spaces is in fact an isomorphism of C* algebras into a subspace of $\mathbf{C}_\infty(\Sigma)$, in which $M(G)$ is equipped with the product given by convolution of measures and $\mathbf{C}_\infty(\Sigma)$ the product given by multiplication of operators in each index σ.

The Peter-Weyl theorem holds, and a version of the Fourier inversion formula (Plancherel's theorem) follows: if $f \in L^2(G)$, then

$$f(g) = \sum_{\sigma \in \Sigma} d_\sigma \mathrm{tr}(\hat{f}(\sigma) U_g^{(\sigma)})$$

where the summation is understood as convergent in the L^2 sense.

The generalization of the Fourier transform to the noncommutative situation has also in part contributed to the development of noncommutative geometry. In this context, a categorical generalization of the Fourier transform to noncommutative groups is Tannaka-Krein duality, which replaces the group of characters with the category of representations. However, this loses the connection with harmonic functions.

Alternatives

In signal processing terms, a function (of time) is a representation of a signal with perfect *time resolution,* but no frequency information, while the Fourier transform has perfect *frequency resolution,* but no time information: the magnitude of the Fourier transform at a point is how much frequency content there is, but location is only given by phase (argument of the Fourier transform at a point), and standing waves are not localized in time – a sine wave continues out to infinity, without decaying. This limits the usefulness of the Fourier transform for analyzing signals that are localized in time, notably transients, or any signal of finite extent.

As alternatives to the Fourier transform, in time-frequency analysis, one uses time-frequency transforms or time-frequency distributions to represent signals in a form that has some time information and some frequency information – by the uncertainty principle, there is a trade-off between these. These can be generalizations of the Fourier transform, such as the short-time Fourier transform or fractional Fourier transform, or can use different functions to represent signals, as in wavelet transforms and chirplet transforms, with the wavelet analog of the

(continuous) Fourier transform being the continuous wavelet transform. (Boashash 2003).

Applications

Analysis of differential equations

Fourier transforms and the closely related Laplace transforms are widely used in solving differential equations. The Fourier transform is compatible with differentiation in the following sense: if $f(x)$ is a differentiable function with Fourier transform $\hat{f}(\xi)$, then the Fourier transform of its derivative is given by $2\pi i \xi \hat{f}(\xi)$. This can be used to transform differential equations into algebraic equations. Note that this technique only applies to problems whose domain is the whole set of real numbers. By extending the Fourier transform to functions of several variables partial differential equations with domain $\mathbf{R}^n$ can also be translated into algebraic equations.

FT-NMR, FT-IR, FT-NIR and MRI

The Fourier transform is also used in nuclear magnetic resonance (NMR) and in other kinds of spectroscopy, e.g. infrared (FT-IR). In NMR an exponentially-shaped free induction decay (FID) signal is acquired in the time domain and Fourier-transformed to a Lorentzian line-shape in the frequency domain. The Fourier transform is also used in magnetic resonance imaging (MRI) and mass spectrometry.

Domain and range of the Fourier transform

It is often desirable to have the most general domain for the Fourier transform as possible. The definition of Fourier transform as an integral naturally restricts the domain to the space of integrable functions. Unfortunately, there is no simple characterizations of which functions are Fourier transforms of integrable functions (Stein & Weiss 1971). It is possible to extend the domain of the Fourier transform in various ways, as discussed in generalizations above. The following list details some of the more common domains and ranges on which the Fourier transform is defined.

- The space of Schwartz functions is closed under the Fourier transform. Schwartz functions are rapidly decaying functions and do not include all functions which are relevant for the Fourier transform. More details may be found in (Stein & Weiss 1971).

- The space L^p maps into the space L^q, where $1/p + 1/q = 1$ and $1 \leq p \leq 2$ (Hausdorff−Young inequality).

- In particular, the space L^2 is closed under the Fourier transform, but here the Fourier transform is no longer defined by integration.

- The space L^1 of Lebesgue integrable functions maps into C_0, the space of continuous functions that tend to zero at infinity − not just into the space L^∞ of bounded functions (the Riemann−Lebesgue lemma).

- The set of tempered distributions is closed under the Fourier transform. Tempered distributions are also a form of generalization of functions. It is in this generality that one can define the Fourier transform of objects like the Dirac comb.

Other notations

Other common notations for $\hat{f}(\xi)$ are: $\tilde{f}(\xi)$, $F(\xi)$, $\mathcal{F}(f)(\xi)$, $(\mathcal{F}f)(\xi)$, $\mathcal{F}(f)$, $\mathcal{F}(\omega)$, $\mathcal{F}(j\omega)$, $\mathcal{F}\{f\}$ and $\mathcal{F}(f(t))$. Though less commonly other notations are used. Denoting the Fourier transform by a capital letter corresponding to the letter of function being transformed (such as $f(x)$ and $F(\xi)$) is especially common in the sciences and engineering. In electronics, the omega (ω) is often used instead of ξ due to its interpretation as angular frequency, sometimes it is written as $F(j\omega)$, where j is the imaginary unit, to indicate its relationship with the Laplace transform, and sometimes it is written informally as $F(2\pi f)$ in order to use ordinary frequency.

The interpretation of the complex function $\hat{f}(\xi)$ may be aided by expressing it in polar coordinate form:
$\hat{f}(\xi) = A(\xi)e^{i\varphi(\xi)}$ in terms of the two real functions $A(\xi)$ and $\varphi(\xi)$ where:

$$A(\xi) = |\hat{f}(\xi)|,$$

is the amplitude and

$$\varphi(\xi) = \arg\left(\hat{f}(\xi)\right),$$

is the phase (see arg function).

Then the inverse transform can be written:

$$f(x) = \int_{-\infty}^{\infty} A(\xi)\ e^{i(2\pi\xi x + \varphi(\xi))}\ d\xi,$$

which is a recombination of all the **frequency components** of *f(x)*. Each component is a complex sinusoid of the form $e^{2\pi i x\xi}$ whose amplitude is *A(ξ)* and whose initial phase angle (at *x* = 0) is *φ(ξ)*.

The Fourier transform may be thought of as a mapping on function spaces. This mapping is here denoted $\mathcal{F}$ and $\mathcal{F}(f)$ is used to denote the Fourier transform of the function *f*. This mapping is linear, which means that $\mathcal{F}$ can also be seen as a linear transformation on the function space and implies that the standard notation in linear algebra of applying a linear transformation to a vector (here the function *f*) can be used to write $\mathcal{F}f$ instead of $\mathcal{F}(f)$. Since the result of applying the Fourier transform is again a function, we can be interested in the value of this function evaluated at the value ξ for its variable, and this is denoted either as $\mathcal{F}(f)(\xi)$ or as $(\mathcal{F}f)(\xi)$. Notice that in the former case, it is implicitly understood that $\mathcal{F}$ is applied first to *f* and then the resulting function is evaluated at ξ, not the other way around.

In mathematics and various applied sciences it is often necessary to distinguish between a function *f* and the value of *f* when its variable equals *x*, denoted *f(x)*. This means that a notation like $\mathcal{F}(f(x))$ formally can be interpreted as the Fourier transform of the values of *f* at *x*. Despite this flaw, the previous notation appears frequently, often when a particular function or a function of a particular variable is to be transformed. For example, $\mathcal{F}(\text{rect}(x)) = \text{sinc}(\xi)$ is sometimes used to express that the Fourier transform of a rectangular function is a sinc function, or $\mathcal{F}(f(x + x_0)) = \mathcal{F}(f(x))e^{2\pi i\xi x_0}$ is used to express the shift property of the Fourier transform. Notice, that the last example is only correct under the assumption that the transformed function is a function of *x*, not of x_0.

Other conventions

There are three common conventions for defining the Fourier transform. The Fourier transform is often written in terms of angular frequency: $\omega = 2\pi\xi$ whose units are radians per second.

The substitution ξ = ω/(2π) into the formulas above produces this convention:

$$\hat{f}(\omega) = \int_{\mathbb{R}^n} f(x)e^{-i\omega\cdot x}\ dx.$$

Under this convention, the inverse transform becomes:

$$f(x) = \frac{1}{(2\pi)^n}\int_{\mathbb{R}^n} \hat{f}(\omega)e^{i\omega\cdot x}\ d\omega.$$

Unlike the convention followed in this article, when the Fourier transform is defined this way, it is no longer a unitary transformation on $L^2(\mathbf{R}^n)$. There is also less symmetry between the formulas for the Fourier transform and its inverse.

Another popular convention is to split the factor of $(2\pi)^n$ evenly between the Fourier transform and its inverse, which leads to definitions:

$$\hat{f}(\omega) = \frac{1}{(2\pi)^{n/2}}\int_{\mathbb{R}^n} f(x)e^{-i\omega\cdot x}\ dx$$

$$f(x) = \frac{1}{(2\pi)^{n/2}} \int_{\mathbb{R}^n} \hat{f}(\omega) e^{i\omega \cdot x} \, d\omega.$$

Under this convention, the Fourier transform is again a unitary transformation on $L^2(\mathbf{R}^n)$. It also restores the symmetry between the Fourier transform and its inverse.

Variations of all three conventions can be created by conjugating the complex-exponential kernel of both the forward and the reverse transform. The signs must be opposites. Other than that, the choice is (again) a matter of convention.

Summary of popular forms of the Fourier transform

ordinary frequency ξ (hertz)	unitary	$\hat{f}_1(\xi) \stackrel{\text{def}}{=} \int_{\mathbb{R}^n} f(x) e^{-2\pi i x \cdot \xi} \, dx = \hat{f}_2(2\pi\xi) = (2\pi)^{n/2} \hat{f}_3(2\pi\xi)$ $f(x) = \int_{\mathbb{R}^n} \hat{f}_1(\xi) e^{2\pi i x \cdot \xi} \, d\xi$
angular frequency ω (rad/s)	non-unitary	$\hat{f}_2(\omega) \stackrel{\text{def}}{=} \int_{\mathbb{R}^n} f(x) e^{-i\omega \cdot x} \, dx = \hat{f}_1\left(\frac{\omega}{2\pi}\right) = (2\pi)^{n/2} \hat{f}_3(\omega)$ $f(x) = \frac{1}{(2\pi)^n} \int_{\mathbb{R}^n} \hat{f}_2(\omega) e^{i\omega \cdot x} \, d\omega$
	unitary	$\hat{f}_3(\omega) \stackrel{\text{def}}{=} \frac{1}{(2\pi)^{n/2}} \int_{\mathbb{R}^n} f(x) \ e^{-i\omega \cdot x} \, dx = \frac{1}{(2\pi)^{n/2}} \hat{f}_1\left(\frac{\omega}{2\pi}\right) = \frac{1}{(2\pi)^{n/2}} \hat{f}_2(\omega)$ $f(x) = \frac{1}{(2\pi)^{n/2}} \int_{\mathbb{R}^n} \hat{f}_3(\omega) e^{i\omega \cdot x} \, d\omega$

The ordinary-frequency convention (which is used in this article) is the one most often found in the mathematics literature. In the physics literature, the two angular-frequency conventions are more commonly used.

As discussed above, the characteristic function of a random variable is the same as the Fourier–Stieltjes transform of its distribution measure, but in this context it is typical to take a different convention for the constants. Typically characteristic function is defined $E\left(e^{it \cdot X}\right) = \int e^{it \cdot x} d\mu_X(x)$. As in the case of the "non-unitary angular frequency" convention above, there is no factor of 2π appearing in either of the integral, or in the exponential. Unlike any of the conventions appearing above, this convention takes the opposite sign in the exponential.

Tables of important Fourier transforms

The following tables record some closed form Fourier transforms. For functions $f(x)$, $g(x)$ and $h(x)$ denote their Fourier transforms by $\hat{f}$, $\hat{g}$, and $\hat{h}$ respectively. Only the three most common conventions are included. It is sometimes useful to notice that entry 105 gives a relationship between the Fourier transform of a function and the original function, which can be seen as relating the Fourier transform and its inverse.

Functional relationships

The Fourier transforms in this table may be found in (Erdélyi 1954) or the appendix of (Kammler 2000).

	Function	Fourier transform unitary, ordinary frequency	Fourier transform unitary, angular frequency	Fourier transform non-unitary, angular frequency	Remarks
	$f(x)$	$\hat{f}(\xi) = \int_{-\infty}^{\infty} f(x)e^{-2\pi i x\xi}\, dx$	$\hat{f}(\omega) = \dfrac{1}{\sqrt{2\pi}} \int_{-\infty}^{\infty} f(x)e^{-i\omega x}\, dx$	$\hat{f}(\nu) = \int_{-\infty}^{\infty} f(x)e^{-i\nu x}\, dx$	Definition
101	$a \cdot f(x) + b \cdot g(x)$	$a \cdot \hat{f}(\xi) + b \cdot \hat{g}(\xi)$	$a \cdot \hat{f}(\omega) + b \cdot \hat{g}(\omega)$	$a \cdot \hat{f}(\nu) + b \cdot \hat{g}(\nu)$	Linearity
102	$f(x - a)$	$e^{-2\pi i a\xi} \hat{f}(\xi)$	$e^{-ia\omega} \hat{f}(\omega)$	$e^{-ia\nu} \hat{f}(\nu)$	Shift in time domain
103	$e^{2\pi i ax} f(x)$	$\hat{f}(\xi - a)$	$\hat{f}(\omega - 2\pi a)$	$\hat{f}(\nu - 2\pi a)$	Shift in frequency domain, dual of 102
104	$f(ax)$	$\dfrac{1}{\lvert a\rvert}\hat{f}\left(\dfrac{\xi}{a}\right)$	$\dfrac{1}{\lvert a\rvert}\hat{f}\left(\dfrac{\omega}{a}\right)$	$\dfrac{1}{\lvert a\rvert}\hat{f}\left(\dfrac{\nu}{a}\right)$	Scaling in the time domain. If $\lvert a\rvert$ is large, then $f(ax)$ is concentrated around 0 and $\dfrac{1}{\lvert a\rvert}\hat{f}\left(\dfrac{\omega}{a}\right)$ spreads out and flattens.
105	$\hat{f}(x)$	$f(-\xi)$	$f(-\omega)$	$2\pi f(-\nu)$	Duality. Here $\hat{f}$ needs to be calculated using the same method as Fourier transform column. Results from swapping "dummy" variables of x and ξ or ω or ν.
106	$\dfrac{d^n f(x)}{dx^n}$	$(2\pi i\xi)^n \hat{f}(\xi)$	$(i\omega)^n \hat{f}(\omega)$	$(i\nu)^n \hat{f}(\nu)$	
107	$x^n f(x)$	$\left(\dfrac{i}{2\pi}\right)^n \dfrac{d^n \hat{f}(\xi)}{d\xi^n}$	$i^n \dfrac{d^n \hat{f}(\omega)}{d\omega^n}$	$i^n \dfrac{d^n \hat{f}(\nu)}{d\nu^n}$	This is the dual of 106

108	$(f*g)(x)$	$\hat{f}(\xi)\hat{g}(\xi)$	$\sqrt{2\pi}\,\hat{f}(\omega)\hat{g}(\omega)$	$\hat{f}(\nu)\hat{g}(\nu)$	The notation $f*g$ denotes the convolution of f and g — this rule is the convolution theorem
109	$f(x)g(x)$	$(\hat{f}*\hat{g})(\xi)$	$\dfrac{(\hat{f}*\hat{g})(\omega)}{\sqrt{2\pi}}$	$\dfrac{1}{2\pi}(\hat{f}*\hat{g})(\nu)$	This is the dual of 108
110	For $f(x)$ a purely real	$\hat{f}(-\xi)=\overline{\hat{f}(\xi)}$	$\hat{f}(-\omega)=\overline{\hat{f}(\omega)}$	$\hat{f}(-\nu)=\overline{\hat{f}(\nu)}$	Hermitian symmetry. $\overline{z}$ indicates the complex conjugate.
111	For $f(x)$ a purely real even function	$\hat{f}(\omega)$, $\hat{f}(\xi)$ and $\hat{f}(\nu)$ are purely real even functions.			
112	For $f(x)$ a purely real odd function	$\hat{f}(\omega)$, $\hat{f}(\xi)$ and $\hat{f}(\nu)$ are purely imaginary odd functions.			

Square-integrable functions

The Fourier transforms in this table may be found in (Campbell & Foster 1948), (Erdélyi 1954), or the appendix of (Kammler 2000).

	Function	Fourier transform unitary, ordinary frequency	Fourier transform unitary, angular frequency	Fourier transform non-unitary, angular frequency	Remarks
	$f(x)$	$\hat{f}(\xi)=\int_{-\infty}^{\infty}f(x)e^{-2\pi ix\xi}\,dx$	$\hat{f}(\omega)=\dfrac{1}{\sqrt{2\pi}}\int_{-\infty}^{\infty}f(x)e^{-i\omega x}\,dx$	$\hat{f}(\nu)=\int_{-\infty}^{\infty}f(x)e^{-i\nu x}\,dx$	
201	$\mathrm{rect}(ax)$	$\dfrac{1}{|a|}\cdot\mathrm{sinc}\left(\dfrac{\xi}{a}\right)$	$\dfrac{1}{\sqrt{2\pi a^2}}\cdot\mathrm{sinc}\left(\dfrac{\omega}{2\pi a}\right)$	$\dfrac{1}{|a|}\cdot\mathrm{sinc}\left(\dfrac{\nu}{2\pi a}\right)$	The rectangular pulse and the *normalized* sinc function, here defined as sinc(x) = sin(πx)/(πx)
202	$\mathrm{sinc}(ax)$	$\dfrac{1}{|a|}\cdot\mathrm{rect}\left(\dfrac{\xi}{a}\right)$	$\dfrac{1}{\sqrt{2\pi a^2}}\cdot\mathrm{rect}\left(\dfrac{\omega}{2\pi a}\right)$	$\dfrac{1}{|a|}\cdot\mathrm{rect}\left(\dfrac{\nu}{2\pi a}\right)$	Dual of rule 201. The rectangular function is an ideal low-pass filter, and the sinc function is the non-causal impulse response of such a filter.

203	$\operatorname{sinc}^2(ax)$	$\dfrac{1}{\lvert a\rvert}\cdot\operatorname{tri}\left(\dfrac{\xi}{a}\right)$	$\dfrac{1}{\sqrt{2\pi a^2}}\cdot\operatorname{tri}\left(\dfrac{\omega}{2\pi a}\right)$	$\dfrac{1}{\lvert a\rvert}\cdot\operatorname{tri}\left(\dfrac{\nu}{2\pi a}\right)$	The function tri(x) is the triangular function
204	$\operatorname{tri}(ax)$	$\dfrac{1}{\lvert a\rvert}\cdot\operatorname{sinc}^2\left(\dfrac{\xi}{a}\right)$	$\dfrac{1}{\sqrt{2\pi a^2}}\cdot\operatorname{sinc}^2\left(\dfrac{\omega}{2\pi a}\right)$	$\dfrac{1}{\lvert a\rvert}\cdot\operatorname{sinc}^2\left(\dfrac{\nu}{2\pi a}\right)$	Dual of rule 203.
205	$e^{-ax}u(x)$	$\dfrac{1}{a+2\pi i\xi}$	$\dfrac{1}{\sqrt{2\pi}(a+i\omega)}$	$\dfrac{1}{a+i\nu}$	The function $u(x)$ is the Heaviside unit step function and $a>0$.
206	$e^{-\alpha x^2}$	$\sqrt{\dfrac{\pi}{\alpha}}\cdot e^{-\frac{(\pi\xi)^2}{\alpha}}$	$\dfrac{1}{\sqrt{2\alpha}}\cdot e^{-\frac{\omega^2}{4\alpha}}$	$\sqrt{\dfrac{\pi}{\alpha}}\cdot e^{-\frac{\nu^2}{4\alpha}}$	This shows that, for the unitary Fourier transforms, the Gaussian function exp($-\alpha x^2$) is its own Fourier transform for some choice of α. For this to be integrable we must have Re(α)>0.
207	$e^{-a\lvert x\rvert}$	$\dfrac{2a}{a^2+4\pi^2\xi^2}$	$\sqrt{\dfrac{2}{\pi}}\cdot\dfrac{a}{a^2+\omega^2}$	$\dfrac{2a}{a^2+\nu^2}$	For $a>0$. That is, the Fourier transform of a decaying exponential function is a Lorentzian function.
208	$\dfrac{J_n(x)}{x}$	$\dfrac{2i}{n}(-i)^n\cdot U_{n-1}(2\pi\xi)$ $\cdot\sqrt{1-4\pi^2\xi^2}\operatorname{rect}(\pi\xi)$	$\sqrt{\dfrac{2}{\pi}}\dfrac{i}{n}(-i)^n\cdot U_{n-1}(\omega)$ $\cdot\sqrt{1-\omega^2}\operatorname{rect}\left(\dfrac{\omega}{2}\right)$	$\dfrac{2i}{n}(-i)^n\cdot U_{n-1}(\nu)$ $\cdot\sqrt{1-\nu^2}\operatorname{rect}\left(\dfrac{\nu}{2}\right)$	The functions $J_n(x)$ are the n-th order Bessel functions of the first kind. The functions $U_n(x)$ are the Chebyshev polynomial of the second kind. See 315 and 316 below.
209	$\operatorname{sech}(ax)$	$\dfrac{\pi}{a}\operatorname{sech}\left(\dfrac{\pi^2}{a}\xi\right)$	$\dfrac{1}{a}\sqrt{\dfrac{\pi}{2}}\operatorname{sech}\left(\dfrac{\pi}{2a}\omega\right)$	$\dfrac{\pi}{a}\operatorname{sech}\left(\dfrac{\pi}{2a}\nu\right)$	Hyperbolic secant is its own Fourier transform

Distributions

The Fourier transforms in this table may be found in (Erdélyi 1954) or the appendix of (Kammler 2000).

Function	Fourier transform unitary, ordinary frequency	Fourier transform unitary, angular frequency	Fourier transform non-unitary, angular frequency	Remarks
$f(x)$	$\hat{f}(\xi) =$ $\int_{-\infty}^{\infty} f(x)e^{-2\pi i x\xi}\,dx$	$\hat{f}(\omega) =$ $\frac{1}{\sqrt{2\pi}}\int_{-\infty}^{\infty} f(x)e^{-i\omega x}\,dx$	$\hat{f}(\nu) =$ $\int_{-\infty}^{\infty} f(x)e^{-i\nu x}\,dx$	
1	$\delta(\xi)$	$\sqrt{2\pi}\cdot\delta(\omega)$	$2\pi\delta(\nu)$	The distribution $\delta(\xi)$ denotes the Dirac delta function.
$\delta(x)$	1	$\frac{1}{\sqrt{2\pi}}$	1	Dual of rule 301.
e^{iax}	$\delta\left(\xi - \frac{a}{2\pi}\right)$	$\sqrt{2\pi}\cdot\delta(\omega - a)$	$2\pi\delta(\nu - a)$	This follows from 103 and 301.
$\cos(ax)$	$\dfrac{\delta\left(\xi - \frac{a}{2\pi}\right) + \delta\left(\xi + \frac{a}{2\pi}\right)}{2}$	$\sqrt{2\pi}\cdot\dfrac{\delta(\omega - a) + \delta(\omega + a)}{2}$	$\pi\left(\delta(\nu - a) + \delta(\nu + a)\right)$	This follows from rules 101 and 303 using Euler's formula: $\cos(ax) = (e^{iax} + e^{-iax})/2.$
$\sin(ax)$	$i\cdot\dfrac{\delta\left(\xi + \frac{a}{2\pi}\right) - \delta\left(\xi - \frac{a}{2\pi}\right)}{2}$	$i\sqrt{2\pi}\cdot\dfrac{\delta(\omega + a) - \delta(\omega - a)}{2}$	$i\pi\left(\delta(\nu + a) - \delta(\nu - a)\right)$	This follows from 101 and 303 using $\sin(ax) = (e^{iax} - e^{-iax})/(2i).$
$\cos(ax^2)$	$\sqrt{\dfrac{\pi}{a}}\cos\left(\dfrac{\pi^2\xi^2}{a} - \dfrac{\pi}{4}\right)$	$\dfrac{1}{\sqrt{2a}}\cos\left(\dfrac{\omega^2}{4a} - \dfrac{\pi}{4}\right)$	$\sqrt{\dfrac{\pi}{a}}\cos\left(\dfrac{\nu^2}{4a} - \dfrac{\pi}{4}\right)$	
$\sin(ax^2)$	$-\sqrt{\dfrac{\pi}{a}}\sin\left(\dfrac{\pi^2\xi^2}{a} - \dfrac{\pi}{4}\right)$	$\dfrac{-1}{\sqrt{2a}}\sin\left(\dfrac{\omega^2}{4a} - \dfrac{\pi}{4}\right)$	$-\sqrt{\dfrac{\pi}{a}}\sin\left(\dfrac{\nu^2}{4a} - \dfrac{\pi}{4}\right)$	
x^n	$\left(\dfrac{i}{2\pi}\right)^n \delta^{(n)}(\xi)$	$i^n\sqrt{2\pi}\delta^{(n)}(\omega)$	$2\pi i^n \delta^{(n)}(\nu)$	Here, n is a natural number and $\delta^{(n)}(\xi)$ is the n-th distribution derivative of the Dirac delta function. This rule follows from rules 107 and 301. Combining this rule with 101, we can transform all polynomials.
$\dfrac{1}{x}$	$-i\pi\,\mathrm{sgn}(\xi)$	$-i\sqrt{\dfrac{\pi}{2}}\,\mathrm{sgn}(\omega)$	$-i\pi\,\mathrm{sgn}(\nu)$	Here $\mathrm{sgn}(\xi)$ is the sign function. Note that $1/x$ is a distribution. It is necessary to use the Cauchy principal value when testing against Schwartz functions. This rule is useful in studying the Hilbert transform.

$\dfrac{1}{x^n} := \dfrac{(-1)^{n-1}}{(n-1)!}\dfrac{d^n}{dx^n}\log|x|$	$-i\pi\dfrac{(-2\pi i\xi)^{n-1}}{(n-1)!}\,\mathrm{sgn}(\xi)$	$-i\sqrt{\dfrac{\pi}{2}}\cdot\dfrac{(-i\omega)^{n-1}}{(n-1)!}\,\mathrm{sgn}(\omega)$	$-i\pi\dfrac{(-i\nu)^{n-1}}{(n-1)!}\,\mathrm{sgn}(\nu)$	$1/x^n$ is the homogeneous distribution, defined by regularizing the singularity via $$\frac{1}{x^n}[\phi]=\int_{-\infty}^{\infty}\frac{\phi(x)-\sum_{k=0}^{n-1}x^k\phi^{(k)}(0)}{x^n}$$
$|x|^\alpha$	$-2\dfrac{\sin(\pi\alpha/2)\Gamma(\alpha+1)}{|2\pi\xi|^{\alpha+1}}$	$\dfrac{-2}{\sqrt{2\pi}}\dfrac{\sin(\pi\alpha/2)\Gamma(\alpha+1)}{|\omega|^{\alpha+1}}$	$-2\dfrac{\sin(\pi\alpha/2)\Gamma(\alpha+1)}{|\nu|^{\alpha+1}}$	If Re $\alpha > -1$, then $|x|^\alpha$ is a locally integrable function, and so it is a tempered distribution. The function $\alpha\mapsto|x|^\alpha$ is a holomorphic function from the right half-plane to the space of tempered distributions. It admits a unique meromorphic extension to a tempered distribution, also denoted $|x|^\alpha$ for $\alpha\neq-2,-4,...$ (See homogeneous distribution.)
$\mathrm{sgn}(x)$	$\dfrac{1}{i\pi\xi}$	$\sqrt{\dfrac{2}{\pi}}\cdot\dfrac{1}{i\omega}$	$\dfrac{2}{i\nu}$	The dual of rule 309. This time the Fourier transforms need to be considered as Cauchy principal value.
$u(x)$	$\dfrac{1}{2}\left(\dfrac{1}{i\pi\xi}+\delta(\xi)\right)$	$\sqrt{\dfrac{\pi}{2}}\left(\dfrac{1}{i\pi\omega}+\delta(\omega)\right)$	$\pi\left(\dfrac{1}{i\pi\nu}+\delta(\nu)\right)$	The function $u(x)$ is the Heaviside unit step function; this follows from rules 101,301, and 312.
$\displaystyle\sum_{n=-\infty}^{\infty}\delta(x-nT)$	$\dfrac{1}{T}\displaystyle\sum_{k=-\infty}^{\infty}\delta\left(\xi-\dfrac{k}{T}\right)$	$\dfrac{\sqrt{2\pi}}{T}\displaystyle\sum_{k=-\infty}^{\infty}\delta\left(\omega-\dfrac{2\pi k}{T}\right)$	$\dfrac{2\pi}{T}\displaystyle\sum_{k=-\infty}^{\infty}\delta\left(\nu-\dfrac{2\pi k}{T}\right)$	This function is known as the Dirac comb function. This result can be derived from 302 and 102, together with the fact that $$\sum_{n=-\infty}^{\infty}e^{inx}=2\pi\sum_{k=-\infty}^{\infty}\delta(x+2\pi k)$$ as distributions.
$J_0(x)$	$\dfrac{2\,\mathrm{rect}(\pi\xi)}{\sqrt{1-4\pi^2\xi^2}}$	$\sqrt{\dfrac{2}{\pi}}\cdot\dfrac{\mathrm{rect}\left(\dfrac{\omega}{2}\right)}{\sqrt{1-\omega^2}}$	$\dfrac{2\,\mathrm{rect}\left(\dfrac{\nu}{2}\right)}{\sqrt{1-\nu^2}}$	The function $J_0(x)$ is the zeroth order Bessel function of first kind.
$J_n(x)$	$\dfrac{2(-i)^n T_n(2\pi\xi)\mathrm{rect}(\pi\xi)}{\sqrt{1-4\pi^2\xi^2}}$	$\sqrt{\dfrac{2}{\pi}}\dfrac{(-i)^n T_n(\omega)\mathrm{rect}\left(\dfrac{\omega}{2}\right)}{\sqrt{1-\omega^2}}$	$\dfrac{2(-i)^n T_n(\nu)\mathrm{rect}\left(\dfrac{\nu}{2}\right)}{\sqrt{1-\nu^2}}$	This is a generalization of 315. The function $J_n(x)$ is the n-th order Bessel function of first kind. The function $T_n(x)$ is the Chebyshev polynomial of the first kind.

Two-dimensional functions

$f(x, y)$	Functions (400 to 402)	Fourier transform unitary, ordinary frequency	Fourier transform unitary, angular frequency
	$\hat{f}(\xi_x, \xi_y) = \iint f(x, y) e^{-2\pi i(\xi_x x + \xi_y y)}\, dx dy$	$\hat{f}(\omega_x, \omega_y) = \dfrac{1}{2\pi} \iint f(x, y) e^{-i(\omega_x x + \omega_y y)}\, dx dy$	$\hat{f}(\nu_x, \nu_y) = \iint f(x, y) e^{-i(\nu_x x + \nu_y y)}\, dx dy$
$e^{-\pi\left(a^2 x^2 + b^2 y^2\right)}$	$\dfrac{1}{\|ab\|} e^{-\pi\left(\xi_x^2/a^2 + \xi_y^2/b^2\right)}$	$\dfrac{1}{2\pi \cdot \|ab\|} e^{\frac{-\left(\omega_x^2/a^2 + \omega_y^2/b^2\right)}{4\pi}}$	$\dfrac{1}{\|ab\|} e^{\frac{-\left(\nu_x^2/a^2 + \nu_y^2/b^2\right)}{4\pi}}$
$\operatorname{circ}\left(\sqrt{x^2 + y^2}\right)$	$\dfrac{J_1\left(2\pi\sqrt{\xi_x^2 + \xi_y^2}\right)}{\sqrt{\xi_x^2 + \xi_y^2}}$	$\dfrac{J_1\left(\sqrt{\omega_x^2 + \omega_y^2}\right)}{\sqrt{\omega_x^2 + \omega_y^2}}$	$\dfrac{2\pi J_1\left(\sqrt{\nu_x^2 + \nu_y^2}\right)}{\sqrt{\nu_x^2 + \nu_y^2}}$

Remarks

To 400: The variables ξ_x, ξ_y, ω_x, ω_y, ν_x and ν_y are real numbers. The integrals are taken over the entire plane.

To 401: Both functions are Gaussians, which may not have unit volume.

To 402: The function is defined by circ(r)=1 0≤r≤1, and is 0 otherwise. This is the Airy distribution, and is expressed using J_1 (the order 1 Bessel function of the first kind). (Stein & Weiss 1971, Thm. IV.3.3)

Formulas for general *n*-dimensional functions

	Function	Fourier transform unitary, ordinary frequency	Fourier transform unitary, angular frequency	Fourier transform non-unitary, angular frequency
500	$f(x)$	$\hat{f}(\xi) = \displaystyle\int_{\mathbb{R}^n} f(x) e^{-2\pi i x \cdot \xi}\, d^n x$	$\hat{f}(\omega) = \dfrac{1}{(2\pi)^{(n/2)}} \displaystyle\int_{\mathbb{R}^n} f(x) e^{-i\omega \cdot x}\, d^n x$	$\hat{f}(\nu) = \displaystyle\int_{\mathbb{R}^n} f(x) e^{-ix \cdot \nu}\, d^n x$
501	$\chi_{[0,1]}(\|x\|)(1 - \|x\|^2)^\delta$	$\pi^{-\delta}\Gamma(\delta + 1)\|\xi\|^{-(n/2)-\delta}$ $\cdot J_{n/2+\delta}(2\pi\|\xi\|)$	$2^{-\delta}\Gamma(\delta + 1)\|\omega\|^{-(n/2)-\delta}$ $\cdot J_{n/2+\delta}(\|\omega\|)$	$\pi^{-\delta}\Gamma(\delta + 1)\left\|\dfrac{\nu}{2\pi}\right\|^{-(n/2)-\delta}$ $\cdot J_{n/2+\delta}(\|\nu\|)$ loc=Thm. 4.13}}
502	$\|x\|^{-\alpha}, \quad 0 < \operatorname{Re}\alpha < n.$	$c_\alpha \|\xi\|^{-(n-\alpha)}$		

Remarks

To 501: The function $\chi_{[0,1]}$ is the indicator function of the interval [0,1]. The function $\Gamma(x)$ is the gamma function. The function $J_{n/2+\delta}$ is a Bessel function of the first kind, with order $n/2+\delta$. Taking $n = 2$ and $\delta = 0$ produces 402. {{harv|Stein|Weiss|1971|

To 502: See Riesz potential. The formula also holds for all $\alpha \neq -n$, $-n-1$, ... by analytic continuation, but then the function and its Fourier transforms need to be understood as suitably regularized tempered distributions. See homogeneous distribution.

See also

- Fourier series
- Fast Fourier transform
- Laplace transform
- Discrete Fourier transform

  - DFT matrix

- Discrete-time Fourier transform
- Fourier–Deligne transform
- Fractional Fourier transform
- Linear canonical transform
- Fourier sine transform
- Short-time Fourier transform
- Fourier inversion theorem
- Analog signal processing
- Transform (mathematics)
- Integral transform

  - Hartley transform
  - Hankel transform

References

- Boashash, B., ed. (2003), *Time-Frequency Signal Analysis and Processing: A Comprehensive Reference*, Oxford: Elsevier Science
- Bochner S., Chandrasekharan K. (1949), *Fourier Transforms*, Princeton University Press
- Bracewell, R. N. (2000), *The Fourier Transform and Its Applications* (3rd ed.), Boston: McGraw-Hill.
- Campbell, George; Foster, Ronald (1948), *Fourier Integrals for Practical Applications*, New York: D. Van Nostrand Company, Inc..
- Duoandikoetxea, Javier (2001), *Fourier Analysis*, American Mathematical Society, ISBN 0-8218-2172-5.
- Dym, H; McKean, H (1985), *Fourier Series and Integrals*, Academic Press, ISBN 978-0122264511.
- Erdélyi, Arthur, ed. (1954), *Tables of Integral Transforms*, **1**, New Your: McGraw-Hill
- Fourier, J. B. Joseph (1822), *Théorie Analytique de la Chaleur* [1], Paris
- Grafakos, Loukas (2004), *Classical and Modern Fourier Analysis*, Prentice-Hall, ISBN 0-13-035399-X.
- Hewitt, Edwin; Ross, Kenneth A. (1970), *Abstract harmonic analysis. Vol. II: Structure and analysis for compact groups. Analysis on locally compact Abelian groups*, Die Grundlehren der mathematischen Wissenschaften, Band 152, Berlin, New York: Springer-Verlag, MR0262773.
- Hörmander, L. (1976), *Linear Partial Differential Operators, Volume 1*, Springer-Verlag, ISBN 978-3540006626.
- James, J.F. (2002), *A Student's Guide to Fourier Transforms* (2nd ed.), New York: Cambridge University Press, ISBN 0-521-00428-4.
- Kaiser, Gerald (1994), *A Friendly Guide to Wavelets*, Birkhäuser, ISBN 0-8176-3711-7
- Kammler, David (2000), *A First Course in Fourier Analysis*, Prentice Hall, ISBN 0-13-578782-3
- Katznelson, Yitzhak (1976), *An introduction to Harmonic Analysis*, Dover, ISBN 0-486-63331-4
- Knapp, Anthony W. (2001), *Representation Theory of Semisimple Groups: An Overview Based on Examples* [2], Princeton University Press, ISBN 978-0-691-09089-4
- Pinsky, Mark (2002), *Introduction to Fourier Analysis and Wavelets*, Brooks/Cole, ISBN 0-534-37660-6
- Polyanin, A. D.; Manzhirov, A. V. (1998), *Handbook of Integral Equations*, Boca Raton: CRC Press, ISBN 0-8493-2876-4.
- Rudin, Walter (1987), *Real and Complex Analysis* (Third ed.), Singapore: McGraw Hill, ISBN 0-07-100276-6.

- Stein, Elias; Shakarchi, Rami (2003), *Fourier Analysis: An introduction*, Princeton University Press, ISBN 0-691-11384-X.
- Stein, Elias; Weiss, Guido (1971), *Introduction to Fourier Analysis on Euclidean Spaces*, Princeton, N.J.: Princeton University Press, ISBN 978-0-691-08078-9.
- Wilson, R. G. (1995), *Fourier Series and Optical Transform Techniques in Contemporary Optics*, New York: Wiley, ISBN 0471303577.
- Yosida, K. (1968), *Functional Analysis*, Springer-Verlag, ISBN 3-540-58654-7.

External links

- Fourier Series Applet [3] (Tip: drag magnitude or phase dots up or down to change the wave form).
- Stephan Bernsee's FFTlab [4] (Java Applet)
- Stanford Video Course on the Fourier Transform [5]
- Tables of Integral Transforms [6] at EqWorld: The World of Mathematical Equations.
- Weisstein, Eric W., "Fourier Transform [7]" from MathWorld.
- Fourier Transform Module by John H. Mathews [8]
- The DFT "à Pied": Mastering The Fourier Transform in One Day [9] at The DSP Dimension
- An Interactive Flash Tutorial for the Fourier Transform [10]

References

[1] http://books.google.com/?id=TDQJAAAAIAAJ&printsec=frontcover&dq=Th%C3%A9orie+analytique+de+la+chaleur&q

[2] http://books.google.com/?id=QCcW1h835pwC

[3] http://www.westga.edu/~jhasbun/osp/Fourier.htm

[4] http://www.dspdimension.com/fftlab/

[5] http://www.academicearth.com/courses/the-fourier-transform-and-its-applications

[6] http://eqworld.ipmnet.ru/en/auxiliary/aux-inttrans.htm

[7] http://mathworld.wolfram.com/FourierTransform.html

[8] http://math.fullerton.edu/mathews/c2003/FourierTransformMod.html

[9] http://www.dspdimension.com/admin/dft-a-pied/

[10] http://www.fourier-series.com/f-transform/index.html

Discrete Fourier transform

Fourier transforms
Continuous Fourier transform
Fourier series
Discrete Fourier transform
Discrete-time Fourier transform
Related transforms

In mathematics, the **discrete Fourier transform (DFT)** is a specific kind of Fourier transform, used in Fourier analysis. It transforms one function into another, which is called the *frequency domain* representation, or simply the *DFT*, of the original function (which is often a function in the time domain). But the DFT requires an input function that is *discrete* and whose non-zero values have a limited (*finite*) duration. Such inputs are often created by sampling a continuous function, like a person's voice. Unlike the discrete-time Fourier transform (DTFT), it only evaluates enough frequency components to reconstruct the finite segment that was analyzed. Using the DFT implies that the finite segment that is analyzed is one period of an infinitely extended periodic signal; if this is not actually true, a window function has to be used to reduce the artifacts in the spectrum. For the same reason, the inverse DFT cannot reproduce the entire time domain, unless the input happens to be periodic (forever). Therefore it is often said that the DFT is a transform for Fourier analysis of finite-domain discrete-time functions. The sinusoidal basis functions of the decomposition have the same properties.

The input to the DFT is a finite sequence of real or complex numbers (with more abstract generalizations discussed below), making the DFT ideal for processing information stored in computers. In particular, the DFT is widely employed in signal processing and related fields to analyze the frequencies contained in a sampled signal, to solve partial differential equations, and to perform other operations such as convolutions or multiplying large integers. A key enabling factor for these applications is the fact that the DFT can be computed efficiently in practice using a fast Fourier transform (FFT) algorithm.

FFT algorithms are so commonly employed to compute DFTs that the term "FFT" is often used to mean "DFT" in colloquial settings. Formally, there is a clear distinction: "DFT" refers to a mathematical transformation or function, regardless of how it is computed, whereas "FFT" refers to a specific family of algorithms for computing DFTs. The terminology is further blurred by the (now rare) synonym finite Fourier transform for the DFT, which apparently predates the term "fast Fourier transform" (Cooley et al., 1969) but has the same initialism.

Definition

The sequence of *N* complex numbers x_0, ..., x_{N-1} is transformed into the sequence of *N* complex numbers X_0, ..., X_{N-1} by the DFT according to the formula:

$$X_k = \sum_{n=0}^{N-1} x_n e^{-\frac{2\pi i}{N}kn} \qquad k = 0, \dots, N-1$$

where i is the imaginary unit and $e^{\frac{2\pi i}{N}}$ is a primitive N'th root of unity. (This expression can also be written in terms of a DFT matrix; when scaled appropriately it becomes a unitary matrix and the X_k can thus be viewed as coefficients of *x* in an orthonormal basis.)

The transform is sometimes denoted by the symbol $\mathcal{F}$, as in $\mathbf{X} = \mathcal{F}\{\mathbf{x}\}$ or $\mathcal{F}(\mathbf{x})$ or $\mathcal{F}\mathbf{x}$.

The **inverse discrete Fourier transform (IDFT)** is given by

$$x_n = \frac{1}{N} \sum_{k=0}^{N-1} X_k e^{\frac{2\pi i}{N} kn} \qquad n = 0, \ldots, N-1.$$

A simple description of these equations is that the complex numbers X_k represent the amplitude and phase of the different sinusoidal components of the input "signal" x_n. The DFT computes the X_k from the x_n, while the IDFT shows how to compute the x_n as a sum of sinusoidal components $(1/N)X_k e^{\frac{2\pi i}{N} kn}$ with frequency k/N cycles per sample. By writing the equations in this form, we are making extensive use of Euler's formula to express sinusoids in terms of complex exponentials, which are much easier to manipulate. In the same way, by writing X_k in polar form, we obtain the sinusoid amplitude A_k/N and phase ϕ_k from the complex modulus and argument of X_k, respectively:

$$A_k = |X_k| = \sqrt{\operatorname{Re}(X_k)^2 + \operatorname{Im}(X_k)^2},$$
$$\varphi_k = \arg(X_k) = \operatorname{atan2}\big(\operatorname{Im}(X_k), \operatorname{Re}(X_k)\big),$$

where atan2 is the two-argument form of the arctan function. Note that the normalization factor multiplying the DFT and IDFT (here 1 and 1/*N*) and the signs of the exponents are merely conventions, and differ in some treatments. The only requirements of these conventions are that the DFT and IDFT have opposite-sign exponents and that the product of their normalization factors be 1/*N*. A normalization of $1/\sqrt{N}$ for both the DFT and IDFT makes the transforms unitary, which has some theoretical advantages, but it is often more practical in numerical computation to perform the scaling all at once as above (and a unit scaling can be convenient in other ways).

(The convention of a negative sign in the exponent is often convenient because it means that X_k is the amplitude of a "positive frequency" $2\pi k/N$. Equivalently, the DFT is often thought of as a matched filter: when looking for a frequency of +1, one correlates the incoming signal with a frequency of –1.)

In the following discussion the terms "sequence" and "vector" will be considered interchangeable.

Properties

Completeness

The discrete Fourier transform is an invertible, linear transformation

$$\mathcal{F} : \mathbb{C}^N \to \mathbb{C}^N$$

with **C** denoting the set of complex numbers. In other words, for any *N* > 0, an *N*-dimensional complex vector has a DFT and an IDFT which are in turn *N*-dimensional complex vectors.

Orthogonality

The vectors $e^{\frac{2\pi i}{N} kn}$ form an orthogonal basis over the set of *N*-dimensional complex vectors:

$$\sum_{n=0}^{N-1} \left(e^{\frac{2\pi i}{N} kn} \right) \left(e^{-\frac{2\pi i}{N} k'n} \right) = N \; \delta_{kk'}$$

where $\delta_{kk'}$ is the Kronecker delta. This orthogonality condition can be used to derive the formula for the IDFT from the definition of the DFT, and is equivalent to the unitarity property below.

The Plancherel theorem and Parseval's theorem

If X_k and Y_k are the DFTs of x_n and y_n respectively then the Plancherel theorem states:

$$\sum_{n=0}^{N-1} x_n y_n^* = \frac{1}{N} \sum_{k=0}^{N-1} X_k Y_k^*$$

where the star denotes complex conjugation. Parseval's theorem is a special case of the Plancherel theorem and states:

$$\sum_{n=0}^{N-1} |x_n|^2 = \frac{1}{N} \sum_{k=0}^{N-1} |X_k|^2.$$

These theorems are also equivalent to the unitary condition below.

Periodicity

If the expression that defines the DFT is evaluated for all integers k instead of just for $k = 0, \ldots, N-1$, then the resulting infinite sequence is a periodic extension of the DFT, periodic with period *N*.

The periodicity can be shown directly from the definition:

$$X_{k+N} \overset{\text{def}}{=} \sum_{n=0}^{N-1} x_n e^{-\frac{2\pi i}{N}(k+N)n} = \sum_{n=0}^{N-1} x_n e^{-\frac{2\pi i}{N}kn} \underbrace{e^{-2\pi i n}}_{1} = \sum_{n=0}^{N-1} x_n e^{-\frac{2\pi i}{N}kn} = X_k.$$

Similarly, it can be shown that the IDFT formula leads to a periodic extension.

The shift theorem

Multiplying x_n by a *linear phase* $e^{\frac{2\pi i}{N}nm}$ for some integer *m* corresponds to a *circular shift* of the output X_k: X_k is replaced by X_{k-m}, where the subscript is interpreted modulo *N* (i.e., periodically). Similarly, a circular shift of the input x_n corresponds to multiplying the output X_k by a linear phase. Mathematically, if $\{x_n\}$ represents the vector **x** then

if $\mathcal{F}(\{x_n\})_k = X_k$

then $\mathcal{F}(\{x_n \cdot e^{\frac{2\pi i}{N}nm}\})_k = X_{k-m}$

and $\mathcal{F}(\{x_{n-m}\})_k = X_k \cdot e^{-\frac{2\pi i}{N}km}$

Circular convolution theorem and cross-correlation theorem

The convolution theorem for the continuous and discrete time Fourier transforms indicates that a convolution of two infinite sequences can be obtained as the inverse transform of the product of the individual transforms. With sequences and transforms of length N, a circularity arises**:**

$$\mathcal{F}^{-1}\{\mathbf{X} \cdot \mathbf{Y}\}_n \overset{\text{def}}{=} \frac{1}{N} \sum_{k=0}^{N-1} X_k \cdot Y_k \cdot e^{\frac{2\pi i}{N}kn}$$

$$= \frac{1}{N} \sum_{k=0}^{N-1} \left(\sum_{l=0}^{N-1} x_l e^{-\frac{2\pi i}{N}kl} \right) \cdot \left(\sum_{m=0}^{N-1} y_m e^{-\frac{2\pi i}{N}km} \right) \cdot e^{\frac{2\pi i}{N}kn}$$

$$= \sum_{l=0}^{N-1} x_l \sum_{m=0}^{N-1} y_m \left(\frac{1}{N} \sum_{k=0}^{N-1} e^{\frac{2\pi i}{N}k(n-l-m)} \right).$$

The quantity in parentheses is 0 for all values of *m* except those of the form $n - l - pN$, where *p* is any integer. At those values, it is 1. It can therefore be replaced by an infinite sum of Kronecker delta functions, and we continue accordingly. Note that we can also extend the limits of *m* to infinity, with the understanding that the *x* and *y* sequences are defined as 0 outside [0,N-1]**:**

$$\mathcal{F}^{-1}\left\{\mathbf{X}\cdot\mathbf{Y}\right\}_n = \sum_{l=0}^{N-1} x_l \sum_{m=-\infty}^{\infty} y_m \left(\sum_{p=-\infty}^{\infty} \delta_{m,(n-l-pN)}\right)$$

$$= \sum_{l=0}^{N-1} x_l \sum_{p=-\infty}^{\infty} \underbrace{\left(\sum_{m=-\infty}^{\infty} y_m \cdot \delta_{m,(n-l-pN)}\right)}_{y_{n-l-pN}}$$

$$= \sum_{l=0}^{N-1} x_l \left(\sum_{p=-\infty}^{\infty} y_{n-l-pN}\right) \overset{\text{def}}{=} (\mathbf{x} * \mathbf{y_N})_n \ ,$$

which is the convolution of the $\mathbf{x}$ sequence with a <u>periodically extended</u> $\mathbf{y}$ sequence defined by:

$$\left(\mathbf{y_N}\right)_n \overset{\text{def}}{=} \sum_{p=-\infty}^{\infty} y_{(n-pN)}.$$

Similarly, it can be shown that:

$$\mathcal{F}^{-1}\left\{\mathbf{X}^*\cdot\mathbf{Y}\right\}_n = \sum_{l=0}^{N-1} x_l^* \cdot (y_N)_{n+l} \overset{\text{def}}{=} (\mathbf{x} \star \mathbf{y_N})_n \ ,$$

which is the cross-correlation of $\mathbf{x}$ and $\mathbf{y_N}$.

A direct evaluation of the convolution or correlation summation (above) requires $O(N^2)$ operations for an output sequence of length N. An indirect method, using transforms, can take advantage of the $O(N\log N)$ efficiency of the fast Fourier transform (FFT) to achieve much better performance. Furthermore, convolutions can be used to efficiently compute DFTs via Rader's FFT algorithm and Bluestein's FFT algorithm.
Methods have also been developed to use circular convolution as part of an efficient process that achieves normal (non-circular) convolution with an $\mathbf{x}$ or $\mathbf{y}$ sequence potentially much longer than the practical transform size (**N**). Two such methods are called overlap-save and overlap-add[1].

Convolution theorem duality

It can also be shown that:

$$\mathcal{F}\left\{\mathbf{x}\cdot\mathbf{y}\right\}_k \overset{\text{def}}{=} \sum_{n=0}^{N-1} x_n \cdot y_n \cdot e^{-\frac{2\pi i}{N}kn}$$

$$= \frac{1}{N}(\mathbf{X} * \mathbf{Y_N})_k, \quad \text{which is the circular convolution of } \mathbf{X} \text{ and } \mathbf{Y}.$$

Trigonometric interpolation polynomial

The trigonometric interpolation polynomial

$$p(t) = \frac{1}{N}\left[X_0 + X_1 e^{it} + \cdots + X_{N/2-1}e^{(N/2-1)it} + X_{N/2}\cos(Nt/2) + X_{N/2+1}e^{(-N/2+1)it} + \cdots + X_{N-1}e\right.$$

N even ,

$$p(t) = \frac{1}{N}\left[X_0 + X_1 e^{it} + \cdots + X_{\lfloor N/2\rfloor}e^{\lfloor N/2\rfloor it} + X_{\lfloor N/2\rfloor+1}e^{-\lfloor N/2\rfloor it} + \cdots + X_{N-1}e^{-it}\right] \text{for } N$$

odd,

where the coefficients X_k are given by the DFT of x_n above, satisfies the interpolation property $p(2\pi n/N) = x_n$ for $n = 0, \ldots, N-1$.

For even N, notice that the Nyquist component $\dfrac{X_{N/2}}{N}\cos(Nt/2)$ is handled specially.

This interpolation is *not unique*: aliasing implies that one could add *N* to any of the complex-sinusoid frequencies (e.g. changing e^{-it} to $e^{i(N-1)t}$) without changing the interpolation property, but giving *different* values in between the x_n points. The choice above, however, is typical because it has two useful properties. First, it consists of sinusoids whose frequencies have the smallest possible magnitudes, and therefore minimizes the mean-square slope $\int |p'(t)|^2 dt$ of the interpolating function. Second, if the x_n are real numbers, then $p(t)$ is real as well.

In contrast, the most obvious trigonometric interpolation polynomial is the one in which the frequencies range from 0 to $N-1$ (instead of roughly $-N/2$ to $+N/2$ as above), similar to the inverse DFT formula. This interpolation does *not* minimize the slope, and is *not* generally real-valued for real x_n; its use is a common mistake.

The unitary DFT

Another way of looking at the DFT is to note that in the above discussion, the DFT can be expressed as a Vandermonde matrix:

$$
\mathbf{F} = \begin{bmatrix}
\omega_N^{0 \cdot 0} & \omega_N^{0 \cdot 1} & \dots & \omega_N^{0 \cdot (N-1)} \\
\omega_N^{1 \cdot 0} & \omega_N^{1 \cdot 1} & \dots & \omega_N^{1 \cdot (N-1)} \\
\vdots & \vdots & \ddots & \vdots \\
\omega_N^{(N-1) \cdot 0} & \omega_N^{(N-1) \cdot 1} & \dots & \omega_N^{(N-1) \cdot (N-1)}
\end{bmatrix}
$$

where

$$
\omega_N = e^{-2\pi i/N}
$$

is a primitive Nth root of unity. The inverse transform is then given by the inverse of the above matrix:

$$
\mathbf{F}^{-1} = \frac{1}{N}\mathbf{F}^*
$$

With unitary normalization constants $1/\sqrt{N}$, the DFT becomes a unitary transformation, defined by a unitary matrix:

$$
\mathbf{U} = \mathbf{F}/\sqrt{N}
$$
$$
\mathbf{U}^{-1} = \mathbf{U}^*
$$
$$
|\det(\mathbf{U})| = 1
$$

where *det()* is the determinant function. The determinant is the product of the eigenvalues, which are always ± 1 or $\pm i$ as described below. In a real vector space, a unitary transformation can be thought of as simply a rigid rotation of the coordinate system, and all of the properties of a rigid rotation can be found in the unitary DFT.

The orthogonality of the DFT is now expressed as an orthonormality condition (which arises in many areas of mathematics as described in root of unity):

$$
\sum_{m=0}^{N-1} U_{km} U_{mn}^* = \delta_{kn}
$$

If $\mathbf{X}$ is defined as the unitary DFT of the vector $\mathbf{x}$ then

$$
X_k = \sum_{n=0}^{N-1} U_{kn} x_n
$$

and the Plancherel theorem is expressed as:

$$
\sum_{n=0}^{N-1} x_n y_n^* = \sum_{k=0}^{N-1} X_k Y_k^*
$$

If we view the DFT as just a coordinate transformation which simply specifies the components of a vector in a new coordinate system, then the above is just the statement that the dot product of two vectors is preserved under a unitary DFT transformation. For the special case $\mathbf{x} = \mathbf{y}$, this implies that the length of a vector is preserved as

well—this is just Parseval's theorem:

$$\sum_{n=0}^{N-1} |x_n|^2 = \sum_{k=0}^{N-1} |X_k|^2$$

Expressing the inverse DFT in terms of the DFT

A useful property of the DFT is that the inverse DFT can be easily expressed in terms of the (forward) DFT, via several well-known "tricks". (For example, in computations, it is often convenient to only implement a fast Fourier transform corresponding to one transform direction and then to get the other transform direction from the first.)

First, we can compute the inverse DFT by reversing the inputs:

$$\mathcal{F}^{-1}(\{x_n\}) = \mathcal{F}(\{x_{N-n}\})/N$$

(As usual, the subscripts are interpreted modulo N; thus, for $n = 0$, we have $x_{N-0} = x_0$.)

Second, one can also conjugate the inputs and outputs:

$$\mathcal{F}^{-1}(\mathbf{x}) = \mathcal{F}(\mathbf{x}^*)^*/N$$

Third, a variant of this conjugation trick, which is sometimes preferable because it requires no modification of the data values, involves swapping real and imaginary parts (which can be done on a computer simply by modifying pointers). Define swap(x_n) as x_n with its real and imaginary parts swapped—that is, if $x_n = a + bi$ then swap(x_n) is $b + ai$. Equivalently, swap(x_n) equals ix_n^*. Then

$$\mathcal{F}^{-1}(\mathbf{x}) = \mathrm{swap}(\mathcal{F}(\mathrm{swap}(\mathbf{x})))/N$$

That is, the inverse transform is the same as the forward transform with the real and imaginary parts swapped for both input and output, up to a normalization (Duhamel *et al.*, 1988).

The conjugation trick can also be used to define a new transform, closely related to the DFT, that is involutary—that is, which is its own inverse. In particular, $T(\mathbf{x}) = \mathcal{F}(\mathbf{x}^*)/\sqrt{N}$ is clearly its own inverse: $T(T(\mathbf{x})) = \mathbf{x}$. A closely related involutary transformation (by a factor of $(1+i)/\sqrt{2}$) is $H(\mathbf{x}) = \mathcal{F}((1+i)\mathbf{x}^*)/\sqrt{2N}$, since the $(1+i)$ factors in $H(H(\mathbf{x}))$ cancel the 2. For real inputs $\mathbf{x}$, the real part of $H(\mathbf{x})$ is none other than the discrete Hartley transform, which is also involutary.

Eigenvalues and eigenvectors

The eigenvalues of the DFT matrix are simple and well-known, whereas the eigenvectors are complicated, not unique, and are the subject of ongoing research.

Consider the unitary form $\mathbf{U}$ defined above for the DFT of length N, where

$$\mathbf{U}_{m,n} = \frac{1}{\sqrt{N}} \omega_N^{(m-1)(n-1)} = \frac{1}{\sqrt{N}} e^{-\frac{2\pi i}{N}(m-1)(n-1)}.$$

This matrix satisfies the equation:

$$\mathbf{U}^4 = \mathbf{I}.$$

This can be seen from the inverse properties above: operating $\mathbf{U}$ twice gives the original data in reverse order, so operating $\mathbf{U}$ four times gives back the original data and is thus the identity matrix. This means that the eigenvalues λ satisfy a characteristic equation:

$$\lambda^4 = 1.$$

Therefore, the eigenvalues of $\mathbf{U}$ are the fourth roots of unity: λ is +1, −1, +i, or −i.

Since there are only four distinct eigenvalues for this $N \times N$ matrix, they have some multiplicity. The multiplicity gives the number of linearly independent eigenvectors corresponding to each eigenvalue. (Note that there are N independent eigenvectors; a unitary matrix is never defective.)

The problem of their multiplicity was solved by McClellan and Parks (1972), although it was later shown to have been equivalent to a problem solved by Gauss (Dickinson and Steiglitz, 1982). The multiplicity depends on the value of N modulo 4, and is given by the following table:

Multiplicities of the eigenvalues λ of the unitary DFT matrix U as a function of the transform size *N* (in terms of an integer *m*).

size *N*	λ = +1	λ = −1	λ = -i	λ = +i
4m	m + 1	m	m	m − 1
4m + 1	m + 1	m	m	m
4m + 2	m + 1	m + 1	m	m
4m + 3	m + 1	m + 1	m + 1	m

No simple analytical formula for general eigenvectors is known. Moreover, the eigenvectors are not unique because any linear combination of eigenvectors for the same eigenvalue is also an eigenvector for that eigenvalue. Various researchers have proposed different choices of eigenvectors, selected to satisfy useful properties like orthogonality and to have "simple" forms (e.g., McClellan and Parks, 1972; Dickinson and Steiglitz, 1982; Grünbaum, 1982; Atakishiyev and Wolf, 1997; Candan *et al.*, 2000; Hanna *et al.*, 2004; Gurevich and Hadani, 2008). However two simple closed-form analytical eigenvectors for special DFT period *N* were found (Kong, 2008):

For DFT period $N = 2L + 1 = 4K + 1$, where *K* is an integer, the following is an eigenvector of DFT:

$$F(m) = \prod_{s=K+1}^{L} \left[\cos\left(\frac{2\pi}{N}m\right) - \cos\left(\frac{2\pi}{N}s\right) \right]$$

For DFT period $N = 2L = 4K$, where *K* is an integer, the following is an eigenvector of DFT:

$$F(m) = \sin\left(\frac{2\pi}{N}m\right) \prod_{s=K+1}^{L-1} \left[\cos\left(\frac{2\pi}{N}m\right) - \cos\left(\frac{2\pi}{N}s\right) \right]$$

The choice of eigenvectors of the DFT matrix has become important in recent years in order to define a discrete analogue of the fractional Fourier transform—the DFT matrix can be taken to fractional powers by exponentiating the eigenvalues (e.g., Rubio and Santhanam, 2005). For the continuous Fourier transform, the natural orthogonal eigenfunctions are the Hermite functions, so various discrete analogues of these have been employed as the eigenvectors of the DFT, such as the Kravchuk polynomials (Atakishiyev and Wolf, 1997). The "best" choice of eigenvectors to define a fractional discrete Fourier transform remains an open question, however.

The real-input DFT

If $x_0, \ldots, x_{N-1}$ are real numbers, as they often are in practical applications, then the DFT obeys the symmetry:

$$X_k = X_{N-k}^*.$$

The star denotes complex conjugation. The subscripts are interpreted modulo *N*.

Therefore, the DFT output for real inputs is half redundant, and one obtains the complete information by only looking at roughly half of the outputs $X_0, \ldots, X_{N-1}$. In this case, the "DC" element X_0 is purely real, and for even *N* the "Nyquist" element $X_{N/2}$ is also real, so there are exactly *N* non-redundant real numbers in the first half + Nyquist element of the complex output *X*.

Using Euler's formula, the interpolating trigonometric polynomial can then be interpreted as a sum of sine and cosine functions.

Generalized/shifted DFT

It is possible to shift the transform sampling in time and/or frequency domain by some real shifts *a* and *b*, respectively. This is sometimes known as a **generalized DFT** (or **GDFT**), also called the **shifted DFT** or **offset DFT**, and has analogous properties to the ordinary DFT:

$$X_k = \sum_{n=0}^{N-1} x_n e^{-\frac{2\pi i}{N}(k+b)(n+a)} \qquad k = 0, \dots, N-1.$$

Most often, shifts of $1/2$ (half a sample) are used. While the ordinary DFT corresponds to a periodic signal in both time and frequency domains, $a = 1/2$ produces a signal that is anti-periodic in frequency domain ($X_{k+N} = -X_k$) and vice-versa for $b = 1/2$. Thus, the specific case of $a = b = 1/2$ is known as an *odd-time odd-frequency* discrete Fourier transform (or O^2 DFT). Such shifted transforms are most often used for symmetric data, to represent different boundary symmetries, and for real-symmetric data they correspond to different forms of the discrete cosine and sine transforms.

Another interesting choice is $a = b = -(N-1)/2$, which is called the **centered DFT** (or **CDFT**). The centered DFT has the useful property that, when *N* is a multiple of four, all four of its eigenvalues (see above) have equal multiplicities (Rubio and Santhanam, 2005)[2]

The discrete Fourier transform can be viewed as a special case of the z-transform, evaluated on the unit circle in the complex plane; more general z-transforms correspond to *complex* shifts *a* and *b* above.

Multidimensional DFT

The ordinary DFT transforms a one-dimensional sequence or array x_n that is a function of exactly one discrete variable *n*. The multidimensional DFT of a multidimensional array $x_{n_1, n_2, \dots, n_d}$ that is a function of *d* discrete variables $n_\ell = 0, 1, \dots, N_\ell - 1$ for ℓ in $1, 2, \dots, d$ is defined by:

$$X_{k_1, k_2, \dots, k_d} = \sum_{n_1=0}^{N_1-1} \left(\omega_{N_1}^{k_1 n_1} \sum_{n_2=0}^{N_2-1} \left(\omega_{N_2}^{k_2 n_2} \cdots \sum_{n_d=0}^{N_d-1} \omega_{N_d}^{k_d n_d} \cdot x_{n_1, n_2, \dots, n_d} \right) \cdots \right),$$

where $\omega_{N_\ell} = \exp(-2\pi i / N_\ell)$ as above and the *d* output indices run from $k_\ell = 0, 1, \dots, N_\ell - 1$. This is more compactly expressed in vector notation, where we define $\mathbf{n} = (n_1, n_2, \dots, n_d)$ and $\mathbf{k} = (k_1, k_2, \dots, k_d)$ as *d*-dimensional vectors of indices from 0 to $\mathbf{N} - 1$, which we define as $\mathbf{N} - 1 = (N_1 - 1, N_2 - 1, \dots, N_d - 1)$:

$$X_{\mathbf{k}} = \sum_{\mathbf{n}=0}^{\mathbf{N}-1} e^{-2\pi i \mathbf{k} \cdot (\mathbf{n}/\mathbf{N})} x_{\mathbf{n}},$$

where the division $\mathbf{n}/\mathbf{N}$ is defined as $\mathbf{n}/\mathbf{N} = (n_1/N_1, \dots, n_d/N_d)$ to be performed element-wise, and the sum denotes the set of nested summations above.

The inverse of the multi-dimensional DFT is, analogous to the one-dimensional case, given by:

$$x_{\mathbf{n}} = \frac{1}{\prod_{\ell=1}^{d} N_\ell} \sum_{\mathbf{k}=0}^{\mathbf{N}-1} e^{2\pi i \mathbf{n} \cdot (\mathbf{k}/\mathbf{N})} X_{\mathbf{k}}.$$

As the one-dimensional DFT expresses the input x_n as a superposition of sinusoids, the multidimensional DFT expresses the input as a superposition of plane waves, or sinusoids. The direction of oscillation in space is $\mathbf{k}/\mathbf{N}$. The amplitudes are $X_{\mathbf{k}}$. This decomposition is of great importance for everything from digital image processing (two-dimensional) to solving partial differential equations. The solution is broken up into plane waves.

The multidimensional DFT can be computed by the composition of a sequence of one-dimensional DFTs along each dimension. In the two-dimensional case x_{n_1, n_2} the N_1 independent DFTs of the rows (i.e., along n_2) are computed first to form a new array . Then the N_2 independent DFTs of *y* along the columns (along n_1) are

computed to form the final result X_{k_1,k_2}. Alternatively the columns can be computed first and then the rows. The order is immaterial because the nested summations above commute.

An algorithm to compute a one-dimensional DFT is thus sufficient to efficiently compute a multidimensional DFT. This approach is known as the *row-column* algorithm. There are also intrinsically multidimensional FFT algorithms.

The real-input multidimensional DFT

For input data $x_{n_1,n_2,...,n_d}$ consisting of real numbers, the DFT outputs have a conjugate symmetry similar to the one-dimensional case above:

$$X_{k_1,k_2,...,k_d} = X^*_{N_1-k_1, N_2-k_2,..., N_d-k_d},$$

where the star again denotes complex conjugation and the ℓ-th subscript is again interpreted modulo N_ℓ (for $\ell = 1, 2, \ldots, d$).

Applications

The DFT has seen wide usage across a large number of fields; we only sketch a few examples below (see also the references at the end). All applications of the DFT depend crucially on the availability of a fast algorithm to compute discrete Fourier transforms and their inverses, a fast Fourier transform.

Spectral analysis

When the DFT is used for spectral analysis, the $\{x_n\}$ sequence usually represents a finite set of uniformly-spaced time-samples of some signal $x(t)$, where t represents time. The conversion from continuous time to samples (discrete-time) changes the underlying Fourier transform of x(t) into a discrete-time Fourier transform (DTFT), which generally entails a type of distortion called aliasing. Choice of an appropriate sample-rate (see Nyquist frequency) is the key to minimizing that distortion. Similarly, the conversion from a very long (or infinite) sequence to a manageable size entails a type of distortion called *leakage*, which is manifested as a loss of detail (aka resolution) in the DTFT. Choice of an appropriate sub-sequence length is the primary key to minimizing that effect. When the available data (and time to process it) is more than the amount needed to attain the desired frequency resolution, a standard technique is to perform multiple DFTs, for example to create a spectrogram. If the desired result is a power spectrum and noise or randomness is present in the data, averaging the magnitude components of the multiple DFTs is a useful procedure to reduce the variance of the spectrum (also called a periodogram in this context); two examples of such techniques are the Welch method and the Bartlett method; the general subject of estimating the power spectrum of a noisy signal is called spectral estimation.

A final source of distortion (or perhaps *illusion*) is the DFT itself, because it is just a discrete sampling of the DTFT, which is a function of a continuous frequency domain. That can be mitigated by increasing the resolution of the DFT. That procedure is illustrated in the discrete-time Fourier transform article.

- The procedure is sometimes referred to as *zero-padding*, which is a particular implementation used in conjunction with the fast Fourier transform (FFT) algorithm. The inefficiency of performing multiplications and additions with zero-valued "samples" is more than offset by the inherent efficiency of the FFT.
- As already noted, leakage imposes a limit on the inherent resolution of the DTFT. So there is a practical limit to the benefit that can be obtained from a fine-grained DFT.

Data compression

The field of digital signal processing relies heavily on operations in the frequency domain (i.e. on the Fourier transform). For example, several lossy image and sound compression methods employ the discrete Fourier transform: the signal is cut into short segments, each is transformed, and then the Fourier coefficients of high frequencies, which are assumed to be unnoticeable, are discarded. The decompressor computes the inverse transform based on this reduced number of Fourier coefficients. (Compression applications often use a specialized form of the DFT, the discrete cosine transform or sometimes the modified discrete cosine transform.)

Partial differential equations

Discrete Fourier transforms are often used to solve partial differential equations, where again the DFT is used as an approximation for the Fourier series (which is recovered in the limit of infinite N). The advantage of this approach is that it expands the signal in complex exponentials e^{inx}, which are eigenfunctions of differentiation: $d/dx\, e^{inx} = in\, e^{inx}$. Thus, in the Fourier representation, differentiation is simple—we just multiply by $i\,n$. (Note, however, that the choice of n is not unique due to aliasing; for the method to be convergent, a choice similar to that in the trigonometric interpolation section above should be used.) A linear differential equation with constant coefficients is transformed into an easily solvable algebraic equation. One then uses the inverse DFT to transform the result back into the ordinary spatial representation. Such an approach is called a spectral method.

Polynomial multiplication

Suppose we wish to compute the polynomial product $c(x) = a(x) \cdot b(x)$. The ordinary product expression for the coefficients of c involves a linear (acyclic) convolution, where indices do not "wrap around." This can be rewritten as a cyclic convolution by taking the coefficient vectors for $a(x)$ and $b(x)$ with constant term first, then appending zeros so that the resultant coefficient vectors $\mathbf{a}$ and $\mathbf{b}$ have dimension $d > \deg(a(x)) + \deg(b(x))$. Then,

$$\mathbf{c} = \mathbf{a} * \mathbf{b}$$

Where $\mathbf{c}$ is the vector of coefficients for $c(x)$, and the convolution operator $*$ is defined so

$$c_n = \sum_{m=0}^{d-1} a_m b_{n-m \ \mathrm{mod} \ d} \qquad n = 0, 1 \ldots, d-1$$

But convolution becomes multiplication under the DFT:

$$\mathcal{F}(\mathbf{c}) = \mathcal{F}(\mathbf{a})\mathcal{F}(\mathbf{b})$$

Here the vector product is taken elementwise. Thus the coefficients of the product polynomial $c(x)$ are just the terms $0, ..., \deg(a(x)) + \deg(b(x))$ of the coefficient vector

$$\mathbf{c} = \mathcal{F}^{-1}(\mathcal{F}(\mathbf{a})\mathcal{F}(\mathbf{b})).$$

With a fast Fourier transform, the resulting algorithm takes O $(N \log N)$ arithmetic operations. Due to its simplicity and speed, the Cooley–Tukey FFT algorithm, which is limited to composite sizes, is often chosen for the transform operation. In this case, d should be chosen as the smallest integer greater than the sum of the input polynomial degrees that is factorizable into small prime factors (e.g. 2, 3, and 5, depending upon the FFT implementation).

Multiplication of large integers

The fastest known algorithms for the multiplication of very large integers use the polynomial multiplication method outlined above. Integers can be treated as the value of a polynomial evaluated specifically at the number base, with the coefficients of the polynomial corresponding to the digits in that base. After polynomial multiplication, a relatively low-complexity carry-propagation step completes the multiplication.

Some discrete Fourier transform pairs

Some DFT pairs

$x_n = \frac{1}{N}\sum_{k=0}^{N-1} X_k e^{i2\pi kn/N}$	$X_k = \sum_{n=0}^{N-1} x_n e^{-i2\pi kn/N}$	Note
$x_n e^{i2\pi n\ell/N}$	$X_{k-\ell}$	Shift theorem
$x_{n-\ell}$	$X_k e^{-i2\pi k\ell/N}$	
$x_n \in \mathbb{R}$	$X_k = X_{N-k}^*$	Real DFT
a^n	$\begin{cases} N & \text{if } a = e^{i2\pi k/N} \\ \frac{1-a^N}{1-a\,e^{-i2\pi k/N}} & \text{otherwise} \end{cases}$	from the geometric progression formula
$\binom{N-1}{n}$	$\left(1 + e^{-i2\pi k/N}\right)^{N-1}$	from the binomial theorem
$\begin{cases} \frac{1}{W} & \text{if } 2n < W \text{ or } 2(N-n) < W \\ 0 & \text{otherwise} \end{cases}$	$\begin{cases} 1 & \text{if } k = 0 \\ \frac{\sin\left(\frac{\pi W k}{N}\right)}{W\sin\left(\frac{\pi k}{N}\right)} & \text{otherwise} \end{cases}$	x_n is a rectangular window function of W points centered on x_0, where W is an odd integer, and X_k is a sinc-like function

Derivation as Fourier series

The DFT can be derived as a truncation of the Fourier series of a periodic sequence of impulses.

Generalizations

Representation theory

The DFT can be interpreted as the complex-valued representation theory of the finite cyclic group. In other words, a sequence of n complex numbers can be thought of as an element of n-dimensional complex space $\mathbf{C}^n$, or equivalently a function from the finite cyclic group of order n to the complex numbers, $\mathbf{Z}/n\mathbf{Z} \to \mathbf{C}$. This latter may be suggestively written $\mathbf{C}^{\mathbf{Z}/n\mathbf{Z}}$ to emphasize that this is a complex vector space whose coordinates are indexed by the n-element set $\mathbf{Z}/n\mathbf{Z}$.

From this point of view, one may generalize the DFT to representation theory generally, or more narrowly to the representation theory of finite groups.

More narrowly still, one may generalize the DFT by either changing the target (taking values in a field other than the complex numbers), or the domain (a group other than a finite cyclic group), as detailed in the sequel.

Other fields

Many of the properties of the DFT only depend on the fact that $e^{-\frac{2\pi i}{N}}$ is a primitive root of unity, sometimes denoted ω_N or W_N (so that $\omega_N^N = 1$). Such properties include the completeness, orthogonality, Plancherel/Parseval, periodicity, shift, convolution, and unitarity properties above, as well as many FFT algorithms. For this reason, the discrete Fourier transform can be defined by using roots of unity in fields other than the complex numbers, and such generalizations are commonly called *number-theoretic transforms* (NTTs) in the case of finite fields. For more information, see number-theoretic transform and discrete Fourier transform (general).

Other finite groups

The standard DFT acts on a sequence $x_0, x_1, \ldots, x_{N-1}$ of complex numbers, which can be viewed as a function {0, 1, $\ldots$, $N-1$} → **C**. The multidimensional DFT acts on multidimensional sequences, which can be viewed as functions

$$\{0, 1, \ldots, N_1 - 1\} \times \cdots \times \{0, 1, \ldots, N_d - 1\} \to \mathbb{C}.$$

This suggests the generalization to Fourier transforms on arbitrary finite groups, which act on functions $G \to$ **C** where G is a finite group. In this framework, the standard DFT is seen as the Fourier transform on a cyclic group, while the multidimensional DFT is a Fourier transform on a direct sum of cyclic groups.

Alternatives

As with other Fourier transforms, there are various alternatives to the DFT for various applications, prominent among which are wavelets. The analog of the DFT is the discrete wavelet transform (DWT). From the point of view of time−frequency analysis, a key limitation of the Fourier transform is that it does not include *location* information, only *frequency* information, and thus has difficulty in representing transients. As wavelets have location as well as frequency, they are better able to represent location, at the expense of greater difficulty representing frequency. For details, see comparison of the discrete wavelet transform with the discrete Fourier transform.

See also

- DFT matrix
- Fast Fourier transform
- List of Fourier-related transforms
- FFTW

References

- Brigham, E. Oran (1988). *The fast Fourier transform and its applications*. Englewood Cliffs, N.J.: Prentice Hall. ISBN 0-13-307505-2.
- Oppenheim, Alan V.; Schafer, R. W.; and Buck, J. R. (1999). *Discrete-time signal processing*. Upper Saddle River, N.J.: Prentice Hall. ISBN 0-13-754920-2.
- Smith, Steven W. (1999). "Chapter 8: The Discrete Fourier Transform" [3]. *The Scientist and Engineer's Guide to Digital Signal Processing* (Second ed.). San Diego, Calif.: California Technical Publishing. ISBN 0-9660176-3-3.
- Cormen, Thomas H.; Charles E. Leiserson, Ronald L. Rivest, and Clifford Stein (2001). "Chapter 30: Polynomials and the FFT". *Introduction to Algorithms* (Second ed.). MIT Press and McGraw-Hill. pp. 822−848. ISBN 0-262-03293-7. esp. section 30.2: The DFT and FFT, pp. 830−838.
- P. Duhamel, B. Piron, and J. M. Etcheto (1988). "On computing the inverse DFT". *IEEE Trans. Acoust., Speech and Sig. Processing* **36** (2): 285−286. doi:10.1109/29.1519.
- J. H. McClellan and T. W. Parks (1972). "Eigenvalues and eigenvectors of the discrete Fourier transformation". *IEEE Trans. Audio Electroacoust.* **20** (1): 66−74. doi:10.1109/TAU.1972.1162342.

- Bradley W. Dickinson and Kenneth Steiglitz (1982). "Eigenvectors and functions of the discrete Fourier transform". *IEEE Trans. Acoust., Speech and Sig. Processing* **30** (1): 25−31. doi:10.1109/TASSP.1982.1163843. (Note that this paper has an apparent typo in its table of the eigenvalue multiplicities: the +i/−i columns are interchanged. The correct table can be found in McClellan and Parks, 1972, and is easily confirmed numerically.)
- F. A. Grünbaum (1982). "The eigenvectors of the discrete Fourier transform". *J. Math. Anal. Appl.* **88** (2): 355−363. doi:10.1016/0022-247X(82)90199-8.
- Natig M. Atakishiyev and Kurt Bernardo Wolf (1997). "Fractional Fourier-Kravchuk transform". *J. Opt. Soc. Am. A* **14** (7): 1467−1477. doi:10.1364/JOSAA.14.001467.
- C. Candan, M. A. Kutay and H. M.Ozaktas (2000). "The discrete fractional Fourier transform". *IEEE Trans. on Signal Processing* **48** (5): 1329−1337. doi:10.1109/78.839980.
- Magdy Tawfik Hanna, Nabila Philip Attalla Seif, and Waleed Abd El Maguid Ahmed (2004). "Hermite-Gaussian-like eigenvectors of the discrete Fourier transform matrix based on the singular-value decomposition of its orthogonal projection matrices". *IEEE Trans. Circ. Syst. I* **51** (11): 2245−2254. doi:10.1109/TCSI.2004.836850.
- Shamgar Gurevich and Ronny Hadani (2009). "On the diagonalization of the discrete Fourier transform". *Applied and Computational Harmonic Analysis* **27** (1): 87−99. doi:10.1016/j.acha.2008.11.003. preprint at arXiv:0808.3281.
- Shamgar Gurevich, Ronny Hadani, and Nir Sochen (2008). "The finite harmonic oscillator and its applications to sequences, communication and radar". *IEEE Transactions on Information Theory* **54** (9): 4239−4253. doi:10.1109/TIT.2008.926440. preprint at arXiv:0808.1495.
- Juan G. Vargas-Rubio and Balu Santhanam (2005). "On the multiangle centered discrete fractional Fourier transform". *IEEE Sig. Proc. Lett.* **12** (4): 273−276. doi:10.1109/LSP.2005.843762.
- J. Cooley, P. Lewis, and P. Welch (1969). "The finite Fourier transform". *IEEE Trans. Audio Electroacoustics* **17** (2): 77−85. doi:10.1109/TAU.1969.1162036.
- F.N. Kong (2008). "Analytic Expressions of Two Discrete Hermite-Gaussian Signals". *IEEE Trans. Circuits and Systems −II: Express Briefs.* **55** (1): 56−60. doi:10.1109/TCSII.2007.909865.

External links

- Interactive flash tutorial on the DFT [4]
- Mathematics of the Discrete Fourier Transform by Julius O. Smith III [5]
- Fast implementation of the DFT - coded in C and under General Public License (GPL) [6]
- Example of how DFT spectral analysis is used in engineering studies of the Otto Struve 2.1m telescope [7]
- The DFT "à Pied": Mastering The Fourier Transform in One Day [9]

References

[1] T. G. Stockham, Jr., "High-speed convolution and correlation," in 1966 *Proc. AFIPS Spring Joint Computing Conf.* Reprinted in Digital Signal Processing, L. R. Rabiner and C. M. Rader, editors, New York: IEEE Press, 1972.

[2] Santhanam, Balu; Santhanam, Thalanayar S. "*Discrete Gauss-Hermite functions and eigenvectors of the centered discrete Fourier transform*" (http://thamakau.usc.edu/Proceedings/ICASSP 2007/pdfs/0301385.pdf), Proceedings of the 32nd IEEE *International Conference on Acoustics, Speech, and Signal Processing* (ICASSP 2007, SPTM-P12.4), vol. III, pp. 1385-1388.

[3] http://www.dspguide.com/ch8/1.htm

[4] http://www.fourier-series.com/fourierseries2/DFT_tutorial.html

[5] http://ccrma.stanford.edu/~jos/mdft/mdft.html

[6] http://www.fftw.org

[7] http://nexus.as.utexas.edu/kuehne/3_4%22.html

Fast Fourier transform

A **fast Fourier transform** (**FFT**) is an efficient algorithm to compute the discrete Fourier transform (DFT) and its inverse. There are many distinct FFT algorithms involving a wide range of mathematics, from simple complex-number arithmetic to group theory and number theory; this article gives an overview of the available techniques and some of their general properties, while the specific algorithms are described in subsidiary articles linked below.

A DFT decomposes a sequence of values into components of different frequencies. This operation is useful in many fields (see discrete Fourier transform for properties and applications of the transform) but computing it directly from the definition is often too slow to be practical. An FFT is a way to compute the same result more quickly: computing a DFT of N points in the naive way, using the definition, takes $O(N^2)$ arithmetical operations, while an FFT can compute the same result in only $O(N \log N)$ operations. The difference in speed can be substantial, especially for long data sets where N may be in the thousands or millions—in practice, the computation time can be reduced by several orders of magnitude in such cases, and the improvement is roughly proportional to $N/\log(N)$. This huge improvement made many DFT-based algorithms practical; FFTs are of great importance to a wide variety of applications, from digital signal processing and solving partial differential equations to algorithms for quick multiplication of large integers.

The most well known FFT algorithms depend upon the factorization of N, but (contrary to popular misconception) there are FFTs with $O(N \log N)$ complexity for all N, even for prime N. Many FFT algorithms only depend on the fact that $e^{-\frac{2\pi i}{N}}$ is an N th primitive root of unity, and thus can be applied to analogous transforms over any finite field, such as number-theoretic transforms.

Since the inverse DFT is the same as the DFT, but with the opposite sign in the exponent and a $1/N$ factor, any FFT algorithm can easily be adapted for it.

Definition and speed

An FFT computes the DFT and produces exactly the same result as evaluating the DFT definition directly; the only difference is that an FFT is much faster. (In the presence of round-off error, many FFT algorithms are also much more accurate than evaluating the DFT definition directly, as discussed below.)

Let $x_0, ..., x_{N-1}$ be complex numbers. The DFT is defined by the formula

$$X_k = \sum_{n=0}^{N-1} x_n e^{-i2\pi k \frac{n}{N}} \qquad k = 0, \ldots, N-1.$$

Evaluating this definition directly requires $O(N^2)$ operations: there are N outputs X_k, and each output requires a sum of N terms. An FFT is any method to compute the same results in $O(N \log N)$ operations. More precisely, all known FFT algorithms require $\Theta(N \log N)$ operations (technically, O only denotes an upper bound), although there is no proof that better complexity is impossible.

To illustrate the savings of an FFT, consider the count of complex multiplications and additions. Evaluating the DFT's sums directly involves N^2 complex multiplications and $N(N-1)$ complex additions [of which $O(N)$ operations can be saved by eliminating trivial operations such as multiplications by 1]. The well-known radix-2 Cooley−Tukey algorithm, for N a power of 2, can compute the same result with only $(N/2) \log_2 N$ complex multiplies (again, ignoring simplifications of multiplications by 1 and similar) and $N \log_2 N$ complex additions. In practice, actual performance on modern computers is usually dominated by factors other than arithmetic and is a complicated subject (see, e.g., Frigo & Johnson, 2005), but the overall improvement from $\Theta(N^2)$ to $\Theta(N \log N)$ remains.

Computational issues

Bounds on complexity and operation counts

A fundamental question of longstanding theoretical interest is to prove lower bounds on the complexity and exact operation counts of fast Fourier transforms, and many open problems remain. It is not even rigorously proved whether DFTs truly require $\Omega(N \log N)$ (i.e., order $N \log N$ or greater) operations, even for the simple case of power of two sizes, although no algorithms with lower complexity are known. In particular, the count of arithmetic operations is usually the focus of such questions, although actual performance on modern-day computers is determined by many other factors such as cache or CPU pipeline optimization.

Following pioneering work by Winograd (1978), a tight $\Theta(N)$ lower bound *is* known for the number of real multiplications required by an FFT. It can be shown that only $4N - 2\log_2^2 N - 2\log_2 N - 4$ irrational real multiplications are required to compute a DFT of power-of-two length $N = 2^m$. Moreover, explicit algorithms that achieve this count are known (Heideman & Burrus, 1986; Duhamel, 1990). Unfortunately, these algorithms require too many additions to be practical, at least on modern computers with hardware multipliers.

A tight lower bound is *not* known on the number of required additions, although lower bounds have been proved under some restrictive assumptions on the algorithms. In 1973, Morgenstern proved an $\Omega(N \log N)$ lower bound on the addition count for algorithms where the multiplicative constants have bounded magnitudes (which is true for most but not all FFT algorithms). Pan (1986) proved an $\Omega(N \log N)$ lower bound assuming a bound on a measure of the FFT algorithm's "asynchronicity", but the generality of this assumption is unclear. For the case of power-of-two N, Papadimitriou (1979) argued that the number $N \log_2 N$ of complex-number additions achieved by Cooley–Tukey algorithms is *optimal* under certain assumptions on the graph of the algorithm (his assumptions imply, among other things, that no additive identities in the roots of unity are exploited). (This argument would imply that at least $2N \log_2 N$ real additions are required, although this is not a tight bound because extra additions are required as part of complex-number multiplications.) Thus far, no published FFT algorithm has achieved fewer than $N \log_2 N$ complex-number additions (or their equivalent) for power-of-two N.

A third problem is to minimize the *total* number of real multiplications and additions, sometimes called the "arithmetic complexity" (although in this context it is the exact count and not the asymptotic complexity that is being considered). Again, no tight lower bound has been proven. Since 1968, however, the lowest published count for power-of-two N was long achieved by the split-radix FFT algorithm, which requires $4N \log_2 N - 6N + 8$ real multiplications and additions for $N > 1$. This was recently reduced to $\sim \frac{34}{9} N \log_2 N$ (Johnson and Frigo, 2007; Lundy and Van Buskirk, 2007).

Most of the attempts to lower or prove the complexity of FFT algorithms have focused on the ordinary complex-data case, because it is the simplest. However, complex-data FFTs are so closely related to algorithms for related problems such as real-data FFTs, discrete cosine transforms, discrete Hartley transforms, and so on, that any improvement in one of these would immediately lead to improvements in the others (Duhamel & Vetterli, 1990).

Accuracy and approximations

All of the FFT algorithms discussed below compute the DFT exactly (in exact arithmetic, i.e. neglecting floating-point errors). A few "FFT" algorithms have been proposed, however, that compute the DFT *approximately*, with an error that can be made arbitrarily small at the expense of increased computations. Such algorithms trade the approximation error for increased speed or other properties. For example, an approximate FFT algorithm by Edelman et al. (1999) achieves lower communication requirements for parallel computing with the help of a fast multipole method. A wavelet-based approximate FFT by Guo and Burrus (1996) takes sparse inputs/outputs (time/frequency localization) into account more efficiently than is possible with an exact FFT. Another algorithm for approximate computation of a subset of the DFT outputs is due to Shentov et al. (1995). Only the Edelman algorithm

works equally well for sparse and non-sparse data, however, since it is based on the compressibility (rank deficiency) of the Fourier matrix itself rather than the compressibility (sparsity) of the data.

Even the "exact" FFT algorithms have errors when finite-precision floating-point arithmetic is used, but these errors are typically quite small; most FFT algorithms, e.g. Cooley−Tukey, have excellent numerical properties. The upper bound on the relative error for the Cooley−Tukey algorithm is O(ε log N), compared to O($\varepsilon N^{3/2}$) for the naïve DFT formula (Gentleman and Sande, 1966), where ε is the machine floating-point relative precision. In fact, the root mean square (rms) errors are much better than these upper bounds, being only O($\varepsilon \sqrt{\log N}$) for Cooley−Tukey and O($\varepsilon \sqrt{N}$) for the naïve DFT (Schatzman, 1996). These results, however, are very sensitive to the accuracy of the twiddle factors used in the FFT (i.e. the trigonometric function values), and it is not unusual for incautious FFT implementations to have much worse accuracy, e.g. if they use inaccurate trigonometric recurrence formulas. Some FFTs other than Cooley−Tukey, such as the Rader-Brenner algorithm, are intrinsically less stable.

In fixed-point arithmetic, the finite-precision errors accumulated by FFT algorithms are worse, with rms errors growing as O($\sqrt{N}$) for the Cooley−Tukey algorithm (Welch, 1969). Moreover, even achieving this accuracy requires careful attention to scaling in order to minimize the loss of precision, and fixed-point FFT algorithms involve rescaling at each intermediate stage of decompositions like Cooley−Tukey.

To verify the correctness of an FFT implementation, rigorous guarantees can be obtained in O(N log N) time by a simple procedure checking the linearity, impulse-response, and time-shift properties of the transform on random inputs (Ergün, 1995).

Algorithms

Cooley−Tukey algorithm

By far the most common FFT is the Cooley−Tukey algorithm. This is a divide and conquer algorithm that recursively breaks down a DFT of any composite size $N = N_1 N_2$ into many smaller DFTs of sizes N_1 and N_2, along with O(N) multiplications by complex roots of unity traditionally called twiddle factors (after Gentleman and Sande, 1966).

This method (and the general idea of an FFT) was popularized by a publication of J. W. Cooley and J. W. Tukey in 1965, but it was later discovered (Heideman & Burrus, 1984) that those two authors had independently re-invented an algorithm known to Carl Friedrich Gauss around 1805 (and subsequently rediscovered several times in limited forms).

The most well-known use of the Cooley−Tukey algorithm is to divide the transform into two pieces of size $N/2$ at each step, and is therefore limited to power-of-two sizes, but any factorization can be used in general (as was known to both Gauss and Cooley/Tukey). These are called the **radix-2** and **mixed-radix** cases, respectively (and other variants such as the split-radix FFT have their own names as well). Although the basic idea is recursive, most traditional implementations rearrange the algorithm to avoid explicit recursion. Also, because the Cooley−Tukey algorithm breaks the DFT into smaller DFTs, it can be combined arbitrarily with any other algorithm for the DFT, such as those described below.

Other FFT algorithms

There are other FFT algorithms distinct from Cooley−Tukey. For $N = N_1 N_2$ with coprime N_1 and N_2, one can use the Prime-Factor (Good-Thomas) algorithm (PFA), based on the Chinese Remainder Theorem, to factorize the DFT similarly to Cooley−Tukey but without the twiddle factors. The Rader-Brenner algorithm (1976) is a Cooley−Tukey-like factorization but with purely imaginary twiddle factors, reducing multiplications at the cost of increased additions and reduced numerical stability; it was later superseded by the split-radix variant of Cooley−Tukey (which achieves the same multiplication count but with fewer additions and without sacrificing accuracy). Algorithms that recursively factorize the DFT into smaller operations other than DFTs include the Bruun

and QFT algorithms. (The Rader-Brenner and QFT algorithms were proposed for power-of-two sizes, but it is possible that they could be adapted to general composite n. Bruun's algorithm applies to arbitrary even composite sizes.) Bruun's algorithm, in particular, is based on interpreting the FFT as a recursive factorization of the polynomial $z^N - 1$, here into real-coefficient polynomials of the form $z^M - 1$ and $z^{2M} + az^M + 1$.

Another polynomial viewpoint is exploited by the Winograd algorithm, which factorizes $z^N - 1$ into cyclotomic polynomials—these often have coefficients of 1, 0, or −1, and therefore require few (if any) multiplications, so Winograd can be used to obtain minimal-multiplication FFTs and is often used to find efficient algorithms for small factors. Indeed, Winograd showed that the DFT can be computed with only $O(N)$ irrational multiplications, leading to a proven achievable lower bound on the number of multiplications for power-of-two sizes; unfortunately, this comes at the cost of many more additions, a tradeoff no longer favorable on modern processors with hardware multipliers. In particular, Winograd also makes use of the PFA as well as an algorithm by Rader for FFTs of *prime* sizes.

Rader's algorithm, exploiting the existence of a generator for the multiplicative group modulo prime N, expresses a DFT of prime size n as a cyclic convolution of (composite) size $N - 1$, which can then be computed by a pair of ordinary FFTs via the convolution theorem (although Winograd uses other convolution methods). Another prime-size FFT is due to L. I. Bluestein, and is sometimes called the chirp-z algorithm; it also re-expresses a DFT as a convolution, but this time of the *same* size (which can be zero-padded to a power of two and evaluated by radix-2 Cooley–Tukey FFTs, for example), via the identity $nk = -(k-n)^2/2 + n^2/2 + k^2/2$.

FFT algorithms specialized for real and/or symmetric data

In many applications, the input data for the DFT are purely real, in which case the outputs satisfy the symmetry

$$X_{N-k} = X_k^*,$$

and efficient FFT algorithms have been designed for this situation (see e.g. Sorensen, 1987). One approach consists of taking an ordinary algorithm (e.g. Cooley–Tukey) and removing the redundant parts of the computation, saving roughly a factor of two in time and memory. Alternatively, it is possible to express an *even*-length real-input DFT as a complex DFT of half the length (whose real and imaginary parts are the even/odd elements of the original real data), followed by O(*N*) post-processing operations.

It was once believed that real-input DFTs could be more efficiently computed by means of the discrete Hartley transform (DHT), but it was subsequently argued that a specialized real-input DFT algorithm (FFT) can typically be found that requires fewer operations than the corresponding DHT algorithm (FHT) for the same number of inputs. Bruun's algorithm (above) is another method that was initially proposed to take advantage of real inputs, but it has not proved popular.

There are further FFT specializations for the cases of real data that have even/odd symmetry, in which case one can gain another factor of (roughly) two in time and memory and the DFT becomes the discrete cosine/sine transform(s) (DCT/DST). Instead of directly modifying an FFT algorithm for these cases, DCTs/DSTs can also be computed via FFTs of real data combined with O(*N*) pre/post processing.

Multidimensional FFTs

As defined in the multidimensional DFT article, the multidimensional DFT

$$X_{\mathbf{k}} = \sum_{\mathbf{n}=0}^{\mathbf{N}-1} e^{-2\pi i \mathbf{k} \cdot (\mathbf{n}/\mathbf{N})} x_{\mathbf{n}}$$

transforms an array $x_{\mathbf{n}}$ with a d-dimensional vector of indices $\mathbf{n} = (n_1, n_2, \ldots, n_d)$ by a set of d nested summations (over $n_j = 0 \ldots N_j - 1$ for each j), where the division $\mathbf{n}/\mathbf{N}$, defined as $\mathbf{n}/\mathbf{N} = (n_1/N_1, \cdots, n_d/N_d)$, is performed element-wise. Equivalently, it is simply the composition of a sequence of d sets of one-dimensional DFTs, performed along one dimension at a time (in any order).

This compositional viewpoint immediately provides the simplest and most common multidimensional DFT algorithm, known as the **row-column** algorithm (after the two-dimensional case, below). That is, one simply performs a sequence of d one-dimensional FFTs (by any of the above algorithms): first you transform along the n_1 dimension, then along the n_2 dimension, and so on (or actually, any ordering will work). This method is easily shown to have the usual $O(N \log N)$ complexity, where $N = N_1 N_2 \cdots N_d$ is the total number of data points transformed. In particular, there are N/N_1 transforms of size N_1, etcetera, so the complexity of the sequence of FFTs is:

$$\frac{N}{N_1} O(N_1 \log N_1) + \cdots + \frac{N}{N_d} O(N_d \log N_d)$$

$$= O\left(N\left[\log N_1 + \cdots + \log N_d\right]\right) = O(N \log N).$$

In two dimensions, the $x_{\mathbf{k}}$ can be viewed as an $n_1 \times n_2$ matrix, and this algorithm corresponds to first performing the FFT of all the rows and then of all the columns (or vice versa), hence the name.

In more than two dimensions, it is often advantageous for cache locality to group the dimensions recursively. For example, a three-dimensional FFT might first perform two-dimensional FFTs of each planar "slice" for each fixed n_1, and then perform the one-dimensional FFTs along the n_1 direction. More generally, an asymptotically optimal cache-oblivious algorithm consists of recursively dividing the dimensions into two groups $(n_1, \cdots, n_{d/2})$ and $(n_{d/2+1}, \cdots, n_d)$ that are transformed recursively (rounding if d is not even) (see Frigo and Johnson, 2005). Still, this remains a straightforward variation of the row-column algorithm that ultimately requires only a one-dimensional FFT algorithm as the base case, and still has $O(N \log N)$ complexity. Yet another variation is to perform matrix transpositions in between transforming subsequent dimensions, so that the transforms operate on contiguous data; this is especially important for out-of-core and distributed memory situations where accessing non-contiguous data is extremely time-consuming.

There are other multidimensional FFT algorithms that are distinct from the row-column algorithm, although all of them have $O(N \log N)$ complexity. Perhaps the simplest non-row-column FFT is the vector-radix FFT algorithm, which is a generalization of the ordinary Cooley–Tukey algorithm where one divides the transform dimensions by a vector $\mathbf{r} = (r_1, r_2, \cdots, r_d)$ of radices at each step. (This may also have cache benefits.) The simplest case of vector-radix is where all of the radices are equal (e.g. vector-radix-2 divides *all* of the dimensions by two), but this is not necessary. Vector radix with only a single non-unit radix at a time, i.e. $\mathbf{r} = (1, \cdots, 1, r, 1, \cdots, 1)$, is essentially a row-column algorithm. Other, more complicated, methods include polynomial transform algorithms due to Nussbaumer (1977), which view the transform in terms of convolutions and polynomial products. See Duhamel and Vetterli (1990) for more information and references.

Other generalizations

An $O(N^{5/2} \log N)$ generalization to spherical harmonics on the sphere S^2 with N^2 nodes was described by Mohlenkamp (1999), along with an algorithm conjectured (but not proven) to have $O(N^2 \log^2 N)$ complexity; Mohlenkamp also provides an implementation in the libftsh library [1]. A spherical-harmonic algorithm with $O(N^2 \log N)$ complexity is described by Rokhlin and Tygert (2006).

Various groups have also published "FFT" algorithms for non-equispaced data, as reviewed in Potts *et al.* (2001). Such algorithms do not strictly compute the DFT (which is only defined for equispaced data), but rather some approximation thereof (a non-uniform discrete Fourier transform, or NDFT, which itself is often computed only approximately).

See also

- Split-radix FFT algorithm
- Prime-factor FFT algorithm
- Bruun's FFT algorithm
- Rader's FFT algorithm
- Bluestein's FFT algorithm
- Butterfly diagram - a diagram used to describe FFTs.
- Odlyzko–Schönhage algorithm applies the FFT to finite Dirichlet series.
- Overlap add/Overlap save - efficient convolution methods using FFT for long signals
- Spectral music (involves application of FFT analysis to musical composition)
- Spectrum analyzers - Devices that perform an FFT
- FFTW "Fastest Fourier Transform in the West" - 'C' library for the discrete Fourier transform (DFT) in one or more dimensions.
- Time Series
- Math Kernel Library

References

- N. Brenner and C. Rader, 1976, A New Principle for Fast Fourier Transformation [2], *IEEE Acoustics, Speech & Signal Processing* **24**: 264-266.
- Brigham, E.O. (2002), *The Fast Fourier Transform*, New York: Prentice-Hall
- Cooley, James W., and John W. Tukey, 1965, "An algorithm for the machine calculation of complex Fourier series," *Math. Comput.* **19**: 297–301.
- Thomas H. Cormen, Charles E. Leiserson, Ronald L. Rivest, and Clifford Stein, 2001. *Introduction to Algorithms*, 2nd. ed. MIT Press and McGraw-Hill. ISBN 0-262-03293-7. Especially chapter 30, "Polynomials and the FFT."
- Pierre Duhamel, 1990, Algorithms meeting the lower bounds on the multiplicative complexity of length- 2^n DFTs and their connection with practical algorithms (doi:10.1109/29.60070), *IEEE Trans. Acoust. Speech. Sig. Proc.* **38**: 1504-151.
- P. Duhamel and M. Vetterli, 1990, Fast Fourier transforms: a tutorial review and a state of the art (doi:10.1016/0165-1684(90)90158-U), *Signal Processing* **19**: 259–299.
- A. Edelman, P. McCorquodale, and S. Toledo, 1999, The Future Fast Fourier Transform? (doi:10.1137/S1064827597316266), *SIAM J. Sci. Computing* **20**: 1094–1114.
- Funda Ergün, 1995, Testing multivariate linear functions: Overcoming the generator bottleneck (doi:10.1145/225058.225167), *Proc. 27th ACM Symposium on the Theory of Computing*: 407–416.
- M. Frigo and S. G. Johnson, 2005, "The Design and Implementation of FFTW3 [3]," *Proceedings of the IEEE* **93**: 216–231.

- Carl Friedrich Gauss, 1866. "Nachlass: Theoria interpolationis methodo nova tractata," *Werke* band **3**, 265–327. Göttingen: Königliche Gesellschaft der Wissenschaften.
- W. M. Gentleman and G. Sande, 1966, "Fast Fourier transforms—for fun and profit," *Proc. AFIPS* **29**: 563–578.
- H. Guo and C. S. Burrus, 1996, Fast approximate Fourier transform via wavelets transform (doi:10.1117/12.255236), *Proc. SPIE Intl. Soc. Opt. Eng.* **2825**: 250–259.
- H. Guo, G. A. Sitton, C. S. Burrus, 1994, The Quick Discrete Fourier Transform (doi:10.1109/ICASSP.1994.389994), *Proc. IEEE Conf. Acoust. Speech and Sig. Processing (ICASSP)* **3**: 445–448.
- Heideman, M. T., D. H. Johnson, and C. S. Burrus, "Gauss and the history of the fast Fourier transform [4]," IEEE ASSP Magazine, 1, (4), 14–21 (1984).
- Michael T. Heideman and C. Sidney Burrus, 1986, On the number of multiplications necessary to compute a length- 2^n DFT [5], *IEEE Trans. Acoust. Speech. Sig. Proc.* **34**: 91-95.
- S. G. Johnson and M. Frigo, 2007. "A modified split-radix FFT with fewer arithmetic operations [6]," *IEEE Trans. Signal Processing* **55** (1): 111–119.
- T. Lundy and J. Van Buskirk, 2007. "A new matrix approach to real FFTs and convolutions of length 2^k," *Computing* **80** (1): 23-45.
- Jacques Morgenstern, 1973, Note on a lower bound of the linear complexity of the fast Fourier transform (doi:10.1145/321752.321761), *J. ACM* **20**: 305-306.
- M. J. Mohlenkamp, 1999, "A fast transform for spherical harmonics", *J. Fourier Anal. Appl.* **5**, 159–184. [7] (preprint [8])
- H. J. Nussbaumer, 1977, Digital filtering using polynomial transforms (doi:10.1049/el:19770280), *Electronics Lett.* **13**: 386-387.
- V. Pan, 1986, The trade-off between the additive complexity and the asyncronicity of linear and bilinear algorithms (doi:10.1016/0020-0190(86)90035-9), *Information Proc. Lett.* **22**: 11-14.
- Christos H. Papadimitriou, 1979, Optimality of the fast Fourier transform (doi:10.1145/322108.322118), *J. ACM* **26**: 95-102.
- D. Potts, G. Steidl, and M. Tasche, 2001. "Fast Fourier transforms for nonequispaced data: A tutorial [9]", in: J.J. Benedetto and P. Ferreira (Eds.), *Modern Sampling Theory: Mathematics and Applications* (Birkhauser).
- Vladimir Rokhlin and Mark Tygert, 2006, "Fast algorithms for spherical harmonic expansions [10]," *SIAM J. Sci. Computing* **27** (6): 1903-1928.
- James C. Schatzman, 1996, Accuracy of the discrete Fourier transform and the fast Fourier transform [11], *SIAM J. Sci. Comput.* **17**: 1150–1166.
- O. V. Shentov, S. K. Mitra, U. Heute, and A. N. Hossen, 1995, Subband DFT. I. Definition, interpretations and extensions (doi:10.1016/0165-1684(94)00103-7), *Signal Processing* **41**: 261–277.
- H. V. Sorensen, D. L. Jones, M. T. Heideman, and C. S. Burrus, 1987, Real-valued fast Fourier transform algorithms [12], *IEEE Trans. Acoust. Speech Sig. Processing* **ASSP-35**: 849–863. See also Corrections to "Real-valued fast Fourier transform algorithms" [13]
- Peter D. Welch, 1969, A fixed-point fast Fourier transform error analysis [14], *IEEE Trans. Audio Electroacoustics* **17**: 151–157.
- S. Winograd, 1978, On computing the discrete Fourier transform [15], *Math. Computation* **32**: 175-199.

External links

- *Fast Fourier Transforms* [16], Connexions online book edited by C. Sidney Burrus, with chapters by C. Sidney Burrus, Ivan Selesnick, Markus Pueschel, Matteo Frigo, and Steven G. Johnson (2008).
- Links to FFT code and information online. [17]
- National Taiwan University - FFT [18]
- FFT programming in C++ — Cooley–Tukey algorithm. [19]
- Online documentation, links, book, and code. [20]
- Using FFT to construct aggregate probability distributions [21]
- Sri Welaratna, "30 years of FFT Analyzers [22]", *Sound and Vibration* (January 1997, 30th anniversary issue). A historical review of hardware FFT devices.
- FFT Basics and Case Study Using Multi-Instrument [23]
- FFT Textbook notes, PPTs [24] at Holistic Numerical Methods Institute.
- ALGLIB FFT Code [25] GPL Licensed multilanguage (VBA, C++, Pascal, etc.) numerical analysis and data processing library.

References

[1] http://www.math.ohiou.edu/~mjm/research/libftsh.html
[2] http://ieeexplore.ieee.org/search/wrapper.jsp?arnumber=1162805
[3] http://fftw.org/fftw-paper-ieee.pdf
[4] http://ieeexplore.ieee.org/xpls/abs_all.jsp?arnumber=1162257
[5] http://ieeexplore.ieee.org/xpl/freeabs_all.jsp?arnumber=1164785
[6] http://www.fftw.org/newsplit.pdf
[7] http://dx.doi.org/10.1007/BF01261607
[8] http://www.math.ohiou.edu/~mjm/research/MOHLEN1999P.pdf
[9] http://www.tu-chemnitz.de/~potts/paper/ndft.pdf
[10] http://pantheon.yale.edu/~mwt7/sph2.pdf
[11] http://portal.acm.org/citation.cfm?id=240432
[12] http://ieeexplore.ieee.org/search/wrapper.jsp?arnumber=1165220
[13] http://ieeexplore.ieee.org/search/wrapper.jsp?arnumber=1165284
[14] http://ieeexplore.ieee.org/search/wrapper.jsp?arnumber=1162035
[15] http://www.jstor.org/view/00255718/di970565/97p0015m/0
[16] http://cnx.org/content/col10550/
[17] http://www.fftw.org/links.html
[18] http://www.cmlab.csie.ntu.edu.tw/cml/dsp/training/coding/transform/fft.html
[19] http://www.librow.com/articles/article-10
[20] http://www.jjj.de/fxt/
[21] http://www.vosesoftware.com/ModelRiskHelp/index.htm#Aggregate_distributions/
    Aggregate_modeling_-_Fast_Fourier_Transform_FFT_method.htm
[22] http://www.dataphysics.com/support/library/downloads/articles/DP-30%20Years%20of%20FFT.pdf
[23] http://www.multi-instrument.com/doc/D1002/FFT_Basics_and_Case_Study_using_Multi-Instrument_D1002.pdf
[24] http://numericalmethods.eng.usf.edu/topics/fft.html
[25] http://www.alglib.net/fasttransforms/fft.php

Fourier transform spectroscopy

Fourier transform spectroscopy is a measurement technique whereby spectra are collected based on measurements of the coherence of a radiative source, using time-domain or space-domain measurements of the electromagnetic radiation or other type of radiation. It can be applied to a variety of types of spectroscopy including optical spectroscopy, infrared spectroscopy (FTIR, FT-NIRS), nuclear magnetic resonance (NMR) and magnetic resonance spectroscopic imaging (MRSI)[1] , mass spectrometry and electron spin resonance spectroscopy. There are several methods for measuring the temporal coherence of the light, including the continuous wave *Michelson* or *Fourier transform* spectrometer and the pulsed Fourier transform spectrograph (which is more sensitive and has a much shorter sampling time than conventional spectroscopic techniques, but is only applicable in a laboratory environment).

The term *Fourier transform spectroscopy* reflects the fact that in all these techniques, a Fourier transform is required to turn the raw data into the actual spectrum.

Conceptual introduction

Measuring an emission spectrum

One of the most basic tasks in spectroscopy is to characterize the spectrum of a light source: How much light is emitted at each different wavelength. The most straightforward way to measure a spectrum is to pass the light through a monochromator, an instrument that blocks all of the light *except* the light at a certain wavelength (the un-blocked wavelength is set by a knob on the monochromator). Then the intensity of this remaining (single-wavelength) light is measured. The measured intensity directly indicates how much light is emitted at that wavelength. By varying the monochromator's wavelength setting, the full spectrum can be measured. This simple scheme in fact describes how *some* spectrometers work.

Fourier transform spectroscopy is a less intuitive way to get the same information. Rather than allowing only one wavelength at a time to pass through to the detector, this technique lets through a beam

An example of a spectrum: The spectrum of light emitted by the blue flame of a butane torch. The horizontal axis is the wavelength of light, and the vertical axis represents how much light is emitted by the torch at that wavelength.

containing many different wavelengths of light at once, and measures the *total* beam intensity. Next, the beam is modified to contain a *different* combination of wavelengths, giving a second data point. This process is repeated many times. Afterwards, a computer takes all this data and works backwards to infer how much light there is at each wavelength.

To be more specific, between the light source and the detector, there is a certain configuration of mirrors that allows some wavelengths to pass through but blocks others (due to wave interference). The beam is modified for each new data point by moving one of the mirrors; this changes the set of wavelengths that can pass through.

As mentioned, computer processing is required to turn the raw data (light intensity for each mirror position) into the desired result (light intensity for each wavelength). The processing required turns out to be a common algorithm called the Fourier transform (hence the name, "Fourier transform spectroscopy"). The raw data is sometimes called an "interferogram".
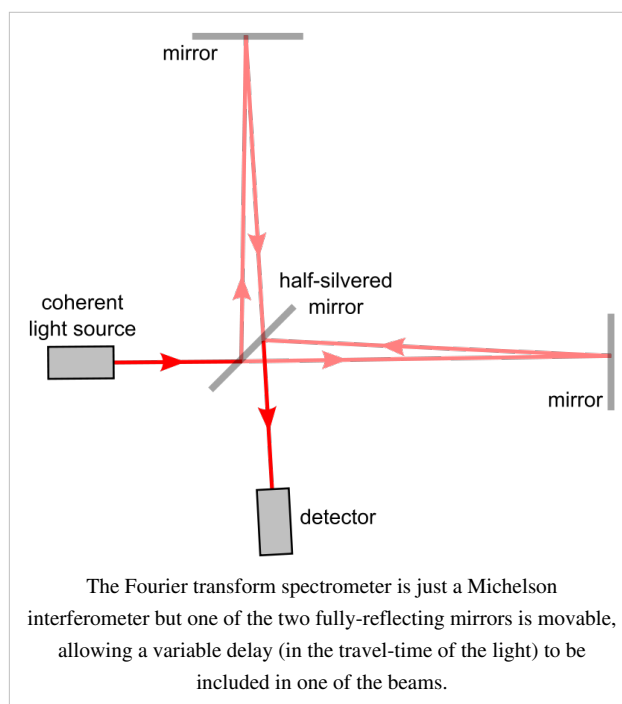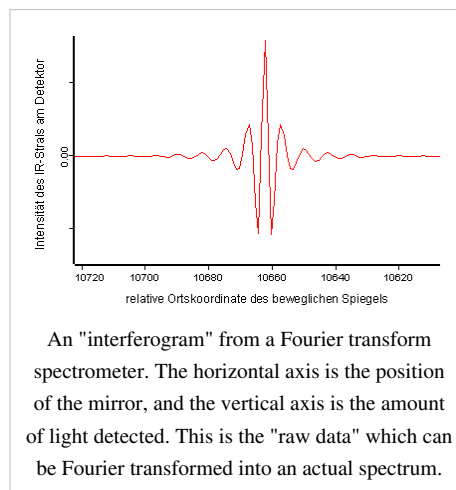
Measuring an absorption spectrum

The method of Fourier transform spectroscopy can also be used for absorption spectroscopy. The primary example is "FTIR Spectroscopy", a common technique in chemistry.

In general, the goal of absorption spectroscopy is to measure how well a sample absorbs or transmits light at each different wavelength. Although absorption spectroscopy and emission spectroscopy are different in principle, they are closely related in practice; any technique for emission spectroscopy can also be used for absorption spectroscopy. First, the emission spectrum of a broadband lamp is measured (this is called the "background spectrum"). Second, the emission spectrum of the same lamp *shining through the sample* is measured (this is called the "sample spectrum"). The sample will absorb some of the light, causing the spectra to be different. The ratio of the "sample spectrum" to the "background spectrum" is directly related to the sample's absorption spectrum.

An "interferogram" from a Fourier transform spectrometer. The horizontal axis is the position of the mirror, and the vertical axis is the amount of light detected. This is the "raw data" which can be Fourier transformed into an actual spectrum.

Accordingly, the technique of "Fourier transform spectroscopy" can be used both for measuring emission spectra (for example, the emission spectrum of a star), *and* absorption spectra (for example, the absorption spectrum of a glass of liquid).

Continuous wave *Michelson* or *Fourier transform* spectrograph

The Michelson spectrograph is similar to the instrument used in the Michelson-Morley experiment. Light from the source is split into two beams by a half-silvered mirror, one is reflected off a fixed mirror and one off a moving mirror which introduces a time delay—the Fourier transform spectrometer is just a Michelson interferometer with a movable mirror. The beams interfere, allowing the temporal coherence of the light to be measured at each different time delay setting, effectively converting the time domain into a spatial coordinate. By making measurements of the signal at many discrete positions of the moving mirror, the spectrum can be reconstructed using a Fourier transform of the temporal coherence of the light. Michelson spectrographs are capable of very high spectral resolution observations of very bright sources. The Michelson or Fourier transform spectrograph was popular for infra-red applications at a time when infra-red astronomy only had single pixel detectors.

The Fourier transform spectrometer is just a Michelson interferometer but one of the two fully-reflecting mirrors is movable, allowing a variable delay (in the travel-time of the light) to be included in one of the beams.

Imaging Michelson spectrometers are a possibility, but in general have been supplanted by imaging Fabry–Pérot instruments which are easier to construct.

Extracting the spectrum

The intensity as a function of the path length difference in the interferometer p and wavenumber $\tilde{\nu} = 1/\lambda$ is [2]

$$I(p, \tilde{\nu}) = I(\tilde{\nu})[1 + \cos(2\pi\tilde{\nu}p)],$$

where $I(\tilde{\nu})$ is the spectrum to be determined. Note that it is not necessary for $I(\tilde{\nu})$ to be modulated by the sample before the interferometer. In fact, most FTIR spectrometers place the sample after the interferometer in the optical path. The total intensity at the detector is

$$I(p) = \int_0^\infty I(p, \tilde{\nu})d\tilde{\nu} = \int_0^\infty I(\tilde{\nu})[1 + \cos(2\pi\tilde{\nu}p)]d\tilde{\nu}.$$

This is just a Fourier cosine transform. The inverse gives us our desired result in terms of the measured quantity $I(p)$:

$$I(\tilde{\nu}) = 4 \int_0^\infty [I(p) - \tfrac{1}{2}I(p=0)] \cos(2\pi\tilde{\nu}p)dp.$$

Pulsed *Fourier transform* spectrometer

A pulsed *Fourier transform* spectrometer does not employ transmittance techniques. In the most general description of pulsed FT spectrometry, a sample is exposed to an energizing event which causes a periodic response. The frequency of the periodic response, as governed by the field conditions in the spectrometer, is indicative of the measured properties of the analyte.

Examples of pulsed Fourier transform spectrometry

In magnetic spectroscopy (EPR, NMR), an RF pulse in a strong ambient magnetic field is used as the energizing event. This turns the magnetic particles at an angle to the ambient field, resulting in gyration. The gyrating spins then induce a periodic current in a detector coil. Each spin exhibits a characteristic frequency of gyration (relative to the field strength) which reveals information about the analyte.

In Fourier transform mass spectrometry, the energizing event is the injection of the charged sample into the strong electromagnetic field of a cyclotron. These particles travel in circles, inducing a current in a fixed coil on one point in their circle. Each traveling particle exhibits a characteristic cyclotron frequency-field ratio revealing the masses in the sample.

Free induction decay

Pulsed FT spectrometry gives the advantage of requiring a single, time-dependent measurement which can easily deconvolute a set of similar but distinct signals. The resulting composite signal, is called a *free induction decay,* because typically the signal will decay due to inhomogeneities in sample frequency, or simply unrecoverable loss of signal due to entropic loss of the property being measured.

Stationary forms of Fourier transform spectrometers

In addition to the scanning forms of Fourier transform spectrometers, there are a number of stationary or self-scanned forms.[3] While the analysis of the interferometric output is similar to that of the typical scanning interferometer, significant differences apply, as shown in the published analyses. Some stationary forms retain the Fellgett multiplex advantage, and their use in the spectral region where detector noise limits apply is similar to the scanning forms of the FTS. In the photon-noise limited region, the application of stationary interferometers is dictated by specific consideration for the spectral region and the application.

Fellgett advantage

One of the most important advantages of Fourier transform spectroscopy was shown by P.B. Fellgett, an early advocate of the method. The Fellgett advantage, also known as the multiplex principle, states that a multiplex spectrometer such as the Fourier transform spectroscopy will produce a gain of the order of the square root of m in the signal-to-noise ratio of the resulting spectrum, when compared with an equivalent scanning monochromator, where m is the number of elements comprising the resulting spectrum when the measurement noise is dominated by detector noise.

Converting spectra from time domain to frequency domain

$$S(t) = \int_{-\infty}^{\infty} I(\nu) e^{-i\nu 2\pi t} \, d\nu$$

The sum is performed over all contributing frequencies to give a signal S(t) in the time domain.

$$I(\nu) = \int_{-\infty}^{\infty} S(t) e^{i\nu 2\pi t} dt$$

gives non-zero value when S(t) contains a component that matches the oscillating function.

Remember that

$$e^{ix} = \cos x + i \sin x$$

See also

- Applied spectroscopy
- Forensic chemistry
- Forensic polymer engineering
- Nuclear Magnetic Resonance
- Infrared spectroscopy

External links

- Description of how a Fourier transform spectrometer works [4]
- The Michelson or Fourier transform spectrograph [5]
- Internet Journal of Vibrational Spectroscopy - How FTIR works [6]
- Fourier Transform Spectroscopy Topical Meeting and Tabletop Exhibit [7]

References

[1] Antoine Abragam. 1968. *Principles of Nuclear Magnetic Resonance.*, Cambridge University Press: Cambridge, UK.

[2] Peter Atkins, Julio De Paula. 2006. *Physical Chemistry*, 8th ed. Oxford University Press: Oxford, UK.

[3] William H. Smith U.S. Patent 4976542 (http://www.google.com/patents?vid=4976542) Digital Array Scanned Interferometer, issued Dec. 11, 1990

[4] http://scienceworld.wolfram.com/physics/FourierTransformSpectrometer.html

[5] http://www.astro.livjm.ac.uk/courses/phys362/notes/

[6] http://www.ijvs.com/volume5/edition5/section1.html#Feature

[7] http://www.osa.org/meetings/topicalmeetings/fts/default.aspx

Nuclear magnetic resonance

Nuclear magnetic resonance (**NMR**) is a property that magnetic nuclei have in a magnetic field and applied electromagnetic (EM) pulse or pulses, which cause the nuclei to absorb energy from the EM pulse and radiate this energy back out. The energy radiated back out is at a specific resonance frequency which depends on the strength of the magnetic field and other factors. This allows the observation of specific quantum mechanical magnetic properties of an atomic nucleus. Many scientific techniques exploit NMR phenomena to study molecular physics, crystals and non-crystalline materials through NMR spectroscopy. NMR is also routinely used in advanced medical imaging techniques, such as in magnetic resonance imaging (MRI).

All stable isotopes that contain an odd number of protons and/or of neutrons (see Isotope) have an intrinsic magnetic moment and angular momentum, in other words a nonzero spin, while all nuclides with even numbers of both have spin 0. The most commonly studied nuclei are ^{1}H (the most NMR-sensitive isotope after the radioactive ^{3}H) and ^{13}C, although nuclei from isotopes of many other elements (e.g. ^{2}H, ^{10}B, ^{11}B, ^{14}N, ^{15}N, ^{17}O, ^{19}F, ^{23}Na, ^{29}Si, ^{31}P, ^{35}Cl, ^{113}Cd, ^{129}Xe, ^{195}Pt) are studied by high-field NMR spectroscopy as well.

A key feature of NMR is that the resonance frequency of a particular substance is directly proportional to the strength of the applied magnetic field. It is this feature that is exploited in imaging techniques; if a sample is placed in a non-uniform magnetic field then the resonance frequencies of the sample's nuclei depend on where in the field they are located. Since the resolution of the

World's First 1 GHz NMR Spectrometer (1000 MHz, 23.5 T) was installed at the new 'Centre de RMN à Très Hauts Champs' in Lyon, France in August 2009

Pacific Northwest National Laboratory's high magnetic field (800 MHz, 18.8 T) NMR spectrometer.

imaging techniques depends on how big the gradient of the field is, many efforts are made to develop more powerful magnets, often using superconductors. The effectiveness of NMR can also be improved using hyperpolarization, and/or using two-dimensional, three-dimensional and higher dimension multi-frequency techniques.

The principle of NMR usually involves two sequential steps:

- The alignment (polarization) of the magnetic nuclear spins in an applied, constant magnetic field $\mathbf{H}_0$.
- The perturbation of this alignment of the nuclear spins by employing an electro-magnetic, usually radio frequency (RF) pulse. The required perturbing frequency is dependent upon the static magnetic field ($\mathbf{H}_0$) and the nuclei of observation.

The two fields are usually chosen to be perpendicular to each other as this maximizes the NMR signal strength. The resulting response by the total magnetization ($\mathbf{M}$) of the nuclear spins is the phenomenon that is exploited in NMR spectroscopy and magnetic resonance imaging. Both use intense applied magnetic fields ($\mathbf{H}_0$) in order to achieve dispersion and very high stability to deliver spectral resolution, the details of which are described by chemical shifts, the Zeeman effect, and Knight shifts (in metals).

NMR phenomena are also utilized in low-field NMR, NMR spectroscopy and MRI in the Earth's magnetic field (referred to as Earth's field NMR), and in several types of magnetometers.

History

Discovery

Nuclear magnetic resonance was first described and measured in molecular beams by Isidor Rabi in 1938,[1] and in 1944, Rabi was awarded the Nobel Prize in physics for this work.[2] In 1946, Felix Bloch and Edward Mills Purcell expanded the technique for use on liquids and solids, for which they shared the Nobel Prize in physics in 1952.[3]

Purcell had worked on the development and radar applications during World War II at Massachusetts Institute of Technology's Radiation Laboratory. His work during that project on the production and detection of RF energy, and on the absorption of such RF energy by matter, preceded his discovery of NMR.

They noticed that magnetic nuclei, like ^{1}H and ^{31}P, could absorb RF energy when placed in a magnetic field of a strength specific to the identity of the nuclei. When this absorption occurs, the nucleus is described as being *in resonance*. Different atomic nuclei within a molecule resonate at different (radio) frequencies for the same magnetic field strength. The observation of such magnetic resonance frequencies of the nuclei present in a molecule allows any trained user to discover essential, chemical and structural information about the molecule.

The development of nuclear magnetic resonance as a technique of analytical chemistry and biochemistry parallels the development of electromagnetic technology and its introduction into civilian use.

Theory of nuclear magnetic resonance

Nuclear spin and magnets

All nucleons, that is neutrons and protons, composing any atomic nucleus, have the intrinsic quantum property of spin. The overall spin of the nucleus is determined by the spin quantum number S. If the number of both the protons and neutrons in a given nuclide are even then $S = 0$, i.e. there is no overall spin; just as electrons pair up in atomic orbitals, so do even numbers of protons or even numbers of neutrons (which are also spin-$\frac{1}{2}$ particles and hence fermions) pair up giving zero overall spin.

However, a proton and neutron will have lower energy when their spins are parallel, **not anti-parallel**, as this parallel spin alignment does not infringe upon the Pauli principle, but instead has to do with the quark structure of these two nucleons. Therefore, the spin ground state for the deuteron (the deuterium nucleus, or the ^{2}H isotope of hydrogen)—that has only a proton and a neutron—corresponds to a spin value of **1**, *not of zero*; the single, isolated deuteron is therefore exhibiting an NMR absorption spectrum characteristic of a quadrupolar nucleus of spin **1**, which in the 'rigid' state at very low temperatures is a characteristic ('Pake') *doublet*, (not a singlet as for a single, isolated ^{1}H, or any other isolated fermion or dipolar nucleus of spin 1/2). On the other hand, because of the Pauli

principle, the (radioactive) tritium isotope has to have a pair of anti-parallel spin neutrons (of total spin zero for the neutron spin couple), plus a proton of spin 1/2; therefore, the character of the tritium nucleus ('triton') is again magnetic dipolar, *not quadrupolar*—like its non-radioactive deuteron neighbor, and the tritium nucleus total spin value is again 1/2, just like for the simpler, abundant hydrogen isotope, ^{1}H nucleus (the *proton*). The NMR absorption (radio) frequency for tritium is however slightly higher than that of ^{1}H because the tritium nucleus has a slightly higher gyromagnetic ratio than ^{1}H. In many other cases of *non-radioactive* nuclei, the overall spin is also non-zero. For example, the ^{27}Al nucleus has an overall spin value $S = \frac{5}{2}$.

A non-zero spin is thus always associated with a non-zero magnetic moment (μ) via the relation $\mu = \gamma S$, where γ is the gyromagnetic ratio. It is this magnetic moment that allows the observation of NMR absorption spectra caused by transitions between nuclear spin levels. Most nuclides (with some rare exceptions) that have both even numbers of protons and even numbers of neutrons, also have zero nuclear magnetic moments-and also have zero magnetic dipole and quadrupole moments; therefore, such nuclides do not exhibit any NMR absorption spectra. Thus, ^{18}O is an example of a nuclide that has no NMR absorption, whereas ^{13}C, ^{31}P, ^{35}Cl and ^{37}Cl are nuclides that do exhibit NMR absorption spectra; the last two nuclei are quadrupolar nuclei whereas the preceding two nuclei (^{13}C and ^{31}P) are dipolar ones.

Electron spin resonance (ESR) is a related technique which detects transitions between electron spin levels instead of nuclear ones. The basic principles are similar; however, the instrumentation, data analysis and detailed theory are significantly different. Moreover, there is a much smaller number of molecules and materials with unpaired electron spins that exhibit ESR (or electron paramagnetic resonance (EPR)) absorption than those that have NMR absorption spectra. Significantly also, is the much greater sensitivity of ESR and EPR in comparison with NMR. Furthermore, ferromagnetic materials and thin films may exhibit 'very unusual', highly resolved ferromagnetic resonance (FMR) spectra, or ferromagnetic spin wave resonance (FSWR) excitations in non-crystalline solids such as ferromagnetic metallic glasses, well beyond the common single-transitions of most routine NMR, FMR and EPR studies.[4] [5]

Values of spin angular momentum

The angular momentum associated with nuclear spin is quantized. This means both that the magnitude of angular momentum is quantized (i.e. S can only take on a restricted range of values), and also that the orientation of the associated angular momentum is quantized. The associated quantum number is known as the magnetic quantum number, m, and can take values from $+S$ to $-S$, in integer steps. Hence for any given nucleus, there is a total of $2S + 1$ angular momentum states.

The z-component of the angular momentum vector (**S**) is therefore $S_z = m\hbar$, where $\hbar$ is the reduced Planck constant. The z-component of the magnetic moment is simply:

$$\mu_z = \gamma S_z = \gamma m \hbar$$

Spin behavior in a magnetic field

Consider nuclei which have a spin of one-half, like ^{1}H, ^{13}C or ^{19}F. The nucleus has two possible spin states: $m = \frac{1}{2}$ or $m = -\frac{1}{2}$ (also referred to as spin-up and spin-down, or sometimes α and β spin states, respectively). These states are degenerate, that is they have the same energy. Hence the number of atoms in these two states will be approximately equal at thermal equilibrium.

If a nucleus is placed in a magnetic field, however, the interaction between the nuclear magnetic moment and the external magnetic field mean the two states no longer have the same energy. The energy of a magnetic moment μ when in a magnetic field $\mathbf{B}_0$ is given by:

Splitting of nuclei spin states in an external magnetic field

$$E = -\mu \cdot \mathbf{B}_0 = -\mu_{\mathrm{x}} B_{0x} - \mu_{\mathrm{y}} B_{0y} - \mu_{\mathrm{z}} B_{0z}.$$

Usually the z axis is chosen to be along $\mathbf{B}_0$, and the above expression reduces to:

$$E = -\mu_{\mathrm{z}} B_0 ,$$

or alternatively:

$$E = -\gamma m \hbar B_0 .$$

As a result the different nuclear spin states have different energies in a non-zero magnetic field. In hand-waving terms, we can talk about the two spin states of a spin $\frac{1}{2}$ as being *aligned* either with or against the magnetic field. If γ is positive (true for most isotopes) then $m = \frac{1}{2}$ is the lower energy state.

The energy difference between the two states is:

$$\Delta E = \gamma \hbar B_0 ,$$

and this difference results in a small population bias toward the lower energy state.

Magnetic resonance by nuclei

Resonant absorption by nuclear spins will occur only when electromagnetic radiation of the correct frequency (e.g., equaling the Larmor precession rate) is being applied to match the energy difference between the nuclear spin levels in a constant magnetic field of the appropriate strength. The energy of an absorbed photon is then $E = h\nu_0$, where ν_0 is the resonance radiofrequency that has to match (that is, it has to be equal to) the Larmor precession frequency ν_L of the nuclear magnetization in the constant magnetic field $\mathbf{B}_0$. Hence, a magnetic resonance absorption will only occur when $\Delta E = h\nu_0$, which is when $\nu_0 = \gamma B_0/(2\pi)$. Such magnetic resonance frequencies typically correspond to the radio frequency (or RF) range of the electromagnetic spectrum for magnetic fields up to ~20 T. It is this magnetic resonant absorption which is detected in NMR.

Nuclear shielding

It might appear from the above that all nuclei of the same nuclide (and hence the same *g*) would resonate at the same frequency. This is not the case. The most important perturbation of the NMR frequency for applications of NMR is the 'shielding' effect of the surrounding electrons. In general, this electronic shielding reduces the magnetic field *at the nucleus* (which is what determines the NMR frequency).

As a result the energy gap is reduced, and the frequency required to achieve resonance is also reduced. This shift in the NMR frequency due to the electrons' molecular orbital coupling to the external magnetic field is called chemical shift, and it explains why NMR is able to probe the chemical structure of molecules which depends on the electron density distribution in the corresponding molecular orbitals. If a nucleus in a specific chemical group is shielded to a higher degree by a higher electron density of its surrounding molecular orbital, then its NMR frequency will be shifted "upfield" (that is, a lower chemical shift), whereas if it is less shielded by such surrounding electron density, then its NMR frequency will be shifted "downfield" (that is, a higher chemical shift).

Unless the local symmetry of such molecular orbitals is very high (leading to "isotropic" shift), the shielding effect will depend on the orientation of the molecule with respect to the external field ($\mathbf{B}_0$). In solid-state NMR spectroscopy, magic angle spinning is required to average out this orientation dependence in order to obtain values close to the average chemical shifts. This is unnecessary in conventional NMR investigations of molecules, since rapid molecular tumbling averages out the chemical shift anisotropy (CSA). In this case, the term "average" chemical shift (ACS) is used.

Relaxation

The process called population relaxation refers to nuclei that return to the thermodynamic state in the magnet. This process is also called T_1, "spin-lattice" or "longitudinal magnetic" relaxation, where T_1 refers to the mean time for an individual nucleus to return to its thermal equilibrium state of the spins. Once the nuclear spin population is relaxed, it can be probed again, since it is in the initial, equilibrium (mixed) state.

The precessing nuclei can also fall out of alignment with each other (returning the net magnetization vector to a non-precessing field) and stop producing a signal. This is called T_2 or *transverse relaxation*. Because of the difference in the actual relaxation mechanisms involved (for example, inter-molecular vs. intra-molecular magnetic dipole-dipole interactions), T_1 is always longer than T_2 (that is, slower spin-lattice relaxation, for example because of smaller dipole-dipole interaction effects). In practice, the value of T^*_2 which is the actually observed decay time of the observed NMR signal, or free induction decay, (to 1/e of the initial amplitude immediately after the resonant RF pulse)-- also depends on the static magnetic field inhomogeneity, which is quite significant. (There is also a smaller but significant contribution to the observed FID shortening from the RF inhomogeneity of the resonant pulse). In the corresponding FT-NMR spectrum—meaning the Fourier transform of the free induction decay--the T^*_2 time is inversely related to the width of the NMR signal in frequency units. Thus, a nucleus with a long T_2 relaxation time gives rise to a very sharp NMR peak in the FT-NMR spectrum for a very homogeneous ("well-shimmed") static magnetic field, whereas nuclei with shorter T_2 values give rise to broad FT-NMR peaks even when the magnet is shimmed well. Both T_1 and T_2 depend on the rate of molecular motions as well as the gyromagnetic ratios of both the resonating and their strongly interacting, next-neighbor nuclei that are not at resonance.

NMR spectroscopy

NMR spectroscopy is one of the principal techniques used to obtain physical, chemical, electronic and structural information about molecules due to either the chemical shift, Zeeman effect, or the Knight shift effect, or a combination of both, on the resonant frequencies of the nuclei present in the sample. It is a powerful technique that can provide detailed information on the topology, dynamics and three-dimensional structure of molecules in solution and the solid state. Thus, structural and dynamic information is obtainable (with or without "magic angle" spinning (MAS)) from NMR studies of quadrupolar nuclei (that is, those nuclei with spin $S > \frac{1}{2}$) even in the presence of magnetic dipole-dipole interaction broadening (or simply, dipolar broadening) which is always much smaller than the quadrupolar interaction strength because it is a magnetic vs. an electric interaction effect.

Additional structural and chemical information may be obtained by performing double-quantum NMR experiments for quadrupolar nuclei such as ^{2}H. Also, nuclear magnetic resonance is one of the techniques that has been used to design quantum automata, and also build elementary quantum computers.[6] [7]

900 MHz, 21.2 T NMR Magnet at HWB-NMR, Birmingham, UK

Continuous wave (CW) spectroscopy

In its first few decades, nuclear magnetic resonance spectrometers used a technique known as continuous-wave spectroscopy (CW spectroscopy). Although NMR spectra could be, and have been, obtained using a fixed magnetic field and sweeping the frequency of the electromagnetic radiation, this more typically involved using a fixed frequency source and varying the current (and hence magnetic field) in an electromagnet to observe the resonant absorption signals. This is the origin of the counterintuitive, but still common, "high" and "low" field terminology for low frequency and high frequency regions respectively of the NMR spectrum.

CW spectroscopy is inefficient in comparison to Fourier techniques (see below) as it probes the NMR response at individual frequencies in succession. As the NMR signal is intrinsically weak, the observed spectra suffer from a poor signal-to-noise ratio. This can be mitigated by signal averaging i.e. adding the spectra from repeated measurements. While the NMR signal is constant between scans and so adds linearly, the random noise adds more slowly—as the square-root of the number of spectra (see Random walk). Hence the overall ratio of the signal to the noise increases as the square-root of the number of spectra measured.

Fourier transform spectroscopy

Most applications of NMR involve full NMR spectra, that is, the intensity of the NMR signal as a function of frequency. Early attempts to acquire the NMR spectrum more efficiently than simple CW methods involved irradiating simultaneously with more than one frequency. A revolution in NMR occurred when short pulses of radio-frequency were used (centered at the middle of the NMR spectrum). In simple terms, a short square pulse of a given "carrier" frequency "contains" a range of frequencies centered about the carrier frequency, with the range of excitation (bandwidth) being inversely proportional to the pulse duration (the Fourier transform (FT) of an approximate square wave contains contributions from all the frequencies in the neighborhood of the principal frequency). The restricted range of the NMR frequencies made it relatively easy to use short (millisecond to microsecond) radiofrequency (RF) pulses to excite the entire NMR spectrum.

Applying such a pulse to a set of nuclear spins simultaneously excites all the single-quantum NMR transitions. In terms of the net magnetization vector, this corresponds to tilting the magnetization vector away from its equilibrium position (aligned along the external magnetic field). The out-of-equilibrium magnetization vector precesses about the external magnetic field vector at the NMR frequency of the spins. This oscillating magnetization vector induces a current in a nearby pickup coil, creating an electrical signal oscillating at the NMR frequency. This signal is known as the free induction decay (FID) and contains the vector-sum of the NMR responses from all the excited spins. In order to obtain the frequency-domain NMR spectrum (NMR absorption intensity vs. NMR frequency) this time-domain signal (intensity vs. time) must be FTed. Fortunately the development of FT NMR coincided with the development of digital computers and Fast Fourier Transform algorithms. FT methods can be applied to many types of spectroscopy; see the general article on Fourier transform spectroscopy.

Richard R. Ernst was one of the pioneers of pulse (FT) NMR and won a Nobel Prize in chemistry in 1991 for his work on FT NMR and his development of multi-dimensional NMR (see below).

Multi-dimensional NMR Spectroscopy

The use of pulses of different shapes, frequencies and durations in specifically-designed patterns or *pulse sequences* allows the spectroscopist to extract many different types of information about the molecule. Multi-dimensional nuclear magnetic resonance spectroscopy is a kind of FT NMR in which there are at least two pulses and, as the experiment is repeated, the pulse sequence is varied. In *multidimensional nuclear magnetic resonance* there will be a sequence of pulses and, at least, one variable time period. In three dimensions, two time sequences will be varied. In four dimensions, three will be varied.

There are many such experiments. In one, these time intervals allow (amongst other things) magnetization transfer between nuclei and, therefore, the detection of the kinds of nuclear-nuclear interactions that allowed for the magnetization transfer. Interactions that can be detected are usually classified into two kinds. There are *through-bond* interactions and *through-space* interactions, the latter usually being a consequence of the nuclear Overhauser effect. Experiments of the nuclear Overhauser variety may be employed to establish distances between atoms, as for example by 2D-FT NMR of molecules in solution.

Although the fundamental concept of 2D-FT NMR was proposed by Jean Jeener from the Free University of Brussels at an International Conference, this idea was largely developed by Richard Ernst who won the 1991 Nobel prize in Chemistry for his work in FT NMR, including multi-dimensional FT NMR, and especially 2D-FT NMR of small molecules.[8] Multi-dimensional FT NMR experiments were then further developed into powerful methodologies for studying biomolecules in solution, in particular for the determination of the structure of biopolymers such as proteins or even small nucleic acids.[9]

Kurt Wüthrich shared (with John B. Fenn) in 2002 the Nobel Prize in Chemistry for his work in protein FT NMR in solution.

Solid-state NMR spectroscopy

This technique complements biopolymer X-ray crystallography in that it is frequently applicable to biomolecules in a liquid or liquid crystal phase, whereas crystallography, as the name implies, is performed on molecules in a solid phase. Though nuclear magnetic resonance is used to study solids, extensive atomic-level biomolecular structural detail is especially challenging to obtain in the solid state. There is little signal averaging by thermal motion in the solid state, where most molecules can only undergo restricted vibrations and rotations at room temperature, each in a slightly different electronic environment, therefore exhibiting a different NMR absorption peak. Such a variation in the electronic environment of the resonating nuclei results in a blurring of the observed spectra—which is often only a broad Gaussian band for non-quadrupolar spins in a solid- thus making the interpretation of such "dipolar" and "chemical shift anisotropy" (CSA) broadened spectra either very difficult or impossible.

Professor Raymond Andrew at Nottingham University in the UK pioneered the development of high-resolution solid-state nuclear magnetic resonance. He was the first to report the introduction of the MAS (magic angle sample spinning; MASS) technique that allowed him to achieve spectral resolution in solids sufficient to distinguish between chemical groups with either different chemical shifts or distinct Knight shifts. In MASS, the sample is spun at several kilohertz around an axis that makes the so-called magic angle θ_m (which is ~54.74°, where $\cos^2\theta_m = 1/3$) with respect to the direction of the static magnetic field $\mathbf{B}_0$; as a result of such magic angle sample spinning, the chemical shift anisotropy bands are averaged to their corresponding average (isotropic) chemical shift values. The above expression involving $\cos^2\theta_m$ has its origin in a calculation that predicts the magnetic dipolar interaction effects to cancel out for the specific value of θ_m called the magic angle. One notes that correct alignment of the sample rotation axis as close as possible to θ_m is essential for cancelling out the dipolar interactions whose strength for angles sufficiently far from θ_m is usually greater than ~10 kHz for C-H bonds in solids, for example, and it is thus greater than their CSA values.

There are different angles for the sample spinning relative to the applied field for the averaging of quadrupole interactions and paramagnetic interactions, correspondingly ~30.6° and ~70.1°

A concept developed by Sven Hartmann and Erwin Hahn was utilized in transferring magnetization from protons to less sensitive nuclei (popularly known as cross-polarization) by M.G. Gibby, Alex Pines and John S. Waugh. Then, Jake Schaefer and Ed Stejskal demonstrated also the powerful use of cross-polarization under MASS conditions which is now routinely employed to detect low-abundance and low-sensitivity nuclei.

Sensitivity

Because the intensity of nuclear magnetic resonance signals and, hence, the sensitivity of the technique depends on the strength of the magnetic field the technique has also advanced over the decades with the development of more powerful magnets. Advances made in audio-visual technology have also improved the signal-generation and processing capabilities of newer machines.

As noted above, the sensitivity of nuclear magnetic resonance signals is also dependent on the presence of a magnetically-susceptible nuclide and, therefore, either on the natural abundance of such nuclides or on the ability of the experimentalist to artificially enrich the molecules, under study, with such nuclides. The most abundant naturally-occurring isotopes of hydrogen and phosphorus (for example) are both magnetically susceptible and readily useful for nuclear magnetic resonance spectroscopy. In contrast, carbon and nitrogen have useful isotopes but which occur only in very low natural abundance.

Other limitations on sensitivity arise from the quantum-mechanical nature of the phenomenon. For quantum states separated by energy equivalent to radio frequencies, thermal energy from the environment causes the populations of the states to be close to equal. Since incoming radiation is equally likely to cause stimulated emission (a transition from the upper to the lower state) as absorption, the NMR effect depends on an excess of nuclei in the lower states. Several factors can reduce sensitivity, including

- Increasing temperature, which evens out the population of states. Conversely, low temperature NMR can sometimes yield better results than room-temperature NMR, providing the sample remains liquid.
- Saturation of the sample with energy applied at the resonant radiofrequency. This manifests in both CW and pulsed NMR; in the first, CW, case this happens by using too much continuous power that keeps the upper spin levels completely populated; in the second case, saturation occurs by pulsing too frequently—without allowing time for the nuclei to return to thermal equilibrium through spin-lattice relaxation. For nuclei such as ^{29}Si this is a serious practical problem as the relaxation time is measured in seconds; for protons in "pure" ice, or ^{19}F in high-purity (undoped) LiF crystals the spin-lattice relaxation time can be on the order of an hour or longer. The use of shorter RF pulses that tip the magnetization by less than 90° can partially solve the problem by allowing spectral acquisition without the complete loss of NMR signal.
- Non-magnetic effects, such as electric-quadrupole coupling of spin-1 and spin-$\frac{3}{2}$ nuclei with their local environment, which broaden and weaken absorption peaks. ^{14}N, an abundant spin-1 nucleus, is difficult to study for this reason. High resolution NMR instead probes molecules using the rarer ^{15}N isotope, which has spin-$\frac{1}{2}$.

Isotopes

Many chemical elements can be used for NMR analysis.[10]

Commonly used nuclei:

- ^{1}H, the most commonly used spin ½ nucleus in NMR investigation, has been studied using many forms of NMR. Hydrogen is highly abundant, especially in biological systems. It is the nucleus most sensitive to NMR signal (apart from ^{3}H which is not commonly used due to its instability and radioactivity). Proton NMR produces narrow chemical shift with sharp signals. The ^{1}H signal has been the sole diagnostic nucleus used for clinical magnetic resonance imaging.
- ^{2}H, a spin 1 nucleus commonly utilized as signal-free medium in the form of deuterated solvents during proton NMR, to avoid signal interference from hydrogen-containing solvents in measurement of ^{1}H solutes. Also used in determining the behavior of lipids in lipid membranes and other solids or liquid crystals as it is a relatively non-perturbing label which can selectively replace ^{1}H. Alternatively, ^{2}H can be detected in media specially labeled with ^{2}H.
- ^{3}He, is very sensitive to NMR. There is a very low percentage in natural helium, and subsequently has to be purified from ^{4}He. It is used mainly in studies of endohedral fullerenes, where its chemical inertness is beneficial to ascertaining the structure of the entrapping fullerene.
- ^{10}B, lower sensitivity than ^{11}B. Quartz tubes must be used as borosilicate glass interferes with measurement.
- ^{11}B, more sensitive than ^{10}B, yields sharper signals. Quartz tubes must be used as borosilicate glass interferes with measurement.
- ^{13}C spin-1/2, is widely used, despite its relative paucity in naturally-occurring carbon (approximately 1%). It is stable to nuclear decay. Since there is a low percentage in natural carbon, spectrum acquisition on samples which have not been experimentally enriched in ^{13}C takes a long time. Frequently used for labeling of compounds in synthetic and metabolic studies. Has low sensitivity and wide chemical shift, yields sharp signals. Low percentage makes it useful by preventing spin-spin couplings and makes the spectrum appear less crowded. Slow relaxation means that spectra are not integrable unless long acquisition times are used.
- ^{14}N, spin-1, medium sensitivity nucleus with wide chemical shift. Its large quadrupole moment interferes in acquisition of high resolution spectra, limiting usefulness to smaller molecules and functional groups with a high degree of symmetry such as the headgroups of lipids.
- ^{15}N, spin-1/2, relatively commonly used. Can be used for labeling compounds. Nucleus very insensitive but yields sharp signals. Low percentage in natural nitrogen together with low sensitivity requires high concentrations or expensive isotope enrichment.
- ^{17}O, spin-5/2, low sensitivity and very low natural abundance (0.037%), wide chemical shifts range (up to 2000 ppm). Quadrupole moment causing a line broadening. Used in metabolic and biochemical studies in studies of

chemical equilibria.

- ^{19}F, spin-1/2, relatively commonly measured. Sensitive, yields sharp signals, has wide chemical shift.
- ^{31}P, spin-1/2, 100% of natural phosphorus. Medium sensitivity, wide chemical shifts range, yields sharp lines. Used in biochemical studies.
- ^{35}Cl and ^{37}Cl, broad signal. ^{35}Cl significantly more sensitive, preferred over ^{37}Cl despite its slightly broader signal. Organic chlorides yield very broad signals, its use is limited to inorganic and ionic chlorides and very small organic molecules.
- ^{43}Ca, used in biochemistry to study calcium binding to DNA, proteins, etc. Moderately sensitive, very low natural abundance.
- ^{195}Pt, used in studies of catalysts and complexes.

Other nuclei (usually used in the studies of their complexes and chemical binding, or to detect presence of the element):

- ^{6}Li, ^{7}Li
- ^{9}Be
- ^{19}F
- ^{21}Ne
- ^{23}Na
- ^{25}Mg
- ^{27}Al
- ^{29}Si
- ^{31}P
- ^{33}S
- ^{39}K, ^{40}K, ^{41}K
- ^{45}Sc
- ^{47}Ti, ^{49}Ti
- ^{50}V, ^{51}V
- ^{53}Cr
- ^{55}Mn
- ^{57}Fe
- ^{59}Co
- ^{61}Ni
- ^{63}Cu, ^{65}Cu
- ^{67}Zn
- ^{69}Ga, ^{71}Ga
- ^{73}Ge
- ^{77}Se
- ^{81}Br
- ^{87}Rb
- ^{87}Sr
- ^{95}Mo
- ^{109}Ag
- ^{113}Cd
- ^{119}Sn
- ^{125}Te
- ^{127}I
- ^{133}Cs
- ^{135}Ba, ^{137}Ba

- ^{139}La
- ^{183}W
- ^{199}Hg

Applications

Medicine

The application of nuclear magnetic resonance best known to the general public is magnetic resonance imaging for medical diagnosis and MR Microscopy in research settings, however, it is also widely used in chemical studies, notably in NMR spectroscopy such as proton NMR, carbon-13 NMR, deuterium NMR and phosphorus-31 NMR. Biochemical information can also be obtained from living tissue (e.g. human brain tumors) with the technique known as in vivo magnetic resonance spectroscopy or chemical shift NMR Microscopy.

These studies are possible because nuclei are surrounded by orbiting electrons, which are charged particles that generate small, local magnetic fields that add to or subtract from the external magnetic field, and so will partially shield the nuclei. The amount of shielding depends

Medical MRI

on the exact local environment. For example, a hydrogen bonded to an oxygen will be shielded differently than a hydrogen bonded to a carbon atom. In addition, two hydrogen nuclei can interact via a process known as spin-spin coupling, if they are on the same molecule, which will split the lines of the spectra in a recognizable way.

As one of the two major spectroscopic techniques used in metabolomics, NMR is used to generate metabolic fingerprints from biological fluids to obtain information about disease states or toxic insults.

Chemistry

By studying the peaks of nuclear magnetic resonance spectra, chemists can determine the structure of many compounds. It can be a very selective technique, distinguishing among many atoms within a molecule or collection of molecules of the same type but which differ only in terms of their local chemical environment. See the articles on carbon-13 NMR and proton NMR for detailed discussions.

By studying T_2*information, a chemist can determine the identity of a compound by comparing the observed nuclear precession frequencies to known frequencies. Further structural data can be elucidated by observing *spin-spin coupling*, a process by which the precession frequency of a nucleus can be influenced by the magnetization transfer from nearby nuclei. Spin-spin coupling is most commonly observed in NMR involving common isotopes, such as Hydrogen-1 (^{1}H NMR).

Because the nuclear magnetic resonance *timescale* is rather slow, compared to other spectroscopic methods, changing the temperature of a T_2*experiment can also give information about fast reactions, such as the Cope rearrangement or about structural dynamics, such as ring-flipping in cyclohexane. At low enough temperatures, a distinction can be made between the axial and equatorial hydrogens in cyclohexane.

An example of nuclear magnetic resonance being used in the determination of a structure is that of buckminsterfullerene (often called "buckyballs", composition C_{60}). This now famous form of carbon has 60 carbon atoms forming a sphere. The carbon atoms are all in identical environments and so should see the same internal H field. Unfortunately, buckminsterfullerene contains no hydrogen and so ^{13}C nuclear magnetic resonance has to be used. ^{13}C spectra require longer acquisition times since carbon-13 is not the common isotope of carbon (unlike hydrogen, where ^{1}H is the common isotope). However, in 1990 the spectrum was obtained by R. Taylor and

co-workers at the University of Sussex and was found to contain a single peak, confirming the unusual structure of buckminsterfullerene.[11]

Non-destructive testing

Nuclear magnetic resonance is extremely useful for analyzing samples non-destructively. Radio waves and static magnetic fields easily penetrate many types of matter and anything that is not inherently ferromagnetic. For example, various expensive biological samples, such as nucleic acids, including RNA and DNA, or proteins, can be studied using nuclear magnetic resonance for weeks or months before using destructive biochemical experiments. This also makes nuclear magnetic resonance a good choice for analyzing dangerous samples.

Acquisition of dynamic information

In addition to providing static information on molecules by determining their 3D structures in solution, one of the remarkable advantages of NMR over X-ray crystallography is that it can be used to obtain important dynamic information including the low-frequency collective motion in proteins and DNA, for example in the Ca^{2+}-calmodulin system.[12] . The low-frequency internal motion in biomacromolecules and its biological functions have been discussed by Chou.[13] .

Data acquisition in the petroleum industry

Another use for nuclear magnetic resonance is data acquisition in the petroleum industry for petroleum and natural gas exploration and recovery. A borehole is drilled into rock and sedimentary strata into which nuclear magnetic resonance logging equipment is lowered. Nuclear magnetic resonance analysis of these boreholes is used to measure rock porosity, estimate permeability from pore size distribution and identify pore fluids (water, oil and gas). These instruments are typically low field NMR spectrometers.

Flow probes for NMR spectroscopy

Recently, real-time applications of NMR in liquid media have been developed using specifically designed flow probes (flow cell assemblies)which can replace standard tube probes. This has enabled techniques that can incorporate the use of high performance liquid chromatography (HPLC) or other continuous flow sample introduction devices.[14]

Process control

NMR has now entered the arena of real-time process control and process optimization in oil refineries and petrochemical plants. Two different types of NMR analysis are utilized to provide real time analysis of feeds and products in order to control and optimize unit operations. Time-domain NMR (TD-NMR) spectrometers operating at low field (2–20 MHz for ^{1}H) yield free induction decay data that can be used to determine absolute hydrogen content values, rheological information, and component composition. These spectrometers are used in mining, polymer production, cosmetics and food manufacturing as well as coal analysis. High resolution FT-NMR spectrometers operating in the 60 MHz range with shielded permanent magnet systems yield high resolution ^{1}H NMR spectra of refinery and petrochemical streams. The variation observed in these spectra with changing physical and chemical properties is modeled using chemometrics to yield predictions on unknown samples. The prediction results are provided to control systems via analogue or digital outputs from the spectrometer.

Earth's field NMR

In the Earth's magnetic field, NMR frequencies are in the audio frequency range, or the very low frequency band of the radio frequency spectrum. Earth's field NMR (EFNMR) is typically stimulated by applying a relatively strong dc magnetic field pulse to the sample and, following the pulse, analyzing the resulting low frequency alternating magnetic field that occurs in the Earth's magnetic field due to free induction decay (FID). These effects are exploited in some types of magnetometers, EFNMR spectrometers, and MRI imagers. Their inexpensive portable nature makes these instruments valuable for field use and for teaching the principles of NMR and MRI.

Quantum computing

NMR quantum computing uses the spin states of molecules as qubits. NMR differs from other implementations of quantum computers in that it uses an ensemble of systems, in this case molecules. The ensemble is initialized to be the thermal equilibrium state (see quantum statistical mechanics).

Magnetometers

Various magnetometers use NMR effects to measure magnetic fields, including proton precession magnetometers (PPM) (also known as proton magnetometers), and Overhauser magnetometers. See also Earth's field NMR.

Makers of NMR equipment

Major NMR instrument makers include Oxford Instruments, Bruker, Spinlock SRL, General Electric, JEOL, Kimble Chase, Philips, Siemens AG and Varian, Inc..

See also

- Carbon-13 NMR
- Chemical shift
- Dynamic nuclear polarisation (DNP)
- Earth's field NMR (EFNMR)
- Free induction decay (FID)
- In vivo magnetic resonance spectroscopy (MRS)
- J-coupling
- Larmor equation (Not to be confused with Larmor formula).
- Larmor precession
- Low field NMR
- Magic angle spinning
- Magnetometer
- Magnetic resonance imaging (MRI)
- NMR spectra database
- NMR spectroscopy
- NMR Microscopy
- Nuclear magnetic resonance in porous media
- Nuclear quadrupole resonance (NQR)
- Protein dynamics
- Protein NMR
- Proton NMR
- Rabi cycle
- Relaxometry

- Relaxation (NMR)
- Solid-state NMR
- Zero field NMR

References

- G.E Martin, A.S. Zekter (1988). *Two-Dimensional NMR Methods for Establishing Molecular Connectivity*. New York: VCH Publishers. p. 59.
- J.W. Akitt, B.E. Mann (2000). *NMR and Chemistry*. Cheltenham, UK: Stanley Thornes. pp. 273, 287. ISBN 0748743448.
- J.P. Hornak. "The Basics of NMR" [15]. Retrieved 2009-02-23.
- J. Keeler (2005). *Understanding NMR Spectroscopy*. John Wiley & Sons. ISBN 0470017864.
- K. Wuthrich (1986). *NMR of Proteins and Nucleic Acids*. New York (NY), USA: Wiley-Interscience. ISBN 0471119172.
- J.M Tyszka, S.E Fraser, R.E Jacobs (2005). "Magnetic resonance microscopy: recent advances and applications". *Current Opinion in Biotechnology* **16** (1): 93–99. doi:10.1016/j.copbio.2004.11.004. PMID 15722021.
- J.C. Edwards. "Principles of NMR" [16]. Process NMR Associates. Retrieved 2009-02-23.
- R.L Haner, P.A. Keifer (2009). *Encyclopedia of Magnetic Resonance*. John Wiley. doi:10.1002/9780470034590.emrstm1085.

External links

Tutorial

- NMR/MRI tutorial [17]
- NMR Library [18] NMR Concepts
- NMR Course Notes [19]

Animations and Simulations

- This animation shows a spin, the modification of spin with magnetic field and HF pulse, spin echo sequences, inversion recovery sequence, gradient echo sequence and relaxation of spin [20]
- Animation of NMR spin $\frac{1}{2}$ precession [21]
- A free interactive simulation of NMR principles [22]

Software

- CARA [23] - Computer Aided Resonance Assignment, freeware, developed at the group of Prof. Kurt Wüthrich
- CCPN [24] NMR software suite from community led Collaborative Computing Project for NMR.
- Janocchio [25] Conformation-dependent coupling and NOE prediction for small molecules.
- Mnova [26] - Multiplatform NMR processing, analysis and prediction software from Mestrelab Research [27].
- NMR processing software from ACD/Labs [28] for 1D [29] and 2D [30] NMR spectra. DB interface available.
- NMR Prediction software ACD/NMR Predictors [31]
- NMR simulation software QSim [32]
- Free software for simulation of spin coupled multiplets and DNMR spectra WINDNMR-Pro [33]
- NMR processing software NMRPipe [34]
- RMN [35] - An NMR data processing program for Macintosh Classic OS 9.
- SPINUS [36] website that uses neural networks to predict NMR spectra from chemical structures

Video

- introduction to NMR and MRI [37]
- Richard Ernst, NL - Developer of Multdimensional NMR techniques [38] Freeview video provided by the Vega Science Trust.
- 'An Interview with Kurt Wuthrich' [39] Freeview video by the Vega Science Trust (Wüthrich was awarded a Nobel Prize in Chemistry in 2002 "for his development of nuclear magnetic resonance spectroscopy for determining the three-dimensional structure of biological macromolecules in solution").

Wiki

- NMR Wiki [40] Open NMR,EPR,MRI web project
- NMR wiki in Chinese [41] Chinese NMR, MRI and EPR community

References

[1] I.I. Rabi, J.R. Zacharias, S. Millman, P. Kusch (1938). "A New Method of Measuring Nuclear Magnetic Moment". *Physical Review* **53**: 318. doi:10.1103/PhysRev.53.318.

[2] Biography of I. Rabi at Nobelprize.org (http://nobelprize.org/nobel_prizes/physics/laureates/1944/rabi-bio.html)

[3] Filler, Aaron (2009). "The History, Development and Impact of Computed Imaging in Neurological Diagnosis and Neurosurgery: CT, MRI, and DTI". *Nature Precedings*. doi:10.1038/npre.2009.3267.5.

[4] I.C. Baianu, K.A. Rubinson, J. Patterson (1979). "Ferromagnetic Resonance and Spin Wave Excitations in Metallic Glasses". *J. Phys. Chem. Solids* **40** (12): 941−950. doi:10.1016/0022-3697(79)90122-7.

[5] I.C. Baianu (1979). "Ferromagnetic resonance and spin wave excitations in metallic glasses: The effects of thermal ageing and long-range magnetic ordering". *Solid State Communications* **29**: i−xvi. doi:10.1016/0038-1098(79)91190-6.

[6] Quantum automaton and quantum computation (http://planetphysics.org/encyclopedia/QuantumComputers.html) (see also references therein)

[7] Rabi, I. I.; Zacharias, J.; Millman, S.; Kusch, P. (1938). "A New Method of Measuring Nuclear Magnetic Moment". *Physical Review* **53** (1): 318. doi:10.1103/PhysRev.53.318. PMID 9981980.

[8] "Nuclear Magnetic Resonance Fourier Transform Spectroscopy" (http://nobelprize.org/nobel_prizes/chemistry/laureates/1991/ernst-lecture.html) Ernst's Nobel lecture. (Includes mention of Jeener's suggestion.)

[9] I.C. Baianu. "Two-dimensional Fourier transforms" (http://planetmath.org/encyclopedia/TwoDimensionalFourierTransforms.html). *2D-FT NMR and MRI*. PlanetMath. . Retrieved 2009-02-22.

[10] Multinuclear NMR (http://chem.ch.huji.ac.il/nmr/techniques/1d/multi.html)

[11] R. Taylor, J.P. Hare, A.K. Abdul-Sada, H.W. Kroto (1990). "Isolation, separation and characterization of the fullerenes C60 and C70: the third form of carbon". *Journal of the Chemical Society, Chemical Communications* **20**: 1423−1425. doi:10.1039/c39900001423.

[12] Chou, J. J., Li, S., Klee, C. B. & Bax, A. (2001). Solution structure of Ca2+-calmodulin reveals flexible hand-like properties of its domains. Nature Structural Biology 8, 990-997.

[13] Kuo-Chen Chou (1988) Low-frequency collective motion in biomacromolecules and its biological functions. Biophys Chem 30, 3-48.

[14] R.L Haner and P.A, Keifer (2009). "Flow Probes for NMR Spectroscopy". *Encyclopedia of Magnetic Resonance*. doi:10.1002/9780470034590.emrstm1085.

[15] http://www.cis.rit.edu/htbooks/nmr/

[16] http://www.process-nmr.com/pdfs/NMR%20Overview.pdf

[17] http://www.cis.rit.edu/htbooks/nmr/inside.htm

[18] http://nmr.chinanmr.cn/guide/eNMR/eNMRindex.html

[19] http://www.grandinetti.org/Teaching/Chem824/NMRNotes

[20] http://www.bigs.de/BLH/en/index.php?option=com_content&view=category&layout=blog&id=51&Itemid=222

[21] http://www.chem.queensu.ca/FACILITIES/NMR/nmr/webcourse/precess.htm

[22] http://vam.anest.ufl.edu/forensic/nmr.html

[23] http://cara.nmr.ch/

[24] http://www.ccpn.ac.uk/

[25] http://janocchio.sourceforge.net

[26] http://mestrelab.com/products/mnova/details.html

[27] http://mestrelab.com/

[28] http://www.acdlabs.com/

[29] http://www.acdlabs.com/products/adh/nmr/1d_man/

[30] http://www.acdlabs.com/nmrworkbook

[31] http://www.acdlabs.com/products/adh/nmr/nmr_pred/

[32] http://www.bpc.lu.se/QSim

[33] http://www.chem.wisc.edu/areas/reich/plt/windnmr.htm

[34] http://spin.niddk.nih.gov/bax/software/NMRPipe

[35] http://www.grandinetti.org/Software/RMN

[36] http://www2.chemie.uni-erlangen.de/services/spinus/

[37] http://www.youtube.com/watch?v=7aRKAXD4dAg

[38] http://www.vega.org.uk/video/programme/21

[39] http://www.vega.org.uk/video/programme/115

[40] http://www.nmrwiki.org

[41] http://wiki.chinanmr.cn

NMR Spectroscopy

Nuclear magnetic resonance spectroscopy, most commonly known as **NMR spectroscopy**, is the name given to a technique which exploits the magnetic properties of certain nuclei. For details regarding this phenomenon and its origins, refer to the nuclear magnetic resonance article. The most important applications for the organic chemist are proton NMR and carbon-13 NMR spectroscopy. In principle, NMR is applicable to any nucleus possessing spin.

Many types of information can be obtained from an NMR spectrum. Much like using infrared spectroscopy (IR) to identify functional groups, analysis of a NMR spectrum provides information on the number and type of chemical entities in a molecule. However, NMR provides much more information than IR.

The impact of NMR spectroscopy on the natural sciences has been substantial. It can, among other things, be used to study mixtures of analytes, to understand dynamic effects such as change in temperature and reaction mechanisms, and is an invaluable tool in understanding protein and

A 900MHz NMR instrument with a 21.2 T magnet at HWB-NMR, Birmingham, UK

nucleic acid structure and function. It can be applied to a wide variety of samples, both in the solution and the solid state.

Basic NMR techniques

When placed in a magnetic field, NMR active nuclei (such as ^{1}H or ^{13}C) absorb at a frequency characteristic of the isotope. The resonant frequency, energy of the absorption and the intensity of the signal are proportional to the strength of the magnetic field. For example, in a 21 tesla magnetic field, protons resonate at 900 MHz. It is common to refer to a 21 T magnet as a 900 MHz magnet, although different nuclei resonate at a different frequency at this field strength.

In the Earth's magnetic field the same nuclei resonate at audio frequencies. This effect is used in Earth's field NMR spectrometers and other instruments. Because these instruments are portable and inexpensive, they are often used for teaching and field work.

Chemical shift

Depending on the local chemical environment, different protons in a molecule resonate at slightly different frequencies. Since both this frequency shift and the fundamental resonant frequency are directly proportional to the strength of the magnetic field, the shift

The NMR sample is prepared in a thin-walled glass tube - an NMR tube.

is converted into a *field-independent* dimensionless value known as the chemical shift. The chemical shift is reported as a relative measure from some reference resonance frequency. (For the nuclei ^{1}H, ^{13}C, and [29]Si, TMS (tetramethylsilane) is commonly used as a reference.) This difference between the frequency of the signal and the frequency of the reference is divided by frequency of the reference signal to give the chemical shift. The frequency shifts are extremely small in comparison to the fundamental NMR frequency. A typical frequency shift might be 100 Hz, compared to a fundamental NMR frequency of 100 MHz, so the chemical shift is generally expressed in parts per million (ppm).[1] To be able to detect such small frequency differences it is necessary, that the external magnetic field varies much less throughout the sample volume. High resolution NMR spectrometers use shims to adjust the homogeneity of the magnetic field to parts per billion (ppb) in a volume of a few cubic centimeters.

By understanding different chemical environments, the chemical shift can be used to obtain some structural information about the molecule in a sample. The conversion of the raw data to this information is called *assigning* the spectrum. For example, for the ^{1}H-NMR spectrum for ethanol (CH_3CH_2OH), one would expect three specific signals at three specific chemical shifts: one for the CH_3 group, one for the CH_2 group and one for the OH group. A typical CH_3 group has a shift around 1 ppm, a CH_2 attached to an OH has a shift of around 4 ppm and an OH has a shift around 2−3 ppm depending on the solvent used.

Because of molecular motion at room temperature, the three methyl protons *average* out during the course of the NMR experiment (which typically requires a few ms). These protons become degenerate and form a peak at the same chemical shift.

The shape and size of peaks are indicators of chemical structure too. In the example above—the proton spectrum of ethanol—the CH_3 peak would be three times as large as the OH. Similarly the CH_2 peak would be twice the size of the OH peak but only 2/3 the size of the CH_3 peak.

Modern analysis software allows analysis of the size of peaks to understand how many protons give rise to the peak. This is known as integration—a mathematical process which calculates the area under a graph (essentially what a spectrum is). The analyst must integrate the peak and not measure its height because the peaks also have *width*—and thus its size is dependent on its area not its height. However, it should be mentioned that the number of protons, or

any other observed nucleus, is only proportional to the intensity, or the integral, of the NMR signal, in the very simplest one-dimensional NMR experiments. In more elaborate experiments, for instance, experiments typically used to obtain carbon-13 NMR spectra, the integral of the signals depends on the relaxation rate of the nucleus, and its scalar and dipolar coupling constants. Very often these factors are poorly known - therefore, the integral of the NMR signal is very difficult to interpret in more complicated NMR experiments.

J-coupling

Multiplicity	Intensity Ratio
Singlet (s)	1
Doublet (d)	1:1
Triplet (t)	1:2:1
Quartet (q)	1:3:3:1
Quintet	1:4:6:4:1
Sextet	1:5:10:10:5:1
Septet	1:6:15:20:15:6:1

Some of the most useful information for structure determination in a one-dimensional NMR spectrum comes from **J-coupling** or **scalar coupling** (a special case of spin-spin coupling) between NMR active nuclei. This coupling arises from the interaction of different spin states through the chemical bonds of a molecule and results in the splitting of NMR signals. These splitting patterns can be complex or simple and, likewise, can be straightforwardly interpretable or deceptive. This coupling provides detailed insight into the connectivity of atoms in a molecule.

Coupling to n equivalent (spin ½) nuclei splits the signal into a $n+1$ **multiplet** with intensity ratios following Pascal's triangle as described on the right. Coupling to additional spins will lead to further splittings of each component of the multiplet e.g. coupling to two different spin ½ nuclei with significantly different coupling constants will lead to a *doublet of doublets* (abbreviation: dd). Note that coupling between nuclei that are chemically equivalent (that is, have the same chemical shift) has no effect of the NMR spectra and couplings between nuclei that are distant (usually more than 3 bonds apart for protons in flexible molecules) are usually too small to cause observable splittings. *Long-range* couplings over more than three bonds can often be observed in cyclic and aromatic compounds, leading to more complex splitting patterns.

For example, in the proton spectrum for ethanol described above, the CH_3 group is split into a *triplet* with an intensity ratio of 1:2:1 by the two neighboring CH_2 protons. Similarly, the CH_2 is split into a *quartet* with an intensity ratio of 1:3:3:1 by the three neighboring CH_3 protons. In principle, the two CH_2 protons would also be split again into a *doublet* to form a *doublet of quartets* by the hydroxyl proton, but intermolecular exchange of the acidic hydroxyl proton often results in a loss of coupling information.

Coupling to any spin ½ nuclei such as phosphorus-31 or fluorine-19 works in this fashion (although the magnitudes of the coupling constants may be very different). But the splitting patterns differ from those described above for nuclei with spin greater than ½ because the spin quantum number has more than two possible values. For instance, coupling to deuterium (a spin 1 nucleus) splits the signal into a *1:1:1 triplet* because the spin 1 has three spin states. Similarly, a spin 3/2 nucleus splits a signal into a *1:1:1:1 quartet* and so on.

Coupling combined with the chemical shift (and the integration for protons) tells us not only about the chemical environment of the nuclei, but also the number of *neighboring* NMR active nuclei within the molecule. In more complex spectra with multiple peaks at similar chemical shifts or in spectra of nuclei other than hydrogen, coupling is often the only way to distinguish different nuclei.

Second-order (or strong) coupling

The above description assumes that the coupling constant is small in comparison with the difference in NMR frequencies between the inequivalent spins. If the shift separation decreases (or the coupling strength increases), the multiplet intensity patterns are first distorted, and then become more complex and less easily analyzed (especially if more than two spins are involved). Intensification of some peaks in a multiplet is achieved at the expense of the remainder, which sometimes almost disappear in the background noise, although the integrated area under the peaks remains constant. In most high-field NMR, however, the distortions are usually modest and the characteristic distortions (*roofing*) can in fact help to identify related peaks.

Second-order effects decrease as the frequency difference between multiplets increases, so that high-field (i.e. high-frequency) NMR spectra display less distortion than lower frequency spectra. Early spectra at 60 MHz were more prone to distortion than spectra from later machines typically operating at frequencies at 200 MHz or above.

Magnetic inequivalence

More subtle effects can occur if chemically equivalent spins (i.e. nuclei related by symmetry and so having the same NMR frequency) have different coupling relationships to external spins. Spins that are chemically equivalent but are not indistinguishable (based on their coupling relationships) are termed magnetically inequivalent. For example, the 4 H sites of 1,2-dichlorobenzene divide into two chemically equivalent pairs by symmetry, but an individual member of one of the pairs has different couplings to the spins making up the other pair. Magnetic inequivalence can lead to highly complex spectra which can only be analyzed by computational modeling. Such effects are more common in NMR spectra of aromatic and other non-flexible systems, while conformational averaging about C-C bonds in flexible molecules tends to equalize the couplings between protons on adjacent carbons, reducing problems with magnetic inequivalence.

Correlation spectroscopy

Correlation spectroscopy is one of several types of two-dimensional nuclear magnetic resonance (NMR) spectroscopy. This type of NMR experiment is best known by its acronym, COSY. Other types of two-dimensional NMR include J-spectroscopy, exchange spectroscopy (EXSY), Nuclear Overhauser effect spectroscopy (NOESY), total correlation spectroscopy (TOCSY) and heteronuclear correlation experiments, such as HSQC, HMQC, and HMBC. Two-dimensional NMR spectra provide more information about a molecule than one-dimensional NMR spectra and are especially useful in determining the structure of a molecule, particularly for molecules that are too complicated to work with using one-dimensional NMR. The first two-dimensional experiment, COSY, was proposed by Jean Jeener, a professor at Université Libre de Bruxelles, in 1971. This experiment was later implemented by Walter P. Aue, Enrico Bartholdi and Richard R. Ernst, who published their work in 1976.[2]

Solid-state nuclear magnetic resonance

A variety of physical circumstances does not allow molecules to be studied in solution, and at the same time not by other spectroscopic techniques to an atomic level, either. In solid-phase media, such as crystals, microcrystalline powders, gels, anisotropic solutions, etc., it is in particular the dipolar coupling and chemical shift anisotropy that become dominant to the behaviour of the nuclear spin systems. In conventional solution-state NMR spectroscopy, these additional interactions would lead to a significant broadening of spectral lines. A variety of techniques allows to establish high-resolution conditions, that can, at least for ^{13}C spectra, be comparable to solution-state NMR spectra.

Two important concepts for high-resolution solid-state NMR spectroscopy are the limitation of possible molecular orientation by sample orientation, and the reduction of anisotropic nuclear magnetic interactions by sample spinning. Of the latter approach, fast spinning around the magic angle is a very prominent method, when the system comprises spin 1/2 nuclei. A number of intermediate techniques, with samples of partial alignment or reduced mobility, is

currently being used in NMR spectroscopy.

Applications in which solid-state NMR effects occur are often related to structure investigations on membrane proteins, protein fibrils or all kinds of polymers, and chemical analysis in inorganic chemistry, but also include "exotic" applications like the plant leaves and fuel cells.

NMR spectroscopy applied to proteins

Much of the recent innovation within NMR spectroscopy has been within the field of protein NMR, which has become a very important technique in structural biology. One common goal of these investigations is to obtain high resolution 3-dimensional structures of the protein, similar to what can be achieved by X-ray crystallography. In contrast to X-ray crystallography, NMR is primarily limited to relatively small proteins, usually smaller than 35 kDa, though technical advances allow ever larger structures to be solved. NMR spectroscopy is often the only way to obtain high resolution information on partially or wholly intrinsically unstructured proteins. It is now a common tool for the determination of Conformation Activity Relationships where the structure before and after interaction with, for example, a drug candidate is compared to its known biochemical activity. Proteins are orders of magnitude larger than the small organic molecules discussed earlier in this article, but the basic NMR techniques and some of the NMR theory also applies. Because of the much higher number of atoms present in a protein molecule in comparison with a small organic compund, the basic 1D spectra become crowded with overlapping signals to an extent where direct spectra analysis becomnes untenable. Therefore, multidimensional (2, 3 or 4D) experiments have been devised to deal with this problem. To facilitate these experiments, it is desirable to isotopically label the protein with ^{13}C and ^{15}N because the predominant naturally occurring isotope ^{12}C is not NMR-active, whereas the nuclear quadrupole moment of the predominant naturally occurring ^{14}N isotope prevents high resolution information to be obtained from this nitrogen isotope. The most important method used for structure determination of proteins utilizes NOE experiments to measure distances between pairs of atoms within the molecule. Subsequently, the obtained distances are used to generate a 3D structure of the molecule by solving a distance geometry problem.

See also

- distance geometry
- In vivo magnetic resonance spectroscopy
- Low field NMR
- Magnetic Resonance Imaging
- Nuclear Magnetic Resonance
- NMR spectra database
- NMR tube - includes a section on sample preparation
- Protein nuclear magnetic resonance spectroscopy
- NMR spectroscopy of stereoisomers

External links

- Protein NMR- A Practical Guide [3] Practical guide to NMR, in particular protein NMR assignment
- James Keeler. "Understanding NMR Spectroscopy" [4] (reprinted at University of Cambridge). University of California, Irvine. Retrieved 2007-05-11.
- The Basics of NMR [15] - A non-technical overview of NMR theory, equipment, and techniques by Dr. Joseph Hornak, Professor of Chemistry at RIT
- NMRWiki.ORG [5] project, a Wiki dedicated to NMR, MRI, and EPR.
- NMR spectroscopy for organic chemistry [6]
- The Spectral Game [7] NMR spectroscopy game.

- Spectra libray [18] NMR spectroscopy library
- Obtaining dihedral angles from ^{3}J coupling constants [8]
- Another Javascript-like NMR coupling constant to dihedral [9]
- NMR Spectroscopy [10] Citizendium article on NMR Spectroscopy

Free NMR processing, analysis and simulation software

- WINDNMR-Pro [33] - simulation software for interactive calculation of first and second-order spin-coupled multiplets and a variety of DNMR lineshapes.
- CARA [11] - resonance assignment software developed at the Wüthrich group
- NMRShiftDB [12] - open database and NMR prediction website
- Spinworks [13]
- SPINUS [36] website that uses neural networks to predict NMR spectra from chemical structures
- MD-jeep [14] : free software for solving distance geometry problems related to NMR data

References

[1] James Keeler. "Chapter 2: NMR and energy levels" (http://www-keeler.ch.cam.ac.uk/lectures/Irvine/chapter2.pdf) (reprinted at University of Cambridge). *Understanding NMR Spectroscopy*. University of California, Irvine. . Retrieved 2007-05-11.

[2] Martin, G.E; Zekter, A.S., *Two-Dimensional NMR Methods for Establishing Molecular Connectivity*; VCH Publishers, Inc: New York, 1988 (p.59)

[3] http://www.protein-nmr.org.uk

[4] http://www-keeler.ch.cam.ac.uk/lectures/Irvine/

[5] http://nmrwiki.org

[6] http://www.organicworldwide.net/nmr.html

[7] http://spectralgame.com

[8] http://www.jonathanpmiller.com/Karplus.html

[9] http://www.spectroscopynow.com/FCKeditor/UserFiles/File/specNOW/HTML%20files/General_Karplus_Calculator.htm

[10] http://en.citizendium.org/wiki/NMR_spectroscopy

[11] http://cara.nmr.ch

[12] http://www.nmrshiftdb.org

[13] http://www.umanitoba.ca/chemistry/nmr/spinworks/

[14] http://www.antoniomucherino.it/en/mdjeep.php

2D-NMR

Correlation spectroscopy (COSY) is one of several types of two-dimensional nuclear magnetic resonance (NMR) spectroscopy. Other types of two-dimensional NMR include **J-spectroscopy**, **exchange spectroscopy** (EXSY), and Nuclear Overhauser effect spectroscopy (NOESY). Two-dimensional NMR spectra provide more information about a molecule than one-dimensional NMR spectra and are especially useful in determining the structure of a molecule, particularly for molecules that are too complicated to work with using one-dimensional NMR. The first two-dimensional experiment, **COSY**, was proposed by Jean Jeener, a professor at the Université Libre de Bruxelles, in 1971. This experiment was later implemented by Walter P. Aue, Enrico Bartholdi and Richard R. Ernst, who published their work in 1976.

Principles

A two-dimensional NMR experiment involves a series of one-dimensional experiments. Each experiment consists of a sequence of radio frequency pulses with delay periods in between them. It is the timing, frequencies, and intensities of these pulses that distinguish different NMR experiments from one another. During some of the delays, the nuclear spins are allowed to freely precess (rotate) for a determined length of time known as the **evolution time**. The frequencies of the nuclei are detected after the final pulse. By incrementing the evolution time in successive experiments, a two-dimensional data set is generated from a series of one-dimensional experiments.

An example of a two-dimension NMR experiment is the homonuclear correlation spectroscopy (COSY) sequence, which consists of a pulse (p1) followed by an evolution time (t1) followed by a second pulse (p2) followed by a measurement time (t2). A computer is used to compile the spectra as a function of the evolution time (t1). Finally, the Fourier transform is used to convert the time-dependent signals into a two-dimensional spectrum.

The two-dimensional spectrum that results from the COSY experiment shows the frequencies for a single isotope (usually hydrogen, ^{1}H) along both axes. (Techniques have also been devised for generating heteronuclear correlation spectra, in which the two axes correspond to different isotopes, such as ^{13}C and ^{1}H.) The intensities of the peaks in the spectrum can be represented using a third dimension. More commonly, intensity is indicated using contours or different colors. The spectrum is interpreted starting from the diagonal, which consists of a series of peaks. The peaks that appear off of the diagonal are called cross-peaks. The cross-peaks are symmetrical (both above and below) along the diagonal and indicate which hydrogen atoms are spin-spin coupled to each other. One can determine which atoms are connected to one another by only a few chemical bonds by matching the center of a cross-peak with the center of each of two corresponding diagonal peaks. The peaks on the diagonal when matched with cross-peaks are coupled to each other.

For example: a $CH_3CH_2COCH_3$ molecule 2-butanone would show three peaks on the diagonal, due to the three distinct hydrogen groups. By drawing a line straight down from a cross-peak to the point on the diagonal directly above or below it, and then drawing a line from the cross-peak directly across to another peak on the diagonal, one can determine which peaks are coupled. This is done in such a way that the lines from the cross-peak form a 90° angle between the two peaks on the diagonal. The matching peaks, as determined by using the cross-peaks, indicate which hydrogens are coupled, giving a clearer understanding of the structure of the molecule under examination.

To the right is an example of a COSY NMR spectrum of progesterone in DMSO-d6. The spectrum that appears along both the x- and y-axes is a regular one dimensional ^{1}H NMR spectrum. The COSY is read along the diagonal - where the bulk of the peaks appear. Cross-peaks appear symmetrically above and below the diagonal.

2D proton-COSY experiment on Progesterone

COSY NMR

COSY-90 is the most common COSY experiment. In COSY-90, the sample is irradiated with a radio frequency pulse, p1, which tilts the nuclear spin by 90°. After p1, the sample is allowed to freely precess during an evolution period (t1). A second 90° pulse, p2, is then applied, after which the experimental data are acquired. This is done repeatedly using a series of different evolution periods (t1). At the conclusion of data acquisition the data is Fourier transformed in each dimension to generate the two dimensional spectrum. It is only because the evolution period is varied that cross-peaks appear in the spectrum.

Cross-peaks result from a phenomenon called magnetization transfer. In COSY, magnetization transfer occurs through the chemical bonds rather than through space.

Another member of the COSY family is **COSY-45**. In COSY-45 a 45° pulse is used instead of a 90° pulse for the first pulse, p1. The advantage of a

In COSY NMR, the resonance signal from the sample is read in period t2 following two experimental magnetic pulses p1 and p2 separated by a variable period t1.

COSY-45 is that the diagonal-peaks are less pronounced, making it simpler to match cross-peaks near the diagonal in a large molecule. Additionally, the relative signs of the coupling constants can be elucidated from a COSY-45 spectrum. This is not possible using COSY-90.[COSY45_vs_COSY90] Overall, the COSY-45 offers a cleaner spectrum while the COSY-90 is more sensitive. Related COSY techniques include double quantum filtered COSY and multiple quantum filtered COSY.

COSY NMR has useful applications. Organic chemists often use COSY to elucidate structural data on molecules that are not satisfactorily represented in a one-dimensional NMR spectrum. Using cross-peaks, along with the diagonal spectrum, one can often discover much about the structure of an unknown molecule.

The 2D - TOCSY experiment is similar to the 2D - COSY experiment, in that cross peaks of coupled protons are observed. However, the additional information obtained in a TOCSY is correlations for all the protons in the spin system. In the case of oligosaccharides, each sugar residue is an isolated spin system, so it is possible to differentiate all the protons of a specific sugar residue. A 1D version of TOCSY is also available and by irradiating a single proton the rest of the spin system can be revealed.

Recent advances in this technique include the 1D - CSSF - TOCSY (Chemical Shift Selective Filter - TOCSY) experiment. This produces higher quality spectra and allows coupling constants to be reliably extracted and used to help determine stereochemistry.

NOESY

In NOESY, the Nuclear Overhauser effect (NOE) between nuclear spins is used to establish the correlations. Hence the cross-peaks in the resulting two-dimensional spectrum connect resonances from spins that are spatially close. NOESY spectra from large biomolecules can often be assigned using Sequential Walking.

The NOESY experiment can also be performed in a one-dimensional fashion by pre-selecting individual resonances. The spectra are read with the pre-selected nuclei giving a large, negative signal while neighboring nuclei are identified by weaker, positive signals. This only reveals which peaks have measurable NOEs to the resonance of interest but obviously takes much less time than the full 2D experiment. In addition, if a pre-selected nucleus changes environment within the time scale of the experiment, multiple negative signals may be observed. This offers exchange information similar to EXSY (i.e. exchange spectroscopy) NMR spectroscopy.

HMBC & HMQC

HMQC (Heteronuclear Multiple Quantum Coherence) and HMBC (Heteronuclear Multiple Bond Coherence) are 2D inverse correlation techniques that allow for the determination of connectivity between two different nuclear species. HMQC is selective for direct coupling and HMBC gives longer range couplings (2-4 bond coupling).

See also

- Exclusive correlation spectroscopy
- Two dimensional correlation analysis

2D-FT NMRI and Spectroscopy

2D-FT Nuclear Magnetic resonance imaging (**2D-FT NMRI**), or **Two-dimensional Fourier transform** magnetic resonance imaging (**NMRI**), is primarily a non--invasive imaging technique most commonly used in biomedical research and medical radiology/nuclear medicine/MRI to visualize structures and functions of the living systems and single cells. For example it can provides fairly detailed images of a human body in any selected cross-sectional plane, such as longitudinal, transversal, sagital, etc. NMRI provides much greater contrast especially for the different soft tissues of the body than computed tomography (CT) as its most sensitive option observes the nuclear spin distribution and dynamics of highly mobile molecules that contain the naturally abundant, stable hydrogen isotope ^{1}H as in plasma water molecules, blood, disolved metabolites and fats. This approach makes it most useful in cardiovascular, oncological (cancer), neurological (brain), musculoskeletal, and cartilage imaging. Unlike CT, it uses no ionizing radiation, and also unlike nuclear imaging it does not employ any radioactive isotopes. Some of the first MRI images reported were published in 1973[1] and the first study performed on a human took place on July 3, 1977.[2] Earlier papers were also published by Peter Mansfield[3] in UK (Nobel Laureate in 2003), and R. Damadian in the USA, (together with an approved patent for magnetic imaging). Unpublished `high-resolution' (50 micron resolution) images of other living systems, such as hydrated wheat grains, were obtained and communicated in UK in 1977-1979, and were subsequently confirmed by articles published in *Nature*.

NMRI Principle

Certain nuclei such as ^{1}H nuclei, or `fermions' have spin-1/2, because there are two spin states, referred to as "up" and "down" states. The nuclear magnetic resonance absorption phenomenon occurs when samples containing such nuclear spins are placed in a static magnetic field and a very short radiofrequency pulse is applied with a center, or carrier, frequency matching that of the transition between the up and down states of the spin-1/2 ^{1}H nuclei that were polarized by the static magnetic field. [4] Very low field schemes have also been recently reported.[5]

Advanced clinical diagnostics and biomedical research NMR Imaging instrument.

Chemical Shifts

NMR is a very useful family of techniques for chemical and biochemical research because of the chemical shift; this effect consists in a frequency shift of the nuclear magnetic resonance for specific chemical groups or atoms as a result of the partial shielding of the corresponding nuclei from the applied, static external magnetic field by the electron orbitals (or molecular orbitals) surrounding such nuclei present in the chemical groups. Thus, the higher the electron density surounding a specific nucleus the larger the chemical shift will be. The resulting magnetic field at the nucleus is thus lower than the applied external magnetic field and the resonance frequencies observed as a result of such shielding are lower than the value that would be observed in the absence of any electronic orbital shielding. Furthermore, in order to obtain a chemical shift value independent of the strength of the applied magnetic field and allow for the direct comparison of spectra obtained at different magnetic field values, the chemical shift is defined by the ratio of the strength of the local magnetic field value at the observed (electron orbital-shielded) nucleus by the external magnetic field strength, H_{loc}/ H_0. The first NMR observations of the chemical shift, with the correct physical chemistry interpretation, were reported for ^{19}F containing compounds in the early 1950's by Herbert S. Gutowsky and Charles P. Slichter from the University of Illinois at Urbana (USA).

NMR Imaging Principles

A number of methods have been devised for combining magnetic field gradients and radiofrequency pulsed excitation to obtain an image. Two major maethods involve either 2D -FT or 3D-FT[6] reconstruction from projections, somewhat similar to Computed Tomography, with the exception of the image interpretation that in the former case must include dynamic and relaxation/contrast enhancement information as well. Other schemes involve building the NMR image either point-by-point or line-by-line. Some schemes use instead gradients in the rf field rather than in the static magnetic field. The majority of NMR images routinely obtained are either by the Two-Dimensional Fourier Transform (2D-FT) technique [7] (with slice selection), or by the Three-Dimensional Fourier Transform (3D--FT) techniques that are however much more time consuming at present. 2D-FT NMRI is sometime called in common parlance a "spin-warp". An NMR image corresponds to a spectrum consisting of a number of `spatial frequencies' at different locations in the sample investigated, or in a patient.[8] A two–dimensional

Fourier transformation of such a "real" image may be considered as a representation of such "real waves" by a matrix of spatial frequencies known as the k−space. We shall see next in some mathematical detail how the 2D-FT computation works to obtain 2D-FT NMR images.

Two-dimensional Fourier transform imaging and spectroscopy

A two-dimensional Fourier transform (2D-FT) is computed numerically or carried out in two stages, both involving `standard', one-dimensional Fourier transforms. However, the second stage Fourier transform is not the inverse Fourier transform (which would result in the original function that was transformed at the first stage), but a Fourier transform in a second variable-- which is `shifted' in value-- relative to that involved in the result of the first Fourier transform. Such 2D-FT analysis is a very powerful method for both NMRI and two-dimensional nuclear magnetic resonance spectroscopy (2D-FT NMRS)[9] that allows the three-dimensional reconstruction of polymer and biopolymer structures at atomic resolution]].[10] for molecular weights (Mw) of dissolved biopolymers in aqueous solutions (for example) up to about 50,000 Mw. For larger biopolymers or polymers, more complex methods have been developed to obtain limited structural resolution needed for partial 3D-reconstructions of higher molecular structures, e.g. for up 900,000 Mw or even oriented microcrystals in aqueous suspensions or single crystals; such methods have also been reported for *in vivo* 2D-FT NMR spectroscopic studies of algae, bacteria, yeast and certain mammalian cells, including human ones. The 2D-FT method is also widely utilized in optical spectroscopy, such as *2D-FT NIR hyperspectral imaging* (2D-FT NIR-HS), or in MRI imaging for research and clinical, diagnostic applications in Medicine. In the latter case, 2D-FT NIR-HS has recently allowed the identification of single, malignant cancer cells surrounded by healthy human breast tissue at about 1 micron resolution, well-beyond the resolution obtainable 2D-FT NMRI for such systems in the limited time available for such diagnostic investigations (and also in magnetic fields up to the FDA approved magnetic field strength $\mathbf{H}_0$ of 4.7 T, as shown in the top image of the state-of-the-art NMRI instrument). A more precise mathematical definition of the `double' (2D) Fourier transform involved in both 2D NMRI and 2D-FT NMRS is specified next, and a precise example follows this generally accepted definition.

2D-FT Definition

A *2D-FT, or two-dimensional Fourier transform*, is a standard Fourier transformation of a function of two variables, $f(x_1, x_2)$, carried first in the first variable x_1, followed by the Fourier transform in the second variable x_2 of the resulting function $F(s_1, x_2)$. Note that in the case of both 2D-FT NMRI and 2D-FT NMRS the two independent variables in this definition are in the time domain, whereas the results of the two successive Fourier transforms have, of course, frequencies as the independent variable in the NMRS, and ultimately spatial coordinates for both 2D NMRI and 2D-FT NMRS following computer structural reconstructions based on special algorithms that are different from FT or 2D-FT. Moreover, such structural algorithms are different for 2D NMRI and 2D-FT NMRS: in the former case they involve macroscopic, or anatomical structure detrmination, whereas in the latter case of 2D-FT NMRS the atomic structure reconstruction algorithms are based on the quantum theory of a microphysical (quantum) process such as nuclear Overhauser enhancement NOE, or specific magnetic dipole-dipole interactions[11] between neighbor nuclei.

Example 1

A 2D Fourier transformation and phase correction is applied to a set of 2D NMR (FID) signals : $s(t_1, t_2)$ yielding a real 2D-FT NMR `spectrum' (collection of 1D FT-NMR spectra) represented by a matrix **S** whose elements are

$$S(\nu_1, \nu_2) = \mathbf{Re} \int \int cos(\nu_1 t_1) exp^{(-i\nu_2 t_2)} s(t_1, t_2) dt_1 dt_2$$

where : ν_1 and : ν_2 denote the discrete indirect double-quantum and single-quantum(detection) axes, respectively, in the 2D NMR experiments. Next, the \emph{covariance matrix} is calculated in the frequency domain according to the following equation

$$C(\nu_2', \nu_2) = S^T S = \sum_{\nu^1} [S(\nu_1, \nu_2') S(\nu_1, \nu_2)],$$ with : ν_2, ν_2' taking all possible single-quantum

frequency values and with the summation carried out over all discrete, double quantum frequencies : ν_1.

Example 2

Atomic Structure from 2D-FT STEM Images [12] of electron distributions in a high-temperature cuprate superconductor `paracrystal' reveal both the domains (or `location') and the local symmetry of the 'pseudo-gap' in the electron-pair correlation band responsible for the high--temperature superconductivity effect (obtained at Cornell University). So far there have been three Nobel prizes awarded for 2D-FT NMR/MRI during 1992-2003, and an additional, earlier Nobel prize for 2D-FT of X-ray data (`CAT scans'); recently the advanced possibilities of 2D-FT techniques in Chemistry, Physiology and Medicine [13] received very significant recognition.[14]

Brief explanation of NMRI diagnostic uses in Pathology

As an example, a diseased tissue such as a malign tumor, can be detected by 2D-FT NMRI because the hydrogen nuclei of molecules in different tissues return to their equilibrium spin state at different relaxation rates, and also because of the manner in which a malign tumor spreads and grows rapidly along the blood vessels adjacent to the tumor, also inducing further vascularization to occur. By changing the pulse delays in the RF pulse sequence employed, and/or the RF pulse sequence itself, one may obtain a `relaxation--based contrast', or contrast enhancement between different types of body tissue, such as normal vs. diseased tissue cells for example. Excluded from such diagnostic observations by NMRI are all patients with ferromagnetic metal implants, (e.g., cochlear implants), and all cardiac pacemaker patients who cannot undergo any NMRI scan because of the very intense magnetic and RF fields employed in NMRI which would strongly interfere with the correct functioning of such pacemakers. It is, however, conceivable that future developments may also include along with the NMRI diagnostic treatments with special techniques involving applied magnetic fields and very high frequency RF. Already, surgery with special tools is being experimented on in the presence of NMR imaging of subjects.Thus, NMRI is used to image almost every part of the body, and is especially useful for diagnosis in neurological conditions, disorders of the muscles and joints, for evaluating tumors, such as in lung or skin cancers, abnormalities in the heart (especially in children with hereditary disorders), blood vessels, CAD, atherosclerosis and cardiac infarcts [15] (courtesy of Dr. Robert R. Edelman)

See also

- Nuclear magnetic resonance (NMR)
- Magnetic resonance microscopy
- Relaxation
- Medical imaging
- Solid-state NMR
- Earth's field NMR (EFNMR)
- Protein nuclear magnetic resonance spectroscopy
- Herbert S. Gutowsky
- Robinson oscillator
- Kurt Wüthrich
- John S. Waugh
- Chemical shift
- Charles P. Slichter
- Computed tomography (CT)
- FT-NIRS (NIR)
- Fourier transform spectroscopy(FTS)
- Magnetic resonance elastography
- Richard R. Ernst

Reference list

[1] Lauterbur, P.C., Nobel Laureate in 2003 (1973). "Image Formation by Induced Local Interactions: Examples of Employing Nuclear Magnetic Resonance". *Nature* **242**: 190−1. doi:10.1038/242190a0.

[2] [http://www.howstuffworks.com/mri.htm/printable Howstuffworks "How MRI Works"

[3] Peter Mansfield. 2003. Nobel Laureate in Physiology and Medicine for (2D and 3D) MRI (http://www.parteqinnovations.com/pdf-doc/fandr-Gaz1006.pdf)

[4] Antoine Abragam. 1968. *Principles of Nuclear Magnetic Resonance.*, 895 pp., Cambridge University Press: Cambridge, UK.

[5] Raftery D (August 2006). "MRI without the magnet" (http://www.pubmedcentral.nih.gov/articlerender.fcgi?tool=pmcentrez&artid=1568902). *Proc Natl Acad Sci USA.* **103** (34): 12657−8. doi:10.1073/pnas.0605625103. PMID 16912110. PMC 1568902.

[6] Wu Y, Chesler DA, Glimcher MJ, *et al* (February 1999). "Multinuclear solid-state three-dimensional MRI of bone and synthetic calcium phosphates" (http://www.pnas.org/cgi/pmidlookup?view=long&pmid=9990066). *Proc. Natl. Acad. Sci. U.S.A.* **96** (4): 1574−8. doi:10.1073/pnas.96.4.1574. PMID 9990066. PMC 15521. .

[7] http://www.math.cuhk.edu.hk/course/mat2071a/lec1_08.ppt

[8] *Haacke, E Mark; Brown, Robert F; Thompson, Michael; Venkatesan, Ramesh (1999). *Magnetic resonance imaging: physical principles and sequence design*. New York: J. Wiley & Sons. ISBN 0-471-35128-8.

[9] Richard R. Ernst. 1992. Nuclear Magnetic Resonance Fourier Transform (2D-FT) Spectroscopy. Nobel Lecture (http://nobelprize.org/nobel_prizes/chemistry/laureates/1991/ernst-lecture.pdf), on December 9, 1992.

[10] http://en.wikipedia.org/wiki/Nuclear_magnetic_resonance#Nuclear_spin_and_magnets Kurt Wutrich in 1982-1986 : 2D-FT NMR of solutions

[11] Charles P. Slichter.1996. *Principles of Magnetic Resonance.* Springer: Berlin and New York, Third Edition., 651pp. ISBN 0-387-50157-6.

[12] http://www.physorg.com/news129395045.html

[13] http://nobelprize.org/nobel_prizes/chemistry/laureates/1991/ernst-lecture.pdf

[14] Protein structure determination in solution by NMR spectroscopy (http://www.ncbi.nlm.nih.gov/entrez/query.fcgi?cmd=Retrieve&db=pubmed&dopt=Abstract&list_uids=2266107&query_hl=33&itool=pubmed_docsum) Wuthrich K. J Biol Chem. 1990 December 25;265(36):22059-62.

[15] http://www.mr-tip.com/serv1.php?type=img&img=Cardiac%20Infarct%20Short%20Axis%20Cine%204

References

- Antoine Abragam. 1968. *Principles of Nuclear Magnetic Resonance.*, 895 pp., Cambridge University Press: Cambridge, UK.

- Charles P. Slichter.1996. *Principles of Magnetic Resonance.* Springer: Berlin and New York, Third Edition., 651pp. ISBN 0-387-50157-6.

- Kurt Wüthrich. 1986, *NMR of Proteins and Nucleic Acids.*, J. Wiley and Sons: New York, Chichester, Brisbane, Toronto, Singapore. (Nobel Laureate in 2002 for 2D-FT NMR Studies of Structure and Function of Biological Macromolecules (http://nobelprize.org/nobel_prizes/chemistry/laureates/2002/wutrich-lecture.pdf)

- Protein structure determination in solution by NMR spectroscopy (http://www.ncbi.nlm.nih.gov/entrez/query.fcgi?cmd=Retrieve&db=pubmed&dopt=Abstract&list_uids=2266107&query_hl=33&itool=pubmed_docsum) Wuthrich K. J Biol Chem. 1990 December 25;265(36):22059-62

- 2D-FT NMRI Instrument image: A JPG color image of a 2D-FT NMRI `monster' Instrument (http://upload.wikimedia.org/wikipedia/en/b/bf/HWB-NMRv900.jpg).

- Richard R. Ernst. 1992. Nuclear Magnetic Resonance Fourier Transform (2D-FT) Spectroscopy. Nobel Lecture (http://nobelprize.org/nobel_prizes/chemistry/laureates/1991/ernst-lecture.pdf), on December 9, 1992.

- Peter Mansfield. 2003. Nobel Laureate in Physiology and Medicine for (2D and 3D) MRI (http://www.parteqinnovations.com/pdf-doc/fandr-Gaz1006.pdf)

- D. Benett. 2007. PhD Thesis. Worcester Polytechnic Institute. PDF of 2D-FT Imaging Applications to NMRI in Medical Research. (http://www.wpi.edu/Pubs/ETD/Available/etd-081707-080430/unrestricted/dbennett.pdf) Worcester Polytechnic Institute. (Includes many 2D-FT NMR images of human brains.)

- Paul Lauterbur. 2003. Nobel Laureate in Physiology and Medicine for (2D and 3D) MRI. (http://nobelprize.org/nobel_prizes/medicine/laureates/2003/)

- Jean Jeener. 1971. Two-dimensional Fourier Transform NMR, presented at an Ampere International Summer School, Basko Polje, unpublished. A verbatim quote follows from Richard R. Ernst's Nobel Laureate Lecture delivered on December 2, 1992, "A new approach to measure two-dimensional (2D) spectra." has been proposed by Jean Jeener at an Ampere Summer School in Basko Polje, Yugoslavia, 1971 (Jean Jeneer,1971}). He suggested a 2D Fourier transform experiment consisting of two $\pi/2$ pulses with a variable time t_1 between the pulses and the time variable t_2 measuring the time elapsed after the second pulse as shown in Fig. 6 that expands the principles of Fig. 1. Measuring the response $s(t_1,t_2)$ of the two-pulse sequence and Fourier-transformation with respect to both time variables produces a two-dimensional spectrum $S(O_1,O_2)$ of the desired form. This two-pulse experiment by Jean Jeener is the forefather of a whole class of $2D$ experiments that can also easily be expanded to multidimensional spectroscopy.

- Dudley, Robert, L (1993). "High-Field NMR Instrumentation". *Ch. 10 in Physical Chemistry of Food Processes* (New York: Van Nostrand-Reinhold) **2**: 421-30. ISBN 0-442-00582-2.

- Baianu, I.C.; Kumosinski, Thomas (August 1993). "NMR Principles and Applications to Structure and Hydration,". *Ch.9 in Physical Chemistry of Food Processes* (New York: Van Nostrand-Reinhold) **2**: 338-420. ISBN 0-442-00582-2.

- Haacke, E Mark; Brown, Robert F; Thompson, Michael; Venkatesan, Ramesh (1999). *Magnetic resonance imaging: physical principles and sequence design*. New York: J. Wiley & Sons. ISBN 0-471-35128-8.

- Raftery D (August 2006). "MRI without the magnet" (http://www.pubmedcentral.nih.gov/articlerender.fcgi?tool=pmcentrez&artid=1568902). *Proc Natl Acad Sci USA*. **103** (34): 12657–8. doi:10.1073/pnas.0605625103. PMID 16912110. PMC 1568902.

- Wu Y, Chesler DA, Glimcher MJ, *et al* (February 1999). "Multinuclear solid-state three-dimensional MRI of bone and synthetic calcium phosphates" (http://www.pnas.org/cgi/pmidlookup?view=long&pmid=9990066). *Proc. Natl. Acad. Sci. U.S.A*. **96** (4): 1574–8. doi:10.1073/pnas.96.4.1574. PMID 9990066. PMC 15521.

External links

- Cardiac Infarct or "heart attack" Imaged in Real Time by 2D-FT NMRI (http://www.mr-tip.com/exam_gifs/cardiac_infarct_short_axis_cine_6.gif)
- 3D Animation Movie about MRI Exam (http://www.patiencys.com/MRI/)
- Interactive Flash Animation on MRI (http://www.e-mri.org) - *Online Magnetic Resonance Imaging physics and technique course*
- International Society for Magnetic Resonance in Medicine (http://www.ismrm.org)
- Danger of objects flying into the scanner (http://www.simplyphysics.com/flying_objects.html)

Related Wikipedia websites

- Medical imaging
- Computed tomography
- Magnetic resonance microscopy
- Fourier transform spectroscopy
- FT-NIRS
- Magnetic resonance elastography

- Nuclear magnetic resonance (NMR)
- Chemical shift
- Relaxation
- Robinson oscillator
- Earth's field NMR (EFNMR)
- Rabi cycle

This article incorporates material by the original author from 2D-FT MR- Imaging and related Nobel awards (http:/ / planetphysics. org/ encyclopedia/ 2DFTImaging. html) *on* PlanetPhysics (http:// planetphysics. org/), *which is licensed under the GFDL.*

Solid-state nuclear magnetic resonance

Solid-state NMR (**SSNMR**) spectroscopy is a kind of nuclear magnetic resonance (NMR) spectroscopy, characterized by the presence of anisotropic (directionally dependent) interactions.

Introduction

Basic concepts A spin interacts with a magnetic or an electric field. Spatial proximity and/or a chemical bond between two atoms can give rise to interactions between nuclei. In general, these interactions are orientation dependent. In media with no or little mobility (e.g. crystals, powders, large membrane vesicles, molecular aggregates), anisotropic interactions have a substantial influence on the behaviour of a system of nuclear spins.

Solid-state 900 MHz (21.1 T[1]) NMR spectrometer at the Canadian National Ultrahigh-field NMR Facility for Solids.

In contrast, in a classical liquid-state NMR experiment, Brownian motion leads to an averaging of anisotropic interactions. In such cases, these interactions can be neglected on the time-scale of the NMR experiment.

Examples of anisotropic nuclear interactions Two directionally dependent interactions commonly found in solid-state NMR are the *chemical shift anisotropy* (CSA) and the internuclear *dipolar coupling*. Many more such interactions exist, such as the anisotropic J-coupling in NMR, or in related fields, such as the *g*-tensor in electron spin resonance. In mathematical terms, all these interactions can be described using the same formalism.
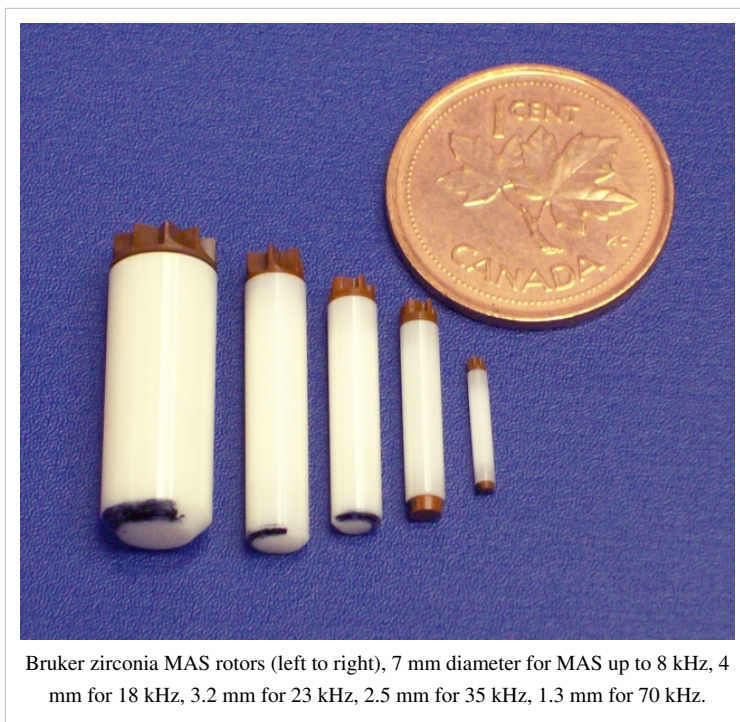
Experimental background Anisotropic interactions modify the nuclear spin energy levels (and hence the resonance frequency) of all sites in a molecule, and often contribute to a line-broadening effect in NMR spectra. However, there is a range of situations when their presence can either not be avoided, or is even particularly desired, as they encode structural parameters, such as orientation information, on the molecule of interest.

High-resolution conditions in solids (in a wider sense) can be established using magic angle spinning (MAS), macroscopic sample orientation, combinations of both of these techniques, enhancement of mobility by highly viscous sample conditions, and a variety of radio frequency (RF) irradiation patterns. While the latter allows decoupling of interactions in spin space, the others facilitate averaging of interactions in real space. In addition, line-broadening effects from microscopic inhomogeneities can be reduced by appropriate methods of sample preparation.

Under decoupling conditions, isotropic interactions can report on the local structure, e.g. by the isotropic chemical shift. In addition, decoupled interactions can be

Bruker zirconia MAS rotors (left to right), 7 mm diameter for MAS up to 8 kHz, 4 mm for 18 kHz, 3.2 mm for 23 kHz, 2.5 mm for 35 kHz, 1.3 mm for 70 kHz.

selectively re-introduced (recoupling"), and used, for example, for controlled de-phasing or transfer of polarization, which allows to derive a number of structural parameters.

Solid-state NMR line widths The residual line width (full width at half max) of ^{13}C nuclei under MAS conditions at 5−15 kHz spinning rate is typically in the order of 0.5−2 ppm, and may be comparable to solution-state NMR conditions. Even at MAS rates of 20 kHz and above, however, non linear groups (not a straight line) of the same nuclei linked via the homonuclear dipolar interactions can only be suppressed partially, leading to line widths of 0.5 ppm and above, which is considerably more than in optimal solution state NMR conditions. Other interactions such as the quadrupolar interaction can lead to line widths of 1000's of ppm due to the strength of the interaction. The first-order quadrupolar broadening is largely suppressed by sufficiently fast MAS, but the second-order quadrupolar broadening has a different angular dependence and cannot be removed by spinning at one angle alone. Ways to achieve isotropic lineshapes for quadrupolar nuclei include spinning at two angles simultaneously (DOR), sequentially (DAS), or through refocusing the second-order quadrupolar interaction with a two-dimensional experiment such as MQMAS or STMAS.

Anisotropic interactions in solution-state NMR From the perspective of solution-state NMR, it can be desirable to reduce motional averaging of dipolar interactions by alignment media. The order of magnitude of these residual dipolar couplings (RDCs) are typically of only a few rad/Hz, but do not destroy high-resolution conditions, and provide a pool of information, in particular on the orientation of molecular domains with respect to each other.

Dipolar truncation The dipolar coupling between two nuclei is inversely proportional to the cube of their distance. This has the effect that the polarization transfer mediated by the dipolar interaction is cut off in the presence of a third nucleus (all of the same kind, e.g. ^{13}C) close to one of these nuclei. This effect is commonly referred to as dipolar truncation. It has been one of the major obstacles in efficient extraction of internuclear distances, which are crucial in the structural analysis of biomolecular structure. By means of labeling schemes or pulse sequences, however, it has become possible to circumvent this problem in a number of ways.

Nuclear spin interactions in the solid phase

Chemical shielding

The chemical shielding is a local property of each nucleus, and depends on the external magnetic field.

Specifically, the external magnetic field induces currents of the electrons in molecular orbitals. These induced currents create local magnetic fields that often vary across the entire molecular framework such that nuclei in distinct molecular environments usually experience unique local fields from this effect.

Under sufficiently fast magic angle spinning, or in solution-state NMR, the directionally dependent character of the chemical shielding is removed, leaving the isotropic chemical shift.

J-coupling

The J-coupling or indirect nuclear spin-spin coupling (sometimes also called "scalar" coupling despite the fact that **J** is a tensor quantity) describes the interaction of nuclear spins through chemical bonds.

Dipolar coupling

Main article: Dipolar coupling (NMR)

Nuclear spins exhibit a dipole moment, which interacts with the dipole moment of other nuclei (dipolar coupling). The magnitude of the interaction is dependent on the spin species, the internuclear distance, and the orientation of the vector connecting the two nuclear spins with respect to the external magnetic field B (see figure). The maximum dipolar coupling is given by the dipolar coupling constant d,

Dipolar coupling vectors

$$d = \frac{\hbar \mu_0}{4\pi} \frac{\gamma_1 \gamma_2}{r^3},$$

where r is the distance between the nuclei, and γ_1 and γ_2 are the gyromagnetic ratios of the nuclei. In a strong magnetic field, the dipolar coupling depends on the orientation of the internuclear vector with the external magnetic field by

$$D \propto 3\cos^2\theta - 1.$$

Consequently, two nuclei with a dipolar coupling vector at an angle of θ_m=54.7° to a strong external magnetic field, which is the angle where D becomes zero, have zero dipolar coupling. θ_m is called the magic angle. One technique for removing dipolar couplings, at least to some extent, is magic angle spinning.

Quadrupolar interaction

Nuclei with a spin greater than one-half have a non spherical charge distribution. This is known as a quadrupolar nucleus. A non spherical charge distribution can interact with an electric field gradient caused by some form of non-symmetry (e.g. in a trigonal bonding atom there are electrons around it in a plane, but not above or below it) to produce a change in the energy level in addition to the Zeeman effect. The quadrupolar interaction is the largest interaction in NMR apart from the Zeeman interaction and they can even become comparable in size. Due to the interaction being so large it can not be treated to just the first order, like most of the other interactions. This means you have a first and second order interaction, which can be treated separately. The first order interaction has an angular dependency with respect to the magnetic field of $(3\cos^2\theta - 1)$ (the P2 Legendre polynomial), this means

that if you spin the sample at $\theta = \arctan \sqrt{2}$(~54.74°) you can average out the first order interaction over one rotor period (all oth interactions apart from Zeeman, Chemical shift, paramagnetic and J coupling also have this angular dependency). However, the second order interaction depends on the P4 Legendre polynomial which has zero points at 30.6° and 70.1°. These can be taken advantage of by either using DOR (DOuble angle Rotation) where you spin at two angles at the same time, or DAS (Double Angle Spinning) where you switch quickly between the two angles. But these techniques suffer from the fact that they require special hardware (probe). A revolutionary advance is Lucio Frydman's multiple quantum magic angle spinning (MQMAS) NMR in 1995 and it has become a routine method for obtaining high resolution solid-state NMR spectra of quadrupolar nuclei[2] [3] . A similar method to MQMAS is satellite transisition magic angle spinning (STMAS) NMR proposed by Zhehong Gan in 2000.

Other interactions

Paramagnetic substances are subject to the Knight shift.

History

See also: nuclear magnetic resonance or NMR spectroscopy articles for an account on discoveries in NMR and NMR spectroscopy in general.

History of discoveries of NMR phenomena, and the development of solid-state NMR spectroscopy:

Purcell, Torrey and Pound: "nuclear induction" on ^{1}H in paraffin 1945, at about the same time Bloch *et al.* on ^{1}H in water.
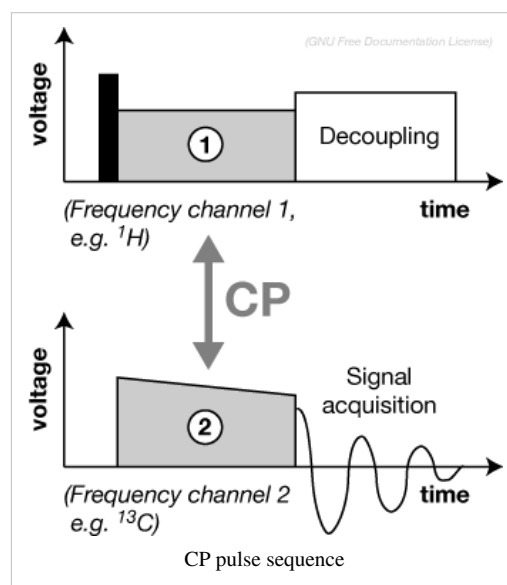
Modern solid-state NMR spectroscopy

Methods and techniques

Basic example

A fundamental RF pulse sequence and building-block in most solid-state NMR experiments is cross-polarization (CP) [Waugh *et al.*]. It can be used to enhance the signal of nuclei with a low gyromagnetic ratio (e.g. [13]C, ^{15}N) by magnetization transfer from nuclei with a high gyromagnetic ratio (e.g. [1]H), or as spectral editing method (e.g. directed [15]N→[13]C CP in protein spectroscopy). In order to establish magnetization transfer, the RF pulses applied on the two frequency channels must fulfill the Hartmann–Hahn condition [Hartmann, 1962]. Under MAS, this condition defines a relationship between the voltage through the RF coil and the rate of sample rotation. Experimental optimization of such conditions is one of the routine tasks in performing a (solid-state) NMR experiment.

CP pulse sequence

CP is a basic building block of most pulse sequences in solid-state NMR spectroscopy. Given its importance, a pulse sequence employing direct excitation of ^{1}H spin polarization, followed by CP transfer to and signal detection of ^{13}C, ^{15}N) or similar nuclei, is itself often referred to as *CP experiment*, or, in conjunction with MAS, as *CP-MAS* [Schaefer and Stejskal, 1976]. It is the typical starting point of an investigation using solid-state NMR spectroscopy.

Decoupling

Nuclear spin interactions need to be removed (decoupled) in order to increase the resolution of NMR spectra, and to isolate spin systems.

A technique that can substantially reduce or remove the chemical shift anisotropy, the dipolar coupling is *sample rotation* (most commonly magic angle spinning, but also off-magic angle spinning).

Homonuclear RF decoupling decouples spin interactions of nuclei which are the same as those which are being detected. *Heteronuclear RF decoupling* decouples spin interactions of other nuclei.

Recoupling

Although the broadened lines are often not desired, dipolar couplings between atoms in the crystal lattice can also provide very useful information. Dipolar coupling are distance dependent, and so they may be used to calculate interatomic distances in isotopically labeled molecules.

Because most dipolar interactions are removed by sample spinning, recoupling experiments are needed to re-introduce desired dipolar couplings so they can be measured.

An example of a recoupling experiment is the Rotational Echo DOuble Resonance (REDOR) experiment [Gullion and Schaefer, 1989].

Applications

Biology

Membrane proteins and amyloid fibrils, the latter related to Alzheimer's disease and Parkinson's disease, are two examples of application where solid-state NMR spectroscopy complements solution-state NMR spectroscopy and beam diffraction methods (e.g. X-ray crystallography, electron microscopy).

Chemistry

Solid-state NMR spectroscopy serves as an analysis tool in organic and inorganic chemistry. SSNMR is also a valuable tool to study local dynamics, kinetics, and thermodynamics of a variety of systems.

References

[1] http://nmr900.ca/instrument_e.html

[2] Isotropic Spectra of Half-Integer Quadrupolar Spins from Bidimensional Magic-Angle Spinning NMR, Lucio Frydman and John S. Hardwood, *J. Am. Chem. Soc.*, **1995**, *117*, 5367—5368, (1995)

[3] Two-dimensional Magic-Angle Spinning Isotropic Reconstruction Sequences for Quadrupolar Nuclei , D. Massiot, B. Touzo, D. Trumeau, J. P. Coutures, J. Virlet, P. Florian and P. J. Grandinetti , *Solid-State NMR* , **6**, 73 (1996)

Suggested readings for beginners

- High Resolution Solid-State NMR of Quadrupolar Nuclei (http://www.grandinetti.org/assets/ GrandinettiRMCBruker2007.pdf) Grandinetti ENC Tutorial
- David D. Laws, Hans-Marcus L. Bitter, and Alexej Jerschow, "Solid-State NMR Spectroscopic Methods in Chemistry", Angewandte Chemie International Edition (engl.), Vol. 41, pp. 3096 (2002) doi:10.1002/1521-3773(20020902)41:17<3096::AID-ANIE3096>3.0.CO;2-X
- Levitt, Malcolm H., *Spin Dynamics: Basics of Nuclear Magnetic Resonance*, Wiley, Chichester, United Kingdom, 2001. (NMR basics, including solids)
- Duer, Melinda J., *Introduction to Solid-State NMR Spectroscopy*, Blackwell, Oxford, 2004. (Some detailed examples of SSNMR spectroscopy)

Advanced readings

Books and major review articles

- McDermott, A, Structure and Dynamics of Membrane Proteins by Magic Angle Spinning Solid-State NMR (http://arjournals.annualreviews.org/doi/abs/10.1146/annurev.biophys.050708.133719) *Annual Review of Biophysics*, v. 38, 2009.
- Mehring, M, *Principles of High Resolution NMR in Solids*, 2nd ed., Springer, Heidelberg, 1983.
- Slichter, C. P., *Principles of Magnetic Resonance*, 3rd ed., Springer, Heidelberg, 1990.
- Gerstein, B. C. and Dybowski, C., *Transient Techniques in NMR of Solids*, Academic Press, San Diego, 1985.
- Schmidt-Rohr, K. and Spiess, H.-W., *Multidimensional Solid-State NMR and Polymers*, Academic Press, San Diego, 1994.
- Dybowski, C. and Lichter, R. L., *NMR Spectroscopy Techniques*, Marcel Dekker, New York, 1987.
- Ramamoorthy, A., *NMR Spectroscopy of Biological Solids*, Taylor & Francis, New York, 2006.

General

References to books and research articles

- Andrew, E. R., Bradbury, A. and Eades, R. G., "Removal of Dipolar Broadening of Nuclear Magnetic Resonance Spectra of Solids by Specimen Rotation," Nature 183, 1802, (1959)
- Ernst, Bodenhausen, Wokaun: *Principles of Nuclear Magnetic Resonance in One and Two Dimensions*
- Hartmann S.R., Hahn E.L., "Nuclear Double Resonance in the Rotating Frame" Phys. Rev. 128 (1962) 2042.
- Pines A., Gibby M.G., Waugh J.S., "Proton-enhanced NMR of dilute spins in solids" J. Chem. Phys. 59, 569-90, (1973)
- Purcell, Torrey and Pound (1945).
- Schaefer, J. and Stejskal, E. O., "Carbon-13 Nuclear Magnetic Resonance of Polymers Spinning at the Magic Angle," Journal of the American Chemical Society 98, 1031 (1976).
- Gullion, T. and Schaefer, J., "Rotational-Echo, Double-Resonance NMR," J. Magn. Reson., 81, 196 (1989).

External links

- *NMRW*iki.ORG (http://www.nmrwiki.org) NMR resource you can edit
- SSNMRBLOG (http://ssnmr.blogspot.com/) Solid-State NMR Literature Blog by Prof. Rob Schurko's Solid-State NMR group at the University of Windsor
- www.ssnmr.org (http://www.ssnmr.org) Rocky Mountain Conference on Solid-State NMR
- Varian Inc (http://www.varianinc.com) NMR system/product manufacturer

Protein nuclear magnetic resonance spectroscopy

Protein nuclear magnetic resonance spectroscopy (usually abbreviated **protein NMR**) is a field of structural biology in which NMR spectroscopy is used to obtain information about the structure and dynamics of proteins. The field was pioneered by, among others, by Richard R. Ernst and Kurt Wüthrich[1]. Protein NMR techniques are continually being used and improved in both academia and the biotech industry. Structure determination by NMR spectroscopy usually consists of several following phases, each using a separate set of highly specialized techniques. The sample is prepared, resonances are assigned, restraints are generated and a structure is calculated and validated.

Pacific Northwest National Laboratory's high magnetic field (800 MHz) NMR spectrometer being loaded with a sample.

Sample preparation

Protein nuclear magnetic resonance is performed on aqueous samples of highly purified protein. Usually the sample consist of between 300 and 600 microlitres with a protein concentration in the range $0.1 - 3$ millimolar. The source of the protein can be either natural or produced in an expression system using recombinant DNA techniques through genetic engineering. Recombinantly expressed proteins are usually easier to produce in sufficient quantity, and makes isotopic labelling possible.

The purified protein is usually dissolved in a buffer solution and adjusted to the desired solvent conditions. The NMR sample is prepared in a thin walled glass tube.

Data collection

Protein NMR utilizes multidimensional nuclear magnetic resonance experiments to obtain information about the protein. Ideally, each distinct nucleus in the molecule experiences a distinct chemical environment and thus has a distinct chemical shift by which it can be recognized. However, in large molecules

The NMR sample is prepared in a thin walled glass tube.

such as proteins the number of resonances can typically be several thousand and a one-dimensional spectrum inevitably has incidental overlaps. Therefore multidimensional experiments are performed which correlate the

frequencies of distinct nuclei. The additional dimensions decrease the chance of overlap and have a larger information content since they correlate signals from nuclei within a specific part of the molecule. Magnetization is

transferred into the sample using pulses of electromagnetic (radiofrequency) energy and between nuclei using delays; the process is described with so-called pulse sequences. Pulse sequences allow the experimenter to investigate and select specific types of connections between nuclei. The array of nuclear magnetic resonance experiments used on proteins fall in two main categories — one where magnetization is transferred through the chemical bonds, and one where the transfer is through space, irrespective of the bonding structure. The first category is used to assign the different chemical shifts to a specific nucleus, and the second is primarily used to generate the distance restraints used in the structure calculation, and in the assignment with unlabelled protein.

Depending on the concentration of the sample, on the magnetic field of the spectrometer, and on the type of experiment, a single multidimensional nuclear magnetic resonance experiment on a protein sample may take hours or even several days to obtain suitable signal-to-noise ratio through signal averaging, and to allow for sufficient evolution of magnetization transfer through the various dimensions of the experiment. Other things being equal, higher-dimensional experiments will take longer than lower-dimensional experiments.

Typically the first experiment to be measured with an isotope-labelled protein is a 2D heteronuclear single quantum correlation (HSQC) spectrum where "heteronuclear" refers to nuclei other than 1H. In theory the heteronuclear single quantum correlation has one peak for each H bound to a heteronucleus. Thus in the 15N-HSQC one signal is expected for each amino acid residue with the exception of proline which has no amide-hydrogen due to the cyclic nature of its backbone. Tryptophan and certain other residues with N-containing sidechains also give rise to additional signals. The 15N-HSQC is often referred to as the fingerprint of a protein because each protein has a unique pattern of signal positions. Analysis of the 15N-HSQC allows researchers to evaluate whether the expected number of peaks is present and thus to identify possible problems due to multiple conformations or sample heterogeneity. The relatively quick heteronuclear single quantum correlation experiment helps determine the feasibility of doing subsequent longer, more expensive, and more elaborate experiments. It is not possible to assign peaks to specific atoms from the heteronuclear single quantum correlation alone.
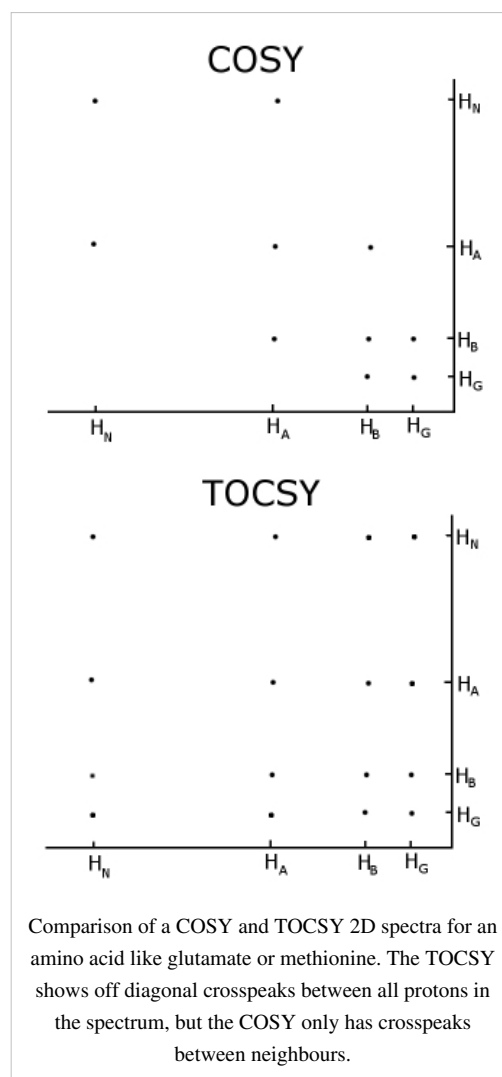
Resonance assignment

In order to analyze the nuclear magnetic resonance data, it is important to get a resonance assignment for the protein. That is to find out which chemical shift corresponds to which atom. This is typically achieved by sequential walking using information derived from several different types of NMR experiment. The exact procedure depends on whether the protein is isotopically labelled or not, since a lot of the assignment experiments depend on carbon-13 and nitrogen-15.
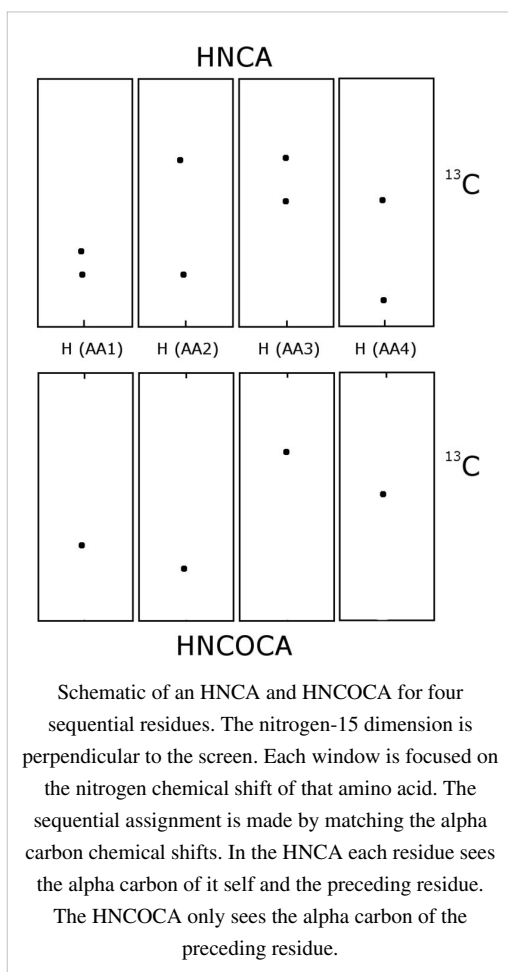
Homonuclear nuclear magnetic resonance

With unlabelled protein the usual procedure is to record a set of two dimensional homonuclear nuclear magnetic resonance experiments through correlation spectroscopy (COSY), of which several types include conventional correlation spectroscopy, *total correlation* spectroscopy (TOCSY) and nuclear Overhauser effect spectroscopy (NOESY).[2] A two-dimensional nuclear magnetic resonance experiment produces a two-dimensional spectrum. The units of both axes are chemical shifts. The COSY and TOCSY transfer magnetization through the chemical bonds between adjacent protons. The conventional correlation spectroscopy experiment is only able to transfer magnetization between protons on adjacent atoms, whereas in the total correlation spectroscopy experiment the protons are able to relay the magnetization, so it is transferred among all the protons that are connected by adjacent atoms. Thus in a conventional correlation spectroscopy, an alpha proton transfers magnetization to the beta protons, the beta protons transfers to the alpha and gamma protons, if any are present, then the gamma proton transfers to the beta and the delta protons, and the process continues. In total correlation spectroscopy, the alpha and all the other protons are able to transfer magnetization to the beta, gamma, delta, epsilon if they are connected by a continuous chain of protons. The continuous chain of protons are the sidechain of the individual amino acids. Thus these two experiments are used to build so called spin systems, that is build a list of resonances of the chemical shift of the peptide proton, the alpha protons and all the protons from each residue's sidechain. Which chemical shifts corresponds to which nuclei in the spin system is determined by the conventional correlation spectroscopy connectivities and the fact that different types of protons have characteristic chemical shifts. To connect the different spinsystems in a sequential order, the nuclear Overhauser effect spectroscopy experiment has to be used. Because this experiment transfers magnetization through space, it will show crosspeaks for all protons that are close in space regardless of whether they are in the same spin system or not. The neighbouring residues are inherently close in space, so the assignments can be made by the peaks in the NOESY with other spin systems.

Comparison of a COSY and TOCSY 2D spectra for an amino acid like glutamate or methionine. The TOCSY shows off diagonal crosspeaks between all protons in the spectrum, but the COSY only has crosspeaks between neighbours.

One important problem using homonuclear nuclear magnetic resonance is overlap between peaks. This occurs when different protons have the same or very similar chemical shifts. This problem becomes greater as the protein becomes larger, so homonuclear nuclear magnetic resonance is usually restricted to small proteins or peptides.

Nitrogen-15 nuclear magnetic resonance

HNCA

H (AA1)   H (AA2)   H (AA3)   H (AA4)

^{13}C

^{13}C

HNCOCA

Schematic of an HNCA and HNCOCA for four sequential residues. The nitrogen-15 dimension is perpendicular to the screen. Each window is focused on the nitrogen chemical shift of that amino acid. The sequential assignment is made by matching the alpha carbon chemical shifts. In the HNCA each residue sees the alpha carbon of it self and the preceding residue. The HNCOCA only sees the alpha carbon of the preceding residue.

Carbon-13 and nitrogen-15 nuclear magnetic resonance

When the protein is labelled with carbon-13 and nitrogen-15 it is possible to record an experiment that transfers magnetisation over the peptide bond, and thus connect different spin systems through bonds. This is usually done using some of the following experiments, HNCO, HNCACO, HNCA,[3] HNCOCA, HNCACB and CBCACONH. All six experiments consist of a HSQC plane expanded with a carbon dimension. In the HNCACO the spectrum contains peaks at the chemical shifts of the carbonyl carbons in the residue of the HSQC peak and the previous one in the sequence. The HNCO only contains the chemical shift from the previous residue, and it is thus possible to assign the carbonyl carbon shifts that corresponds to each HSQC peak and the one previous to that one. Sequential assignment can then be undertaken by matching the shifts of each spin system's own and previous carbons. The HNCA and HNCOCA works similarly, just with the alpha carbons rather than the carbonyls, and the HNCACB and the CBCACONH contains both the alpha carbon and the beta carbon. Usually several of these experiments are required to resolve overlap in the carbon dimension. This procedure is usually less ambiguous than the NOESY based method, since it is based on through bond transfer. In the NOESY-based methods additional peaks that are close in space but not belonging to the sequential residues will appear confusing the assignment process. When the sequential assignment has been made it is usually possible to assign the sidechains using HCCH-TOCSY, which is basically a TOCSY experiment resolved in an additional carbon dimension.

Restraint generation

In order to make structure calculations a number of experimentially determined restraints have to be generated. These fall into different categories, the most widely used is distance restraints and angle restraints.

Distance restraints

A crosspeak in a NOESY experiment signifies spatial proximity between the two nuclei in question. Thus each peak can be converted in to a maximum distance between the nuclei, usually between 1,8 and 6 angstroms. The intensity of a noesy peak is proportional to the distance to the minus 6th power, so the distance is determined according to intensity of the peak. The intensity-distance relationship is not exact, so usually a distance range is used.

It is of great importance to assign the noesy peaks to the correct nuclei based on the chemical shifts. If this task is performed manually it is usually very labor intensive, since proteins usually have thousands of noesy peaks. Some computer programs such as UNIO[4] , CYANA[5] and ARIA[6] /CNS perform this task automatically, coupled to a structure calculation.

To obtain as accurate assignments as possible it is a great advantage to have access to carbon-13 and nitrogen-15 noesy experiments, since they help to resolve overlap in the proton dimension. This leads to faster and more reliable

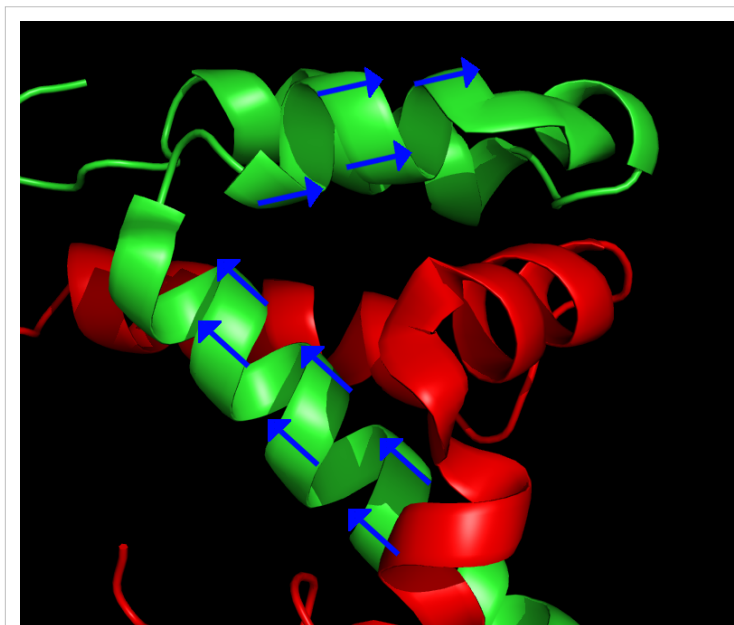assignments, and in turn to better structures.

Angle restraints

In addition to distance restraints, restraints on the torsion angles of the chemical bonds, typically the psi and phi angles can be generated. One approach is to use the Karplus equation, to generate angle restraints from coupling constants. Another approach uses the chemical shifts to generate angle restraints. Both methods use the fact that the geometry around the alpha carbon affects the coupling constants and chemical shifts, so given the coupling constants or the chemical shifts, a qualified guess can be made about the torsion angles.

Orientation restraints

The analyte molecules in a sample can be partially ordered with respect to the external magnetic field of the spectrometer by manipulating the sample conditions. Common techniques include addition of bacteriophages or bicelles to the sample, or preparation of the sample in a stretched polyacrylamide gel. This creates a local environment that favours certain orientations of nonspherical molecules. Normally in solution NMR the dipolar couplings between nuclei are averaged out because of the fast tumbling of the molecule. The slight overpopulation of one orientation means that a residual dipolar coupling remains to be observed. The dipolar coupling is commonly used in solid state NMR and provides information about the relative orientation of the bond vectors relative to a single global reference frame.
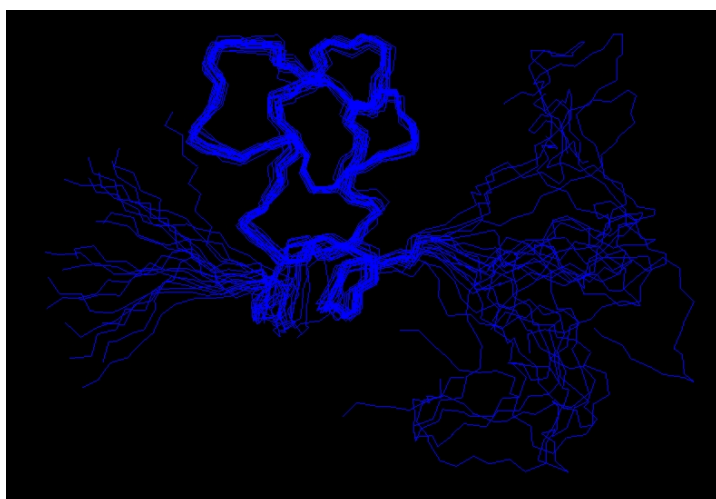
The blue arrows represent the orientation of the N - H bond of selected peptide bonds. By determining the orientation of a sufficient amount of bonds relative to the external magnetic field, the structure of the protein can be determined. From PDB record 1KBH

Typically the orientation of the N-H vector is probed in a HSQC like experiment. Initially residual dipolar couplings were used for refinement of previously determined structures, but attempts at de novo structure determination have also been made.[7]

Hydrogen-Deuterium exchange

NMR spectroscopy is nuclei specific. Thus it can distinguish between hydrogen and deuterium. The amide protons in the protein exchange readily with the solvent, and if the solvent contains a different isotope, typically deuterium, the reaction can be monitored by NMR spectroscopy. How rapidly a given amide exchanges reflects its solvent accessibility. Thus amide exchange rates can give information on which parts of the protein are buried, hydrogen bonded etc. A common application is to compare the exchange of a free form versus a complex. The amides that become protected in the complex, are assumed to be in the interaction interface.

Structure calculation

Nuclear magnetic resonance structure determination generates an ensemble of structures. The structures will only converge if the data is sufficient to dictate a specific fold. In these structures, it is only the case for a part of the structure. From PDB 1SSU.

The experimentially determined restraints can be used as input for the structure calculation process. Researchers, using computer programs such as CYANA (Software) or XPLOR-NIH,[8] attempt to satisfy as many of the restraints as possible, in addition to general properties of proteins such as bond lengths and angles. The algorithms convert the restraints and the general protein properties into energy terms, and thus tries to minimize the energy. The process results in an ensemble of structures that, if the data were sufficient to dictate a certain fold, will converge.

Dynamics

In addition to structures, nuclear magnetic resonance can yield information on the dynamics of various parts of the protein. This usually involves measuring relaxation times such as T_1 and T_2 to determine order parameters, correlation times, and chemical exchange rates. NMR relaxation is a consequence of local fluctuating magnetic fields within a molecule. Local fluctuating magnetic fields are generated by molecular motions. In this way measurements of relaxation times can provide information of motions within a molecule on the atomic level. In NMR studies of protein dynamics the nitrogen-15 isotope is the preferred nucleus to study, because its relaxation times are relatively simple to relate to molecular motions, which however requires isotope labeling of the protein. The T_1 and T_2 relaxation times can be measured using various types of HSQC based experiments. The types of motions, which can be detected, are motions that occur on a time-scale ranging from about 10 picoseconds to about 10 nanoseconds. In addition slower motions, which take place on a time-scale ranging from about 10 microseconds to 100 milliseconds can also be studied. However, since nitrogen atoms are mainly found in the backbone of a protein, the results mainly reflect the motions of the backbone, which is the most rigid part of a protein molecule. Thus, the results obtained from nitrogen-15 relaxation measurements may not be representative for the whole protein. Therefore techniques utilizing relaxation measurements of carbon-13 and deuterium have recently been developed, which enables systematic studies of motions of the amino acid side chains in proteins.

NMR spectroscopy on large proteins

Traditionally nuclear magnetic resonance spectroscopy has been limited to relatively small proteins or protein domains. This is in part caused by problems resolving overlapping peaks in larger proteins, but this has been alleviated by the introduction of isotope labelling and multidimensional experiments. Another more serious problem is the fact that in large proteins the magnetization relaxes faster, which means there is less time to detect the signal. This in turn causes the peaks to become broader and weaker, and eventually disappear. Two techniques have been introduced to attenuate the relaxation: transverse relaxation optimized spectroscopy (TROSY)[9] and deuteration[10] of proteins. By using these techniques it has been possible to study proteins in complex with the 900 kDa chaperone GroES-GroEL.[11]

Automation of the process

Structure determination by NMR has traditionally been a time consuming process, requiring interactive analysis of the data by a highly trained scientist. There has been a considerable interest in automating the process to increase the throughput of structure determination and to make protein NMR accessible to non-experts (See structural genomics). The two most time consuming processes involved are the sequence-specific resonance assignment (backbone and side-chain assignment) and the NOE assignment tasks. Several different computer programs have been published that target individual parts of the overall NMR structure determination process in an automated fashion. Most progress have been achieved for the task of automated NOE assignment. So far, only the FLYA and the UNIO approach were proposed to perform the entire protein NMR structure determination process in an automated manner without any human intervention [5] aria. Efforts have also been made to standardize the structure calculation protocol to make it quicker and more amenable to automation.[12]

See also

- 2D-FT NMRI and Spectroscopy
- X-ray crystallography
- Nuclear magnetic resonance
- NMR spectroscopy
- Protein crystallization
- Protein dynamics

References

General references

- T. Kevin Hitchens; Gordon S. Rule (2005). *Fundamentals of Protein NMR Spectroscopy (Focus on Structural Biology)* [13]. Berlin: Springer. ISBN 1-4020-3499-7.
- Quincy Teng (2005). *Structural biology: practical NMR applications*. Berlin: Springer. ISBN 0-387-24367-4.
- Mark Rance; Cavanagh, John; Wayne J. Fairbrother; Arthur W. Hunt III; Skelton, Nicholas J. (2007). *Protein NMR spectroscopy: principles and practice* (2nd ed.). Boston: Academic Press. ISBN 0-12-164491-X.
- Kurt Wüthrich (1986). *NMR of proteins and nucleic acids*. New York: Wiley. ISBN 0-471-82893-9.

Related links

- NOESY-Based Strategy for Assignments of Backbone and Side Chain Resonances of Large Proteins without Deuteration (a protocol) [14]
- ProSA-web [15] Web service for the recognition of errors in experimentally or theoretically determined protein structures
- *NMRW*iki.ORG [40] NMR resource you can edit
- Protein NMR [16] Protein NMR experiments

References

[1] http://www.nature.com/nsmb/journal/v8/n11/full/nsb1101-923.html

[2] Wüthrich K (December 1990). "Protein structure determination in solution by NMR spectroscopy". *J. Biol. Chem.* **265** (36): 22059−62. PMID 2266107.

[3] Bax A, Ikura M (May 1991). "An efficient 3D NMR technique for correlating the proton and 15N backbone amide resonances with the alpha-carbon of the preceding residue in uniformly 15N/13C enriched proteins". *J. Biomol. NMR* **1** (1): 99−104. doi:10.1007/BF01874573. PMID 1668719.

[4] Herrmann T (2010). "Protein structure calculation and automated NOE restraints". *Encycl. Magn. Res.*. doi:10.1002/9780470034590.emrstm1151.

[5] Güntert P (2004). "Automated NMR structure calculation with CYANA". *Methods Mol. Biol.* **278**: 353−78. doi:10.1385/1-59259-809-9:353. PMID 15318003.

[6] Rieping W, Habeck M, Bardiaux B, Bernard A, Malliavin TE, Nilges M (February 2007). "ARIA2: automated NOE assignment and data integration in NMR structure calculation". *Bioinformatics* **23** (3): 381−2. doi:10.1093/bioinformatics/btl589. PMID 17121777.

[7] de Alba E, Tjandra N (2004). "Residual dipolar couplings in protein structure determination". *Methods Mol. Biol.* **278**: 89−106. doi:10.1385/1-59259-809-9:089. PMID 15317993.

[8] Schwieters CD, Kuszewski JJ, Tjandra N, Clore GM (January 2003). "The Xplor-NIH NMR molecular structure determination package". *J. Magn. Reson.* **160** (1): 65−73. doi:10.1016/S1090-7807(02)00014-9. PMID 12565051.

[9] Pervushin K, Riek R, Wider G, Wüthrich K (November 1997). "Attenuated T2 relaxation by mutual cancellation of dipole-dipole coupling and chemical shift anisotropy indicates an avenue to NMR structures of very large biological macromolecules in solution" (http://www.pubmedcentral.nih.gov/articlerender.fcgi?tool=pmcentrez&artid=24947). *Proc. Natl. Acad. Sci. U.S.A.* **94** (23): 12366−71. doi:10.1073/pnas.94.23.12366. PMID 9356455. PMC 24947.

[10] Markus MA, Dayie KT, Matsudaira P, Wagner G (October 1994). "Effect of deuteration on the amide proton relaxation rates in proteins. Heteronuclear NMR experiments on villin 14T". *J Magn Reson B* **105** (2): 192−5. doi:10.1006/jmrb.1994.1122. PMID 7952934.

[11] Fiaux J, Bertelsen EB, Horwich AL, Wüthrich K (July 2002). "NMR analysis of a 900K GroEL GroES complex". *Nature* **418** (6894): 207−11. doi:10.1038/nature00860. PMID 12110894.

[12] Liu G, Shen Y, Atreya HS, *et al.* (July 2005). "NMR data collection and analysis protocol for high-throughput protein structure determination" (http://www.pubmedcentral.nih.gov/articlerender.fcgi?tool=pmcentrez&artid=1180791). *Proc. Natl. Acad. Sci. U.S.A.* **102** (30): 10487−92. doi:10.1073/pnas.0504338102. PMID 16027363. PMC 1180791.

[13] http://www.springer.com/1-4020-3499-7

[14] http://www.natureprotocols.com/2006/11/09/noesybased_strategy_for_assign.php

[15] https://prosa.services.came.sbg.ac.at/prosa.php

[16] http://nmr.chinanmr.cn/guide/eNMR/proteins/protindex.html

Magnetic resonance microscopy

Magnetic Resonance Microscopy (MRM, μMRI) is Magnetic Resonance Imaging (MRI) at a microscopic level. A strict definition is MRI having voxel resolutions of better than 100 μm³ [1] .

Nomenclature

Many scientist in the field consider the name Magnetic Resonance Microscopy to be a misnomer, since the images produced are much worse than those produced by even a marginal optical or electron microscope. As such, the name High Resolution Magnetic Resonance Imaging is often preferred in scientific literature on the subject. In fact, the term is most widely used by the High Resolution Magnetic Resonance Imaging group from Duke University, headed by Allan Johnson.

Differences between MRI and MRM

- Resolution: Typical medical MRI resolution is about 1 mm³; the desired resolution of MRM is 100 μm³ or smaller.
- Specimen size: Medical MRI machines are designed so that a patient may fit inside. MRM chambers are usually small, typically less than 1 cm³.

Current status of MRM

Although MRI is very common for medical applications, MRM is still developed in laboratories. The major barriers for practical MRM include:

- Magnetic field gradient: High gradient focus the magnetic resonance in a smaller volume (smaller point spread function), results in a better spatial resolution. The gradients for MRM are typically 50 to 100 times those of clinical systems. However, the construction of radio frequency (RF) coil used in MRM does not allow ultrahigh gradient.
- Sensitivity: Because the voxels for MRM can be 1/100,000 of those in MRI, the signal will be proportionately weaker [2] .

Alternative MRM

Magnetic Resonance Force Microscopy (MRFM) is claimed to have nm³-scale resolutions. It improves the sensitivity issue by introducing microfabricated cantilever to measure tiny signals. The magnetic gradient is generated by a micrometre-scale magnetic tip, yielding a typical gradient 10 million times larger than those of clinical systems. This technique is still in the beginning stage. Because the specimen need to be in high vacuum at cryogenic temperatures, MRFM can be only used for solid state matters.

External links

- Introduction to Magnetic Resonance Microscopy [3] Auditory Research Laboratory at the Univ. of North Carolina.

References

[1] P. Glover and P. Mansfield, Limits to magnetic resonance microscopy, Rep. Prog. Phys. 65 1489–1511, 2002

[2] R. Maronpot Applications of Magnetic Resonance Microscopy, Toxicologic Pathology, 32(Suppl. 2):42–48, 2004

[3] http://cbaweb2.med.unc.edu/henson_mrm/pages/mrmfaq.html#MRMAnchor

Imaging

Medical imaging

Medical imaging is the technique and process used to create images of the human body (or parts and function thereof) for clinical purposes (medical procedures seeking to reveal, diagnose or examine disease) or medical science (including the study of normal anatomy and physiology). Although imaging of removed organs and tissues can be performed for medical reasons, such procedures are not usually referred to as medical imaging, but rather are a part of pathology.

As a discipline and in its widest sense, it is part of biological imaging and incorporates radiology (in the wider sense), nuclear medicine, investigative radiological sciences, endoscopy, (medical) thermography, medical photography and microscopy (e.g. for human pathological investigations).

Measurement and recording techniques which are not primarily designed to produce images, such as electroencephalography (EEG), magnetoencephalography (MEG), Electrocardiography (EKG) and others, but which produce data susceptible to be represented as maps (i.e. containing positional information), can be seen as forms of medical imaging.

Overview

In the clinical context, medical imaging is generally equated to radiology or "clinical imaging" and the medical practitioner responsible for interpreting (and sometimes acquiring) the images is a radiologist. Diagnostic radiography designates the technical aspects of medical imaging and in particular the acquisition of medical images. The *radiographer* or *radiologic technologist* is usually responsible for acquiring medical images of diagnostic quality, although some radiological interventions are performed by radiologists. While radiology is an evaluation of anatomy, nuclear medicine provides functional assessment.

As a field of scientific investigation, medical imaging constitutes a sub-discipline of biomedical engineering, medical physics or medicine depending on the context: Research and development in the area of instrumentation, image acquisition (e.g. radiography), modelling and quantification are usually the preserve of biomedical engineering, medical physics and computer science; Research into the application and interpretation of medical images is usually the preserve of radiology and the medical sub-discipline relevant to medical condition or area of medical science (neuroscience, cardiology, psychiatry, psychology, etc.) under investigation. Many of the techniques developed for medical imaging also have scientific and industrial applications.

Medical imaging is often perceived to designate the set of techniques that noninvasively produce images of the internal aspect of the body. In this restricted sense, medical imaging can be seen as the solution of mathematical inverse problems. This means that cause (the properties of living tissue) is inferred from effect (the observed signal). In the case of ultrasonography the probe consists of ultrasonic pressure waves and echoes inside the tissue show the internal structure. In the case of projection radiography, the probe is X-ray radiation which is absorbed at different rates in different tissue types such as bone, muscle and fat.

The term noninvasive is a term based on the fact that following medical imaging modalities do not penetrate the skin physically. But on the electromagnetic and radiation level, they are quite invasive. From the high energy photons in X-Ray Computed Tomography, to the 2+ Tesla coils of an MRI device, these modalities alter the physical and chemical reactions of the body in order to obtain data.

Radiography

Two forms of radiographic images are in use in medical imaging; projection radiography and fluoroscopy, with the latter being useful for intraoperative and catheter guidance. These 2D techniques are still in wide use despite the advance of 3D tomography due to the low cost, high resolution, and depending on application, lower radiation dosages. This imaging modality utilizes a wide beam of x rays for image acquisition and is the first imaging technique available in modern medicine.
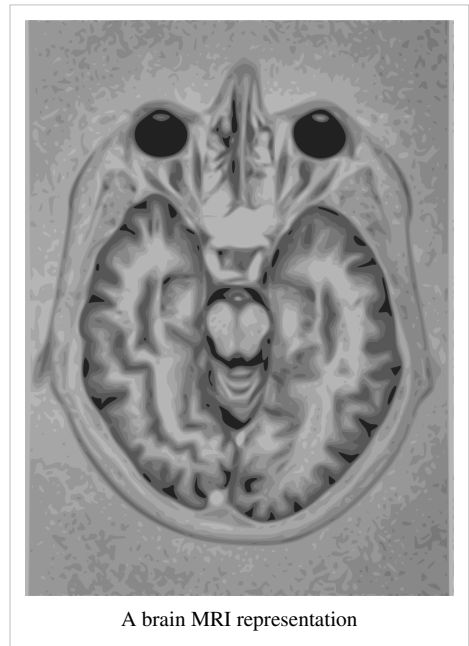
- *Fluoroscopy* produces real-time images of internal structures of the body in a similar fashion to radiography, but employs a constant input of x-rays, at a lower dose rate. Contrast media, such as barium, iodine, and air are used to visualize internal organs as they work. Fluoroscopy is also used in image-guided procedures when constant feedback during a procedure is required. An image receptor is required to convert the radiation into an image after it has passed through the area of interest. Early on this was a fluorescing screen, which gave way to an Image Amplifier (IA) which was a large vacuum tube that had the receiving end coated with cesium iodide, and a mirror at the opposite end. Eventually the mirror was replaced with a TV camera.

- *Projectional radiographs*, more commonly known as x-rays, are often used to determine the type and extent of a fracture as well as for detecting pathological changes in the lungs. With the use of radio-opaque contrast media, such as barium, they can also be used to visualize the structure of the stomach and intestines - this can help diagnose ulcers or certain types of colon cancer.

Magnetic resonance imaging (MRI)

A magnetic resonance imaging instrument (MRI scanner), or "nuclear magnetic resonance (NMR) imaging" scanner as it was originally known, uses powerful magnets to polarise and excite hydrogen nuclei (single proton) in water molecules in human tissue, producing a detectable signal which is spatially encoded, resulting in images of the body. MRI uses three electromagnetic fields: a very strong (on the order of units of teslas) static magnetic field to polarize the hydrogen nuclei, called the static field; a weaker time-varying (on the order of 1 kHz) field(s) for spatial encoding, called the gradient field(s); and a weak radio-frequency (RF) field for manipulation of the hydrogen nuclei to produce measurable signals, collected through an RF antenna.

Like CT, MRI traditionally creates a two dimensional image of a thin "slice" of the body and is therefore considered a tomographic imaging technique. Modern MRI instruments are capable of producing images in the form of 3D blocks, which may be considered a generalisation of the single-slice, tomographic, concept. Unlike CT, MRI does not involve the use of ionizing radiation and is therefore not associated

A brain MRI representation

with the same health hazards. For example, because MRI has only been in use since the early 1980s, there are no known long-term effects of exposure to strong static fields (this is the subject of some debate; see 'Safety' in MRI) and therefore there is no limit to the number of scans to which an individual can be subjected, in contrast with X-ray and CT. However, there are well-identified health risks associated with tissue heating from exposure to the RF field and the presence of implanted devices in the body, such as pace makers. These risks are strictly controlled as part of the design of the instrument and the scanning protocols used.

Because CT and MRI are sensitive to different tissue properties, the appearance of the images obtained with the two techniques differ markedly. In CT, X-rays must be blocked by some form of dense tissue to create an image, so the image quality when looking at soft tissues will be poor. In MRI, while any nucleus with a net nuclear spin can be

used, the proton of the hydrogen atom remains the most widely used, especially in the clinical setting, because it is so ubiquitous and returns a large signal. This nucleus, present in water molecules, allows the excellent soft-tissue contrast achievable with MRI.

Nuclear medicine

Nuclear medicine encompasses both diagnostic imaging and treatment of disease, and may also be referred to as molecular medicine or molecular imaging & therapeutics [1] . Nuclear medicine uses certain properties of isotopes and the energetic particles emitted from radioactive material to diagnose or treat various pathology. Different from the typical concept of anatomic radiology, nuclear medicine enables assessment of physiology. This function-based approach to medical evaluation has useful applications in most subspecialties, notably oncology, neurology, and cardiology. *Gamma cameras* are used in e.g. scintigraphy, SPECT and PET to detect regions of biologic activity that may be associated with disease. Relatively short lived isotope, such as ^{123}I is administered to the patient. Isotopes are often preferentially absorbed by biologically active tissue in the body, and can be used to identify tumors or fracture points in bone. Images are acquired after collimated photons are detected by a crystal that gives off a light signal, which is in turn amplified and converted into count data.

- *Scintigraphy* ("scint") is a form of diagnostic test wherein radioisotopes are taken internally, for example intravenously or orally. Then, gamma camera capture and form two-dimensional[2] images from the radiation emitted by the radiopharmaceuticals. For example, technetium-labeled isoniazid (INH) and ethambutol (EMB) has been used for tubercular imaging for early diagnosis of tuberculosis [3] .

- *SPECT* is a 3D tomographic technique that uses gamma camera data from many projections and can be reconstructed in different planes. A dual detector head gamma camera combined with a CT scanner, which provides localization of functional SPECT data, is termed a SPECT/CT camera, and has shown utility in advancing the field of molecular imaging.In most other medical imaging modalities, energy is passed through the body and the reaction or result is read by detectors. In SPECT imaging, the patient is injected with a radioisotope, most commonly Thallium 201TI, Technetium 99mTC, Iodine 123I, and Gallium 68Ga [4]

. The radioactive gamma rays are emitted through the body as the natural decaying process of these isotopes takes place. The emissions of the gamma rays are captured by detectors that surround the body. This essentially means that the human is now the source of the radioactivity, rather than the medical imaging devices such as X-Ray, CT, or Ultrasound.

- *Positron emission tomography* (PET) uses coincidence detection to image functional processes. Short-lived positron emitting isotope, such as ^{18}F, is incorporated with an organic substance such as glucose, creating F18-fluorodeoxyglucose, which can be used as a marker of metabolic utilization. Images of activity distribution throughout the body can show rapidly growing tissue, like tumor, metastasis, or infection. PET images can be viewed in comparison to computed tomography scans to determine an anatomic correlate. Modern scanners combine PET with a CT, or even MRI, to optimize the image reconstruction involved with positron imaging. This is performed on the same equipment without physically moving the patient off of the gantry. The resultant hybrid of functional and anatomic imaging information is a useful tool in non-invasive diagnosis and patient management.

Photoacoustic imaging

Photoacoustic imaging is a recently developed hybrid biomedical imaging modality based on the photoacoustic effect. It combines the advantages of optical absorption contrast with ultrasonic spatial resolution for deep imaging in (optical) diffusive or quasi-diffusive regime. Recent studies have shown that photoacoustic imaging can be used in vivo for tumor angiogenesis monitoring, blood oxygenation mapping, functional brain imaging, and skin melanoma detection, etc.

Breast Thermography

Digital infrared imaging thermography is based on the principle that metabolic activity and vascular circulation in both pre-cancerous tissue and the area surrounding a developing breast cancer is almost always higher than in normal breast tissue. Cancerous tumors require an ever-increasing supply of nutrients and therefore increase circulation to their cells by holding open existing blood vessels, opening dormant vessels, and creating new ones (neoangiogenesis). This process frequently results in an increase in regional surface temperatures of the breast. Digital infrared imaging uses extremely sensitive medical infrared cameras and sophisticated computers to detect, analyze, and produce high-resolution diagnostic images of these temperature variations. Because of DII's sensitivity, these temperature variations may be among the earliest signs of breast cancer and/or a pre-cancerous state of the breast[5] .

Tomography

Tomography is the method of imaging a single plane, or slice, of an object resulting in a tomogram. There are several forms of tomography:

- Linear tomography: This is the most basic form of tomography. The X-ray tube moved from point "A" to point "B" above the patient, while the cassette holder (or "bucky") moves simultaneously under the patient from point "B" to point "A." The fulcrum, or pivot point, is set to the area of interest. In this manner, the points above and below the focal plane are blurred out, just as the background is blurred when panning a camera during exposure. No longer carried out and replaced by computed tomography.
- Poly tomography: This was a complex form of tomography. With this technique, a number of geometrical movements were programmed, such as hypocycloidic, circular, figure 8, and elliptical. Philips Medical Systems [6] produced one such device called the 'Polytome.' This unit was still in use into the 1990s, as its resulting images for small or difficult physiology, such as the inner ear, was still difficult to image with CTs at that time. As the resolution of CTs got better, this procedure was taken over by the CT.
- Zonography: This is a variant of linear tomography, where a limited arc of movement is used. It is still used in some centres for visualising the kidney during an intravenous urogram (IVU).
- Orthopantomography (OPT or OPG): The only common tomographic examination in use. This makes use of a complex movement to allow the radiographic examination of the mandible, as if it were a flat bone. It is often referred to as a "Panorex", but this is incorrect, as it is a trademark of a specific company.
- Computed Tomography (CT), or Computed Axial Tomography (CAT: A CT scan, also known as a CAT scan), is a helical tomography (latest generation), which traditionally produces a 2D image of the structures in a thin section of the body. It uses X-rays. It has a greater ionizing radiation dose burden than projection radiography; repeated scans must be limited to avoid health effects. CT is based on the same principles as X-Ray projections but in this case, the patient is enclosed in a surrounding ring of detectors assigned with 500-1000 scintillation detectors[4]

. This being the fourth-generation X-Ray CT scanner geometry. Previously in older generation scanners, the X-Ray beam was paired by a translating source and detector.

Ultrasound

Medical ultrasonography uses high frequency broadband sound waves in the megahertz range that are reflected by tissue to varying degrees to produce (up to 3D) images. This is commonly associated with imaging the fetus in pregnant women. Uses of ultrasound are much broader, however. Other important uses include imaging the abdominal organs, heart, breast, muscles, tendons, arteries and veins. While it may provide less anatomical detail than techniques such as CT or MRI, it has several advantages which make it ideal in numerous situations, in particular that it studies the function of moving structures in real-time, emits no ionizing radiation, and contains speckle that can be used in elastography. Ultrasound is also used as a popular research tool for capturing raw data,

that can be made available through an Ultrasound research interface, for the purpose of tissue characterization and implementation of new image processing techniques. The concepts of ultrasound differ from other medical imaging modalities in the fact that it is operated by the transmission and receipt of sound waves. The high frequency sound waves are sent into the tissue and depending on the composition of the different tissues; the signal will be attenuated and returned at separate intervals. A path of reflected sound waves in a multilayered structure can be defined by an input acoustic impedance(Ultrasound sound wave) and the Reflection and transmission coefficients of the relative structures[4] . It is very safe to use and does not appear to cause any adverse effects, although information on this is not well documented. It is also relatively inexpensive and quick to perform. Ultrasound scanners can be taken to critically ill patients in intensive care units, avoiding the danger caused while moving the patient to the radiology department. The real time moving image obtained can be used to guide drainage and biopsy procedures. Doppler capabilities on modern scanners allow the blood flow in arteries and veins to be assessed.

Medical imaging topics

Maximizing imaging procedure use

The amount of data obtained in a single MR or CT scan is very extensive. Some of the data that radiologists discard could save patients time and money, while reducing their exposure to radiation and risk of complications from invasive procedures.[7]

Creation of three-dimensional images

Recently, techniques have been developed to enable CT, MRI and ultrasound scanning software to produce 3D images for the physician.[8] Traditionally CT and MRI scans produced 2D static output on film. To produce 3D images, many scans are made, then combined by computers to produce a 3D model, which can then be manipulated by the physician. 3D ultrasounds are produced using a somewhat similar technique. In diagnosing disease of the viscera of abdomen,ultrasound is particularly sensitive on imaging of biliary tract,urinary tract and female reproductive organs(ovary,fallopian tubes).As for example,diagnosis of gall stone by dilatation of common bile duct and stone in common bile duct . With the ability to visualize important structures in great detail, 3D visualization methods are a valuable resource for the diagnosis and surgical treatment of many pathologies. It was a key resource for the famous, but ultimately unsuccessful attempt by Singaporean surgeons to separate Iranian twins Ladan and Laleh Bijani in 2003. The 3D equipment was used previously for similar operations with great success.

Other proposed or developed techniques include:

- Diffuse optical tomography
- Elastography
- Electrical impedance tomography
- Optoacoustic imaging
- Ophthalmology
  - A-scan
  - B-scan
  - Corneal topography
  - Optical coherence tomography
  - Scanning laser ophthalmoscopy

Some of these techniques are still at a research stage and not yet used in clinical routines.

Compression of medical images

Medical imaging techniques produce very large amounts of data, especially from CT, MRI and PET modalities. As a result, storage and communications of electronic image data are prohibitive without the use of compression. JPEG 2000 is the state-of-the-art image compression DICOM standard for storage and transmission of medical images. The cost and feasibility of accessing large image data sets over low or various bandwidths are further addressed by use of another DICOM standard, called JPIP, to enable efficient streaming of the JPEG 2000 compressed image data.

Non-diagnostic imaging

Neuroimaging has also been used in experimental circumstances to allow people (especially disabled persons) to control outside devices, acting as a brain computer interface.

Archiving and recording

Used primarily in ultrasound imaging, capturing the image a medical imaging device is required for archiving and telemedicine applications. In most scenarios, a frame grabber is used in order to capture the video signal from the medical device and relay it to a computer for further processing and operations.[9]

Open source software for medical image analysis

Several open source software packages are available for performing analysis of medical images:

- ImageJ
- 3D Slicer
- ITK
- OsiriX
- GemIdent
- MicroDicom
- FreeSurfer

Use in pharmaceutical clinical trials

Medical imaging has become a major tool in clinical trials since it enables rapid diagnosis with visualization and quantitative assessment.

A typical clinical trial goes through multiple phases and can take up to eight years. Clinical endpoints or outcomes are used to determine whether the therapy is safe and effective. Once a patient reaches the endpoint, he/she is generally excluded from further experimental interaction. Trials that rely solely on clinical endpoints are very costly as they have long durations and tend to need large number of patients.

In contrast to clinical endpoints, surrogate endpoints have been shown to cut down the time required to confirm whether a drug has clinical benefits. Imaging biomarkers (a characteristic that is objectively measured by an imaging technique, which is used as an indicator of pharmacological response to a therapy) and surrogate endpoints have shown to facilitate the use of small group sizes, obtaining quick results with good statistical power.[10]

Imaging is able to reveal subtle change that is indicative of the progression of therapy that may be missed out by more subjective, traditional approaches. Statistical bias is reduced as the findings are evaluated without any direct patient contact.

For example, measurement of tumour shrinkage is a commonly used surrogate endpoint in solid tumour response evaluation. This allows for faster and more objective assessment of the effects of anticancer drugs. In evaluating the extent of Alzheimer's disease, it is still prevalent to use behavioural and cognitive tests. MRI scans on the entire brain can accurately pinpoint hippocampal atrophy rate while PET scans is able to measure the brain's metabolic activity by measuring regional glucose metabolism.[10]

An imaging-based trial will usually be made up of three components:

1. A realistic imaging protocol. The protocol is an outline that standardizes (as far as practically possible) the way in which the images are acquired using the various modalities (PET, SPECT, CT, MRI). It covers the specifics in which images are to be stored, processed and evaluated.

2. An imaging centre that is responsible for collecting the images, perform quality control and provide tools for data storage, distribution and analysis. It is important for images acquired at different time points are displayed in a standardised format to maintain the reliability of the evaluation. Certain specialised imaging contract research organizations provide to end medical imaging services, from protocol design and site management through to data quality assurance and image analysis.

3. Clinical sites that recruit patients to generate the images to send back to the imaging centre.

See also

- Preclinical imaging
- Cardiac PET
- Biomedical informatics
- Digital Imaging and Communications in Medicine
- Digital Mammography and PACS
- EMMI European Master in Molecular Imaging
- eMix
- Fotofinder
- Full-body scan
- VoluMedic

- Magnetic field imaging
- Medical examination
- Medical radiography
- Medical test

- Neuroimaging
- Non-invasive (medical)
- PACS
- JPEG 2000 compression
- JPIP streaming

- Pneumoencephalogram
- Radiology information system
- Segmentation (image processing)
- Signal-to-noise ratio

- Society for Imaging Science and Technology
- Tomogram
- Virtopsy

Further reading

- Burger, Wilhelm; Burge, Mark James, eds (2008). *Digital Image Processing: An Algorithmic Introduction using Java*. Texts in Computer Science series. New York: Springer Science+Business Media. doi:10.1007/978-1-84628-968-2. ISBN 978-1-84628-379-6.
- Baert, Albert L., ed (2008). *Encyclopedia of Diagnostic Imaging*. Berlin: Springer-Verlag. doi:10.1007/978-3-540-35280-8. ISBN 978-3-540-35278-5.
- Tony F. Chan and Jackie Shen (2005). *Image Processing and Analysis - Variational, PDE, Wavelet, and Stochastic Methods* [11]. SIAM
- Terry Yoo(Editor) (2004), *Insight into Images*.
- Robb, RA (1999). *Biomedical Imaging, Visualization, and Analysis*. John Wiley & Sons, Inc. ISBN 0471283533.
- *Journal of Digital Imaging* (New York: Springer Science+Business Media). ISSN 0897-1889.
- Using JPIP for Standard-Compliant Sharing of Medical Image Data [12] a white paper by Aware Inc. [13]

External links

- Medical imaging [14] at the Open Directory Project
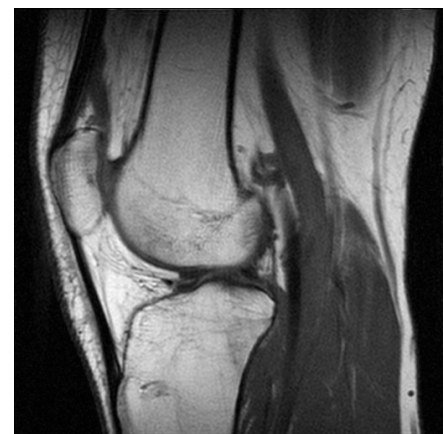- Medical Image Database [15] Free Indexed Online Images
- http://www.aware.com/imaging/accuradjpip.htm What is JPIP?

References

[1] Society of Nuclear Medicine (http://www.snm.org)

[2] thefreedictionary.com - scintigraphy (http://medical-dictionary.thefreedictionary.com/scintigraphy) Citing: Dorland's Medical Dictionary for Health Consumers, 2007 by Saunders; Saunders Comprehensive Veterinary Dictionary, 3 ed. 2007; McGraw-Hill Concise Dictionary of Modern Medicine, 2002 by The McGraw-Hill Companies

[3] Singh, Namrata Singh. Clinical Evaluation of Radiolabeled Drugs for Tubercular Imaging. LAP Lambert Academic Publishing (2010). ISBN-13: 978-3838378381

[4] Dhawan P, A. (2003). Medical Imaging Analysis. Hoboken, NJ: Wiley-Interscience Publication

[5] http://www.breastthermography.com/breast_thermography_mf.htm

[6] http://www.medical.philips.com/main/index.asp

[7] Freiherr G. Waste not, want not: Getting the most from imaging procedures (http://www.diagnosticimaging.com/news/display/article/113619/1541872). *Diagnostic Imaging.* March 19, 2010.

[8] Udupa, J.K. and Herman, G. T., 3D Imaging in Medicine, 2nd Edition, CRC Press, 2000

[9] Treating Medical Ailments in Real Time (http://www.epiphan.com/solutions_new/?arid=16)

[10] Hajnal, J. V., Hawkes, D. J., & Hill, D. L. (2001). Medical Image Registration. CRC Press.

[11] http://jackieneoshen.googlepages.com/ImagingNewEra.html

[12] http://www.aware.com/imaging/whitepapers/wp_jpipwado.htm

[13] http://www.aware.com/imaging/whitepapers.htm

[14] http://www.dmoz.org/Health/Medicine/Imaging//

[15] http://rad.usuhs.edu/medpix/index.html?

MRI

Magnetic resonance imaging (**MRI**), or **nuclear magnetic resonance imaging** (**NMRI**), is primarily a noninvasive medical imaging technique used in radiology to visualize detailed internal structure and limited function of the body. MRI provides much greater contrast between the different soft tissues of the body than computed tomography (CT) does, making it especially useful in neurological (brain), musculoskeletal, cardiovascular, and oncological (cancer) imaging.

Unlike CT, MRI uses no ionizing radiation. Rather, it uses a powerful magnetic field to align the nuclear magnetization of (usually) hydrogen atoms in water in the body. Radio frequency (RF) fields are used to systematically alter the alignment of this magnetization. This causes the hydrogen nuclei to produce a rotating magnetic field detectable by the scanner. This signal can be manipulated by additional magnetic fields to build up enough information to construct an image of the body.[1] :36
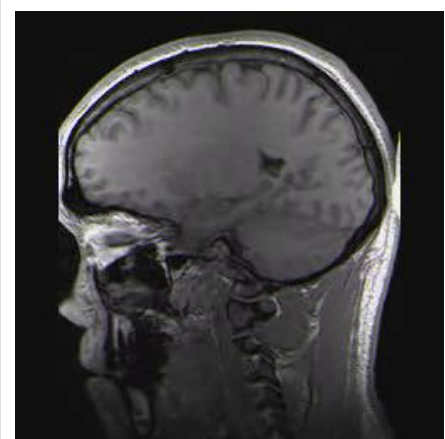

Sagittal MR image of the knee

Magnetic resonance imaging is a relatively new technology. The first MR image was published in 1973[2] [3] and the first cross-sectional

image of a living mouse was published in January 1974.[4] The first studies performed on humans were published in 1977.[5] [6] By comparison, the first human X-ray image was taken in 1895.

Magnetic resonance imaging is a development of nuclear magnetic resonance. Originally, the technique was referred to as nuclear magnetic resonance imaging (NMRI). However, because the word *nuclear* was associated in the public mind with ionizing radiation exposure, it is generally now referred to simply as MRI. Scientists still use the term NMRI when discussing non-medical devices operating on the same principles. The term magnetic resonance tomography (MRT) is also sometimes used.

Para-sagittal MRI of the head, with aliasing artifacts (nose and forehead appear at the back of the head)

How MRI works

The body is largely composed of water molecules. Each water molecule has two hydrogen nuclei or protons. When a person goes inside the powerful magnetic field of the scanner, the magnetic moments of some of these protons changes, and aligns with the direction of the field.

In an MRI machine a radio frequency transmitter is briefly turned on, producing an electromagnetic field. The photons of this field have just the right energy, known as the resonance frequency, to flip the spin of the aligned protons in the body. As the intensity and duration of application of the field increase, more aligned spins are affected. After the field is turned off, the protons decay to the original spin-down state and the difference in energy between the two states is released as a photon. It is these photons that produce the electromagnetic signal that the scanner detects. The frequency the protons resonate at depends on the strength of the magnetic field. As a result of conservation of energy, this also dictates the frequency of the released photons. The photons released when the field is removed have an energy — and therefore a frequency — due to the amount of energy the protons absorbed while the field was active.

It is this relationship between field-strength and frequency that allows the use of nuclear magnetic resonance for imaging. Additional magnetic fields are applied during the scan to make the magnetic field strength depend on the position within the patient, in turn making the frequency of the released photons dependent on position in a predictable manner. Position information can then be recovered from the resulting signal by the use of a Fourier transform. These fields are created by passing electric currents through specially-wound solenoids, known as gradient coils. Since these coils are within the bore of the scanner, there are large forces between them and the main field coils, producing most of the noise that is heard during operation. Without efforts to dampen this noise, it can approach 130 decibels (dB) with strong fields [7] (see also the subsection on acoustic noise).

An image can be constructed because the protons in different tissues return to their equilibrium state at different rates, which is a difference that can be detected. By changing the parameters on the scanner, this effect is used to create contrast between different types of body tissue or between other properties, as in fMRI and diffusion MRI.

Contrast agents may be injected intravenously to enhance the appearance of blood vessels, tumors or inflammation. Contrast agents may also be directly injected into a joint in the case of arthrograms, MRI images of joints. Unlike CT, MRI uses no ionizing radiation and is generally a very safe procedure. Nonetheless the strong magnetic fields and radio pulses can affect metal implants, including cochlear implants and cardiac pacemakers. In the case of cardiac pacemakers, the results can sometimes be lethal,[8] so patients with such implants are generally not eligible

for MRI.

MRI is used to image every part of the body, and is particularly useful for tissues with many hydrogen nuclei and little density contrast, such as the brain, muscle, connective tissue and most tumors.

Applications

In clinical practice, MRI is used to distinguish pathologic tissue (such as a brain tumor) from normal tissue. One advantage of an MRI scan is that it is believed to be harmless to the patient. It uses strong magnetic fields and non-ionizing radiation in the radio frequency range, unlike CT scans and traditional X-rays, which both use ionizing radiation.

While CT provides good spatial resolution (the ability to distinguish two separate structures an arbitrarily small distance from each other), MRI provides comparable resolution with far better contrast resolution (the ability to distinguish the differences between two arbitrarily similar but not identical tissues). The basis of this ability is the complex library of *pulse sequences* that the modern medical MRI scanner includes, each of which is optimized to provide *image contrast* based on the chemical sensitivity of MRI.

For example, with particular values of the *echo time* (T_E) and the *repetition time* (T_R), which are basic parameters of image acquisition, a sequence takes on the property of T_2-weighting. On a T_2-weighted scan, water- and fluid-containing tissues are bright (most modern T_2 sequences are actually *fast T_2* sequences) and fat-containing tissues are dark. The reverse is true for T_1-weighted images. Damaged tissue tends to develop edema, which makes a T_2-weighted sequence sensitive for pathology, and generally able to distinguish pathologic tissue from normal tissue. With the addition of an additional radio frequency pulse and additional manipulation of the magnetic gradients, a T_2-weighted sequence can be converted to a **FLAIR** sequence, in which free water is now dark, but edematous tissues remain bright. This sequence in particular is currently the most sensitive way to evaluate the brain for demyelinating diseases, such as multiple sclerosis.

The typical MRI examination consists of 5–20 sequences, each of which are chosen to provide a particular type of information about the subject tissues. This information is then synthesized by the interpreting physician.

Basic MRI scans

T_1-weighted MRI

T_1-weighted scans use a gradient echo (GRE) sequence, with short T_E and short T_R. This is one of the basic types of MR contrast and is a commonly run clinical scan. The T_1 weighting can be increased (improving contrast) with the use of an inversion pulse as in an MP-RAGE sequence. Due to the short repetition time (T_R) this scan can be run very fast allowing the collection of high resolution 3D datasets. A T_1 reducing gadolinium contrast agent is also commonly used, with a T_1 scan being collected before and after administration of contrast agent to compare the difference. In the brain T_1-weighted scans provide good gray matter/white matter contrast; in other words, T_1-weighted images highlights fat deposition.

T_2-weighted MRI

T_2-weighted scans use a spin echo (SE) sequence, with long T_E and long T_R. They have long been the clinical workhorse as the spin echo sequence is less susceptible to inhomogeneities in the magnetic field. They are particularly well suited to edema as they are sensitive to water content (edema is characterized by increased water content). In other words, put more simply, T2 weighted images light up liquid on the images being visualized.

T^*_2-weighted MRI

T^*_2 (pronounced "T 2 star") weighted scans use a gradient echo (GRE) sequence, with long T_E and long T_R. The gradient echo sequence used does not have the extra refocusing pulse used in spin echo so it is subject to additional losses above the normal T_2 decay (referred to as $T_2{'}$), these taken together are called T^*_2. This also makes it more prone to susceptibility losses at air/tissue boundaries, but can increase contrast for certain types of tissue, such as venous blood.

Spin density weighted MRI

Spin density, also called proton density, weighted scans try to have no contrast from either T_2 or T_1 decay, the only signal change coming from differences in the amount of available spins (hydrogen nuclei in water). It uses a spin echo or sometimes a gradient echo sequence, with short T_E and long T_R.
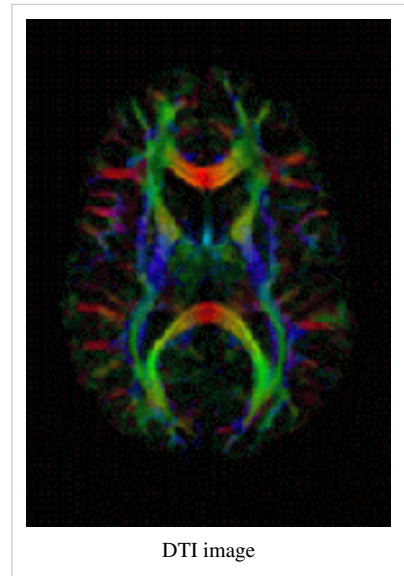
Specialized MRI scans

Diffusion MRI

Diffusion MRI measures the diffusion of water molecules in biological tissues.[9] In an isotropic medium (inside a glass of water for example) water molecules naturally move randomly according to turbulence and Brownian motion. In biological tissues however, where the Reynold's number is low enough for flows to be laminar, the diffusion may be anisotropic. For example a molecule inside the axon of a neuron has a low probability of crossing the myelin membrane. Therefore the molecule moves principally along the axis of the neural fiber. If we know that molecules in a particular voxel diffuse principally in one direction we can make the assumption that the majority of the fibers in this area are going parallel to that direction.

DTI image

The recent development of diffusion tensor imaging (DTI)[3] enables diffusion to be measured in multiple directions and the fractional anisotropy in each direction to be calculated for each voxel. This enables researchers to make brain maps of fiber directions to examine the connectivity of different regions in the brain (using tractography) or to examine areas of neural degeneration and demyelination in diseases like Multiple Sclerosis.

Another application of diffusion MRI is diffusion-weighted imaging (DWI). Following an ischemic stroke, DWI is highly sensitive to the changes occurring in the lesion.[10] It is speculated that increases in restriction (barriers) to water diffusion, as a result of cytotoxic edema (cellular swelling), is responsible for the increase in signal on a DWI scan. The DWI enhancement appears within 5–10 minutes of the onset of stroke symptoms (as compared with computed tomography, which often does not detect changes of acute infarct for up to 4–6 hours) and remains for up to two weeks. Coupled with imaging of cerebral perfusion, researchers can highlight regions of "perfusion/diffusion mismatch" that may indicate regions capable of salvage by reperfusion therapy.

Like many other specialized applications, this technique is usually coupled with a fast image acquisition sequence, such as echo planar imaging sequence.

Magnetization Transfer MRI

Magnetization transfer (MT) refers to the transfer of longitudinal magnetization from free water protons to hydration water protons in NMR and MRI.

In magnetic resonance imaging of molecular solutions, such as protein solutions, two types of water molecules, free (bulk) and hydration (bound), are found. Free water protons have faster average rotational frequency and hence less fixed water molecules that may cause local field inhomogeneity. Because of this uniformity, most free water protons have resonance frequency lying narrowly around the normal proton resonance frequency of 63 MHz (at 1.5 teslas). This also results in slower transverse magnetization dephasing and hence longer T_2. Conversely, hydration water molecules are slowed down by interaction with solute molecules and hence create field inhomogeneities that lead to wider resonance frequency spectrum.

Fluid attenuated inversion recovery (FLAIR)

Fluid Attenuated Inversion Recovery (FLAIR)[11] is an inversion-recovery pulse sequence used to null signal from fluids. For example, it can be used in brain imaging to suppress cerebrospinal fluid (CSF) so as to bring out the periventricular hyperintense lesions, such as multiple sclerosis (MS) plaques. By carefully choosing the inversion time TI (the time between the inversion and excitation pulses), the signal from any particular tissue can be suppressed.

Magnetic resonance angiography

Magnetic resonance angiography (MRA) generates pictures of the arteries to evaluate them for stenosis (abnormal narrowing) or aneurysms (vessel wall dilatations, at risk of rupture). MRA is often used to evaluate the arteries of the neck and brain, the thoracic and abdominal aorta, the renal arteries, and the legs (called a "run-off"). A variety of techniques can be used to generate the pictures, such as administration of a paramagnetic contrast agent (gadolinium) or using a technique known as "flow-related enhancement" (e.g. 2D and 3D time-of-flight sequences), where most of the signal on an image is due to blood that recently moved into that plane, see also FLASH MRI. Techniques involving phase accumulation (known as phase contrast angiography) can also be used to generate flow velocity maps easily and accurately. Magnetic resonance venography (MRV) is a similar procedure that is used to image veins. In this

Magnetic Resonance Angiography

method, the tissue is now excited inferiorly, while signal is gathered in the plane immediately superior to the excitation plane—thus imaging the venous blood that recently moved from the excited plane.[12]
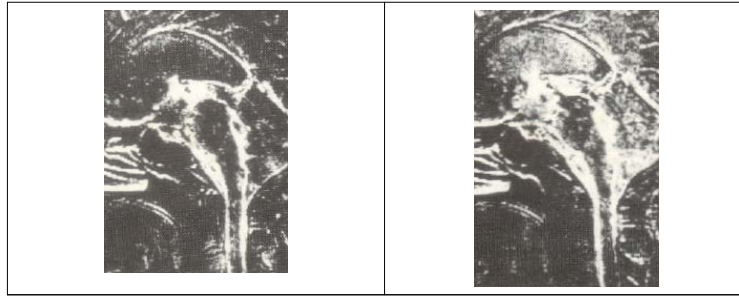
Magnetic resonance gated intracranial CSF dynamics (MR-GILD)

Magnetic resonance gated intracranial cerebrospinal fluid (CSF) or liquor dynamics (MR-GILD) technique is an MR sequence based on bipolar gradient pulse used to demonstrate CSF pulsatile flow in ventricles, cisterns, aqueduct of Sylvius and entire intracranial CSF pathway. It is a method for analyzing CSF circulatory system dynamics in patients with CSF obstructive lesions such as normal pressure hydrocephalus. It also allows visualization of both arterial and venous pulsatile blood flow in vessels without use of contrast agents.[13] [14]

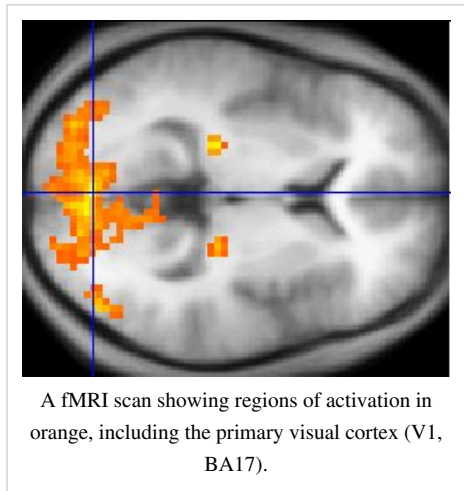| Diastolic time data acquisition (DTDA). | Systolic time data acquisition (STDA). |

Magnetic resonance spectroscopy

Magnetic resonance spectroscopy (MRS) is used to measure the levels of different metabolites in body tissues. The MR signal produces a spectrum of resonances that correspond to different molecular arrangements of the isotope being "excited". This signature is used to diagnose certain metabolic disorders, especially those affecting the brain,[15] and to provide information on tumor metabolism.[16]

Magnetic resonance spectroscopic imaging (MRSI) combines both spectroscopic and imaging methods to produce spatially localized spectra from within the sample or patient. The spatial resolution is much lower (limited by the available SNR), but the spectra in each voxel contains information about many metabolites. Because the available signal is used to encode spatial and spectral information, MRSI requires high SNR achievable only at higher field strengths (3 T and above).

Functional MRI

Functional MRI (fMRI) measures signal changes in the brain that are due to changing neural activity. The brain is scanned at low resolution but at a rapid rate (typically once every 2–3 seconds). Increases in neural activity cause changes in the MR signal via T^*_2 changes;[17] this mechanism is referred to as the BOLD (blood-oxygen-level dependent) effect. Increased neural activity causes an increased demand for oxygen, and the vascular system actually overcompensates for this, increasing the amount of oxygenated hemoglobin relative to deoxygenated hemoglobin. Because deoxygenated hemoglobin attenuates the MR signal, the vascular response leads to a signal increase that is related to the neural activity. The precise nature of the relationship between neural activity and the BOLD signal is a subject of current research. The BOLD effect also allows for the generation of high resolution 3D maps of the venous vasculature within neural tissue.

A fMRI scan showing regions of activation in orange, including the primary visual cortex (V1, BA17).

While BOLD signal is the most common method employed for neuroscience studies in human subjects, the flexible nature of MR imaging provides means to sensitize the signal to other aspects of the blood supply. Alternative techniques employ arterial spin labeling (ASL) or weight the MRI signal by cerebral blood flow (CBF) and cerebral blood volume (CBV). The CBV method requires injection of a class of MRI contrast agents that are now in human clinical trials. Because this method has been shown to be far more sensitive than the BOLD technique in preclinical studies, it may potentially expand the role of fMRI in clinical applications. The CBF method provides more quantitative information than the BOLD signal, albeit at a significant loss of detection sensitivity.

Interventional MRI

The lack of harmful effects on the patient and the operator make MRI well-suited for "interventional radiology", where the images produced by a MRI scanner are used to guide minimally invasive procedures. Of course, such procedures must be done without *any* ferromagnetic instruments.

A specialized growing subset of interventional MRI is that of intraoperative MRI in which the MRI is used in the surgical process. Some specialized MRI systems have been developed that allow imaging concurrent with the surgical procedure. More typical, however, is that the surgical procedure is temporarily interrupted so that MR images can be acquired to verify the success of the procedure or guide subsequent surgical work.

Radiation therapy simulation

Because of MRI's superior imaging of soft tissues, it is now being utilized to specifically locate tumors within the body in preparation for radiation therapy treatments. For therapy simulation, a patient is placed in specific, reproducible, body position and scanned. The MRI system then computes the precise location, shape and orientation of the tumor mass, correcting for any spatial distortion inherent in the system. The patient is then marked or tattooed with points that, when combined with the specific body position, permits precise triangulation for radiation therapy.

Current density imaging

Current density imaging (CDI) endeavors to use the phase information from images to reconstruct current densities within a subject. Current density imaging works because electrical currents generate magnetic fields, which in turn affect the phase of the magnetic dipoles during an imaging sequence. To date no successful CDI has been performed using biological currents, but several studies have been published that involve currents applied through a pair of electrodes.

Magnetic resonance guided focused ultrasound

In MRgFUS therapy, ultrasound beams are focused on a tissue—guided and controlled using MR thermal imaging—and due to the significant energy deposition at the focus, temperature within the tissue rises to more than 65 °C (150 °F), completely destroying it. This technology can achieve precise ablation of diseased tissue. MR imaging provides a three-dimensional view of the target tissue, allowing for precise focusing of ultrasound energy. The MR imaging provides quantitative, real-time, thermal images of the treated area. This allows the physician to ensure that the temperature generated during each cycle of ultrasound energy is sufficient to cause thermal ablation within the desired tissue and if not, to adapt the parameters to ensure effective treatment.

Multinuclear imaging

Hydrogen is the most frequently imaged nucleus in MRI because it is present in biological tissues in great abundance. However, any nucleus with a net nuclear spin could potentially be imaged with MRI. Such nuclei include helium-3, carbon-13, fluorine-19, oxygen-17, sodium-23, phosphorus-31 and xenon-129. ^{23}Na, ^{31}P and ^{17}O are naturally abundant in the body, so can be imaged directly. Gaseous isotopes such as ^{3}He or ^{129}Xe must be hyperpolarized and then inhaled as their nuclear density is too low to yield a useful signal under normal conditions. ^{17}O, ^{13}C and ^{19}F can be administered in sufficient quantities in liquid form (e.g. ^{17}O-water, ^{13}C-glucose solutions or perfluorocarbons) that hyperpolarization is not a necessity.

Multinuclear imaging is primarily a research technique at present. However, potential applications include functional imaging and imaging of organs poorly seen on ^{1}H MRI (e.g. lungs and bones) or as alternative contrast agents. Inhaled hyperpolarized ^{3}He can be used to image the distribution of air spaces within the lungs. Injectable solutions containing ^{13}C or stabilized bubbles of hyperpolarized ^{129}Xe have been studied as contrast agents for angiography and perfusion imaging. ^{31}P can potentially provide information on bone density and structure, as well as functional imaging of the brain.

Susceptibility weighted imaging (SWI)

Susceptibility weighted imaging (SWI), is a new type of contrast in MRI different from spin density, T_1, or T_2 imaging. This method exploits the susceptibility differences between tissues and uses a fully velocity compensated, three dimensional, RF spoiled, high-resolution, 3D gradient echo scan. This special data acquisition and image processing produces an enhanced contrast magnitude image very sensitive to venous blood, hemorrhage and iron storage. It is used to enhance the detection and diagnosis of tumors, vascular and neurovascular diseases (stroke and hemorrhage, multiple sclerosis, Alzheimer's), and also detects traumatic brain injuries that may not be diagnosed using other methods"Radiology" [18]. Retrieved 2 August 2010. **(subscription required)**</ref></ref>

Other specialized MRI techniques

MRI is a new and active field of research and new methods and variants are often published when they are able to get better results in specific fields. Examples of these recent improvements are T_2^*-weighted turbo spin-echo (T_2 TSE MRI), double inversion recovery MRI (DIR-MRI) or phase-sensitive inversion recovery MRI (PSIR-MRI), all of them able to improve imaging of the brain lesions.[19] [20] Another example is MP-RAGE (magnetization-prepared rapid acquisition with gradient echo),[21] which improves images of multiple sclerosis cortical lesions.[22]

Portable instruments

Portable magnetic resonance instruments are available for use in education and field research. Using the principles of Earth's field NMR, they have no powerful polarizing magnet, so that such instruments can be small and inexpensive. Some can be used for both EFNMR spectroscopy and MRI imaging.[23] The low strength of the Earth's field results in poor signal to noise ratios, requiring long scan times to capture spectroscopic data or build up MRI images.

Research with atomic magnetometers have discussed the possibility for cheap and portable MRI instruments without the large magnet.[24] [25]

MRI versus CT

A computed tomography (CT) scanner uses X-rays, a type of ionizing radiation, to acquire its images, making it a good tool for examining tissue composed of elements of a higher atomic number than the tissue surrounding them, such as bone and calcifications (calcium based) within the body (carbon based flesh), or of structures (vessels, bowel). MRI, on the other hand, uses non-ionizing radio frequency (RF) signals to acquire its images and is best suited for non-calcified tissue, though MR images can also be acquired from bones and teeth[26] as well as fossils.[27]

CT may be enhanced by use of contrast agents containing elements of a higher atomic number than the surrounding flesh such as iodine or barium. Contrast agents for MRI have paramagnetic properties, e.g., gadolinium and manganese.

Both CT and MRI scanners are able to generate multiple two-dimensional cross-sections (slices) of tissue and three-dimensional reconstructions. Unlike CT, which uses only X-ray attenuation to generate image contrast, MRI has a long list of properties that may be used to generate image contrast. By variation of scanning parameters, tissue contrast can be altered and enhanced in various ways to detect different features. (See Applications above.)

MRI can generate cross-sectional images in any plane (including oblique planes). In the past, CT was limited to acquiring images in the axial (or near axial) plane. The scans used to be called Computed *Axial* Tomography scans (CAT scans). However, the development of multi-detector CT scanners with near-isotropic resolution, allows the CT scanner to produce data that can be retrospectively reconstructed in any plane with minimal loss of image quality.

For purposes of tumor detection and identification in the brain, MRI is generally superior.[28] [29] [30] However, in the case of solid tumors of the abdomen and chest, CT is often preferred due to less motion artifact. Furthermore, CT usually is more widely available, faster, less expensive, and may be less likely to require the person to be sedated or anesthetized.

MRI is also best suited for cases when a patient is to undergo the exam several times successively in the short term, because, unlike CT, it does not expose the patient to the hazards of ionizing radiation.

Economics of MRI

MRI equipment is expensive. 1.5 tesla scanners often cost between $1 million and $1.5 million USD. 3.0 tesla scanners often cost between $2 million and $2.3 million USD. Construction of MRI suites can cost up to $500,000 USD, or more, depending on project scope.

MRI scanners have been significant sources of revenue for healthcare providers in the US. This is because of favorable reimbursement rates from insurers and federal government programs. Insurance reimbursement is provided in two components, an equipment charge for the actual performance of the MRI scan and professional charge for the radiologist's review of the images and/or data. In the US Northeast, an equipment charge might be $3,500 and a professional charge might be $350 [31] although the actual fees received by the equipment owner and interpreting physician are often significantly less and depend on the rates negotiated with insurance companies or determined by governmental action as in the Medicare Fee Schedule. For example, an

Looking through an MRI scanner.

orthopedic surgery group in Illinois billed a charge of $1,116 for a knee MRI in 2007 but the Medicare reimbursement in 2007 was only $470.91.[32] Many insurance companies require preapproval of an MRI procedure as a condition for coverage.

In the US, the Deficit Reduction Act of 2007 significantly reduced reimbursement rates paid by federal insurance programs for the equipment component of many scans, shifting the economic landscape. Many private insurers have followed suit.

Installation of the MRI unit

Heavy lifting equipment is used to install the MRI unit.

An MRI unit is a rather large item, typically requiring heavy equipment (such as cranes) to move the unit to its final location. Once the MRI unit is in place, the room that houses it is usually "built up" around the unit itself. See this page [33] for an example of the complexity involved in installing an MRI unit in a clinical setting.[34]

Safety

Death and injuries have occurred from projectiles created by the magnetic field, although few compared to the millions of examinations administered.[35] [36] MRI makes use of powerful magnetic fields that, though not known to cause direct biological damage, can interfere with metallic and electromechanical devices. Additional (small) risks are presented by the radio frequency systems, components or elements of the MRI system's operation, elements of the scanning procedure and medications that may be administered to facilitate MRI imaging.

Of great concern is the dramatic increase in the number of reported MRI accidents to the U.S. Food and Drug Administration (FDA). Since 2004, the last year in which a decline in the number of MRI accidents was reported, the full spectrum of MRI accidents has increased significantly in the following years. The 2008 FDA accident report data [37] culminates in a 277% increase over the 2004 rate.

There are many steps that the MRI patient and referring physician can take to help reduce the remaining risks, including providing a full, accurate and thorough medical history to the MRI provider.

Several of the specific MRI safety considerations are identified below:

Implants and foreign bodies

Pacemakers are generally considered an absolute contraindication towards MRI scanning, though highly specialized protocols have been developed to permit scanning of select pacing devices. Several cases of arrhythmia or death have been reported in patients with pacemakers who have undergone MRI scanning without appropriate precautions. Other electronic implants have varying contraindications, depending upon scanner technology, and implant properties, scanning protocols and anatomy being imaged.

Many other forms of medical or biostimulation implants may be contraindicated for MRI scans. These may include vagus nerve stimulators, implantable cardioverter-defibrillators, loop recorders, insulin pumps, cochlear implants, deep brain stimulators, and many others. Medical device patients should always present complete information (manufacturer, model, serial number and date of implantation) about all implants to both the referring physician and to the radiologist or technologist before entering the room for the MRI scan.

While these implants pose a current problem, scientists and manufacturers are working on improved designs that reduce risks to medical device operations. One such development in the works is a nano-coating for implants intended to screen them from the radio frequency waves, helping to make MRI exams available to patients currently prohibited from receiving them. The current article [38] for this is from New Scientist.

Ferromagnetic foreign bodies (e.g. shell fragments), or metallic implants (e.g. surgical prostheses, aneurysm clips) are also potential risks, and safety aspects need to be considered on an individual basis. Interaction of the magnetic and radio frequency fields with such objects can lead to trauma due to movement of the object in the magnetic field, thermal injury from radio-frequency induction heating of the object, or failure of an implanted device. These issues are especially problematic when dealing with the eye. Most MRI centers require an orbital x-ray to be performed on anyone suspected of having metal fragments in their eyes, something not uncommon in metalworking.

Because of its non-ferromagnetic nature and poor electrical conductivity, titanium and its alloys are useful for long term implants and surgical instruments intended for use in image-guided surgery. In particular, not only is titanium safe from movement from the magnetic field, but artifacts around the implant are less frequent and less severe than with more ferromagnetic materials e.g. stainless steel. Artifacts from metal frequently appear as regions of empty space around the implant—frequently called 'black-hole artifact'. E.g. a 3 mm titanium alloy coronary stent may appear as a 5 mm diameter region of empty space on MRI, whereas around a stainless steel stent, the artifact may extend for 10–20 mm or more.

In 2006, a new classification system for implants and ancillary clinical devices has been developed by ASTM International and is now the standard supported by the US Food and Drug Administration:

MR-Safe — The device or implant is completely non-magnetic, non-electrically conductive, and non-RF reactive, eliminating all of the primary potential threats during an MRI procedure.

MR Safe sign

MR-Conditional — A device or implant that may contain magnetic, electrically conductive or RF-reactive components that is safe for operations in proximity to the MRI, provided the conditions for safe operation are defined and observed (such as 'tested safe to 1.5 teslas' or 'safe in magnetic fields below 500 gauss in strength').

MR Conditional sign

MR-Unsafe — Nearly self-explanatory, this category is reserved for objects that are significantly ferromagnetic and pose a clear and direct threat to persons and equipment within the magnet room.

Though the current classification system was originally developed for regulatory-approved medical devices, it is being applied to all manner of items, appliances and equipment intended for use in the MR environment.

In the case of pacemakers, the risk is thought to be primarily RF induction in the pacing electrodes/wires causing inappropriate pacing of the heart, rather than the magnetic field affecting the pacemaker itself. Much research and development is being undertaken, and many tools are being developed to predict RF field effects inside the body.

MR Unsafe sign

Projectile or missile effect

As a result of the very high strength of the magnetic field needed to produce scans (frequently up to 60,000 times the Earth's own magnetic field effects), there are several incidental safety issues addressed in MRI facilities. Missile-effect accidents, where ferromagnetic objects are attracted to the center of the magnet, have resulted in injury and death.[35] [36]

To reduce the risks of projectile accidents, ferromagnetic objects and devices are typically prohibited in proximity to the MRI scanner, with non-ferromagnetic versions of many tools and devices typically retained by the scanning facility. Patients undergoing MRI examinations are required to remove all metallic objects, often by changing into a gown or scrubs.

Ferromagnetic detection devices are used by some sites as a supplement conventional screening techniques, and are now recommended by the American College of Radiology's *Guidance Document for Safe MR Practices*[39] and the United States Department of Veterans Affairs[40] .

The magnetic field and the associated risk of missile-effect accidents remains a permanent hazard, as superconductive MRI magnets are kept permanently energized and so retain their magnetic field in the event of a power outage.

Radio frequency energy

A powerful radio transmitter is needed for excitation of proton spins. This can heat the body to the point of risk of hyperthermia in patients, particularly in obese patients or those with thermoregulation disorders. Several countries have issued restrictions on the maximum specific absorption rate that a scanner may produce.

Peripheral nerve stimulation (PNS)

The rapid switching on and off of the magnetic field gradients is capable of causing nerve stimulation. Volunteers report a twitching sensation when exposed to rapidly switched fields, particularly in their extremities. The reason the peripheral nerves are stimulated is that the changing field increases with distance from the center of the gradient coils (which more or less coincides with the center of the magnet). Note however that when imaging the head, the heart is far off-center and induction of even a tiny current into the heart must be avoided at all costs. Although PNS was not a problem for the slow, weak gradients used in the early days of MRI, the strong, rapidly switched gradients used in techniques such as EPI, fMRI, diffusion MRI, etc. are indeed capable of inducing PNS. American and European regulatory agencies insist that manufacturers stay below specified $d\mathbf{B}/dt$ limits ($d\mathbf{B}/dt$ is the change in field per unit time) or else prove that no PNS is induced for any imaging sequence. As a result of $d\mathbf{B}/dt$ limitation, commercial MRI systems cannot use the full rated power of their gradient amplifiers.

Acoustic noise

Switching of field gradients causes a change in the Lorentz force experienced by the gradient coils, producing minute expansions and contractions of the coil itself. As the switching is typically in the audible frequency range, the resulting vibration produces loud noises (clicking or beeping). This is most marked with high-field machines and rapid-imaging techniques in which sound intensity can reach 120 dB(A) (equivalent to a jet engine at take-off).[41] As a reference, 120 dB is the threshold of loudness causing sensation in the human ear canal — tickling, and 140 dB is the threshold of ear pain. Since decibel is a logarithmic measurement, a 10 dB increase equates to a 10-fold increase in intensity—which, in acoustics, is roughly equal to a doubling of loudness.

Appropriate use of ear protection is essential for anyone inside the MRI scanner room during the examination.[42]

Cryogens

As described above in #Scanner construction and operation, many MRI scanners rely on cryogenic liquids to enable superconducting capabilities of the electromagnetic coils within. Though the cryogenic liquids used are non-toxic, their physical properties present specific hazards.

An unintentional shut-down of a superconducting electromagnet, an event known as "quench", involves the rapid boiling of liquid helium from the device. If the rapidly expanding helium cannot be dissipated through an external vent, sometimes referred to as 'quench pipe', it may be released into the scanner room where it may cause displacement of the oxygen and present a risk of asphyxiation.[43]

Liquid helium, the most commonly used cryogen in MRI, undergoes near explosive expansion as it changes from liquid to a gaseous state. Rooms built in support of superconducting MRI equipment should be equipped with pressure relief mechanisms[44] and an exhaust fan, in addition to the required quench pipe.

Since a quench results in rapid loss of all cryogens in the magnet, recommissioning the magnet is expensive and time-consuming. Spontaneous quenches are uncommon, but may also be triggered by equipment malfunction, improper cryogen fill technique, contaminants inside the cryostat, or extreme magnetic or vibrational disturbances.

Contrast agents

The most commonly used intravenous contrast agents are based on chelates of gadolinium. In general, these agents have proved safer than the iodinated contrast agents used in X-ray radiography or CT. Anaphylactoid reactions are rare, occurring in approx. 0.03–0.1%.[45] Of particular interest is the lower incidence of nephrotoxicity, compared with iodinated agents, when given at usual doses—this has made contrast-enhanced MRI scanning an option for patients with renal impairment, who would otherwise not be able to undergo contrast-enhanced CT.[46]

Although gadolinium agents have proved useful for patients with renal impairment, in patients with severe renal failure requiring dialysis there is a risk of a rare but serious illness, nephrogenic systemic fibrosis, that may be linked to the use of certain gadolinium-containing agents. The most frequently linked is gadodiamide, but other agents have been linked too.[47] Although a causal link has not been definitively established, current guidelines in the United States are that dialysis patients should only receive gadolinium agents where essential, and that dialysis should be performed as soon as possible after the scan to remove the agent from the body promptly.[48] In Europe, where more gadolinium-containing agents are available, a classification of agents according to potential risks has been released.[49] [50] Recently a new contrast agent named gadoxetate, brand name Eovist (US) or Primovist (EU), was approved for diagnostic use: this has the theoretical benefit of a dual excretion path.[51]

Pregnancy

No effects of MRI on the fetus have been demonstrated.[52] In particular, MRI avoids the use of ionizing radiation, to which the fetus is particularly sensitive. However, as a precaution, current guidelines recommend that pregnant women undergo MRI only when essential. This is particularly the case during the first trimester of pregnancy, as organogenesis takes place during this period. The concerns in pregnancy are the same as for MRI in general, but the fetus may be more sensitive to the effects—particularly to heating and to noise. However, one additional concern is the use of contrast agents; gadolinium compounds are known to cross the placenta and enter the fetal bloodstream, and it is recommended that their use be avoided.

Despite these concerns, MRI is rapidly growing in importance as a way of diagnosing and monitoring congenital defects of the fetus because it can provide more diagnostic information than ultrasound and it lacks the ionizing radiation of CT. MRI without contrast agents is the imaging mode of choice for pre-surgical, in-utero diagnosis and evaluation of fetal tumors, primarily teratomas, facilitating open fetal surgery, other fetal interventions, and planning for procedures (such as the EXIT procedure) to safely deliver and treat babies whose defects would otherwise be fatal.

Claustrophobia and discomfort

Due to the construction of some MRI scanners, they can be potentially unpleasant to lie in. Older models of closed bore MRI systems feature a fairly long tube or tunnel. The part of the body being imaged must lie at the center of the magnet, which is at the absolute center of the tunnel. Because scan times on these older scanners may be long (occasionally up to 40 minutes for the entire procedure), people with even mild claustrophobia are sometimes unable to tolerate an MRI scan without management. Modern scanners may have larger bores (up to 70 cm) and scan times are shorter. This means that claustrophobia is less of an issue, and many patients now find MRI an innocuous and easily tolerated procedure.

Nervous patients may still find the following strategies helpful:

- Advance preparation
  - visiting the scanner to see the room and practice lying on the table
  - visualization techniques
  - chemical sedation
  - general anesthesia
- Coping while inside the scanner
  - holding a "panic button"
  - closing eyes as well as covering them (e.g. washcloth, eye mask)
  - listening to music on headphones or watching a movie with a Head-mounted display while in the machine

Alternative scanner designs, such as open or upright systems, can also be helpful where these are available. Though open scanners have increased in popularity, they produce inferior scan quality because they operate at lower magnetic fields than closed scanners. However, commercial 1.5 tesla open systems have recently become available, providing much better image quality than previous lower field strength open models.[53]

For babies and young children chemical sedation or general anesthesia are the norm, as these subjects cannot be instructed to hold still during the scanning session. Obese patients and pregnant women may find the MRI machine to be a tight fit. Pregnant women may also have difficulty lying on their backs for an hour or more without moving.

Guidance

Safety issues, including the potential for biostimulation device interference, movement of ferromagnetic bodies, and incidental localized heating, have been addressed in the American College of Radiology's *White Paper on MR Safety,* which was originally published in 2002 and expanded in 2004. The *ACR White Paper on MR Safety* has been rewritten and was released early in 2007 under the new title *ACR Guidance Document for Safe MR Practices* [54].

In December 2007, the Medicines in Healthcare product Regulation Agency (MHRA), a UK healthcare regulatory body, issued their *Safety Guidelines for Magnetic Resonance Imaging Equipment in Clinical Use* [55].

In February 2008, the Joint Commission, a US healthcare accrediting organization, issued a Sentinel Event Alert #38 [56], their highest patient safety advisory, on MRI safety issues.

In July 2008, the United States Veterans Administration, a federal governmental agency serving the healthcare needs of former military personnel, issued a substantial revision to their *MRI Design Guide* [57], which includes physical or facility safety considerations.

The European Physical Agents Directive

The European Physical Agents (Electromagnetic Fields) Directive is legislation adopted in European legislature. Originally scheduled to be required by the end of 2008, each individual state within the European Union must include this directive in its own law by the end of 2012. Some member nations passed complying legislation and are now attempting to repeal their state laws in expectation that the final version of the EU Physical Agents Directive will be substantially revised prior to the revised adoption date.

The directive applies to occupational exposure to electromagnetic fields (not medical exposure) and was intended to limit workers' acute exposure to strong electromagnetic fields, as may be found near electricity substations, radio or television transmitters or industrial equipment. However, the regulations impact significantly on MRI, with separate sections of the regulations limiting exposure to static magnetic fields, changing magnetic fields and radio frequency energy. Field strength limits are given, which may not be exceeded. An employer may commit a criminal offense by allowing a worker to exceed an exposure limit, if that is how the Directive is implemented in a particular member state.

The Directive is based on the international consensus of established effects of exposure to electromagnetic fields, and in particular the advice of the European Commissions's advisor, the International Commission on Non-Ionizing Radiation Protection (ICNIRP). The aims of the Directive, and the ICNIRP guidelines it is based on, are to prevent exposure to potentially harmful fields. The actual limits in the Directive are very similar to the limits advised by the Institute of Electrical and Electronics Engineers, with the exception of the frequencies produced by the gradient coils, where the IEEE limits are significantly higher.

Many Member States of the EU already have either specific EMF regulations or (as in the UK) a general requirement under workplace health and safety legislation to protect workers against electromagnetic fields. In almost all cases the existing regulations are aligned with the ICNIRP limits so that the Directive should, in theory, have little impact on any employer already meeting their legal responsibilities.

The introduction of the Directive has brought to light an existing potential issue with occupational exposures to MRI fields. There are at present very few data on the number or types of MRI practice that might lead to exposures in excess of the levels of the Directive.[58] [59] There is a justifiable concern amongst MRI practitioners that if the Directive were to be enforced more vigorously than existing legislation, the use of MRI might be restricted, or working practices of MRI personnel might have to change.

In the initial draft a limit of static field strength to 2 T was given. This has since been removed from the regulations, and whilst it is unlikely to be restored as it was without a strong justification, some restriction on static fields may be reintroduced after the matter has been considered more fully by ICNIRP. The effect of such a limit might be to restrict the installation, operation and maintenance of MRI scanners with magnets of 2 T and stronger. As the increase in field strength has been instrumental in developing higher resolution and higher performance scanners, this would be a significant step back. This is why it is unlikely to happen without strong justification.

Individual government agencies and the European Commission have now formed a working group to examine the implications on MRI and to try to address the issue of occupational exposures to electromagnetic fields from MRI.

Three-dimensional (3D) image reconstruction

The principle

Because contemporary MRI scanners offer isotropic, or near isotropic, resolution, display of images does not need to be restricted to the conventional axial images. Instead, it is possible for a software program to build a volume by 'stacking' the individual slices one on top of the other. The program may then display the volume in an alternative manner.

3D rendering techniques

Surface rendering

A threshold value of greyscale density is chosen by the operator (e.g. a level that corresponds to fat). A threshold level is set, using edge detection image processing algorithms. From this, a 3-dimensional model can be constructed and displayed on screen. Multiple models can be constructed from various different thresholds, allowing different colors to represent each anatomical component such as bone, muscle, and cartilage.

However, the interior structure of each element is not visible in this mode of operation.

Volume rendering

Surface rendering is limited in that it only displays surfaces that meet a threshold density, and only displays the surface closest to the imaginary viewer. In volume rendering, transparency and colors are used to allow a better representation of the volume to be shown in a single image - e.g. the bones of the pelvis could be displayed as semi-transparent, so that even at an oblique angle, one part of the image does not conceal another.

Image segmentation

Where different structures have similar threshold density, it can become impossible to separate them simply by adjusting volume rendering parameters. The solution is called segmentation, a manual or automatic procedure that can remove the unwanted structures from the image.

2003 Nobel Prize

Reflecting the fundamental importance and applicability of MRI in medicine, Paul Lauterbur of the University of Illinois at Urbana-Champaign and Sir Peter Mansfield of the University of Nottingham were awarded the 2003 Nobel Prize in Physiology or Medicine for their "discoveries concerning magnetic resonance imaging". The Nobel citation acknowledged Lauterbur's insight of using magnetic field gradients to determine spatial localization, a discovery that allowed rapid acquisition of 2D images. Mansfield was credited with introducing the mathematical formalism and developing techniques for efficient gradient utilization and fast imaging. The actual research that won the prize was done almost 30 years before, while Paul Lauterbur was at Stony Brook University in New York.

The award was vigorously protested by Raymond Vahan Damadian, founder of FONAR Corporation, who claimed that he invented the MRI,[3] and that Lauterbur and Mansfield had merely refined the technology.[60] An ad hoc group, called "The Friends of Raymond Damadian", took out full-page advertisements in the *New York Times* and *The Washington Post* entitled "The Shameful Wrong That Must Be Righted", demanding that he be awarded at least a share of the Nobel Prize.[61] Also, even earlier, in the Soviet Union, Vladislav Ivanov filed (in 1960) a document with the USSR State Committee for Inventions and Discovery at Leningrad for a Magnetic Resonance Imaging device,[62] although this was not approved until the 1970s.[63] In a letter to *Physics Today*, Herman Carr pointed out his own even earlier use of field gradients for one-dimensional MR imaging.[64]

See also

- Earth's field NMR (EFNMR)
- Electron-spin resonance (spin physics)
- History of brain imaging
- Medical imaging
- Magnetic immunoassay
- Jemris (open source MRI simulator)

- *Magnetic Resonance Imaging (journal)*
- Magnetic resonance microscopy
- Magnetic Particle Imaging (MPI)
- Magnetic resonance elastography
- Neuroimaging software
- Nephrogenic fibrosing dermopathy
- Nobel Prize controversies

- Nuclear magnetic resonance (NMR)
- 2D-FT NMRI and Spectroscopy
- Relaxation
- Robinson oscillator
- Rabi cycle
- Virtopsy

Further reading

- Simon, Merrill; Mattson, James S (1996). *The pioneers of NMR and magnetic resonance in medicine: The story of MRI*. Ramat Gan, Israel: Bar-Ilan University Press. ISBN 0-9619243-1-4.
- Haacke, E Mark; Brown, Robert F; Thompson, Michael; Venkatesan, Ramesh (1999). *Magnetic resonance imaging: Physical principles and sequence design*. New York: J. Wiley & Sons. ISBN 0-471-35128-8.
- Lee, S. C. et al., (2001). One Micrometer Resolution NMR Microscopy. *J. Magn. Res.*, **150**: 207-213.

External links

- A Guided Tour of MRI: An introduction for laypeople [65] National High Magnetic Field Laboratory
- The Basics of MRI [66]. *Underlying physics and technical aspects*.
- Video: What to Expect During Your MRI Exam [67] from the Institute for Magnetic Resonance Safety, Education, and Research (IMRSER)
- International Society for Magnetic Resonance in Medicine [68]
- Trends in Biotechnology Volume 28, Issue 7, July 2010, Pages 363-370 [69]

References

[1] Squire LF, Novelline RA (1997). *Squire's fundamentals of radiology* (5th ed.). Harvard University Press. ISBN 0-674-83339-2.

[2] Lauterbur PC (1973). "Image Formation by Induced Local Interactions: Examples of Employing Nuclear Magnetic Resonance". *Nature* **242**: 190−191. doi:10.1038/242190a0.

[3] Filler AG (2010). "The history, development, and impact of computed imaging in neurological diagnosis and neurosurgery: CT, MRI, DTI". *Internet Journal of Neurosurgery* (http://www.ispub.com/journal/the_internet_journal_of_neurosurgery/volume_7_number_1_39/article/the-history-development-and-impact-of-computed-imaging-in-neurological-diagnosis-and-neurosurgery-ct-mri-and-dti.html) **7** (1).

[4] Lauterbur PC (1974). "Magnetic resonance zeugmatography". *Pure and Applied Chemistry* **40**: 149−157. doi:10.1351/pac197440010149.

[5] Damadian R, Goldsmith M, Minkoff L (1977). "NMR in cancer: XVI. Fonar image of the live human body". *Physiological Chemistry and Physics* **9**: 97−100.

[6] Hinshaw DS, Bottomley PA, Holland GN (1977). "Radiographic thin-section image of the human wrist by nuclear magnetic resonance". *Nature* **270**: 722−723. doi:10.1038/270722a0.

[7] Allen Counter, Åke Olofsson, S.; Olofsson, A.; Borg, E.; Bjelke, B.; Häggström, A.; Grahn, H. (2000). "Analysis of Magnetic Resonance Imaging Acoustic Noise Generated by a 4.7 T Experimental System". *Acta Oto-Laryngologica* **120** (6): 739−743. doi:10.1080/000164800750000270. PMID 11099151.

[8] Luechinger, R.; Duru, F.; Candinas, R.; Boesiger, P. (2004). "Safety considerations for magnetic resonance imaging of pacemaker and ICD patients". *Herzschrittmachertherapie und Elektrophysiologie* **15**: 73. doi:10.1007/s00399-004-0401-5.

[9] Le Bihan D, Breton E, Lallemand D, Grenier P, Cabanis E, Laval-Jeantet M. (November 1986). "MR imaging of intravoxel incoherent motions: Application to diffusion and perfusion in neurologic disorders.". *Radiology.* **161** (2): 401−7. PMID 3763909.

[10] Moseley ME, Cohen Y, Mintorovitch J, Chileuitt L, Shimizu H, Kucharczyk J, Wendland MF, Weinstein PR. (1990). "Early detection of regional cerebral ischemia in cats: Comparison of diffusion- and T_2-weighted MRI and spectroscopy". *Magn Reson Med* **14** (2): 330−46. doi:10.1002/mrm.1910140218. PMID 2345513.

[11] De Coene B, Hajnal JV, Gatehouse P, Longmore DB, White SJ, Oatridge A, Pennock JM, Young IR, Bydder GM. (November 1992). "MR of the brain using fluid-attenuated inversion recovery (FLAIR) pulse sequences". *Am J Neuroradiol* **13** (6): 1555−64. PMID 1332459.

[12] Haacke, E Mark; Brown, Robert F; Thompson, Michael; Venkatesan, Ramesh (1999). *Magnetic resonance imaging: Physical principles and sequence design*. New York: J. Wiley & Sons. ISBN 0-471-35128-8.

[13] Ridgway JP, Smith MA (June 1986). "A technique for velocity imaging using magnetic resonance imaging". *Br J Radiol* **59** (702): 603−7. doi:10.1259/0007-1285-59-702-603 (inactive 2010-08-16). PMID 3708269.

[14] Njemanze PC, Beck OJ (1989). "MR-gated intracranial CSF dynamics: Evaluation of CSF pulsatile flow". *AJNR Am J Neuroradiol* **10** (1): 77−80. PMID 2492733.

[15] Rosen Y, Lenkinski RE (2007). "The Recent advances in magnetic resonance neurospectroscopy.". *Neurotherapeutics* **27** (3): 330−45. doi:10.1016/j.nurt.2007.04.009. PMID 17599700.

[16] Golder W (2007). "Magnetic resonance spectroscopy in clinical oncology.". *Onkologie* **27** (3): 304−9. doi:10.1159/000077983. PMID 15249722.

[17] Thulborn KR, Waterton JC, Matthews PM, Radda GK (February 1982). "Oxygenation dependence of the transverse relaxation time of water protons in whole blood at high field" (http://linkinghub.elsevier.com/retrieve/pii/0304-4165(82)90333-6). *Biochim. Biophys. Acta* **714** (2): 265−70. PMID 6275909. .

[18] http://radiology.rsna.org/content/204/1/272.long

[19] Wattjes MP, Lutterbey GG, Gieseke J, *et al.* (1 January 2007). "Double inversion recovery brain imaging at 3T: Diagnostic value in the detection of multiple sclerosis lesions" (http://www.ajnr.org/cgi/pmidlookup?view=long&pmid=17213424). *AJNR Am J Neuroradiol* **28** (1): 54–9. PMID 17213424. .

[20] Nelson F, Poonawalla AH, Hou P, Huang F, Wolinsky JS, Narayana PA (October 2007). "Improved identification of intracortical lesions in multiple sclerosis with phase-sensitive inversion recovery in combination with fast double inversion recovery MR imaging". *AJNR Am J Neuroradiol* **28** (9): 1645–9. doi:10.3174/ajnr.A0645. PMID 17885241.

[21] Nelson F, Poonawalla A, Hou P, Wolinsky JS, Narayana PA (November 2008). "3D MPRAGE improves classification of cortical lesions in multiple sclerosis" (http://www.pubmedcentral.nih.gov/articlerender.fcgi?tool=pmcentrez&artid=2650249). *Mult Scler.* **14** (9): 1214–9. doi:10.1177/1352458508094644. PMID 18952832. PMC 2650249.

[22] Brant-Zawadzki M, Gillan GD, Nitz WR (March 1992). "MP RAGE: A three-dimensional, T_1-weighted, gradient-echo sequence—initial experience in the brain" (http://radiology.rsnajnls.org/cgi/pmidlookup?view=long&pmid=1535892). *Radiology* **182** (3): 769–75. PMID 1535892. .

[23] "Terranova-MRI Earth's Field MRI teaching system" (http://www.magritek.com/terranova.html). Magritek.com. . Retrieved 2010-08-02.

[24] I. M. Savukov and M. V. Romalis (2005). "MNR Detection with an Atomic Magnetometer" (http://www.atomic.princeton.edu/romalis/magnetometer/papers/Savukov and Romalis - NMR Detection with an Atomic Magnetometer.pdf) (PDF). *Physical Review Letters* **94**. . Blog comment:
  - "Hi-res, cheap & portable MRI" (http://neurophilosophy.wordpress.com/2006/09/06/hi-res-cheap-portable-mri/). Neurophilosophy (blog). .

[25] Raftery D (August 2006). "MRI without the magnet" (http://www.pubmedcentral.nih.gov/articlerender.fcgi?tool=pmcentrez&artid=1568902). *Proc Natl Acad Sci USA.* **103** (34): 12657–8. doi:10.1073/pnas.0605625103. PMID 16912110. PMC 1568902.

[26] Wu Y, Chesler DA, Glimcher MJ, *et al.* (February 1999). "Multinuclear solid-state three-dimensional MRI of bone and synthetic calcium phosphates" (http://www.pnas.org/cgi/pmidlookup?view=long&pmid=9990066). *Proc. Natl. Acad. Sci. U.S.A.* **96** (4): 1574–8. doi:10.1073/pnas.96.4.1574. PMID 9990066. PMC 15521. .

[27] Mietchen, D.; Aberhan, M.; Manz, B.; Hampe, O.; Mohr, B.; Neumann, C.; Volke, F. (2008). "Three-dimensional Magnetic Resonance Imaging of fossils across taxa" (http://direct.sref.org/1726-4189/bg/2008-5-25). *Biogeosciences* **5** (1): 25–41. doi:10.5194/bg-5-25-2008. . Retrieved 2008-04-08.

[28] Colosimo C, Celi G, Settecasi C, Tartaglione T, Di Rocco C, Marano P. (1995 October). "Magnetic resonance and computerized tomography of posterior cranial fossa tumors in childhood. Differential diagnosis and assessment of lesion extent" (in Italian). *Radiol Med* (Torino) **90** (4): 386–95. PMID 8552814.

[29] Allen ED, Byrd SE, Darling CF, Tomita T, Wilczynski MA. (1993). "The clinical and radiological evaluation of primary brain neoplasms in children, Part II: Radiological evaluation." (http://www.pubmedcentral.nih.gov/articlerender.fcgi?tool=pmcentrez&artid=2568155). *J Natl Med Assoc.* **85** (7): 546–53. PMID 8350377. PMC 2568155.

[30] Deck MD, Henschke C, Lee BC, Zimmerman RD, Hyman RA, Edwards J, Saint Louis LA, Cahill PT, Stein H, Whalen JP. (March 1989). "Computed tomography versus magnetic resonance imaging of the brain. A collaborative interinstitutional study". *Clin Imaging* **13** (1): 2–15. doi:10.1016/0899-7071(89)90120-4. PMID 2743188.

[31] Stamford Hospital price quotation October 2008, Stamford CT US

[32] Gordon AC, et al "Over-utilization of MRI in the osteoarthritis patient" AAOS meeting 2008; P145.

[33] http://www.lfmi.ninds.nih.gov/img117arrive.php

[34] "LFMI - Home Page" (http://www.lfmi.ninds.nih.gov/img117arrive.php). Lfmi.ninds.nih.gov. . Retrieved 2010-08-02.

[35] Randal C. Archibold, " Hospital Details Failures Leading to M.R.I. Fatality (http://query.nytimes.com/gst/fullpage.html?res=9C04E4D91731F931A1575BC0A9679C8B63)", *The New York Times*, August 22, 2001

[36] Donald G. McNeil Jr, " M.R.I.'s Strong Magnets Cited in Accidents (http://www.nytimes.com/2005/08/19/health/19magnet.html)", *The New York Times*, August 19, 2005.

[37] http://www.accessdata.fda.gov/scripts/cdrh/cfdocs/cfMAUDE/search.CFM

[38] http://www.newscientist.com/article.ns?id=dn3771

[39] "ACR Guidance Document for Safe MR Practices: 2007" (http://www.acr.org/SecondaryMainMenuCategories/quality_safety/MRSafety/safe_mr07.aspx). . Retrieved 2 August 2010.

[40] "MRI Design Guide" (http://www.Mednovus.com/downloads/VA_MRI_Design_Guide-08.pdf). . Retrieved 2 August 2010.

[41] Price DL, de Wilde JP, Papadaki AM, Curran JS, Kitney RI (January 2001). "Investigation of acoustic noise on 15 MRI scanners from 0.2 T to 3 T.". *Journal of Magnetic Resonance Imaging* **13** (2): 288–293. doi:10.1002/1522-2586(200102)13:2<288::AID-JMRI1041>3.0.CO;2-P. PMID 11169836.

[42] The Open University 2007: *Understanding Cardiovascular Diseases*, course book for the lesson *SK121 Understanding cardiovascular diseases* (http://www3.open.ac.uk/courses/bin/p12.dll?C01SK121), printed by University Press, Cambridge, ISBN 9780749226770 (can be found at OUW (http://www.ouw.co.uk/)), pages 220 and 224.

[43] *Kanal E, Barkovich AJ, Bell C, et al. (2007). "ACR Guidance Document for Safe MR Practices: 2007"* (http://www.acr.org/SecondaryMainMenuCategories/quality_safety/MRSafety/safe_mr07.aspx). *AJR Am J Roentgenol.* **188** *(6): 1–27. doi:10.2214/AJR.06.1616. PMID 17515363. . page 22.*

[44] International Electrotechnical Commission 2008: *Medical Electrical Equipment - Part 2-33: Particular requirements for basic safety and essential performance of magnetic resonance equipment for medical diagnosis*, manufacturers' trade standards (http://webstore.iec.ch/

Webstore/webstore.nsf/0/EC11496F487C406DC125742C000B2805), published by International Electrotechnical Commission, ISBN 2-8318-9626-6 (can be found for purchase at).

[45] Murphy KJ, Brunberg JA, Cohan RH (1 October 1996). "Adverse reactions to gadolinium contrast media: A review of 36 cases" (http://www.ajronline.org/cgi/pmidlookup?view=long&pmid=8819369). *AJR Am J Roentgenol* **167** (4): 847−9. PMID 8819369. .

[46] " ACR guideline (http://www.guideline.gov/summary/summary.aspx?doc_id=8283), 2005"

[47] H.S. Thomsen, S.K. Morcos and P. Dawson (November 2006). "Is there a causal relation between the administration of gadolinium-based contrast media and the development of nephrogenic systemic fibrosis (NSF)?". *Clinical Radiology* **61** (11): 905−6. doi:10.1016/j.crad.2006.09.003. PMID 17018301.

[48] " FDA Public Health Advisory: Gadolinium-containing Contrast Agents for Magnetic Resonance Imaging (http://www.fda.gov/cder/drug/advisory/gadolinium_agents.htm)"

[49] (http://www.mhra.gov.uk/home/idcplg?IdcService=GET_FILE&dID=35149&noSaveAs=0&Rendition=WEB)

[50] "ismrm.org MRI Questions and Answers" (http://www.ismrm.org/special/EMEA2.pdf) (PDF). . Retrieved 2010-08-02.

[51] "Response to the FDA's May 23, 2007, Nephrogenic Systemic Fibrosis Update1 — Radiology" (http://radiology.rsna.org/content/246/1/11.full?searchid=1&HITS=10&hits=10&sortspec=relevance&resourcetype=HWCIT&maxtoshow=&RESULTFORMAT=&author1=kanal&FIRSTINDEX=0). Radiology.rsna.org. 2007-09-12. . Retrieved 2010-08-02.

[52] Ibrahim A. Alorainy, Fahad B. Albadr, Abdullah H. Abujamea (2006). "Attitude towards MRI safety during pregnancy" (http://www.saudiannals.net/pdfs/06-201.pdf). *Ann Saudi Med* **26** (4): 306−9. PMID 16885635. .

[53] "Siemens Introduces First 1.5 Tesla Open Bore MRI" (http://www.medical.siemens.com/webapp/wcs/stores/servlet/PressReleaseView~q_catalogId~e_-1~a_catTree~e_100005,13839,17712~a_langId~e_-1~a_pageId~e_50677~a_storeId~e_10001.htm). Medical.siemens.com. 2004-07-29. . Retrieved 2010-08-02.

[54] http://www.acr.org/SecondaryMainMenuCategories/quality_safety/MRSafety/safe_mr07.aspx

[55] http://www.mhra.gov.uk/home/idcplg?IdcService=GET_FILE&dDocName=CON2033065&RevisionSelectionMethod=LatestReleased

[56] http://www.jointcommission.org/SentinelEvents/SentinelEventAlert/sea_38.htm

[57] http://www.va.gov/facmgt/standard/dg_imag.asp

[58] Bassen, H; Schaefer, D J. ; Zaremba, L; Bushberg, J; Ziskin, M [S]; Foster, K R. (2005). "IEEE Committee on Man and Radiation (COMAR) technical information statement "Exposure of medical personnel to electromagnetic fields from open magnetic resonance imaging systems"". *Health Physics* **89** (6): 684−9. doi:10.1097/01.HP.0000172545.71238.15. PMID 16282801.

[59] HSE 2007, RR570:Assessment of electromagnetic fields around magnetic resonance (MRI) equipment (http://www.hse.gov.uk/research/rrpdf/rr570.pdf). MCL-T Ltd, London

[60] Filler, AG (2009). "The history, development, and impact of computed imaging in neurological diagnosis and neurosurgery: CT, MRI, DTI". *Nature Precedings*. doi:10.1038/npre.2009.3267.2.

[61] H.F. Judson (20 October 2003). "No Nobel Prize for whining". *New York Times*.

[62] MacWilliams, Bryon (2003). "News & Views: Russian claims first in magnetic imaging". *Nature* **426** (6965): 375. doi:10.1038/426375a. PMID 14647349.

[63] "Best Regards to Alfred Nobel" (http://www.inauka.ru/english/article36919.html). . Retrieved 2009-10-16.

[64] Carr, Herman (2004). "Letter: Field Gradients in Early MRI". *Physics Today* **57** (7): 83. doi:10.1063/1.1784322.}

[65] http://www.magnet.fsu.edu/education/tutorials/magnetacademy/mri/

[66] http://www.cis.rit.edu/htbooks/mri/

[67] http://www.imrser.org/PatientVideo.html

[68] http://www.ismrm.org

[69] http://dx.doi.org/10.1016/j.tibtech.2010.04.002

ESR Spectroscopy and Microspectroscopy

ESR

Electron paramagnetic resonance (EPR) or **electron spin resonance** (ESR) spectroscopy is a technique for studying chemical species that have one or more unpaired electrons, such as organic and inorganic free radicals or inorganic complexes possessing a transition metal ion. The basic physical concepts of EPR are analogous to those of nuclear magnetic resonance (NMR), but it is electron spins that are excited instead of spins of atomic nuclei. Because most stable molecules have all their electrons paired, the EPR technique is less widely used than NMR. However, this limitation to paramagnetic species also means that the EPR technique is one of great specificity, since ordinary chemical solvents and matrices do not give rise to EPR spectra.

EPR was first observed in Kazan State University by Soviet physicist Yevgeny Zavoisky in 1944, and was developed independently at the same time by Brebis Bleaney at Oxford University.
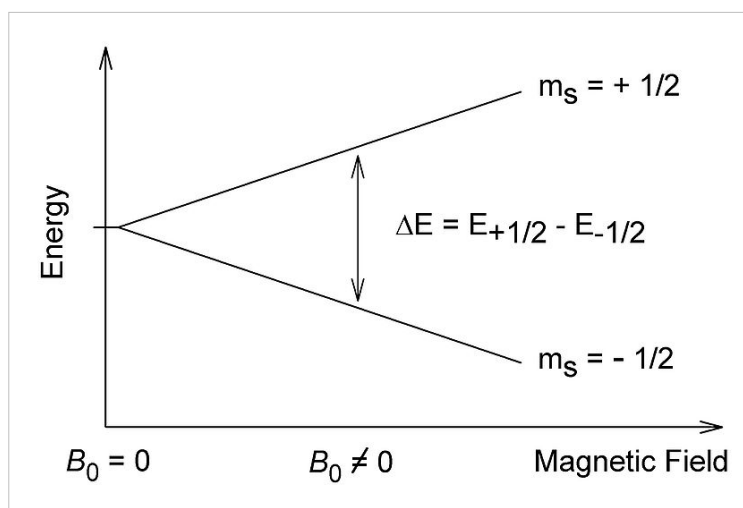
Theory

Origin of an EPR signal

Every electron has a magnetic moment and spin quantum number s = 1/2, with magnetic components m_s = +1/2 and m_s = -1/2. In the presence of an external magnetic field with strength B_0, the electron's magnetic moment aligns itself either parallel (m_s = -1/2) or antiparallel (m_s = +1/2) to the field, each alignment having a specific energy (see the Zeeman effect). The parallel alignment corresponds to the lower energy state, and the separation between it and the upper state is $\triangle E = g_e \mu_B B_0$, where g_e is the electron's

EPR spectrometer

so-called g-factor (see also the Landé g-factor) and μ_B is the Bohr magneton. This equation implies that the splitting of the energy levels is directly proportional to the magnetic field's strength, as shown in the diagram below.
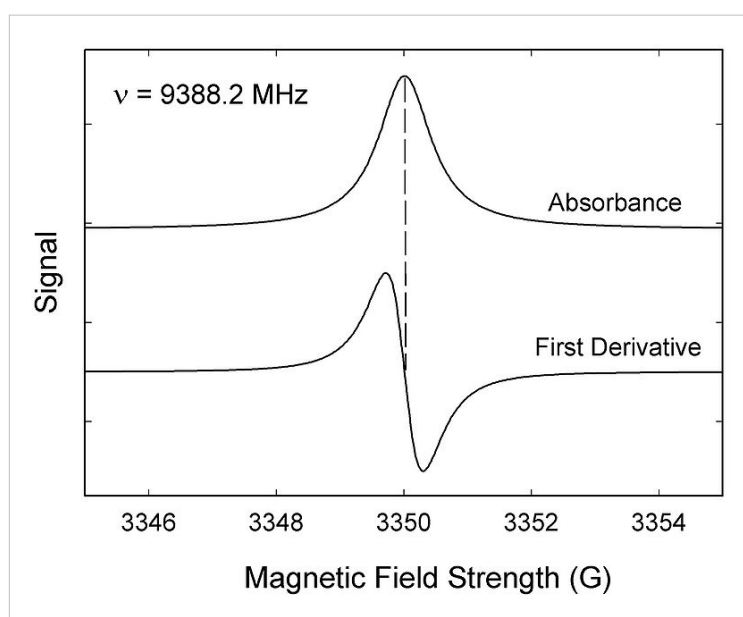
An unpaired electron can move between the two energy levels by either absorbing or emitting electromagnetic radiation of energy $\epsilon = h\nu$ such that the resonance condition, $\epsilon = \triangle E$, is obeyed. Substituting in $\epsilon = h\nu$ and $\triangle E = g_e \mu_B B_0$ leads to the fundamental equation of EPR spectroscopy: $h\nu = g_e \mu_B B_0$. Experimentally, this equation permits a large combination of frequency and magnetic field values, but the great majority of EPR measurements are made with microwaves in the $9000 - 10000$ MHz ($9 - 10$ GHz) region, with fields corresponding to about 3500 G (0.35 T). See below for other field-frequency combinations.

In principle, EPR spectra can be generated by either varying the photon frequency incident on a sample while holding the magnetic field constant, or doing the reverse. In practice, it is usually the frequency which is kept fixed. A collection of paramagnetic centers, such as free radicals, is exposed to microwaves at a fixed frequency. By increasing an external magnetic field, the gap between the $m_s = +1/2$ and $m_s = -1/2$ energy states is widened until it matches the energy of the microwaves, as represented by the double-arrow in the diagram above. At this point the unpaired electrons can move between their two spin states. Since there typically are more electrons in the lower state, due to the Maxwell-Boltzmann distribution (see below), there is a net absorption of energy, and it is this absorption which is monitored and converted into a spectrum.

As an example of how $h\nu = g_e \mu_B B_0$ can be used, consider the case of a free electron, which has $g_e = 2.0023$,[1] and the simulated spectrum shown at the right in two different forms. For the microwave frequency of 9388.2 MHz, the predicted resonance position is a magnetic field of about $B_0 = h\nu / g_e \mu_B = 0.3350$ tesla = 3350 gauss, as shown. Note that while two forms of the same spectrum are presented in the figure, most EPR spectra are recorded and published only as first derivatives.

Because of electron-nuclear mass differences, the magnetic moment of an electron is substantially larger than the corresponding quantity for any nucleus, so

that a much higher electromagnetic frequency is needed to bring about a spin resonance with an electron than with a nucleus, at identical magnetic field strengths. For example, for the field of 3350 G shown at the right, spin resonance occurs near 9388.2 MHz for an electron compared to only about 14.3 MHz for ^{1}H nuclei. (For NMR spectroscopy,

the corresponding resonance equation is $h\nu = g_N\mu_N B_0$ where g_N and μ_N depend on the nucleus under study.)

Maxwell-Boltzmann distribution

In practice, EPR samples consist of collections of many paramagnetic species, and not single isolated paramagnetic centers. If the population of radicals is in thermodynamic equilibrium, its statistical distribution is described by the Maxwell-Boltzmann equation

$$\frac{n_{\text{upper}}}{n_{\text{lower}}} = \exp\left(-\frac{E_{\text{upper}} - E_{\text{lower}}}{kT}\right) = \exp\left(-\frac{\Delta E}{kT}\right) = \exp\left(-\frac{\epsilon}{kT}\right) = \exp\left(-\frac{h\nu}{kT}\right)$$

where n_{upper} is the number of paramagnetic centers occupying the upper energy state, k is the Boltzmann constant, and T is the temperature in kelvins. At 298 K, X-band microwave frequencies ($\nu \approx 9.75$ GHz) give $n_{\text{upper}}/n_{\text{lower}} \approx 0.998$, meaning that the upper energy level has a smaller population than the lower one. Therefore, transitions from the lower to the higher level are more probable than the reverse, which is why there is a net absorption of energy.

The sensitivity of the EPR method (i.e., the minimum number of detectable spins N_{min}) depends on the photon frequency ν according to

$$N_{\text{min}} = \frac{k_1 V}{Q_0 k_f \nu^2 P^{1/2}}$$

where k_1 is a constant, V is the sample's volume, Q_0 is the unloaded quality factor of the microwave cavity (sample chamber), k_f is the cavity filling coefficient, and P is the microwave power in the spectrometer cavity. With k_f and P being constants, $N_{\text{min}} \sim (Q_0\nu^2)^{-1}$, i.e., $N_{\text{min}} \sim \nu^{-\alpha}$, where $\alpha \approx 1.5$. In practice, α can change varying from 0.5 to 4.5 depending on spectrometer characteristics, resonance conditions, and sample size. In other words, the higher the spectrometer frequency the lower the detection limit (N_{min}), meaning greater sensitivity.

Spectral parameters

In real systems, electrons are normally not solitary, but are associated with one or more atoms. There are several important consequences of this:

1. An unpaired electron can gain or lose angular momentum, which can change the value of its *g*-factor, causing it to differ from g_e. This is especially significant for chemical systems with transition-metal ions.
2. If an atom with which an unpaired electron is associated has a non-zero nuclear spin, then its magnetic moment will affect the electron. This leads to the phenomenon of hyperfine coupling, analogous to J-coupling in NMR, splitting the EPR resonance signal into doublets, triplets and so forth.
3. Interactions of an unpaired electron with its environment influence the shape of an EPR spectral line. Line shapes can yield information about, for example, rates of chemical reactions.
4. The *g*-factor and hyperfine coupling in an atom or molecule may not be the same for all orientations of an unpaired electron in an external magnetic field. This anisotropy depends upon the electronic structure of the atom or molecule (e.g., free radical) in question, and so can provide information about the atomic or molecular orbital containing the unpaired electron.

The *g* factor

Knowledge of the *g*-factor can give information about a paramagnetic center's electronic structure. An unpaired electron responds not only to a spectrometer's applied magnetic field B_0, but also to any local magnetic fields of atoms or molecules. The effective field B_{eff} experienced by an electron is thus written

$$B_{\text{eff}} = B_0(1 - \sigma)$$

where σ includes the effects of local fields (σ can be positive or negative). Therefore, the $h\,\nu = g_e\mu_B B_{\text{eff}}$ resonance condition (above) is rewritten as follows:

$$h\nu = g_{\text{e}}\mu_B B_{\text{eff}} = g_{\text{e}}\mu_B B_0(1 - \sigma)$$

The quantity $g_{\text{e}}(1 - \sigma)$ is denoted g and called simply the *g*-factor, so that the final resonance equation becomes

$$h\nu = g\mu_B B_0$$

This last equation is used to determine g in an EPR experiment by measuring the field and the frequency at which resonance occurs. If g does not equal g_{e} the implication is that the ratio of the unpaired electron's spin magnetic moment to its angular momentum differs from the free electron value. Since an electron's spin magnetic moment is constant (approximately the Bohr magneton), then the electron must have gained or lost angular momentum through spin-orbit coupling. Because the mechanisms of spin-orbit coupling are well understood, the magnitude of the change gives information about the nature of the atomic or molecular orbital containing the unpaired electron.

Hyperfine coupling

Since the source of an EPR spectrum is a change in an electron's spin state, it might be thought that all EPR spectra would consist of a single line. However, the interaction of an unpaired electron, by way of its magnetic moment, with nearby nuclear spins, results in additional allowed energy states and, in turn, multi-lined spectra. In such cases, the spacing between the EPR spectral lines indicates the degree of interaction between the unpaired electron and the perturbing nuclei. The hyperfine coupling constant of a nucleus is directly related to the spectral line spacing and, in the simplest cases, is essentially the spacing itself.

Two common mechanisms by which electrons and nuclei interact are the Fermi contact interaction and by dipolar interaction. The former applies largely to the case of isotropic interactions (independent of sample orientation in a magnetic field) and the latter to the case of anisotropic interactions (spectra dependent on sample orientation in a magnetic field). Spin polarization is a third mechanism for interactions between an unpaired electron and a nuclear spin, being especially important for π-electron organic radicals, such as the benzene radical anion. The symbols "*a*" or "*A*" are used for isotropic hyperfine coupling constants while "*B*" is usually employed for anisotropic hyperfine coupling constants.[2]
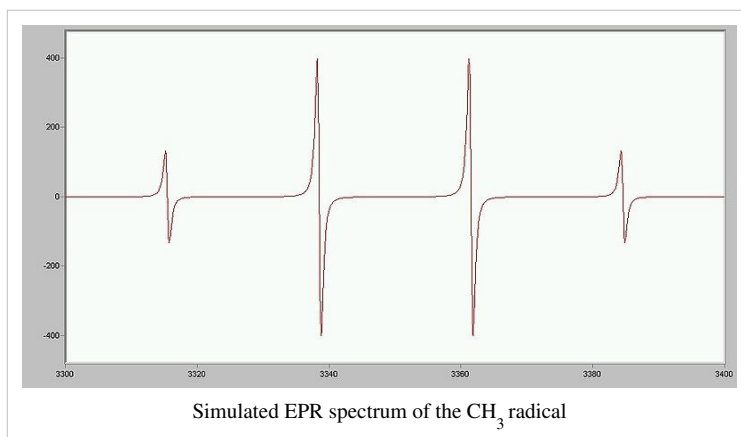
In many cases, the isotropic hyperfine splitting pattern for a radical freely tumbling in a solution (isotropic system) can be predicted.

- For a radical having *M* equivalent nuclei, each with a spin of *I*, the number of EPR lines expected is $2MI + 1$. As an example, the methyl radical, CH_3, has three ^{1}H nuclei each with $I = 1/2$, and so the number of lines expected is $2MI + 1 = 2(3)(1/2) + 1 = 4$, which is as observed.

- For a radical having M_1 equivalent nuclei, each with a spin of I_1, and a group of M_2 equivalent nuclei, each with a spin of I_2, the number of lines expected is $(2M_1 I_1 + 1)(2M_2 I_2 + 1)$. As an example, the methoxymethyl radical, $H_2C(OCH_3)$, has two equivalent ^{1}H nuclei each with $I = 1/2$ and three equivalent ^{1}H nuclei each with $I = 1/2$, and so the number of lines expected is $(2M_1 I_1 + 1)(2M_2 I_2 + 1) = [2(2)(1/2) + 1][2(3)(1/2) + 1] = [3][4] = 12$, again as observed.
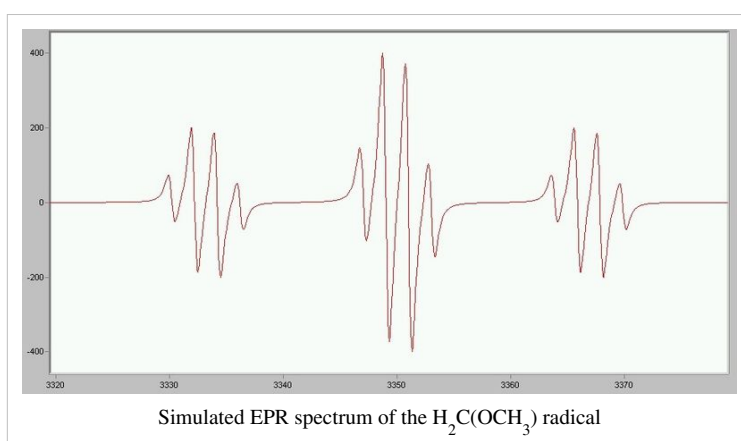
- The above can be extended to predict the number of lines for any number of nuclei.

While it is easy to predict the number of lines a radical's EPR spectrum should show, the reverse problem, unraveling a complex multi-line EPR spectrum and assigning the various spacings to specific nuclei, is more difficult.

In the oft-encountered case of $I = 1/2$ nuclei (e.g., ^{1}H, ^{19}F, ^{31}P), the line intensities produced by a population of radicals, each

Simulated EPR spectrum of the CH_3 radical

possessing M equivalent nuclei, will follow Pascal's triangle. For example, the spectrum at the right shows that the three ^{1}H nuclei of the CH_3 radical give rise to $2MI + 1 = 2(3)(1/2) + 1 = 4$ lines with a 1:3:3:1 ratio. The line spacing gives a hyperfine coupling constant of $a_H = 23$ G for each of the three ^{1}H nuclei. Note again that the lines in this spectrum are *first derivatives* of absorptions.

As a second example, consider the methoxymethyl radical, $H_2C(OCH_3)$. The two equivalent methyl hydrogens will give an overall 1:2:1 EPR pattern, each component of which is further split by the three methoxy hydrogens into a 1:3:3:1 pattern to give a total of $3 \times 4 = 12$ lines, a triplet of quartets. A simulation of the observed EPR spectrum is shown at the right, and agrees with the 12-line prediction and the expected line intensities. Note that the smaller coupling constant (smaller line spacing) is due to the three methoxy hydrogens, while the larger coupling constant (line spacing) is from the two

Simulated EPR spectrum of the $H_2C(OCH_3)$ radical

hydrogens bonded directly to the carbon atom bearing the unpaired electron. It is often the case that coupling constants decrease in size with distance from a radical's unpaired electron, but there are some notable exceptions, such as the ethyl radical (CH_2CH_3).

Resonance linewidth definition

Resonance linewidths are defined in terms of the magnetic induction B, and its corresponding units, and are measured along the x axis of an EPR spectrum, from a line's center to a chosen reference point of the line. These defined widths are called halfwidths and possess some advantages: for asymmetric lines values of left and right halfwidth can be given. The halfwidth ΔB_h is the distance measured from the line's center to the point in which absorption value has half of maximal absorption value in the center of resonance line. First inclination width $\Delta B_{1/2}$ is a distance from center of the line to the point of maximal absorption curve inclination. In practice, a full definition of linewidth is used. For symmetric lines, halfwidth $\Delta B_{1/2} = 2\Delta B_h$, and full inclination width $\Delta B_{max} = 2\Delta B_{1s}$

Applications

EPR spectroscopy is used in various branches of science, such as chemistry and physics, for the detection and identification of free radicals and paramagnetic centers such as F centers. EPR is a sensitive, specific method for studying both radicals formed in chemical reactions and the reactions themselves. For example, when frozen water (solid H_2O) is decomposed by exposure to high-energy radiation, radicals such as H, OH, and HO_2 are produced. Such radicals can be identified and studied by EPR. Organic and inorganic radicals can be detected in electrochemical systems and in materials exposed to UV light. In many cases, the reactions to make the radicals and the subsequent reactions of the radicals are of interest, while in other cases EPR is used to provide information on a radical's geometry and the orbital of the unpaired electron.

Medical and biological applications of EPR also exist. Although radicals are very reactive, and so do not normally occur in high concentrations in biology, special reagents have been developed to spin-label molecules of interest. These reagents are particularly useful in biological systems. Specially-designed nonreactive radical molecules can attach to specific sites in a biological cell, and EPR spectra can then give information on the environment of these so-called spin-label or spin-probes.

A type of dosimetry system has been designed for reference standards and routine use in medicine, based on EPR signals of radicals from irradiated polycrystalline α-alanine(the alanine deamination radical, the hydrogen abstraction radical, and the $(CO^-(OH))=C(CH_3)NH_2^+$ radical) . This method is suitable for measuring gamma and x-rays, electrons, protons, and high-linear energy transfer (LET) radiation of doses in the 1 Gy to 100 kGy range.[3]

EPR spectroscopy can only be applied to systems in which the balance between radical decay and radical formation keeps the free-radicals concentration above the detection limit of the spectrometer used. This can be a particularly severe problem in studying reactions in liquids. An alternative approach is to slow down reactions by studying samples held at cryogenic temperatures, such as 77 K (liquid nitrogen) or 4.2 K (liquid helium). An example of this work is the study of radical reactions in single crystals of amino acids exposed to x-rays, work that sometimes leads to activation energies and rate constants for radical reactions.

The study of radiation-induced free radicals in biological substances (for cancer research) poses the additional problem that tissue contains water, and water (due to its electric dipole moment) has a strong absorption band in the microwave region used in EPR spectrometers.

EPR also has been used by archaeologists for the dating of teeth. Radiation damage over long periods of time creates free radicals in tooth enamel, which can then be examined by EPR and, after proper calibration, dated. Alternatively, material extracted from the teeth of people during dental procedures can be used to quantify their cumulative exposure to ionizing radiation. People exposed to radiation from the Chernobyl disaster have been examined by this method.[4] [5]
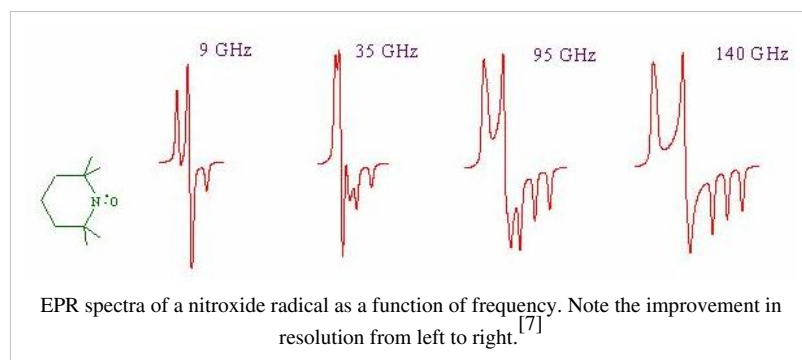
Radiation-sterilized foods have been examined with EPR spectroscopy, the aim being to develop methods to determine if a particular food sample has been irradiated and to what dose.

Because of its high sensitivity, EPR was used recently to measure the quantity of energy used locally during a mechanochemical milling process.[6]

High-field high-frequency measurements

High-field-high-frequency EPR measurements are sometimes needed to detect subtle spectroscopic details. However, for many years the use of electromagnets to produce the needed fields above 1.5 T was impossible, due principally to limitations of traditional magnet materials. The first multifunctional millimeter EPR spectrometer with a superconducting solenoid was described in the early 1970s by Prof. Y. S. Lebedev's group (Russian Institute of Chemical Physics, Moscow) in collaboration with L. G. Oranski's group (Ukrainian Physics and Technics Institute, Donetsk) which began working in the Institute of Problems of Chemical Physics, Chernogolovka around 1975.[7] Two decades later, a W-band EPR spectrometer was produced as a small commercial line by the German Bruker

Company, initiating the expansion of W-band EPR techniques into medium-sized academic laboratories. Today there still are only a few scientific centers in the world capable of high-field-high-frequency EPR, among them are the Grenoble High Magnetic Field Laboratory in Grenoble, France, the Physics Department in Freie Universität Berlin, the National High Magnetic Field Laboratory in Tallahassee, US, the National Center for Advanced ESR Technology (ACERT) at Cornell University in Ithaca, US, the Department of Physiology and Biophysics at Albert Einstein College of Medicine, Bronx, NY, the IFW in Dresden, Germany, the Institute of Physics of Complex Matter in Lausanne in Switzerland, and the Institute of Physics of the Leiden University, Netherlands.

EPR spectra of a nitroxide radical as a function of frequency. Note the improvement in resolution from left to right.[7]

Waveband	L	S	C	X	P	K	Q	U	V	E	W	F	D	—	J	—
λ/mm	300	100	75	30	20	12.5	8.5	6	4.6	4	3.2	2.7	2.1	1.6	1.1	0.83
ν/GHz	1	3	4	10	15	24	35	50	65	75	95	111	140	190	285	360
B_0/T	0.03	0.11	0.14	0.33	0.54	0.86	1.25	1.8	2.3	2.7	3.5	3.9	4.9	6.8	10.2	12.8

The EPR waveband is stipulated by the frequency or wavelength of a spectrometer's microwave source (see Table).

EPR experiments often are conducted at X and, less commonly, Q bands, mainly due to the ready availability of the necessary microwave components (which originally were developed for radar applications). A second reason for widespread X and Q band measurements is that electromagnets can reliably generate fields up to about 1 tesla. However, the low spectral resolution over g-factor at these wavebands limits the study of paramagnetic centers with comparatively low anisotropic magnetic parameters. Measurements at $\nu > 40\,\mathrm{GHz}$, in the millimeter wavelength region, offer the following advantages:

1. EPR spectra are simplified due to the reduction of second-order effects at high fields.
2. Increase in orientation selectivity and sensitivity in the investigation of disordered systems.
3. The informativity and precision of pulse methods, e.g., ENDOR also increase at high magnetic fields.
4. Accessibility of spin systems with larger zero-field splitting due to the larger microwave quantum energy $h\nu$.
5. The higher spectral resolution over g-factor, which increases with irradiation frequency ν and external magnetic field B_0. This is used to investigate the structure, polarity, and dynamics of radical microenvironments in spin-modified organic and biological systems through the spin label and probe method. The figure shows how spectral resolution improves with increasing frequency.
6. Saturation of paramagnetic centers occurs at a comparatively low microwave polarizing field B_1, due to the exponential dependence of the number of excited spins on the radiation frequency ν. This effect can be successfully used to study the relaxation and dynamics of paramagnetic centers as well as of superslow motion in the systems under study.
7. The cross-relaxation of paramagnetic centers decreases dramatically at high magnetic fields, making it easier to obtain more-precise and more-complete information about the system under study.[7]

See also

- Ferromagnetic resonance
- Spin labels
- Site-directed spin labeling
- Spin trapping

Further reading

Many good books and papers are available on the subject of EPR spectroscopy, including those listed here. Essentially all details in this article can be found in these.

- Altshuler, S. A.; Kozirev, B. M. (1964). *Electron Paramagnetic Resonance*. New York: Academic Press.

- Carrington, A.; McLachlan A. (1967). *Introduction to Magnetic Resonance*. London: Harper and Row. ISBN 0470265728.

- Galkin, A. A.; Grinberg, O. Y., Dubinskii, A. A., Kabdin, N. N., Krymov, V. N., Kurochkin, V. I., Lebedev, Y. S., Oransky, L. G., Shuvalov, V. F. (1977). "EPR Spectrometer in 2-mm Range for Chemical Research". *Instrum. Experim. Techn.* **20** (4): 1229.

- Krinichnyi, V. I. (1995). *2-mm Wave Band EPR Spectroscopy of Condensed Systems*. Boca Raton, Florida: CRC Press.

- Lebedev, Y. S. (1994). "2". *High-Field ESR in* Electron Spin Resonance. **14**. Cambridge: Royal Society of Chemistry. p. 63.

- Rhodes, C. J. (2000). *Toxicology of the Human Environment - The Critical Role of Free Radicals*. Taylor and Francis. ISBN 0748409165. - Provides an overview of the role of free radicals in biology and of the use of electron spin resonance in their detection.

- Symons, M. (1978). *Chemical and Biochemical Aspects of Electron-Spin Resonance Spectroscopy*. New York: Wiley. ISBN 0442302290.

- Weil, J. A.; Bolton, J. R., Wertz, J. E. (2001). *Electron Paramagnetic Resonance: Elementary Theory and Practical Applications*. New York: Wiley-Interscience. ISBN 0471572349.

- Weltner, W. (1983). *Magnetic Atoms and Molecules*. New York: Van Nostrand Reinhold. ISBN 0442292066.

- Wertz, J. E.; Bolton, J. R. (1972). *Electron Spin Resonance: Elementary Theory and Practical Applications*. New York: McGraw-Hill. ISBN 0070694540.

- Protein structure elucidation by EPR: Steinhoff, H.-J. (2002). "Methods for study of protein dynamics and protein-protein interaction in protein-ubiquitination by electron paramagnetic resonance spectroscopy". *Frontiers in Bioscience* **7**: 97–110. doi:10.2741/stein.

External links

- NMRWiki.ORG [5] project
- Electron Magnetic Resonance Program [8] National High Magnetic Field Laboratory

References

[1] Odom, B.; Hanneke, D.; D'Urso, B.; and Gabrielse, G. (2006). "New Measurement of the Electron Magnetic Moment Using a One-Electron Quantum Cyclotron". *Phyical Review Letters* **97**: 030801. doi:10.1103/PhysRevLett.97.030801.
[2] Strictly speaking, "*a*" refers to the hyperfine splitting constant, a line spacing measured in magnetic field units, while *A* and *B* refer to hyperfine coupling constants measured in frequency units. Splitting and coupling constants are proportional, but not identical. The book by Wertz and Bolton has more information (pp. 46 and 442).
[3] "Dosimetry Systems". *Journal of the ICRU* **8** (5). 2008. doi:10.1093/jicru/ndn027.

[4] Gualtieri, G.; Colacicchia, S, Sgattonic, R., Giannonic, M. (2001). "The Chernobyl Accident: EPR Dosimetry on Dental Enamel of Children". *Applied Radiation and Isotopes* **55** (1): 71 − 79. doi:10.1016/S0969-8043(00)00351-1. PMID 11339534.

[5] Chumak, V.; Sholom, S.; Pasalskaya, L. (1999). "Application of High Precision EPR Dosimetry with Teeth for Reconstruction of Doses to Chernobyl Populations" (http://rpd.oxfordjournals.org/cgi/content/abstract/84/1-4/515). *Radiation Protection Dosimetry* **84**: 515–520. .

[6] Baron, M., Chamayou, A., Marchioro, L., Raffi, J. (2005). "Radicalar probes to measure the action of energy on granular materials". *Adv. Powder Technol* **16** (3): 199–212. doi:10.1163/1568552053750242.

[7] EPR of low-dimensional systems (http://hf-epr.sitesled.com)

[8] http://www.magnet.fsu.edu/usershub/scientificdivisions/emr/overview.html

Article Sources and Contributors

Relaxation *Source*: http://en.wikipedia.org/w/index.php?oldid=378960658 *Contributors*: Aleph Infinity, Alex Bakharev, AshishG, Barf73, Bensaccount, Bfg, Bobo192, CodeMonk, David Shankbone, Dental, Dina, DmitTrix, Douzzer, EddieVanZant, Elfguy, Ermeyers, Fredrik, Gary King, Hathserv, Hillman, Hyacinth, IMSoP, Interiot, JHunterJ, Jerzy, Jhose, Jossi, Karol Langner, KasugaHuang, Kku, Lambiam, Lion Info, Marie Poise, Mr-Natural-Health, Mwanner, Omid Parto, Pastafarian Nights, Patrick, Pigsonthewing, Prajya, Primetime, RJHall, Rpresser, Skywalker, Stepa, Tanner-Christopher, TechTranslate35, Template namespace initialisation script, Tide rolls, Vildricianus, WLU, Wolfkeeper, Xyzzyplugh, Zana Dark, 24 anonymous edits

Chemical Shift *Source*: http://en.wikipedia.org/w/index.php?oldid=365193121 *Contributors*: Abscurtiss, Art LaPella, Bci2, Blotwell, Bryan Derksen, ChemistHans, Chutinyi, Cmdrjameson, DMacks, Ewlyahoocom, Fantumphool, G-W, Gaius Cornelius, Gene Nygaard, Ghiles, GreatWhiteNortherner, H Padleckas, Headbomb, Isison, Jaerik, Johny83, Kjaergaard, Ksei, Lee-Jon, Lifer21, Marx Gomes, Michael Hardy, Mion, Pdch, PhiLiP, RG2, Ruittenb, Stokerm, Tijmz, Tsuji, V8rik, Zoicon5, 74 anonymous edits

Knight shift *Source*: http://en.wikipedia.org/w/index.php?oldid=322758711 *Contributors*: Michael Hardy, Proofreader77, RJFJR, Salsb, Spiralhighway, The wub, 4 anonymous edits

Robinson oscillator *Source*: http://en.wikipedia.org/w/index.php?oldid=87014408 *Contributors*: Hooperbloob, Jpbowen, Pacula

Fourier transform *Source*: http://en.wikipedia.org/w/index.php?oldid=379850760 *Contributors*: A Doon, Abecedare, Admartch, Adoniscik, Ahoerstemeier, Akbg, Alejo2083, Alipson, Amaher, AnAj, Andrei Polyanin, Angalla, Anna Lincoln, Ap, Army1987, Arondals, Avicennasis, AxelBoldt, Barak Sh, Bci2, Bdmy, BenFrantzDale, BigJohnHenry, Bo Jacoby, Bob K, Bobblewik, Bobo192, Bugnot, Burhem, Butala, CSTAR, Caio2112, Cassandra B, Catslash, Cburnett, Ch mad, Charles Matthews, Chris the speller, ClickRick, Cmghim925, Complexica, Compsonheir, Coppertwig, CrisKatz, Crisófilax, DX-MON, Da nuke, DabMachine, DavidCBryant, Demosta, Discospinster, DmitTrix, Dmmaus, Dougweller, Dr Dec, DrBob, Drew335, Drilnoth, Dysprosia, EconoPhysicist, Ed g2s, Eliyak, Elkman, Enochlau, Feline Hymnic, Feraudyh, Fizyxnrd, Fr33kman, Fred Bradstadt, Fropuff, Futurebird, Gaius Cornelius, Gareth Owen, Giftlite, Glenn, GuidoGer, GyroMagician, H2g2bob, HappyCamper, Heimstern, Hesam7, HirsuteSimia, Hrafeiro, Ht686rg90, I am a mushroom, Igny, Ivan Shmakov, Iwfyita, Jaakobou, Jdorje, Jhealy, Joerite, JohnQPedia, Joriki, Justwantedtofixonething, KHamsun, KYN, Keenan Pepper, Kevmitch, Kostmo, Kunaporn, Larsobrien, Linas, Looxix, Lovibond, Luciopaiva, Lupin, M1ss1ontomars2k4, Manik762007, MathKnight, Maxim, Mckee, Metacomet, Michael Hardy, Mikeblas, Moxfyre, Mr. PIM, NTUDISP, Naddy, Nbarth, Nihil, Nishantjr, Njerseyguy, Nmnogueira, NokMok, Od Mishehu, Oleg Alexandrov, Oli Filth, Omegatron, Ouzel Ring, PAR, Pak21, Papa November, Paul August, Pedrito, Petergans, Phasmatisnox, Phils, PhotoBox, PigFlu Oink, Poincarecon, PtDw832, Publichealthguru, Quintote, Qwfp, R.e.b., Rainwarrior, Rbj, Red Winged Duck, Riesz, Rifleman 82, Rijkbenik, Rjwilmsi, RobertHannah89, Rror, Rs2, Rurz2007, SKvalen, Safenner1, Sai2020, Sbyrnes321, SebastianHelm, Sepia tone, Sgreddin, Shreevatsa, Silly rabbit, Slawekb, SlimDeli, Snigbrook, Snoyes, Sohale, SpaceFlight89, Stevenj, Stpasha, StradivariusTV, Sunev, Sverdrup, Sylvestersteele, Sławomir Biały, THEN WHO WAS PHONE?, TakuyaMurata, Tetracube, The Thing That Should Not Be, Thenub314, Thermochap, Thinking of England, Tim Goodwyn, Tim Starling, Tinos, Tobias Bergemann, TranceThrust, Ujjalpatra, User A1, Vadik wiki, Vasiľ, Verdy p, VeryNewToThis, VictorAnyakin, Vidalian Tears, WLior, Wikiscient, Wile E. Heresiarch, Writer130, Wwheaton, Ybhatti, YouRang?, Zoz, Zvika, 404 anonymous edits

Discrete Fourier transform *Source*: http://en.wikipedia.org/w/index.php?oldid=376335717 *Contributors*: Alberto Orlandini, Alexjs, Arialblack, Arthur Rubin, AxelBoldt, BD2412, Bill411432, Bmitov, Bo Jacoby, Bob K, Bob.v.R, Bongomatic, Booyabazooka, Borching, Bryan Derksen, CRGreathouse, Cburnett, Centrx, Charles Matthews, ChrisRuvolo, Connelly, Conversion script, CoolBlue1234, Crazyvas, Cybedu, Cyp, Dcoetzee, Dicklyon, DopefishJustin, DrBob, Dysprosia, Dzordzm, EconoPhysicist, Ed g2s, Edward, Emvee, Epolk, EverettColdwell, Evil saltine, Foobaz, Fru1tbat, Furrykef, Galaxiaad, Gareth Owen, Gauge, Gene Nygaard, Geoeg, Giftlite, Glogger, Graham87, GregRM, Hanspi, HappyCamper, Helwr, Hesam7, Humatronic, Iyerkri, Java410, JeromeJerome, Jitse Niesen, Kohtala, Kompik, Kramer, Kvng, LMB, Lockeownzj00, Loisel, Madmardigan53, Man It's So Loud In Here, Martynas Patasius, MathMartin, Matithyahu, Mcclurmc, Mckee, Mdebets, Metacomet, Michael Hardy, MightyWarrior, MikeJ9919, Minesweeper, Minghong, Mjb, Msuzen, Nbarth, Nikai, Nitin.mehta, NormDor, Oleg Alexandrov, Oli Filth, Omegatron, OrgasGirl, Ospalh, Oyz, PAR, Pak21, Paul Matthews, Phil Boswell, Poslfit, Pseudomonas, Qz, Rabbanis, Rdrk, Recognizance, Robin S, Ronhjones, Sam Hocevar, Sampletalk, SebastianHelm, Swagato Barman Roy, Sharpoo7, SheeEttin, Silsor, Srleffler, Ssd, Stevenj, Sverdrup, Svick, Swagato Barman Roy, Tbackstr, TheMightyOrb, Thenub314, Thorwald, Uncia, Uncle Dick, User A1, Verdy p, Wikid77, Wile E. Heresiarch, Woohookitty, Zundark, Zvika, Zxcvbnm, Пика Пика, 200 anonymous edits

Fast Fourier transform *Source*: http://en.wikipedia.org/w/index.php?oldid=373140907 *Contributors*: 16@r, 2ganesh, Adam Zivner, Adashiel, Akoesters, Amitparikh, Apexfreak, Artur Nowak, Avalcarce, AxelBoldt, Bartosz, BehnamFarid, Bemoeial, Bender2k14, Blablahblablah, Bmitov, Cameronc, Captain Disdain, Coneslayer, Conversion script, Crossz, Cxxl, Daniel Brockman, David spector, Dcoetzee, Dcwill1285, DeadTotoro, Decrease789, Delirium, Djg2006, Dmsar, Domitori, Donarreiskoffer, DrBob, Efryevt, Eras-mus, Excirial, Eyreland, Faestning, Francium12, Fredrik, Fresheneesz, Furrykef, Gareth Owen, Gene93k, Geoffeg, Giftlite, Glutamin, Gopimanne, GreenSpigot, Grendelkhan, Gunnar Larsson, H2g2bob, HalfShadow, Hashar, Helwr, HenningThielemann, Herry41341, Herve661, Hess88, Hmo, Ixfd64, Jaredwf, Jeltz, Jitse Niesen, Johnbibby, JustUser, Kellybundybrain, Klokbaske, Kuashio, LMB, Lavaka, LeoTrottier, LiDaobing, LouScheffer, Lupo, MarylandArtLover, MaxSem, Maxim, Michael Hardy, Mschlindwein, Mwilde, Nagesh Anupindi, Nbarth, Nixdorf, Norm mit, Ntsimp, Oleg Alexandrov, Oli Filth, Omkar lon, Palfrey, Pankajp, Pit, Pt, QueenCake, Quibik, Quintote, Qwertyus, Qwfp, R.e.b., Requestion, Rjwilmsi, Roadrunner, Robertvan1, Rogerbrent, Rubin joseph 10, Sam Hocevar, Sangwine, SebastianHelm, Solongmarriane, Spectrogram, Squell, Stevenj, TakuyaMurata, Tarquin, Teorth, The Anome, The Yowser, Thenub314, Tim32, TimBentley, Timendum, Tuhinbhakta, Twexcom, Ulterior19802005, Unyoyega, Vincent kraeutler, Wik, Wikicheng, Yacht, Ylai, ZeroOne, Zven, Zxcvbnm, 170 anonymous edits

Fourier transform spectroscopy *Source*: http://en.wikipedia.org/w/index.php?oldid=378775338 *Contributors*: 123Mike456Winston789, AJim, Asterion, Bci2, Bersbers, Berserkerus, BigFatBuddha, Bobby1011, Christopherlin, Conversion script, Damian Yerrick, Deglr6328, E104421, EndersJ, Epbr123, Graeme Bartlett, Graham87, Greggklein, Guillom, Hankwang, Harold f, Haydarkustu, HelgeStenstrom, Jaraalbe, Jcwf, John.lindner, Jonathan F, Kcordina, Kingpin13, Kkmurray, Martyjmch, Matanbz, Materialscientist, Michael Hardy, Nikai, Nitrogen15, PBSurf, Peter, Peterlewis, Publicly Visible, Quibik, Rifleman 82, Rnt20, Ronningt, Roybb95, Sbyrnes321, Seidenstud, Skier Dude, Slapidus, Smeyer1, Stannered, Stepan Roucka, Stokerm, Sverdrup, Taw, Thinkinnng, Tim Starling, Vataro, Veinor, Victorsong, Vsmith, Whasmith, 76 anonymous edits

Nuclear magnetic resonance *Source*: http://en.wikipedia.org/w/index.php?oldid=377198176 *Contributors*: 12boats, 207.172.11.xxx, 2IzSz, 777sms, Abecedare, Abrech, Afiller, Agateller, Akita86, Alansohn, Aleckwyq, Amaher, Amitgujar, Amwestover, Anagram4819, Arisa, Arthena, AutumnSnow, AxelBoldt, Baccyak4H, BailesB, Banano03, Bci2, Beetstra, BenFrantzDale, Bensaccount, Berland, Bigbadjoe, Biophysik, Bruker, Bssquirrel, CMuirPrice, Cacycle, Captain Infinity, Ceyockey, Charles Matthews, ChemistHans, Christopherlin, Colonies Chris, Control.valve, Correo dani, Crazy Demon, Cubbi, Czerinas, DJoe, DMacks, DV8 2XL, DVdm, Daniel.Cardenas, Dantepusiol, Darrien, Davehi1, Deglr6328, DerHexer, Derlay, Dirac66, DixonD, Djdaedalus, Dkontyko, Dreadstar, Dwmyers, Dynabee, DynamicDes, Dysprosia, ERcheck, Edgar181, Edupedro, Ejteye, Eras-mus, Falcon8765, Fantumphool, Flogiston, Foobar, Franamax, G-W, G.hartig, Gadolinist, Gehtnix, Gene Nygaard, Gentgeen, Ghiles, Giftlite, Glhann17, Gogo Dodo, Graham87, GregorB, Greudin, Griffinofwales, Gurch, H Padleckas, Haham hanuka, Hankwang, Haydarkustu, Headbomb, Herbee, Hibernianteas, HolIgor, Iain99, Icairns, Ike9898, Ilws, IlyaV, Improv, Indiedan, Iorsh, IowaStateUniversity, Ixfd64, JBancroftBrown, JWB, Jamesscottbrown, Jayvyas, Jcepna, Jcm, Jcwf, Jens-Erik, Jketola, Jlin, Jmcc150, Jopires, Jpbowen, Jrizor8504, Jsmoreira, Jujutacular, Jurgenfd, JustJuthan, Jxr, KasugaHuang, Katherine Folsom, Kaysette, Kc8ukw, Keenan Pepper, Kevin Ryde, Khilari, King himself88, Kjaergaard, KrakatoaKatie, La goutte de pluie, Latch, Lee-Jon, Lexi Marie, Lfh, Linas, LinguisticDemographer, Linmhall, Little.pig.microphone, Loeffler, Loening, Low-frequency internal, Lucamauri, M stone, Macholl, Magnus Manske, Markber, MartinSaunders, Marx Gomes, Materialscientist, Mav, Michael Hardy, Mietchen, MikeW25, Mkeranat, Morten Cools, Mrmiller24, Naffer, NamfFohyr, Nergaal, Nick Mks, Nickptar, Nicolasbock, Nonoelmo, O18, OMCV, Odie5533, Ole@look, Olivierlopez1, Orelena, Paintman, Paulyche, Peregrine981, Peterlin, PhiRho, Potatoswatter, Pr3cursor, Pt, Quoth, R'win, RSido, Ramamoor, Rednblu, Reinoutr, Rich Farmbrough, Rijkbenik, Rintrah, Rjwilmsi, Rkisling, Rmhermen, Rob Hooft, Robert Hiller, Roy Hoffman, Rvlaw, SCZenz, Salsb, ScAvenger, Shaddack, Sieg6529, Silverchemist, Skier Dude, SlipperyHippo, Snarfevs, Spincore, Spiralhighway, Spree4567, Stan Sykora, Stewartadcock, Tadint, Tamfang, TenOfAllTrades, Terhorstj, The Thing That Should Not Be, TheCoffee, Tim Starling, Timo Honkasalo, Timwi, TomyDuby, Tony Sidaway, Tony27587, Uwcchem, V8rik, Van helsing, Varioustoxins, Voorlandt, Vuo, Walkerma, Waylah, Welsh, Wik, Wikiblaz, Wknight94, XRiffRaffx, Xiaopo, Xris0, Yamamoto Ichiro, Ygramul, Zereshk, Zipz0p, Zosma, 395 anonymous edits

NMR Spectroscopy *Source*: http://en.wikipedia.org/w/index.php?oldid=176585327 *Contributors*: Aihre, Akita86, Aleckwyq, Alex, Andy M. Wang, Anilp83, Antony-22, Atmoz, AxelBoldt, Bci2, Beetstra, Benandjonice, Biophysik, Borisovav, Bruker, CaneryMBurns, Carstensen, Ceyockey, ChemistHans, Chutznik, Cryptophile, DMacks, Djdaedalus, Flogiston, Freestyle-69, G-W, GeeJo, Gehtnix, Gene Nygaard, Ghiles, Graeme Bartlett, Gronan, Hammer1980, Headbomb, Jamesscottbrown, Jclerman, Jenpen, Jingxin, Jrizor8504, Jtepper, Julesd, Kafziel, Kaiserkarl13, Karelj, Keraman, Kjaergaard, Kkmurray, La goutte de pluie, Lee-Jon, LinguisticDemographer, Linmhall, Mac Davis, Markjoseph125, Mboverload, Measure4Measure, Mike.lifeguard, Neparis, OMCV, Oxymoron83, Pekaje, Peterlewis, Pingveno, Quantockgoblin, RG2, Raidon Kane, Ribol, Rifleman 82, Runningonbrains, Salsb, Santiago Dominguez, Santiagoagentino, Shalom Yechiel, Shrew, Sikkema, Smokefoot, Spellmaster, Srnec, Stepa, Takometer, TenOfAllTrades, Tkircher, Tranh Nguyen, Troodon, V8rik, Walkerma, WhatamIdoing, Xenonice, Zosma, 69 anonymous edits

2D-NMR *Source*: http://en.wikipedia.org/w/index.php?oldid=40053741 *Contributors*: Annabel, Biophys, Carstensen, DMacks, DRHagen, Discospinster, Firsfron, Ilikeeatingwaffles, KasugaHuang, Kkmurray, La goutte de pluie, Mkayatta, Sangak, StaticGull, Temporaluser, The wub, V8rik, 28 anonymous edits

2D-FT NMRI and Spectroscopy *Source*: http://en.wikipedia.org/w/index.php?oldid=376470276 *Contributors*: Bci2

Solid-state nuclear magnetic resonance *Source*: http://en.wikipedia.org/w/index.php?oldid=368764268 *Contributors*: BWDuncan, Bluemoose, Cameron barnard, Catgut, Davesnyd, Dharmadeva, ESkog, Fyyer, Gene Nygaard, H Padleckas, Jcwf, KasugaHuang, Kjaergaard, Ksei, La goutte de pluie, Leyo, Martad87, Michael Hardy, NawlinWiki, Nomadr, Ramamoor, Rich Farmbrough, Rvlaw, Salsb, Sangak, Skier Dude, Speeding Cars, Steve Quinn, Sugarkandee1, Teamturnz, Thatjenn, Thue, Whitesoftrice, Wsmitchell3, 62 anonymous edits

Protein nuclear magnetic resonance spectroscopy *Source*: http://en.wikipedia.org/w/index.php?oldid=373836061 *Contributors*: Aleckwyq, Bci2, Bdekker, Beyazid, Biophys, Cmdrjameson, DJoe, Devolk, Długosz, Flogiston, Gaius Cornelius, Jtonejc, Jurgenfd, KangMin, Katherine Folsom, Keilana, Kjaergaard, La goutte de pluie, LostLucidity, Malo, Marx Gomes, Measure4Measure, Miguel Andrade, Neffk, Ocatecir, Opticmountain, Panoramix303, RDBrown, Ragesoss, Rdoherty, Rifleman 82, Rogerb67, Salsb, Sangak, Snowmanradio, Sunil060902, TheLastNinja, Trevyn, Wheedhee, WillowW, 65 anonymous edits

Magnetic resonance microscopy *Source*: http://en.wikipedia.org/w/index.php?oldid=375431439 *Contributors*: Basawala, Bobblewik, Gloy, Joechao, Mindmatrix, STHayden, Simon12, Woohookitty, 6 anonymous edits

Medical imaging *Source*: http://en.wikipedia.org/w/index.php?oldid=379061360 *Contributors*: 01bambern77, A314268, AED, AXu.VSI, Action potential, Adw2000, Alex.tan, Altenmann, Altzinn, AndreasJS, Andrel, Anupam, Appraiser, Arcadian, Auntminnie, Aushulz, Austegard, Bazzargh, Beetstra, Beevee, Beland, Benjaminevans82, Berland, Beth.farrell, Bignoter, Binksternet, Blowdart, Bme591wikiproject, Bradhegg, Btunell, CMD Beaker, CaffeinatedPonderer, Cameron.walsh, Can't sleep, clown will eat me, Canis Lupus, Cozmog, Cuthbertwong, DHN, DMacks, Darklilac, David.Monniaux, Dicklyon, Dina, Discospinster, DocWatson42, Doczilla, Download, Dozen, Dr Zak, Draligus, Elsys, Erikp, Esprit15d, Ferengi, Flowerheaven, Freedomworks, Fumitol, Fuzzball!, G3pro, Ganesha Freya, GargoyleMT, Gene Nygaard, Giftlite, Glitzy queen00, GoingBatty, Goldencuboid, GordyB, Gradient11, GreatWhiteNortherner, GregorB, Gwernol, Hamanibrave, Harrydevoil, HenryLi, Hoof Hearted, Hu12, IXICOexpert, Ian Pitchford, Ihealthbuzz, Imroy, Iweber2003, J04n, JVinocur, JaGa, Jamelan, JamesAM, Jengod, Jfdwolff, JimVC3, Jmanzanares, Jmsc312, John.d.van.horn, Joshnpowell, Karada, Karnesky, Katiem222, Kauczuk, Khalid hassani, Khanafer, Kl4m-AWB, Klar sagen, Kram9, Krisdickie, Ksiddiqui, Kubanczyk, LilHelpa, Loode, Louislemieux, LuisIbanez, Lynnflint, MGlosenger, MMA Texas, Madmedea, Majeka, Mako098765, Mandy0147, Manwichosu, Marcika, Maximus Rex, Maxxicum, Mco44, Mdd, Mechanistic, Med imaging, Melchoir, Mendaliv, Michael Snow, Miguel Andrade, Mikael Häggström, Mirada Medical, Moonriddengirl, Morenus, MrOllie, Nachiketgokhale, NerdyNSK, Nevit, Oclatz, Ohnoitsjamie, Oli Filth, OrangeDog, Oxymoron83, Paranoid, Pde, Peter-NJITWILL, Peterclipston, Peterkmoch, Petersam, Philipcosson, Philippe Nicolai-Dashwood, Pion, Playmobilonhishorse, Publicoption, Pvosta, Radrounds, Rafaela.lamy, RedWolf, Research new, Rhcastilhos, Rich Farmbrough, Rick Sidwell, Rjwilmsi, Robofish, Rphilipp, Rsabbatini, S0uj1r0, SYSS Mouse, Sabry hassouna, Sarahb87, Scottandrewhutchins, Seabhcan, ShakingSpirit, Shunpiker, Sietse Snel, Simeon antonov, Sistromc, Sjschen, Slicky, Smocking, Snoogans1984, Solok7, Soundray, Spencer, Splmko, Stuartghall, Supten, Talented Mr Miller, The Anome, The Rationalist, TheRealNightRider, Thekohser, Themfromspace, Thor Waldsen, Tpl, User A1, UzEE, Van helsing, Wavelength, Way4thesub, Weregerbil, Wilhelm Bauer, Woohookitty, Xanzzibar, Xiggelee, Yoderj, Zereshk, 224 anonymous edits

MRI *Source*: http://en.wikipedia.org/w/index.php?oldid=290480116 *Contributors*: 01bambern77, 0xFFFF, 2T, 95j, 99Perfectos, A314268, A930913, AFdeCH, Aafari, Aarchiba, Abdullahkhurram, Abecedare, Achromatic, Acrabb, Acroterion, Action potential, Adhanali, AdjustShift, Aetheling, Afiller, Afpdv, Agateller, Ageeksgal, Ahmad.ghamdi.24, Ahoerstemeier, AirdishStraus, Alaniaris, Alansohn, Albany NY, Aldaron, Ale jrb, Alex.tan, Amaher, Amberroom, AndonicO, Andre Engels, AndreasJS, Andrewhart1, Angyal8, Animum, Anirishwoman, Antandrus, Antony-22, Anupam, Aplushacks, Apollyon48, Appraiser, Arachnid8124, Arcadian, ArglebargleIV, Argon233, Arteitle, Artemis6234, AtomicDragon, AtticusX, Axl, BBerryhill, Baggio10, Bandy, Banus, Bart133, Bci2, Beao, Beaumont, Bebenko, Benjaminevans82, Binaryblade, Binksternet, Biomed123, Blinking Spirit, Bmeguru, Bobo192, Bodnotbod, Boing! said Zebedee, Boivie, Boris Barowski, Bovineone, Bradhegg, Brandongalbraith, Brewhaha@edmc.net, BrianWren, Brownturkey, Brysonborg, Btunell, Bugnot, Bulbeck, Butros, C.Bluck, Cachorrito, Cajolingwilhelm, Calton, CanadianLinuxUser, Capricorn42, CardinalDan, Caspian, Chantoke, Chet nc, Chris La Mantia, Chris the speller, Christopher Thomas, ChumpusRex, Ck lostsword, DHN, DMacks, DVdm, Da monster under your bed, Daniel.Cardenas, DanielCD, Darrien, David s graff, David.Monniaux, Dawtsf, Deglr6328, Deli nk, Delldot, Deor, Dgbenn, DiamonDie, Diberri, Dick Bos, Dieselbub, Difu Wu, Dirac66, Dj manton, Dlohcierekim's sock, DocWatson42, Dochar, Doctormatt, Doczilla, Dodgethis, Dogcow, Doregan, Dowew, Dreish, Drgeorgek, Duncharris, Dwayne Reed, Ekotkie, El aprendelenguas, Epbr123, Eras-mus, Eric-Wester, Erik Neves, Euyyn, Evahala, Eykanal, Falcon8765, Favonian, Fdpetty, Femto, Ferdinangus, Fernkes, Fig wright, FirstPrinciples, Fixed Phil, Flamebroil, Fleminra, Floppster, Fnielsen, Francis felix, Friginator, Fwayne, Fxqf, G-W, G3pro, Gaius Cornelius, Garrick1a, Gary Cziko, Gene Nygaard, Giftlite, GinaDana, Ginsengbomb, Glenlan, Glennwells, Goalguard33, Gradient11, Graham87, Graldensblud, Gramsaystuart, Grim23, Gsmgm, Gtstricky, Gurchzilla, Gurukeng, GyroMagician, H2g2bob, Hadal, Haham hanuka, Hassaanq, Havaska, Headbomb, Heathd, Hermoye, Heron, Hibana, Hmasoom, Huggles4life, Huitzil, HumphreyW, Husond, Hydrargyrum, Hydrogen Iodide, Hyperdeath, ICAPTCHA, Ian.thomson, Ibuprofen101, Icairns, IceUnshattered, Igoldste, Ihealthbuzz, Ikiroid, ImLookingThruYou, Imagin8or, Improv, Indium, Iridescent, Islander, Isntbrain, Iweber2003, Ixfd64, J.delanoy, JForget, JVinocur, JaGa, Jag123, Jaganath, James Kanjo, JamesMLane, Jan van Male, JdH, Jdrewitt, Je at uwo, Jeffrey O. Gustafson, Jfdwolff, Jfrahm, Jht4060, Jiang, Jimbobl, Jlewis, Jmarchn, Jmjanzen, Jnothman, JoeAnderson, Joelholdsworth, Joema, John.d.van.horn, JohnOwens, Johnkennedyjohn, Jonas2818, Jonathanlewney, Jonboy01, Jong pom chu, Jossi, Jpbowen, Jprawn, Jrockley, Js9530, Jscott.trapp, Jtact, Juansempere, Judicious moron, Jumping cheese, K Eliza Coyne, KDesk, Katieh5584, Keenan Pepper, Khalid hassani, Khened, Kilbad, King himself88, Kitb, Kjkolb, Kjramesh, Kmarhef, Kmpatterson, KnowledgeOfSelf, Koganlikesdick, Kostmo, Kowey, Kpmiyapuram, Kram9, Kshenoy06, Kslays, Kubanczyk, Kuru, Kvahed, Kwamikagami, Kyoko, Lcjohnso, Lcolson, LeadSongDog, Leafyplant, Leszek Jańczuk, Light current, Linas, Liverpool Scouse, LostIntel, LostLeviathan, Luca Balbi, Lucamauri, Lzhang, MAG1, MG1968, MMcCallister, MONGO, Macserv, Macy, MakVal, Mani1, Marek69, Mark83, Master of Puppets, Materialscientist, Matrad6781, Mattabat, Maxxicum, Mco44, Mcsee, Medconn, Mgiganteus1, Michael Hardy, Michaelbusch, Mietchen, Miquonranger03, Missy Sunshine, Mmoneypenny, Mogk, MoraSique, Mossig, MrShim, Mrs.meganmmc, Myanw, N.vanstrien, Naniwako, Nasukaren, NeilUK, Neparis, Nephron, NerdyNSK, Nergaal, Nick Mks, Nigholith, Nightryder84, Nikevich, NonNegative, Nowa, Nulzilla, Nyctea, O18, Oaktree b, Obituarist, Ofirglazer, Oli Filth, Omegatron, Optigan13, Osm agha, Osquar F, Oxymoron83, P g chris, PDH, PMJ, PTSE, Paintman, Pakaran, Papadopc, Paraphelion, Parker007, Pasboudin, Pascal666, Peaceful horizon, Peregrine Fisher, Petemorris, Peterlin, Ph.eyes, Phaked, Philippe Nicolai-Dashwood, Phreed100, Picapica, PierreCA22, Pietrow, PigFlu Oink, Pigsonthewing, Pinball22, Pince Nez, Pinethicket, PloniAlmoni, PoccilScript, Pointillist, Porqin, Potatophysics, Pproctor, Pro crast in a tor, Professorial, Promodulus, QASIMARA, Qrc2006, Quantumobserver, RDBrown, Radeditor, Rasmus Faber, Read-write-services, Reconsider the static, Reedy, Reisio, RelentlessRecusant, Remmus4, Reuben, RexNL, Rich Farmbrough, Richard Arthur Norton (1958-), Richwil, Rickterp, Ridow, Rji, Rjwilmsi, Roadrunner, Robertwharvey, Rod57, Romanm, Romeu, Ronz, RoyBoy, Rstehr, S Roper, SBarnes, SDC, Salsb, Sam Hocevar, SamSim, SanGatiche, Sandstein, Saravask, Savedthat, Sayeth, Schobeiri, Schulte, ScienceApologist, ScottAlanHill, Scottmsg, Sedoc, Sesquiculus1, Sfahey, Shanes, Shavec, Sherool, Shoeofdeath, Shohit, Simoes, Sjschen, Sjö, Skippyjones, Smartwords, Smocking, Sneakygreek, Solipsist, Sorchah, Soundray, Spellwanderer, Spick And Span, Spidermonkey, Spiderman, Spongefrog, Stan Sykora, StaticGull, Stepa, StephanieM, Stevenfruitsmaak, Sthubertus, Stone, Sturm br, Sumersethi, Sunborn, Suruena, SusanLesch, Symane, Taggard, TantalumTelluride, TenOfAllTrades, Tgilk, The Anome, The Hybrid, The JPS, The Random Editor, The Thing That Should Not Be, The undertow, The.Filsouf, TheBrain, TheGlenlivet, Themfromspace, Thisisnotapipe, Thorpe, Threestain, Thumperward, Tide rolls, TimothyFreeman, Timtrent, Timwi, Titoxd, Togo, Tomattea, Tommy2010, Tommytao, TomyDuby, Triddle, Triksox, Una Smith, Unschool, Useight, UtherSRG, Uvo, Valde.maximus, Valentinp14, Van helsing, Vantey, VashiDonsk, Vaughan, Vespristiano, Vicarious, Vicki Rosenzweig, Voice of All, Vonspringer, Vpdvpd, Vuo, Wavelength, Weregerbil, Wernher, Wetman, Widefox, WikHead, Wiki alf, Wimt, Wintonian, Wolf530, Wolfmankurd, Wouterstomp, Writtenright, Wtmitchell, Xangsane181818, Xhead12, Xiggelee, Ygavet, Ystar, Zaak, ZalleZack, Zandperl, Zephalis, Zereshk, Ziggyc, Zureks, Ömer Cengiz Çelebi, Þjóðólfr, 1073 anonymous edits

ESR *Source*: http://en.wikipedia.org/w/index.php?oldid=377268191 *Contributors*: Ahheiss, Astrochemist, Bci2, Brewhaha@edmc.net, Brichcja, Bruker, Chem-awb, Cybercobra, DarkArcher25, Der Marc, EDC105, Ehotze, Falconflyer94, Gene Nygaard, Greyhood, Jauhienij, Jcwf, Jotomicron, K Eliza Coyne, Kbk, Kivirus, Kkmurray, LouisBB, Materialscientist, Nafradi, Oxymoron83, Pavel Dusek, Rjwilmsi, Sbyrnes321, Shiroi Hane, Simetrical, Skier Dude, Spectro Sci, Stan Sykora, StaticGull, Stephen.c.johnson, Tarotcards, Tetracube, Thaejas, Transmobilator, Untifler, V8rik, Van helsing, Wtmitchell, Xenonice, Yuckfoo, علی ویکی, 47 anonymous edits

Image Sources, Licenses and Contributors

Image:NMR alkenes.png *Source*: http://en.wikipedia.org/w/index.php?title=File:NMR_alkenes.png *License*: GNU Free Documentation License *Contributors*: V8rik

Image:NMR alkynes.png *Source*: http://en.wikipedia.org/w/index.php?title=File:NMR_alkynes.png *License*: GNU Free Documentation License *Contributors*: V8rik

Image:Function ocsillating at 3 hertz.svg *Source*: http://en.wikipedia.org/w/index.php?title=File:Function_ocsillating_at_3_hertz.svg *License*: Creative Commons Attribution-Sharealike 3.0 *Contributors*: User:Thenub314

Image:Onfreq.svg *Source*: http://en.wikipedia.org/w/index.php?title=File:Onfreq.svg *License*: Creative Commons Attribution-Sharealike 3.0 *Contributors*: Original: Nicholas Longo, SVG conversion: DX-MON (Richard Mant)

Image:Offfreq.svg *Source*: http://en.wikipedia.org/w/index.php?title=File:Offfreq.svg *License*: Creative Commons Attribution-Sharealike 3.0 *Contributors*: User:Thenub314

Image:Fourier transform of oscillating function.svg *Source*: http://en.wikipedia.org/w/index.php?title=File:Fourier_transform_of_oscillating_function.svg *License*: Creative Commons Attribution-Sharealike 3.0 *Contributors*: User:Thenub314

File:Rectangular function.svg *Source*: http://en.wikipedia.org/w/index.php?title=File:Rectangular_function.svg *License*: unknown *Contributors*: Axxgreazz, Bender235, Darapti, Omegatron

File:Sinc function (normalized).svg *Source*: http://en.wikipedia.org/w/index.php?title=File:Sinc_function_(normalized).svg *License*: unknown *Contributors*: Bender235, Juiced lemon, Omegatron, Pieter Kuiper

File:Spectrum of blue flame.svg *Source*: http://en.wikipedia.org/w/index.php?title=File:Spectrum_of_blue_flame.svg *License*: GNU Free Documentation License *Contributors*: user:Deglr6328 on english wikipedia. Recreated from orginal data

File:Ftir-interferogram.png *Source*: http://en.wikipedia.org/w/index.php?title=File:Ftir-interferogram.png *License*: GNU Free Documentation License *Contributors*: User:Butenbremer

Image:Interferometer.svg *Source*: http://en.wikipedia.org/w/index.php?title=File:Interferometer.svg *License*: GNU Free Documentation License *Contributors*: User:Stannered

Image:Bruker Avance1000.jpg *Source*: http://en.wikipedia.org/w/index.php?title=File:Bruker_Avance1000.jpg *License*: Creative Commons Attribution 3.0 *Contributors*: Haydarkustu

Image:Nuclear Magnetic Resonance Spectrometer.jpg *Source*: http://en.wikipedia.org/w/index.php?title=File:Nuclear_Magnetic_Resonance_Spectrometer.jpg *License*: Public Domain *Contributors*: EMSL at Pacific Northwest National Laboratory

Image:NMR splitting.gif *Source*: http://en.wikipedia.org/w/index.php?title=File:NMR_splitting.gif *License*: Public Domain *Contributors*: IngerAlHaosului, JBancroftBrown

Image:HWB-NMR - 900MHz - 21.2 Tesla.jpg *Source*: http://en.wikipedia.org/w/index.php?title=File:HWB-NMR_-_900MHz_-_21.2_Tesla.jpg *License*: Public Domain *Contributors*: Original uploader was MartinSaunders at en.wikipedia

File:MRI-Philips.JPG *Source*: http://en.wikipedia.org/w/index.php?title=File:MRI-Philips.JPG *License*: Creative Commons Attribution 3.0 *Contributors*: User:Ainali

Image:NMR sample.JPG *Source*: http://en.wikipedia.org/w/index.php?title=File:NMR_sample.JPG *License*: Public Domain *Contributors*: User:Kjaergaard

Image:progesteroneCOSY.png *Source*: http://en.wikipedia.org/w/index.php?title=File:ProgesteroneCOSY.png *License*: GNU Free Documentation License *Contributors*: User:Nonoelmo

Image:Pulsefrequency1.png *Source*: http://en.wikipedia.org/w/index.php?title=File:Pulsefrequency1.png *License*: Public Domain *Contributors*: User:Nonoelmo

Image:Modern 3T MRI.JPG *Source*: http://en.wikipedia.org/w/index.php?title=File:Modern_3T_MRI.JPG *License*: Creative Commons Attribution-Sharealike 2.5 *Contributors*: User:KasugaHuang

Image:900 magnet new.jpg *Source*: http://en.wikipedia.org/w/index.php?title=File:900_magnet_new.jpg *License*: GNU Free Documentation License *Contributors*: Gene Nygaard, Speeding Cars, 1 anonymous edits

Image:Bruker MAS rotors.jpg *Source*: http://en.wikipedia.org/w/index.php?title=File:Bruker_MAS_rotors.jpg *License*: GNU Free Documentation License *Contributors*: Speeding Cars, 1 anonymous edits

Image:SSNMR dip coupl vect.png *Source*: http://en.wikipedia.org/w/index.php?title=File:SSNMR_dip_coupl_vect.png *License*: GNU Free Documentation License *Contributors*: Ksei, PDH, 1 anonymous edits

Image:Cross-polarization.png *Source*: http://en.wikipedia.org/w/index.php?title=File:Cross-polarization.png *License*: GNU Free Documentation License *Contributors*: Ksei

Image:Pacific Northwest National Laboratory 800 MHz NMR Spectrometer.jpg *Source*: http://en.wikipedia.org/w/index.php?title=File:Pacific_Northwest_National_Laboratory_800_MHz_NMR_Spectrometer.jpg *License*: Public Domain *Contributors*: Pacific Northwest National Laboratory

Image:Tocsycosy.jpg *Source*: http://en.wikipedia.org/w/index.php?title=File:Tocsycosy.jpg *License*: Public Domain *Contributors*: User:Kjaergaard

Image:hncahncoca.jpg *Source*: http://en.wikipedia.org/w/index.php?title=File:Hncahncoca.jpg *License*: Public Domain *Contributors*: User:Kjaergaard

Image:RDC and protein structure.png *Source*: http://en.wikipedia.org/w/index.php?title=File:RDC_and_protein_structure.png *License*: Public Domain *Contributors*: DrKjaergaard, Edgar181, Florentyna, 1 anonymous edits

Image:Ensemble of NMR structures.jpg *Source*: http://en.wikipedia.org/w/index.php?title=File:Ensemble_of_NMR_structures.jpg *License*: Public Domain *Contributors*: Kjaergaard

Image:Brain Mri nevit.svg *Source*: http://en.wikipedia.org/w/index.php?title=File:Brain_Mri_nevit.svg *License*: GNU Free Documentation License *Contributors*: Nevit Dilmen

Image:MR Knee.jpg *Source*: http://en.wikipedia.org/w/index.php?title=File:MR_Knee.jpg *License*: GNU Free Documentation License *Contributors*: Blurpeace, Cookie, Fryed-peach, Grook Da Oger, Hellerhoff, Jarekt, Mats Halldin, SBarnes, Test21

File:Structural MRI animation.ogv *Source*: http://en.wikipedia.org/w/index.php?title=File:Structural_MRI_animation.ogv *License*: GNU Free Documentation License *Contributors*: User:Sherool

File:Illus dti.gif *Source*: http://en.wikipedia.org/w/index.php?title=File:Illus_dti.gif *License*: unknown *Contributors*: Lipothymia, 2 anonymous edits

Image:mra1.jpg *Source*: http://en.wikipedia.org/w/index.php?title=File:Mra1.jpg *License*: Creative Commons Attribution 2.5 *Contributors*: Original uploader was Ofirglazer at en.wikipedia

Image:MRI-DTDA.psd.jpg *Source*: http://en.wikipedia.org/w/index.php?title=File:MRI-DTDA.psd.jpg *License*: Public Domain *Contributors*: Dr Philip C. Njemanze

Image:MRI-STDA.psd.jpg *Source*: http://en.wikipedia.org/w/index.php?title=File:MRI-STDA.psd.jpg *License*: Public Domain *Contributors*: Dr Philip C. Njemanze

Image:FMRI.jpg *Source*: http://en.wikipedia.org/w/index.php?title=File:FMRI.jpg *License*: Public Domain *Contributors*: Frank C. Müller, Solipsist, Superborsuk, Was a bee, 2 anonymous edits

File:2009 niams oai hi.jpg *Source*: http://en.wikipedia.org/w/index.php?title=File:2009_niams_oai_hi.jpg *License*: unknown *Contributors*: unknown

File:MRI installation.jpg *Source*: http://en.wikipedia.org/w/index.php?title=File:MRI_installation.jpg *License*: unknown *Contributors*: Laboratory of Functional and Molecular Imaging, NINDS, NIH

Image:MR safe sign.svg *Source*: http://en.wikipedia.org/w/index.php?title=File:MR_safe_sign.svg *License*: Public Domain *Contributors*: User:Ahnode

Image:MR conditional sign.svg *Source*: http://en.wikipedia.org/w/index.php?title=File:MR_conditional_sign.svg *License*: Public Domain *Contributors*: User:Ahnode

Image:MR unsafe sign.svg *Source*: http://en.wikipedia.org/w/index.php?title=File:MR_unsafe_sign.svg *License*: Public Domain *Contributors*: User:WolfWings

Image:EPR spectometer.JPG *Source*: http://en.wikipedia.org/w/index.php?title=File:EPR_spectometer.JPG *License*: GNU Free Documentation License *Contributors*: Photo made by Przemyslaw "Tukan" Grudnik

Image:EPR splitting.jpg *Source*: http://en.wikipedia.org/w/index.php?title=File:EPR_splitting.jpg *License*: Public Domain *Contributors*: Original uploader was Astrochemist at en.wikipedia

Image:EPR lines.jpg *Source*: http://en.wikipedia.org/w/index.php?title=File:EPR_lines.jpg *License*: Public Domain *Contributors*: Original uploader was Astrochemist at en.wikipedia

Image:EPR methyl.jpg *Source*: http://en.wikipedia.org/w/index.php?title=File:EPR_methyl.jpg *License*: Public Domain *Contributors*: Astrochemist

Image:EPR methoxymethyl.jpg *Source*: http://en.wikipedia.org/w/index.php?title=File:EPR_methoxymethyl.jpg *License*: Public Domain *Contributors*: Astrochemist, Keenan Pepper

Image:EPR multifrequency spectra.jpg *Source*: http://en.wikipedia.org/w/index.php?title=File:EPR_multifrequency_spectra.jpg *License*: Public Domain *Contributors*: Astrochemist, Simetrical

License